Feasibility of the tandem reaction of isomerization-telomerization

Torrente Murciano, Laura

Award date:
2007

Awarding institution:
University of Bath

FEASIBILITY OF THE TANDEM REACTION OF ISOMERIZATION – TELOMERIZATION

Laura Torrente Murciano

A thesis submitted for the degree of Doctor of Philosophy

University of Bath
Department of Chemical Engineering

August 2007

Laura Torrente Murciano

ProQuest LLC
789 East Eisenhower Parkway
P.O. Box 1346
Ann Arbor, MI 48106-1346

ABSTRACT

The aim of this project consists of determining the feasibility of a new tandem reaction comprising isomerization and telomerization steps starting from internal diolefins. This type of reactions achieves not only a minimization of the number of steps but also potentially reduces waste formation and process capital costs, thus fulfilling the main objectives of Green Chemistry towards the design of sustainable processes. Telomerization is a 100% atom efficient route to the formation of functionalized long chain molecules. However, only telomerization of terminal conjugated dienes has been reported which limits its applications due to the thermodynamically unfavourable presence of terminal dienes in natural feedstocks. If proved feasible, the proposed tandem reaction would open opportunities for the utilization of new feedstocks and a potentially significant industrial impact.

Titanate nanotubes was found to be a good support for metal catalysts (Pd, Rh, Ru), showing high activity in the isomerization of diolefins and very high selectivity for the reaction with allylbenzene. A novel Ru-PPh_3-resin catalyst was also highly active in diolefins isomerization (including linoleic acid) with similar catalytic activity than homogeneous catalysts and the possibility of being reused without loss of activity.

Screening of homogeneous catalysts based on phosphorus and carbene ligands was carried out for the telomerization reaction and the influence of different operation conditions such as temperature, initial concentration and the nature of nucleophiles was investigated. Heterogeneous catalysts based on DVB resins were also studied, revealing an unusual selectivity to tail-to-head products by Pd-(dvds)-PPh_3-resin in the reaction of isoprene with methanol. The telomerization reaction was extended to 1,3-hexadiene when long-chain alcohols are used as nucleophiles and Pd(Imes)(dvds) as catalyst, opening opportunities for long-chain reactants.

Finally, the feasibility of tandem reactions was successfully demonstrated with the best results obtained with homogeneous isomerization and telomerization catalysts in the presence of free carbene ligands in the reaction medium.

ACKNOWLEDGMENTS

This thesis would not have been possible without many people; so, I would like thank all the people who have participated in my great experience during the last three years in Bath including all staff and students in the Department of Chemical Engineering at the University of Bath. Specifically, to my lab and office mates. I am particularly grateful to my supervisor Dr. Alexei Lapkin for his time and support, for giving me opportunities to develop myself as a scientist and as a person and believing in me.

I am greatly indebted to all my family and friends in Spain and Bath for their support and encouragement. Specially mention to my sister Natalia, mum María, dad Antoliano and my best (boy)friend Raúl. I love you all!!.

TABLE OF CONTENTS

LIST OF FIGURES

LIST OF TABLES

Chapter 1

INTRODUCTION

1.1 RESEARCH CONTEXT

Green Chemistry is the use of chemistry and chemical engineering techniques and methodologies to design products and chemical processes that reduce or eliminate the use of non – renewable feedstocks, by-products, solvents, reagents, etc. that are hazardous to human health or the environment [1]. Thus, Green Chemistry supposes a fundamental change in which the science approaches the design and synthesis of chemical substances, an alternative to the traditional pollute-and-then-clean-up practice. Its goals are summarized in the twelve principles of Green Chemistry which are [2]:

1. Prevention: It is better to prevent pollution than to clean up pollution.
2. Atom economy: maximum incorporation of initial materials in the final products.
3. Less hazardous chemicals syntheses: use of materials and production of products with less possible toxicity to human health and the environment.

4. Designing safer chemicals: minimizing the toxicity maintaining the desired function.
5. Safer solvents and auxiliaries: minimizing the use of solvents, separation agents, etc. or substituting them by less toxic or innocuous ones.
6. Design for energy efficiency: process conditions should approximate as possible to ambient temperature and pressure to minimize costs and environmental impact.
7. Use of renewable feedstocks: if it is technically and economically possible, raw materials should be renewable rather than depleting.
8. Reduce derivatives: minimization or substitution of chemical steps which can produce waste.
9. Catalysis: heterogeneous and selective catalysts decrease the waste.
10. Design for degradation: design of chemical products which do not persist in the environment but degrade to innocuous substances.
11. Real-time analysis for pollution prevention: control of pollution before the formation of hazardous substances.
12. Inherently safer chemistry for accident prevention: chemical processes should be designed to minimize the potential of releases, explosions and any type of accidents.

Chemical manufacturing is the most pollutanting industrial sector releasing more than four times the amount of toxic substances into air, land and water than the next highest sector (extraction of primary metals) [1], contributing to the contamination of air, ground and water. Nowadays, due to the importance of the Sustainability Principles in the political discussions and the social concern about Global Warming and its possible consequences, many governments around the world have already seen the necessity of Environmental Agencies such as the European Environmental Agency and the U.S Environmental Protection Agency, responsible for the European and American environmental polices respectively. Their main actions are the incorporation of environmental taxes in order to pay for the environmental impacts that the companies cause as well as the creation of new and each time more restrictive environmental laws.

Comparing with the previous approaches to the environmental protection which consisted of the minimization of the exposure and the control and treatment of the pollution, Green Chemistry is focusing on accomplishing pollution prevention. While in the first case, processing, disposal and treatment of contaminants are highly economically costly, Green Chemistry's approaches are not only environmentally benign but also economically. If there is not pollution formation, there is not any cost in pollution treatment or extra taxes at the same time than environmental laws are achieved satisfying the efficacy, efficiency and economic criteria.

Thus, the main activities of Green Chemistry are the development of new or the improvement of existing chemical products and processes with a lower environmental impact. One of the most interesting approaches is the reduction of the number of steps in a process combining several reactions in a single reactor, so called "**tandem reaction**". This approach also contributes indirectly towards improved safety, reduced energy consumption and reduced capital costs.

Tandem olefin reactions found in the literature include the initial olefin isomerization followed by hydroaminomethylation [3], different tandem hydroformylation reactions in the presence of N-nucleophiles and with additional C-C bond formations [4], tandem hydroformylation-Wittig olefin hydrogenation process [5].

1.2 RESEARCH SCOPE

The main aim of this project is to establish the feasibility of a tandem reaction involving isomerization of internal linear dienes into 1,3-conjugated dienes combined with telomerization, leading to functionalized molecules. Both reactions are characterised by 100% atom economy and could be performed in environmentally acceptable solvents or solventless and close to ambient conditions. This potential combination is represented in Figure 1.1.

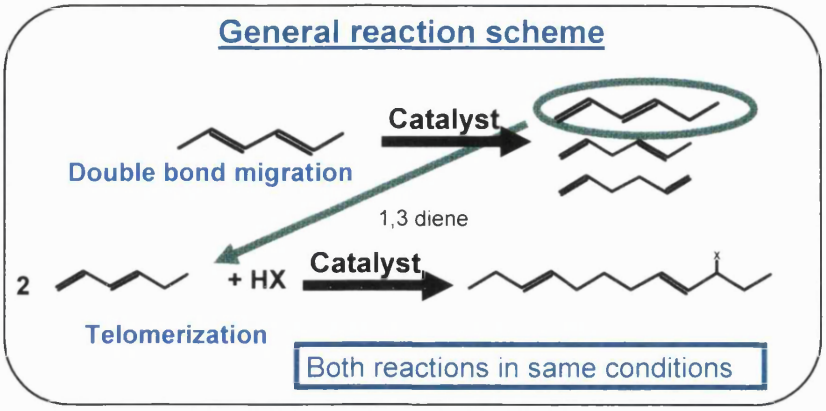

Figure 1.1: Scheme of the proposed tandem isomerization-telomerization reaction.

Beginning with a diene chain with internal double bonds, the first step is the isomerization to obtain a distribution of different isomers. In any double-bond isomer distribution, terminal alkenes are thermodynamically unfavourable, with an equilibrium concentration of the terminal isomer usually less than 5%. In the next step, the telomerization reaction takes place. Telomerization is defined as dimerization of two 1,3-dienes with the concomitant addition of a nucleophile leading to the formation of carbon-carbon and carbon-heteroatom bonds yielding long chain functional molecules which have important uses as a precursors for polymerization, surfactants, etc. In this way, terminal diene formed in the isomerization step will be thermodynamically trapped by the telomerization reaction.

The present project has been carried out in two UK research groups, Professor Kingsley Cavell, Dr Ian Fallis and Dr David Nielsen in the Chemistry Department at Cardiff University and Dr Alexei Lapkin in the Chemical Engineering Department at University of Bath, with the support from Professor Matthias Beller in Rostock, Germany.

The main tasks of our group at Bath include the study of the first reaction in the tandem, the double bond migration reaction, comprising the screening of different homogenous and heterogeneous catalysts, investigation of the kinetics of the double bond migration in conjugated dienes, calculations of the rates of reaction and isomer distributions. The use of heterogeneous catalysts would ensure no

contamination of the telomerization catalysts; however, their main problem is the need to control undesirable reactions, especially hydrogenation.

The Cardiff and Rostock groups are in charge of the synthesis and testing of telomerization catalysts based on palladium-carbenes complexes. These ligands are able to form a weak chelate with the metal centre, and hence stabilise complexes and reaction intermediates. Different dienes and nucleophiles are investigated in Bath, especially the possibility of extending the telomerization reaction to long-chain dienes.

Finally, our group works on the tandem reaction tests including the selection of a reaction medium which allows both isomerization and telomerization reactions to proceed in the same reactor and the selection of complementary or compatible catalysts avoiding the suppression of either reaction. The main challenges of this project are to ensure that the isomerization catalyst remains active in the presence of the telomerization catalyst and both catalysts are inactive for the double bond hydrogenation.

Success in the specific tandem reaction sequence creates exciting opportunities in Green Chemistry using renewable resources. In the telomerization reaction, many pairs of dienes and nucleophiles (water, amines, alcohols, carboxylic acids, carbon dioxide, ketones, aldehides, etc.) have already been investigated. Nevertheless, extending telomerization to long-chain dienes would open new opportunities for building high molecular weight and high value-added of functionalized molecules. An attractive source of long-chain dienes is fatty acids obtained from crops.

1.3 DISSEMINATION

Some of the results obtained during this investigation have been already published in international journals and the papers are shown in Appendix III, others are being prepared:

- L. Torrente-Murciano, A. Lapkin, D. Bavykin, F. Walsh and K. Wilson, "Highly selective Pd/titanate nanotubes catalysts for the double-bond migration reaction", Journal of Catalysis, 245 (2007) 270 – 276.
- D. Bavykin, A. Lapkin, P. Plucinski, L. Torrente-Muciano, J. Friedrich and F. Walsh. "Deposition of Pt, Pd, Ru and Au on the surfaces of titanate nanotubes", Topics in Catalysis, 39 (2006) 151 – 160.
- F. Walsh, D. Bavykin, L. Torrente-Murciano, A. Lapkin and B. Cressey, "Synthesis of novel composite materials via the deposition of precious metals onto protonated titanate nanotubes", Transactions of the Institute of Metal Finishing, 84 (2006) 293 – 299. Awarded the Johnson Matthey Silver Medal 2007.

Several oral and poster presentations were made concerning scientific aspects of the research. These presentations were made at a number of international conferences including: 2nd International Conference on Green and Sustainable Chemistry by ACS (2005), 3rd Spanish Congress in Sustainable Chemistry (2005), 1st European Chemistry Congress (2006), 3rd International Conference on Green and Sustainable Chemistry (2007) and Europacat VIII (2007).

1.4 THESIS STRUCTURE

The results obtained in this thesis are organized as follows:

In Chapter 2, all experimental systems used and procedures followed for the diverse studies are described in detail as well as the analytical techniques used in the characterization of both products and catalysts.

Chapter 3 comprises the synthesis and characterization of the different non-commercialized catalysts studied. This includes both homogeneous and heterogeneous catalysts for double bond migration and telomerization reactions.

Chapter 4 starts with the state of art of the isomerization reactions with both homogeneous and heterogeneous catalysts and proposed mechanisms. Isomerization of allylbenzene was used as a model reaction, screening the performance of different metals supported onto novel titanate nanotubes. It also presents results obtained in the study of the isomerization of dienes such as pentadienes, hexadienes and linoleic acid, screening different homogeneous and heterogeneous catalysts using supports such as titanate nanotubes, silica supports, carbon and resins.

Chapter 5 includes the literature review of the telomerization reaction followed by the results of the kinetic studies carried out with palladium-carbene and palladium/phosphines catalysts using isoprene and 1,3-pentadiene as reactant dienes. Other parameters such as the influence of initial concentration of reactant and different nucleophiles are also studied. The possibility of extending the reaction to longer molecules such as hexadienes was also considered. Finally, telomerization studies with heterogeneous catalysts based in resins are shown.

Chapter 6 includes the latest advances in tandem reactions found in the literature as well as the results obtained for the proposed tandem. Both homogeneous and heterogeneous catalysts were used for both reactions, studying the influence of different parameters such as temperature or presence of base.

Finally, Chapter 7 summarises all the achievements reached in the presented study as well as the limitations found and the future work proposed to continue the project.

Chapter 2

EXPERIMENTAL PART

In the present project, a number of experimental rigs were used in order to perform different studies. In this chapter, the reaction systems and procedures followed for the catalytic experiments are described. The analytical techniques and specific parameters used in each one are summarized.

2.1 REACTION EXPERIMENTS

2.1.1 BATCH REACTIONS SYSTEM AND PROCEDURE

Most reactions were carried out in a batch reactor system which consists of a three neck glass flask heated by an oil bath. The heater plate was controlled by a Pt100 sensor inside the reaction medium and a temperature controller. Both, the medium of reaction and the oil bath were stirred vigorously by magnetic stirrers in order to ensure uniform temperature and homogeneous mix of reactants. To avoid loss of solvent a reflux system was used with tap water as cooler when the reaction

temperature is lower than the boiling point of the mixture and a cold finger filled with dry ice when the temperature is above the boiling point. In the other neck of the reactor, a septum was fixed through which samples were collected with a long stainless steel tube and a syringe.

The batch reaction system was used for both, homogeneous and heterogeneous reactions. In the heterogeneous case, a solution with the reactant is introduced into the reactor. The reaction temperature is fixed and controlled by the magnetic heating plate. In order to reach a constant temperature, forty minutes are allowed before the start of an experiment. Once reaction temperature is reached, the solid catalyst is introduced into the system and the reaction time is started. Periodically, samples of the reaction medium are taken with a syringe, filtered with a Nylaflo® membrane 0.2 μm filters, cooled and analyzed by gas chromatography.

In a typical homogeneous reaction, the appropriate quantity of catalyst is pre-dissolved in solvent and heated up to the reaction temperature. When the temperature is stable, the reactant is added into the reaction mixture. During the reaction, the same procedure described for the heterogeneous case is followed.

2.1.2 PRESSURE TUBE SYSTEM

Homogeneous and heterogeneous reactions were carried out using Ace Pressure Tubes of 15 mL of volume supplied by Sigma Aldrich. Tubes are equipped with a FETFE® O-ring which sits under the top rim of a PTFE bushing. The heavy-wall borosilicate glass tubes are pressure rated to 11 bars.

A heater plate controlled by a Pt100 sensor is used to set the reaction temperature. The oil bath is pre-heated for forty minutes before starting a reaction. In a typical experiment, homogeneous and/or heterogeneous catalyst, solvent, reactant and a stirrer are introduced inside the tube and nitrogen is bubbled to remove air. An initial sample is taken to be analyzed by gas chromatography. The tube is tightly closed and introduced into the oil bath and reaction time is started. After a certain

period of time, the tube is introduced inside an ice-bath to stop the reaction and condense the vapours. Then, a final sample is taken for chromatography analysis.

2.2 ANALYTICAL TECHNIQUES

2.2.1 GAS CHOMATOGRAPHY

Gas chromatography analyses were carried out to determine product distribution and conversion during catalytic tests. Depending on the nature of reactants, two different systems were used, a VARIAN chromatograph model CP-3800 equipped with a non-polar capillary column WCOT Fused Silica model CP-SIL 5CB (15 m x 0.25 mm) or a VARIAN chromatograph model CP-3900 equipped with a non-polar capillary column AT-5 (5% phenyl / 95% methylpolysiloxane) (30 m x 0.32 mm). Both of them have a Flame Ionization Detector (FID), an autosampler and a split injector.

In Table 2.1, the methods used for the different analyses are summarised. When allylbenzene was used as reactant in isomerization reactions, method 1 was used. Methods 2 and 3 were used in analyses during isomerization and telomerization reactions of linear diolefins respectively. Finally, method 4 was used in the analyses during linoleic acid isomerization.

Table 2.1: Methods used in Gas Chromatography analyses.

Method n.	1	2
Carrier gas	Helium	Helium
Injector Temperature	250°C	300°C
Flow	1 mL/min	0.5 mL/min
Temperature program	65°C hold for 0.75 min, to 110°C @ 7°C/min, hold for 1 min	40°C hold for 5 min, to 80°C @ 5°C/min, to 200°C @ 15°C/min
Detector Temperature	300°C	300°C
Split ratio	40	15
Sample volume	0.5 µL	1 µL

Method n.	3	4
Carrier gas	Helium	Helium
Injector Temperature	250°C	260°C
Flow	1 mL/min	0.9 mL/min
Temperature program	40°C hold for 5 min, to 100°C @ 10°C/min, to 180°C @ 8°C/min, to 220°C @ 20°C/min	150°C hold for 0.5 min, to 230°C @ 7°C/min, to 290°C @ 5°C/min, hold for 10 min
Detector Temperature	315°C	290°C
Split ratio	15	20
Sample volume	1 µL	1 µL

Samples taken from the reaction mixture were analyzed without further preparation but dilution in some cases. However, in order to analyze samples in the linoleic isomerization studies, silylation reactions were performed based on the procedure proposed by Bernas et al [6]. A typical preparation consists of the addition of 200µL of sample into a methyl tert-butyl ether (MTBE) washed vial. 200µL of

0.01 M methanol solution of decane is added as internal standard. MTBE and solvent are evaporated and vials are dried in vacuum at 40°C during 20 minutes. After this time, the residue in the vial is dissolved in 100 μL of pyridine, 400 μL of N,O-bis(trimethylsilyl)trifluoroacetamide (BSTFA) and 200 μL of trimethylchlorosilane (TMCS). The solution is kept in oven at 70°C for 45 minutes and thereafter it is ready for GC analysis.

2.2.2 TRANSMISSION ELECTRON MICROSCOPY (TEM)

A JEOL 2011 high resolution transmission electron microscope was used to obtain images of the morphology of metal nanoparticles supported onto titanate nanotubes. The samples for electron microscopy were prepared by suspending them in water and sonicating. Several drops of the suspension were placed on 3 nm carbon film in a copper grid following the standard method before being analyzed.

2.2.3 SCANNING ELECTON MICROSCOPY (SEM)

A JEOL JSM-6310 scanning electron microscopy was used to obtain images of the morphology and chemical structure of catalyst. The analysed samples were attached to a disk using a carbon-based paste. The disks were coated with a fine layer of carbon to enhance conductivity before the analyses.

2.2.4 ATOMIC ABSORPTION SPECTROSCOPY (AAS)

In order to analyse the content of different metals (palladium, rhodium and ruthenium) in solutions, a Varian (model AA-275 series) spectrometer was used. Different hollow cathode lamps were used with the wavelengths and slit width shown in Table 2.2 for each of the metals.

Table 2.2: Parameters used in the AAS analysis.

Metal	Wavelength	Slit width
Palladium	349.9 nm	0.2 nm
Rhodium	343.5 nm	0.5 nm
Ruthenium	244.8 nm	0.2 nm

2.2.5 X-RAY PHOTOELECTRON SPECTROSCOPY (XPS)

XPS measurements were performed in the University of York by Dr. Karen Wilson using a Kratos Axis HSi instrument equipped with a Mg$K\alpha$ X-ray source and charge neutraliser. Spectra were acquired using a pass energy of 20 eV with an X-ray power of 169W. Spectra were energy-referenced using valence band and adventitious carbon, whereas quantification and deconvolution was performed using CASA-XPS version 2.3.9 software.

2.2.6 ACCELERATED SURFACE AREA AND POROSIMETRY (ASAP)

A Micrometrics Accelerated Surface Area and Porosimetry (ASAP) 2010 analyser was used in order to analyze surface area and pores size distribution of different catalytic supports. 0.1 g of sample was weighed into a glass sample tube sealed with a TranSeal^{TM} stopper. Before the analysis, the sample was degassed at 150°C under vacuum overnight in order to remove residual moisture and vapours. After that, the sample was again weighed to obtain its dry mass for subsequent analysis data. Analyses consisted of adsorption and desorption of nitrogen at 77 K until equilibrium was reached. Helium was used to measure the cold and warm freespace in the sample tubes needed for data correction.

In order to determine surface area of the supports from the physisorption isotherm data, the Brunauer-Emmett-Teller (BET) method was used. The Barret, Joyner and Halenda (BJH) method was used to obtain pore size distribution.

2.2.7 INFRA-RED SPECTROSCOPY

Infrared spectra of different compounds and catalysts were obtained using an EQUINOX 55 spectrometer using a DTGS detector. Sample pellets were analyzed with a scanner velocity of 10.0 kHz, a resolution of 12 cm^{-1} and an iris aperture of 6000 microns.

Sample pellets consisted of 0.2 g of KBr and a determined sample quantity (normally a KBr:sample ratio of 1:100 but it depends on the sample IR absorbance). Both were ground into a fine powder before being compressed into a pellet under a pressure of 7 bars for ten minutes. A reference pellet was composed of only KBr.

2.2.8 RAMAN SPECTROSCOPY

Raman spectra of different samples were obtained using a BWTech i-Raman instrument equipped with a TE cooled 2048CCD array detector with a spectral resolution of 5-6 cm^{-1} and a digitizer resolution of 250 kHz. Before the analysis, a dark spectrum was taken with the laser closed and a reference spectrum of the analysis medium.

Sample pellets were prepared in order to avoid scattering. Samples were ground into fine powder before being compressed into a pellet under a pressure of 7 bars for 10 minutes. The location of the pellet was manually adjusted for each case.

2.2.9 INDUCTIVE COUPLING PLASMA (ICP)

The content of palladium in different resins was analyzed using a Varian VISTA AX inductive coupling plasma (ICP) equipment. Before the analyses, organic compounds were dissolved by an acid treatment with sulphuric acid, heating up to boiling point until dryness, followed by a calcination at 750°C in order to eliminate organic compounds. The ash was treated with sulphuric acid, hydrofluoric acid and water at high temperatures obtaining a solution of the metals.

Chapter 3

SYNTHESIS AND CHARACTERIZATION OF CATALYSTS

In the present project, different homogeneous and heterogeneous catalysts have been tested for isomerization and telomerization reactions in order to study their conversion and selectivity to the desired products. Some of these catalysts, especially homogeneous ones for isomerization reaction are commercial, however, others have been synthesised in the laboratory. This chapter includes a detailed description of all catalysts used, synthesis procedures and characterizations of non-commercial ones.

In the first place, isomerization catalysts are considered. Heterogeneous catalysts have been synthesised supporting different metals, exploring suitability of the novel heterogeneous support: titanate nanotubes. Other supports such as carbon, resins, zeolite ZSM-5 and mesoporous material SBA-15 have been also used to study the influence of the support.

For the telomerization reaction, homogeneous catalysts based on carbene ligands have been synthesised by Dr David Nielsen in the University of Cardiff in conjunction with Rostock University (Germany). Heterogeneous palladium catalysts based on DVB resins have also been synthesised and characterised.

3.1 CATALYSTS FOR ISOMERIZATION REACTION

3.1.1 HOMOGENEOUS CATALYSTS

Different homogeneous catalysts for isomerization reactions have been screened. Most of them are commercial and have been purchased from Sigma-Aldrich or Fisher. $RuHCl(CO)(PPh_3)_3$ catalyst was synthesised, following the procedure described below.

In the Figure 3.1, chemical structures and names of all homogenous catalysts used and how they are referred to in this thesis henceforth are shown.

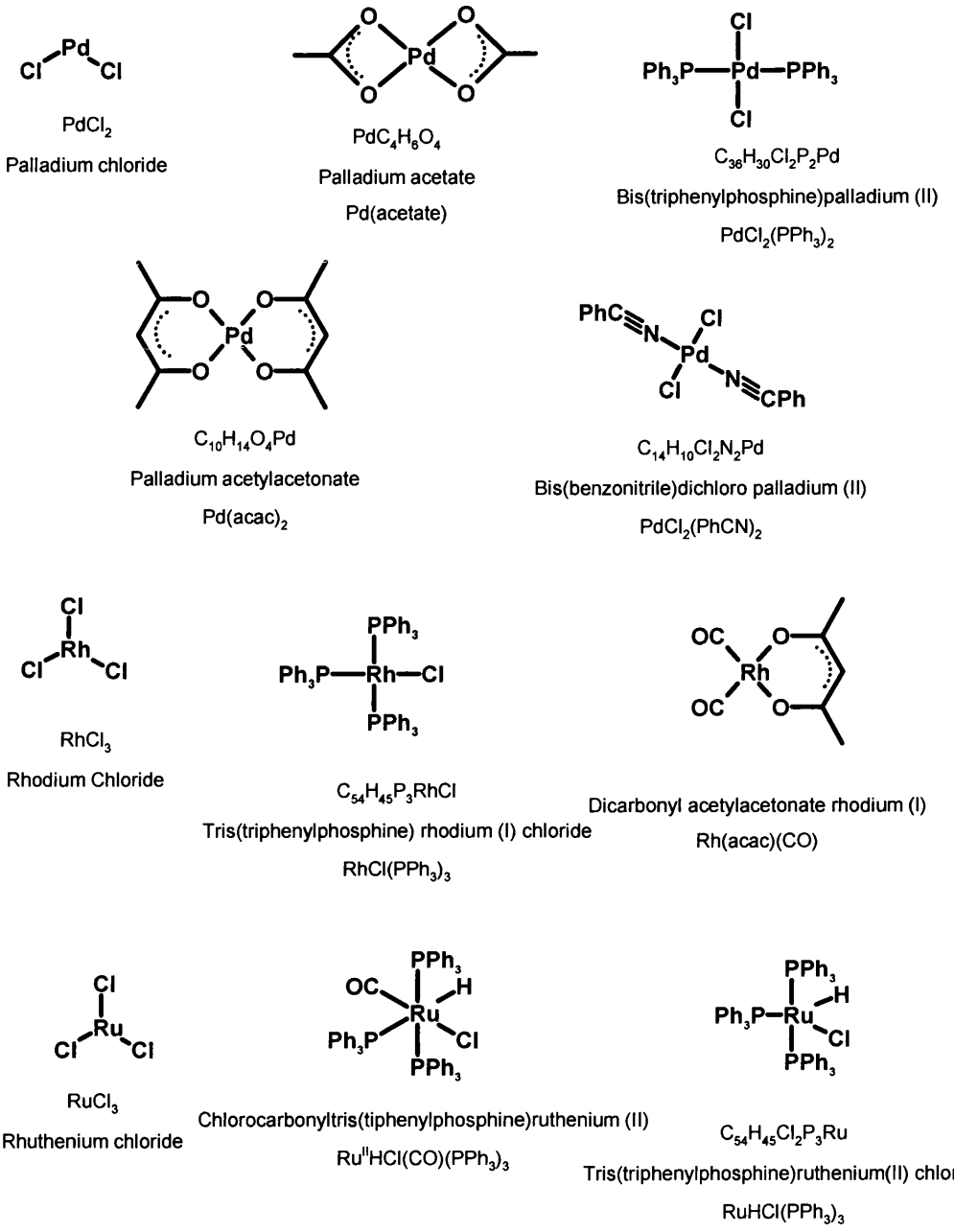

Figure 3.1: Homogeneous isomerization catalysts.

3.1.1.1 Synthesis of $Ru^{II}HCl(CO)(PPh_3)_3$

Carbonyl chlorohydridotris (triphenylphosphine) ruthenium (II) was synthesised according with the procedure described earlier in [7]. Solutions of hydrated ruthenium trichloride (0.26 g, 1 mmol) in 20 mL of butanol and 20 mL of 40% wt

aqueous formaldehyde were added successively to a boiling solution of triphenylphosphine (1.58 g, 6 mmol) in 60 mL of butanol under stirring. The mixture was heated under reflux for 10 minutes and then allowed to cool to room temperature. The formed precipitate was filtered and washed with ethanol, water, ethanol and n-hexane and dried in vacuum. Cream-white nanocrystals were obtained with a yield of 63% based on $RuCl_3 \cdot 3H_2O$.

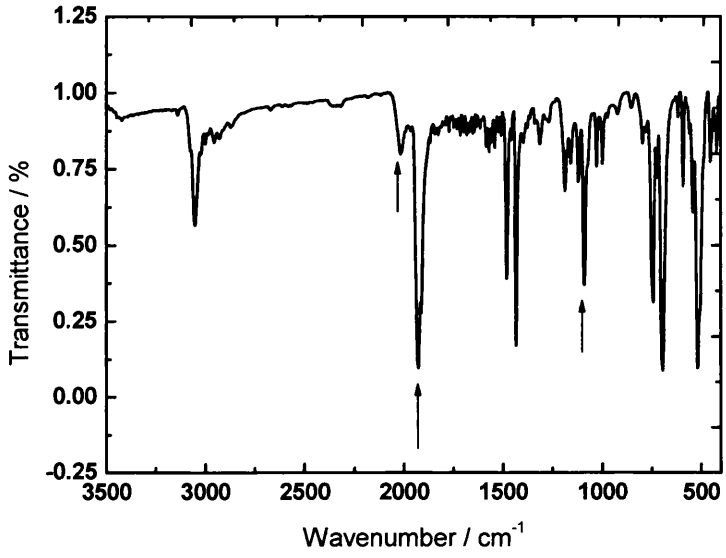

Figure 3.2: IR spectrum of $RuClH(CO)(PPh_3)_3$.

The characteristic infra-red spectrum for $RuClH(CO)(PPh_3)_3$ should show bands at 2020, 1922 and 1903 cm^{-1} attributed to ν(CO) and ν(RuH) bonds [7]. In Figure 3.2, one can observe the three mentioned bands of the synthesised compound in the IR spectrum.

3.1.2 HETEROGENEOUS CATALYSTS

3.1.2.1 Titanate nanotubes

Nanotubular titanate is a novel studied material which possesses a unique combination of physicochemical properties. Its characteristics include high ion-exchange capacity for cations of different metals, open mesoporous morphology, high specific surface area [8] and relatively good stability of the alkali metal saturated form of the nanotubes at elevated temperatures. This nanomaterial has a well developed lamellar structure corresponding to the crystal structure and general formulae of a trititanate, $H_2Ti_3O_7$. The material shows promise in a variety of applications including hydrogen sensors, a substrate for sorption, photocatalysis, acid catalysis, ion-exchange, etc.

Titanate nanotubes (Ti-NT) are of great interest for catalysis since their high cation exchange capacity provides the possibility of achieving a high loading of active catalyst with an even distribution and high dispersion. Besides, the open mesoporous morphology of nanotubes, the high specific surface area and absence of micropores facilitate transport of reagents to the active sites during the catalytic reaction. The semiconducting properties of titanate nanotubes result in strong electronic interaction between the support and a catalyst. Currently, there are few demonstrated examples of successful utilisation of titanate nanotubes as a mesoporous catalyst support for different nanoparticles: CdS decorated titanate nanotubes [9, 10] in reaction of photocatalytic oxidation of dyes, Pd/titanate nanotubes catalyst for electro-oxidation of methanol [11], Pt/titanate nanotubes photocatalyst for generation of H_2 [12], Au/titanate nanotubes catalyst for water-gas shift reaction [13], RuO_2/titanate nanotubes electro-catalyst for reduction of CO_2 [14] and ruthenium (III) hydrated oxide deposited on titanate nanotubes for selective oxidation of alcohols [15].

The nanotubular morphology of titanate could also be exploited in enantioselective and shape-selective catalysis. Deposition of catalysts onto the internal cavities of titanate nanotubes only might provide the possibility of adjusting catalyst

selectivity to favour the formation of non-bulky molecules by adjusting the diameter of the nanotubes. To study this hypothesis it is necessary to develop a method of deposition of catalyst nanoparticles inside the internal cavities of titanate nanotubes.

Preparation of titanate nanotubes

Titanate nanotubes (Ti-NT) were prepared by the hydrothermal method described in detail in [8]. 20-24 g of titanium dioxide (anatase) were added to 300 mL of 10 M NaOH solution and mixed in a PTFE beaker. The solution was placed in an autoclave and heated. For an optimal preparation, in the first instance a high heating rate was applied to reach 170 °C for 30 minutes and after this time the temperature was maintained at 130 °C for 20 hours. The autoclave was then cooled down to ambient temperature.

The white powder of titanate nanotubes obtained was filtered from the NaOH solution, washed several times with water and dried at 120 °C in an oven. When the powder is dried, large accumulated particles of dried powder were broken in a mortar and sieved to 1.7 mm size to avoid physical accumulations. After this, the powder was washed repeatedly with water and 0.1 M HCl solution in order to eliminate the possible remaining NaOH until the pH is around 7. The sample was dried on air at 120 °C overnight.

Characterization of titanate nanotubes

The typical titanate nanotubes structure (Figure 3.3) consists of four concentrical walls with an inner diameter between 4 to 10 nanometers and a distance between layers of 0.72 nm.

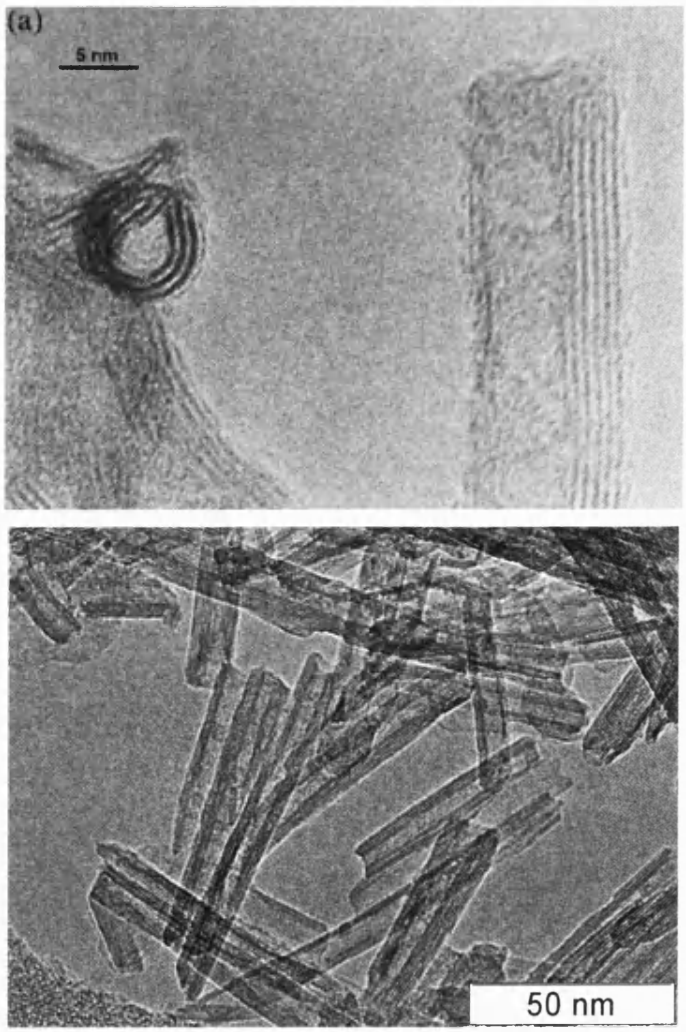

Figure 3.3: TEM images of the titanate nanotubes structure.

The X-ray diffraction (XRD) pattern of the titanate nanotubes is shown in Figure 3.4. It corresponds well with the reflections of a trititanate $H_2Ti_3O_7$, which is believed to be most likely the structure of the nanotubes [16].

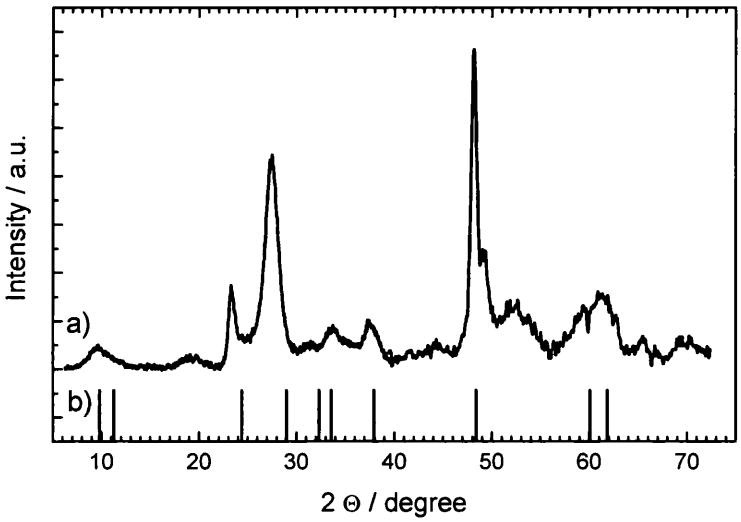

Figure 3.4: XRD pattern of nanotubes: a. spectrum of as prepared sample, b. reflections of trititanate [16].

Nitrogen adsorption analyses were done obtaining the isotherm shown in Figure 3.5. The shape of the isotherm is a typically type IV in the IUPAC classification which reveals that titanate nanotubes have mesopores with an average pore size of 3.5 nm calculated by the BJH method with desoprtion data (Figure 3.6) and a BET surface area around 260.64 ± 7.56 m^2/g.

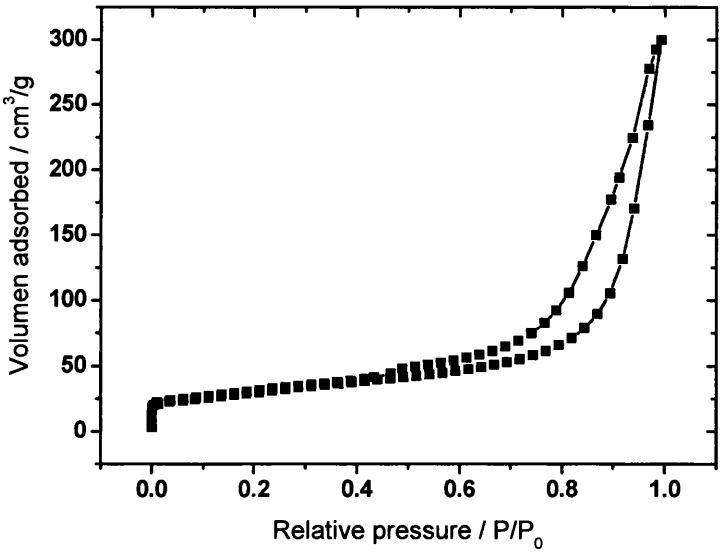

Figure 3.5: Isotherm of adsorption of N_2 on titanate nanotubes at 77K.

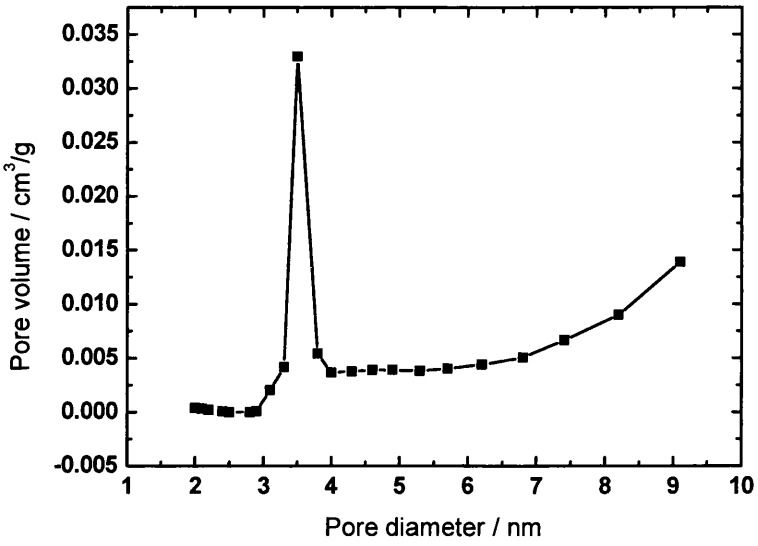

Figure 3.6: Pore size distribution of titanate nanotubes.

Raman characterizations of the TiO_2 starting material and the titanate nanotubes are shown in Figure 3.7. TiO_2 starting material (from Fisher) shows three well-defined peaks at 397, 514 and 639 cm^{-1} which correspond to the anatase structure [17]. None of these peaks are observed in titanate nanotubes whose spectra shows bands at 275, 375, 446, 660 and 905 cm^{-1}.

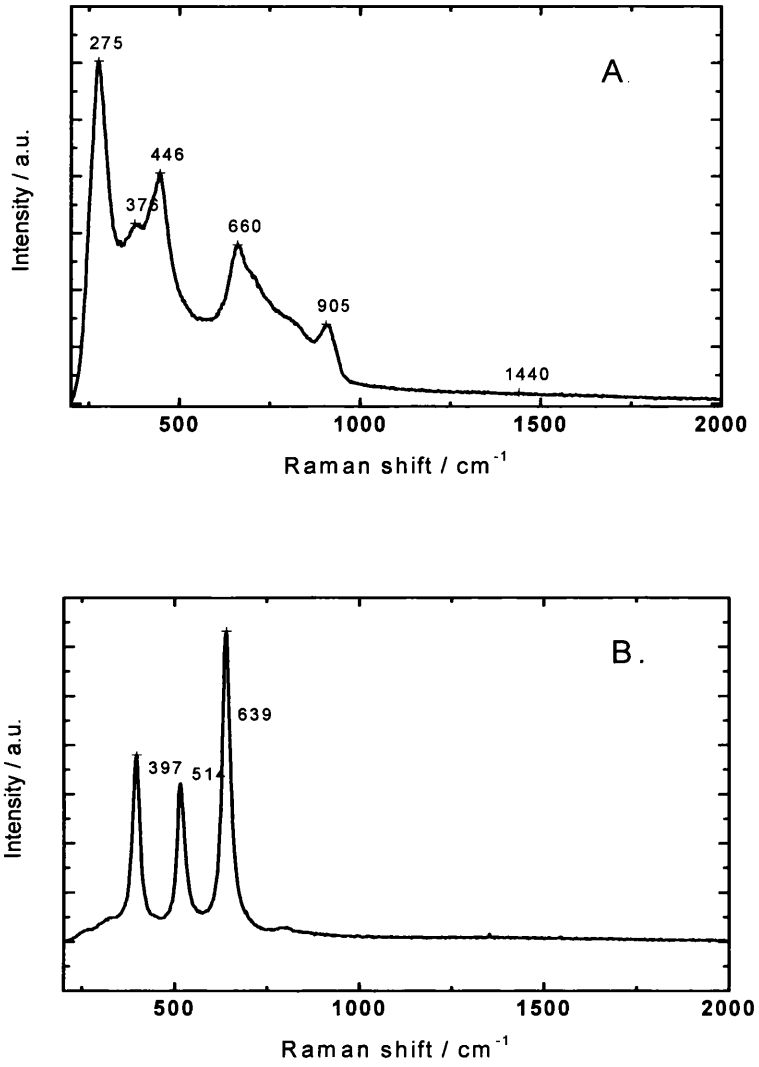

Figure 3.7: Raman spectra of A. titanate nanotubes and B. TiO_2 starting material.

Deposition of metals onto titanate nanotubes

Palladium (II) was supported onto titanate nanotubes by ion exchange. Solutions of different concentrations of $PdCl_2$ were prepared depending on the desired loading. HCl was added to the $PdCl_2$ solutions in order to avoid precipitation of palladium black. The $PdCl_2$ solutions were mixed with a determined quantity of titanante nanotubes at room temperature under stirring over two hours. During the ion exchange, the surface protons of the titanate nanotubes are exchanged with Pd^{2+}.

The catalysts were filtered and washed with demineralised water. The remained solution was collected and analyzed for Pd content by atomic absorption spectroscopy in order to determine the total quantity of palladium deposited. The catalysts had an orange/brown colour depending on the quantity of supported palladium.

To reduce palladium (II) supported onto the titanate nanotubes, a 0.1M solution of $NaBH_3$ was used. 50 mL of this solution was mixed with 0.45 mg of Pd^{2+}/titanate nanotubes catalyst at room temperature for two hours. After this time, the catalyst was filtered and dried overnight at 120 °C. The catalysts change from an orange/brown colour to a grey/black one, depending on palladium loading.

The same procedure was followed to support rhodium and ruthenium onto titanate nanotubes. $RhCl_3 \cdot x\ H_2O$ and $RuCl_3$ were used as a rhodium and ruthenium sources respectively.

Characterization of Pd/titanate nanotubes

The isotherm of adsorption of palladium onto titanate nanotubes was determined at room temperature by measuring the initial and equilibrium concentration after ion exchange of palladium by atomic absorption. These concentrations are summarized in Table 3.1.

The amount of adsorbed metal was determined using Equation (3.1).

$$a\left[\frac{mol\ Pd}{mol\ TiO_2}\right] = \frac{80 \cdot (C_0 - C) \cdot V}{m} \qquad \textbf{(3.1)}$$

And the percentage by weight of palladium loading was calculated by Equation (3.2).

$$\%\ wt\ of\ Pd = \frac{(C_0 - C) \cdot V \cdot M_{w\,Pd}}{(m + (C_0 - C) \cdot V \cdot M_{w\,Pd})} \cdot 100 \qquad \textbf{(3.2)}$$

where C_0 is the initial concentration of metal salt, C is the concentration of metal salt after adsorption, m is the mass of titanate nanotubes, V is the volume of solution and $M_{w\,Pd}$ is the molecular weight of palladium.

Table 3.1: Adsorption data of palladium onto titanate nanotubes at 25°C.

Initial [Pd] (mmol/L)	Equilibrium [Pd] (mmol/L)	Molar ratio (mol Pd/ mol titanate)	% wt Pd
0.374	$9.39 \cdot 10^{-4}$	0.0078	0.9
1.127	$9.39 \cdot 10^{-4}$	0.0225	2.9
1.879	$9.39 \cdot 10^{-4}$	0.0376	4.7
3.012	0.0375	0.0595	6.9
3.758	0.1034	0.0731	8.8
4.510	0.5920	0.0784	9.4
6.023	1.7854	0.0848	10.1

The isotherm of adsorption of palladium onto titanate nanotubes at room temperature is shown in Figure 3.8. The ion-exchange deposition method results in high loadings (up to 10.1 wt%) of palladium metal nanoparticles supported on the surface of the nanotubes. This also indicates the high degree of palladium proton exchange, *e.g.* the reaction of Pd (II) with protons in the titanate nanotubes from a 2 mM solution of $PdCl_2$ results in the ratio Pd^{2+}/Ti 0.08, whereas the maximum 0.33 would correspond to $PdTi_3O_7$. In other words, almost 25 % of all titanate nanotubes protons can be replaced by Pd (II) from relatively diluted solution of a salt. The isotherm of adsorption is characterised by a very sharp increase in metal loading with a small increase in the concentration of the stock solution: nearly quantitative sorption of Pd (II) results in negligible residual equilibrium concentration in solution. Such a small equilibrium concentration of Pd (II) in water suspension of palladium exchanged titanate nanotubes would provide a small rate of palladium leaching from the catalyst.

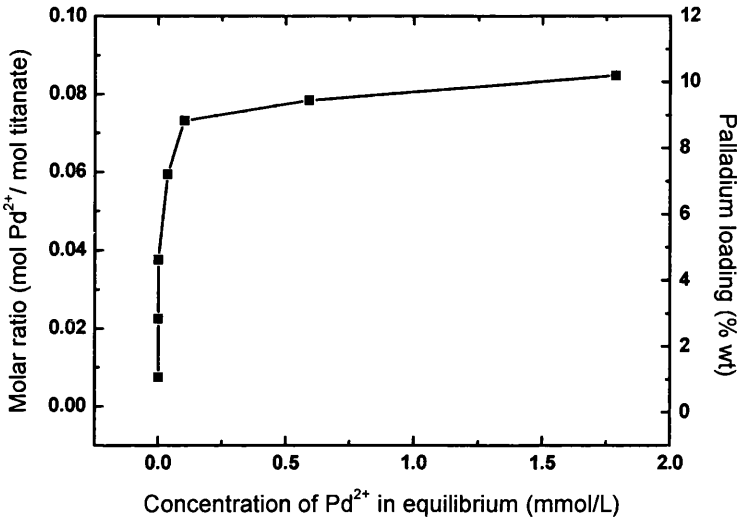

Figure 3.8: Isotherm of adsorption of palladium from $PdCl_2$ aqueous solution onto titanate nanotubes at 25°C.

The variation of pH during the ion-exchange of palladium for the 6.9% wt Pd sample is shown in Figure 3.9. Each catalyst has a different initial pH value, depending of the initial palladium concentration in the solution (double excess of HCl than palladium is added into the palladium salt solution to avoid its precipitation). The ion-exchange rate is very high in the first minutes, being completed within the first twenty minutes. This suggests that the mixing method of the titanate nanotubes and the palladium solution could determine the homogeneity of the sample.

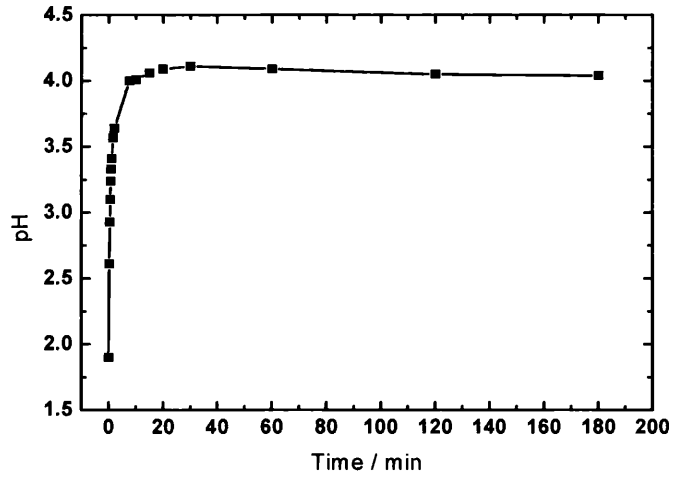

Figure 3.9: Variation of pH during ion-exchange of catalyst 6.9% wt Pd/titanate nanotubes.

The TEM images of titanate nanotubes supporting palladium nanoparticles for various palladium loadings are shown in Figure 3.10. The distribution of Pd particles in the 4.7 wt% sample is not uniform; areas of nanotubes with small density of Pd particles are accompanied by areas with high density of metal particles. For the samples of 6.9 wt% and 8.8 wt% the deposition of metal particles is more uniform. However, the size and shape of metal particles over all tested metal loadings are very similar, with the particle sizes ranging between 1.9-4.8 nm and a spherical, slightly flattened shape of the metal particles. A similar non-uniform deposition was also found in the case of Pt/titanate nanotubes catalysts [18]. The non-uniform deposition of Pd at low metal loadings may be due to non-uniformity of the nanotubes sample: the parts of a sample with higher surface energy react first, leaving remaining nanotubes bare. However, it is also feasible that non-uniformity in metal deposition is due to the method of ion exchange and under different preparation conditions (vigorous stirring and slow addition of diluted metal salt solution, or simultaneous addition of metal salt and the nanotubes powder/dispersion) the uniformity could be improved.

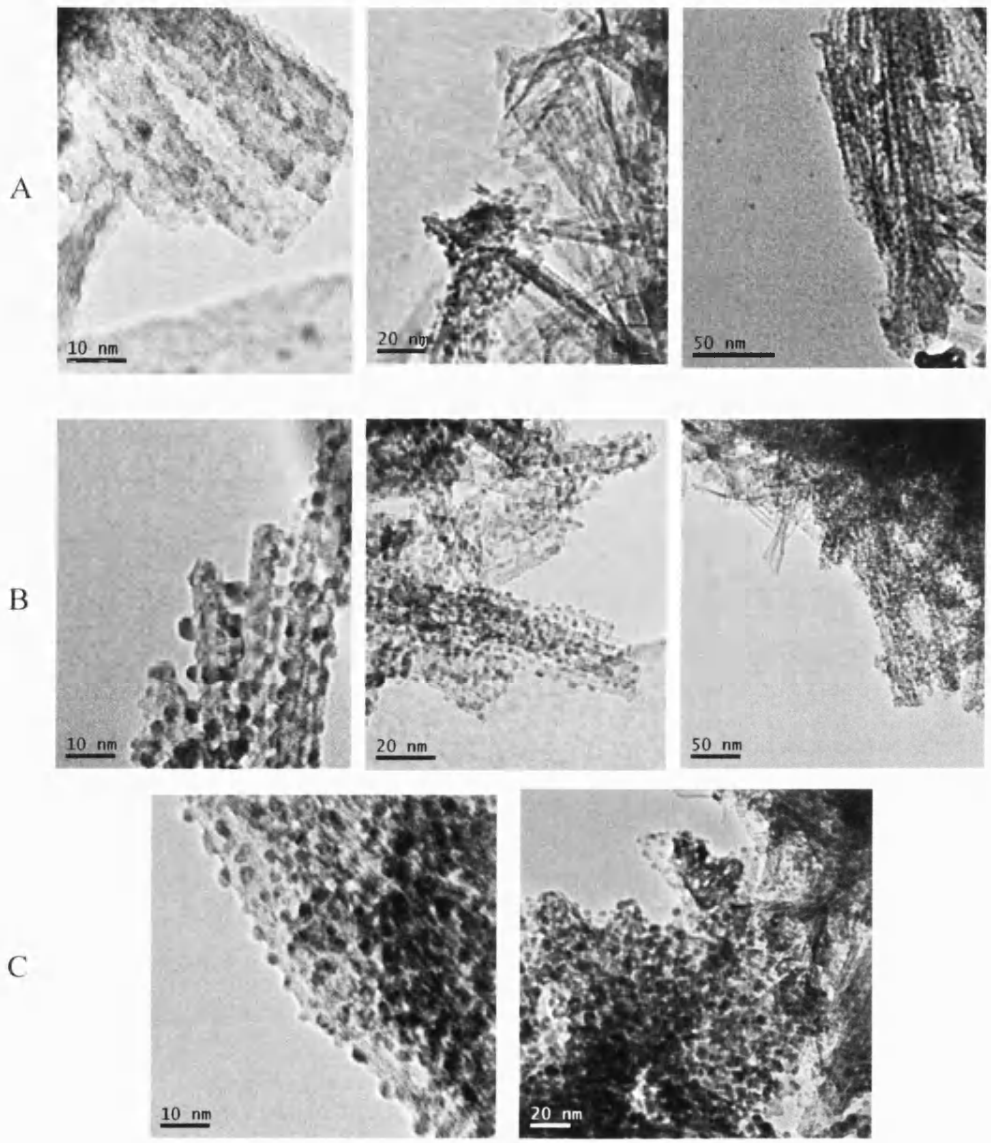

Figure 3.10: TEM images of as prepared Pd(II)/titanante nanotubes catalysts: (A) 4.7 %wt Pd, (B) 6.9 %wt (Pd), (C) 8.8 %wt Pd.

The X-ray analysis of palladium onto titanate nanotubes is shown in Figure 3.11. Titanium and oxygen peaks correspond to the titanate nanotubes. Small peaks of palladium are also easy to distinguish, caused by the metal loading. Sodium peaks might be due to the NaOH solution used for the titanate synthesis. Finally the carbon peak corresponds to the carbon film used to support the sample during the analysis.

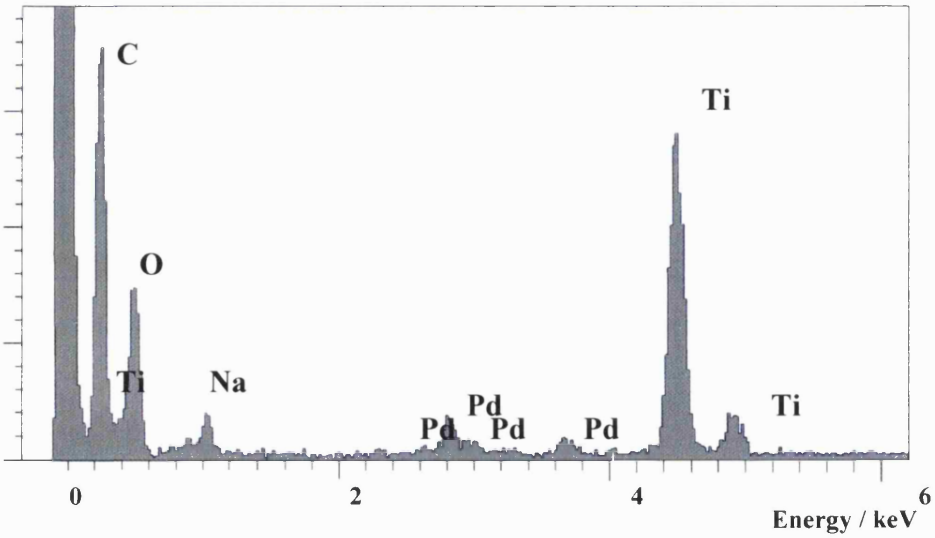

Figure 3.11: X-ray analysis of Pd particles (2.9 wt%) onto titanate nanotubes.

Figure 3.12 shows the Pd 3d XPS spectra for the Pd/titanate nanotubes samples with 0.9, 4.7 and 8.8 wt% palladium loading. The spectra can be deconvoluted into two components with Pd $3d_{5/2}$ binding energies of 337.1 and 335.5 eV which are consistent with Pd (II) and Pd(0) respectively. This reveals that fresh catalysts are formed by a mixture of Pd(II) and Pd(0).

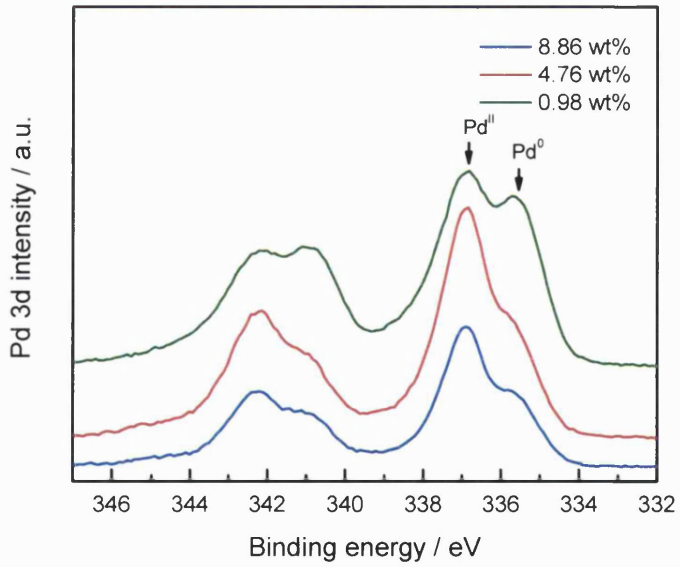

Figure 3.12: XPS spectra of Pd(II)/titanate nanotubes catalyst of different Pd loadings.

Figure 3.13 shows that the percentage of the Pd (II) component decreases with bulk Pd content which is consistent with the Pd clusters becoming more metallic at higher loadings. Quantification of the XPS spectra revealed the surface Pd loadings for the series of catalysts were in the range 18-42 wt%, which are somewhat higher than the bulk Pd content. Such observations are however consistent with attenuation of the underlying Ti 2p signal occurring through exclusive coating of the external surface of the nanotubes with Pd, which is in accord with the observations from TEM.

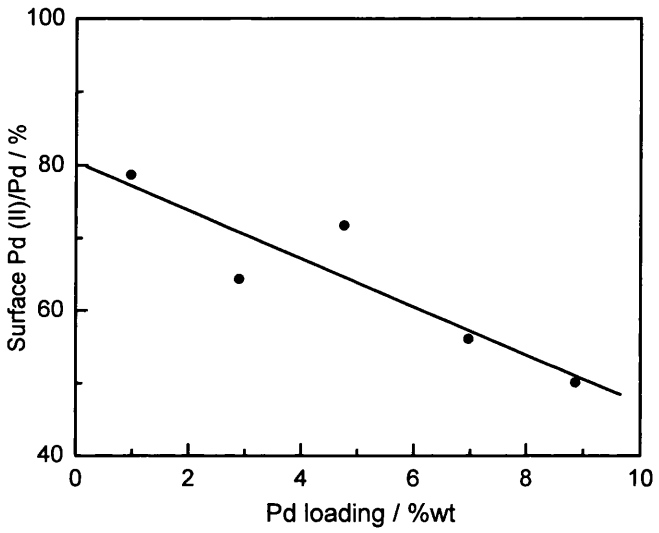

Figure 3.13: Percentage of Pd(II) and Pd(0) of Pd(II)/titanate nanotubes at different Pd loadings.

Characterization of Rh/titanate nanotubes

The isotherm of adsorption of rhodium onto titanate nanotubes at room temperature is shown in Figure 3.14. It was calculated in the same way as the palladium one (Equations (3.1) and (3.2)). The initial and equilibrium concentrations, molar ratio and percentage of supported rhodium are summarized in Table 3.2.

Table 3.2: Adsorption data of rhodium onto titanate nanotubes at 25°C.

Initial [Rh] (mmol/L)	Equilibrium [Rh] (mmol/L)	Molar ratio (mol Rh/ mol titanate)	% wt Rh
1.166	0.233	0.0186	2.3
2.217	0.349	0.0373	4.5
3.097	0.972	0.0425	5.1
4.664	2.041	0.0525	6.3

The isotherm of adsorption of rhodium onto titanate nanotubes at room temperature is shown in Figure 3.14. For an equal equilibrium concentration, the quantity of supported rhodium is lower than that of palladium. The shape of the isotherm suggests that the saturation has not been reached, being possible to exchange more rhodium in the titanate nanotubes surface.

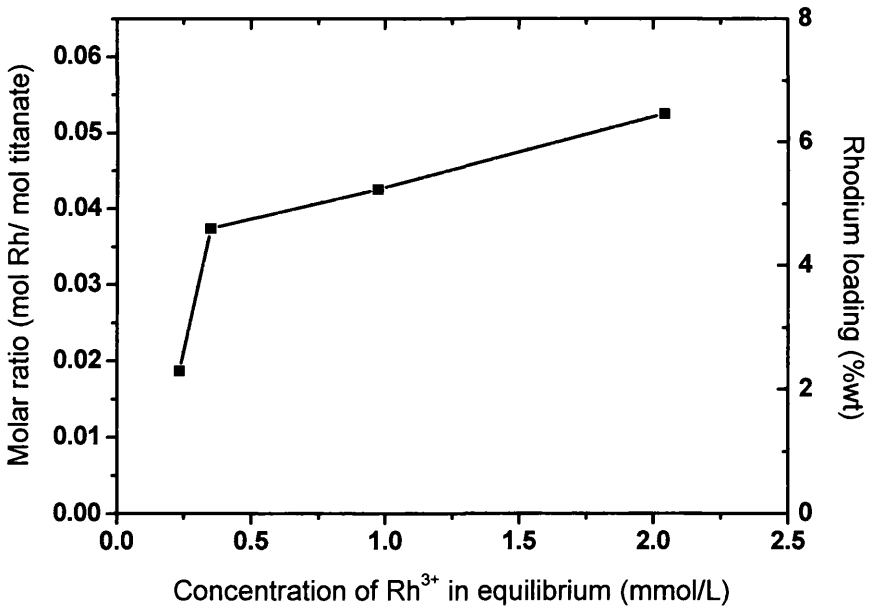

Figure 3.14: Isotherm of adsorption of rhodium from $RhCl_3$ aqueous solutions onto titanate nanotubes at 25°C.

The variation of pH during the ion-exchange of rhodium with the titanate nanotubes for the sample with a final Rh loading of 4.6% wt is shown in

Figure 3.15. The ion-exchange is completed within the first 15 minutes similar to the case of palladium.

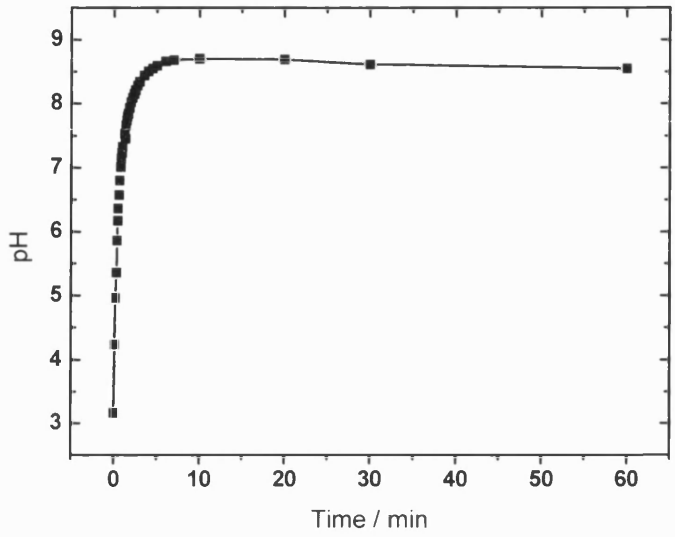

Figure 3.15: Variation of pH during ion-exchange of catalyst 4.5% wt Rh/Ti-NT.

Samples with different loadings of rhodium (2.3, 4.6 and 5.2 %wt) have been analyzed by XPS in order to determine the oxidation state of rhodium. Figure 3.16 shows the Rh 3d spectra which can be deconvoluted into two components with Rh 3d binding energies of 310.9 and 308.9 eV corresponding to Rh (III) and Rh (I) respectively. This result means that the catalysts are formed by a mixture of Rh(III) and Rh(I) with a negligible presence of Rh(0) (less than 1% of the total Rh loading).

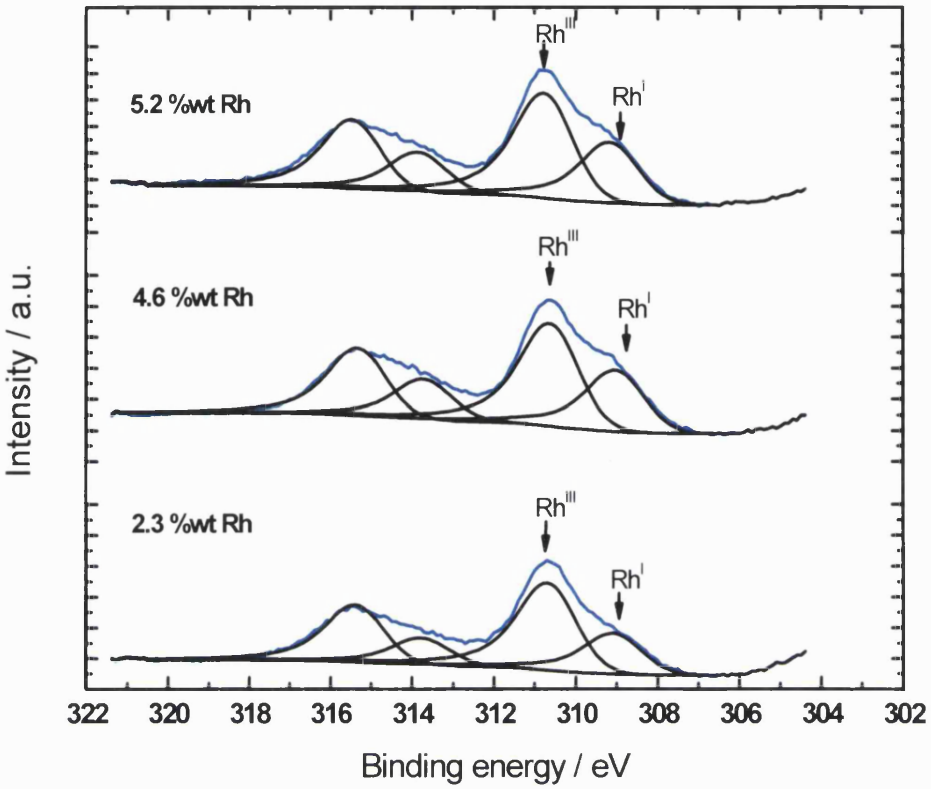

Figure 3.16: XPS spectra of Rh/titanate nanotubes catalysts of different Rh loadings.

Figure 3.17 represents the percentage of rhodium (III) and rhodium (I) in catalysts with different rhodium loadings. The percentage of rhodium (III) decreases slightly as the rhodium loading increases. Same tendency was observed with the palladium catalysts (Figure 3.13).

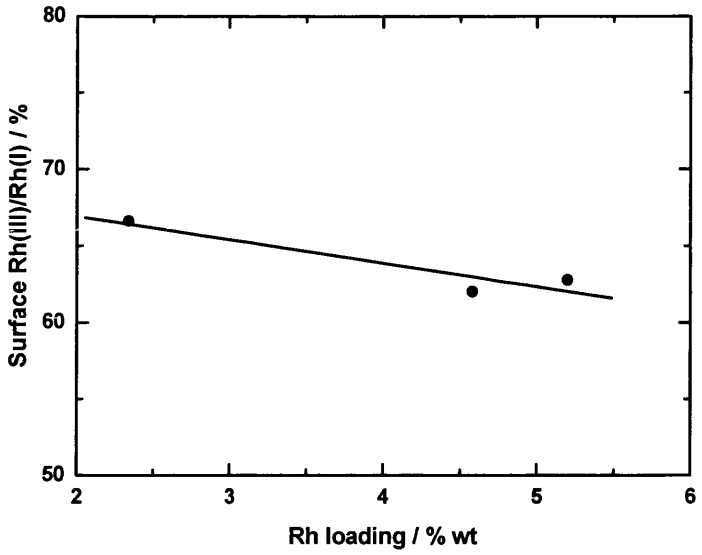

Figure 3.17: Percentage of Rh(III) and Rh(I) in Rh(III)/titanate nanotubes at different Rh loadings.

Characterization of Ru/titanate nanotubes

Same characterization than in case of palladium and rhodium was done in the case of ruthenium. Figure 3.18 shows the isotherm of adsorption of ruthenium onto titanate nanotubes support. Comparing to the isotherms of palladium (Figure 3.8) and rhodium (Figure 3.14), maximum metal loading was obtained in the case of palladium (more than 10 % by weight) although saturation was not reached in the other two cases. Ion-exchange affinity decreases in the order of palladium, ruthenium and rhodium. This means that for a given metal loading, less concentration in equilibrium is needed in the case of palladium than in ruthenium and rhodium.

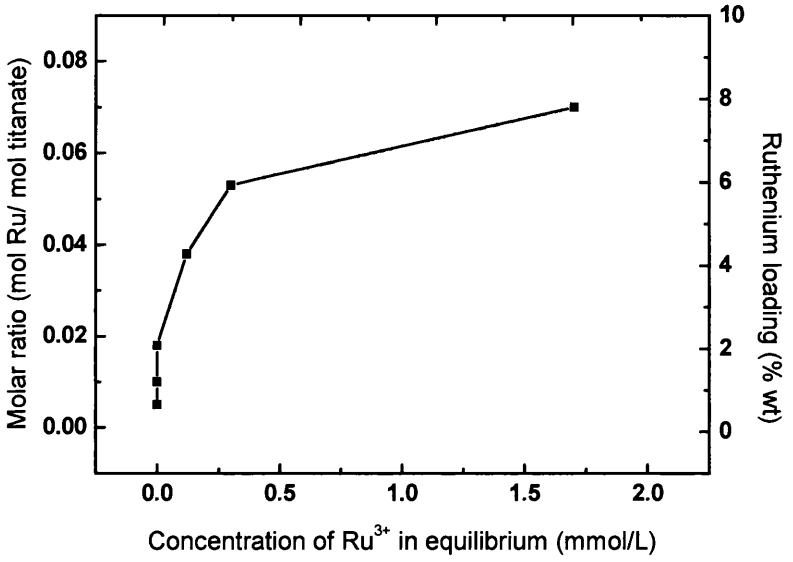

Figure 3.18: Isotherm of adsorption of ruthenium from $RuCl_3$ aqueous solutions onto titanate nanotubes at 25°C.

Variation of pH during ion-exchange of ruthenium in the titanate nanotubes surface is shown in Figure 3.19. A high increment of pH values was observed during the first ten minutes, reaching a steady value after this time. Very similar times were observed during ion-exchange of palladium (Figure 3.9) and rhodium (Figure 3.15).

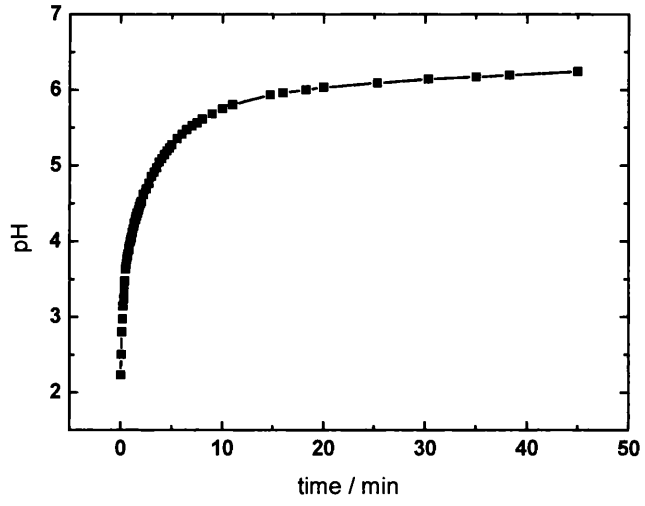

Figure 3.19: Variation of pH during ion-exchange of catalyst 5% wt Ru/titanate nanotubes.

3.1.2.2 Silica supports

Preparation of SBA-15

SBA-15 was synthesized following the procedure by Zhao et al. [19]. Pluronic 123 ($EO_{20}PO_{70}EO_{20}$) (2 g) was dissolved in deionised water (52.5 g) and HCl (12.01 g, 36.5% concentration). Once it was completely dissolved, tetraethyl orthosilicate (TEOS) (4.28 g, 0.02 moles) was added and stirred for 20 hours at 40 °C (313K).

The mixture was aged for 24 hours at 90°C (363K). After that, the precipitate was filtered, washed with deionised water and dried at room temperature for one day. The sample was calcinated under O_2 flux reaching 723 K during 8 hours (around 1°C/min) and maintaining this temperature for further 6 hours.

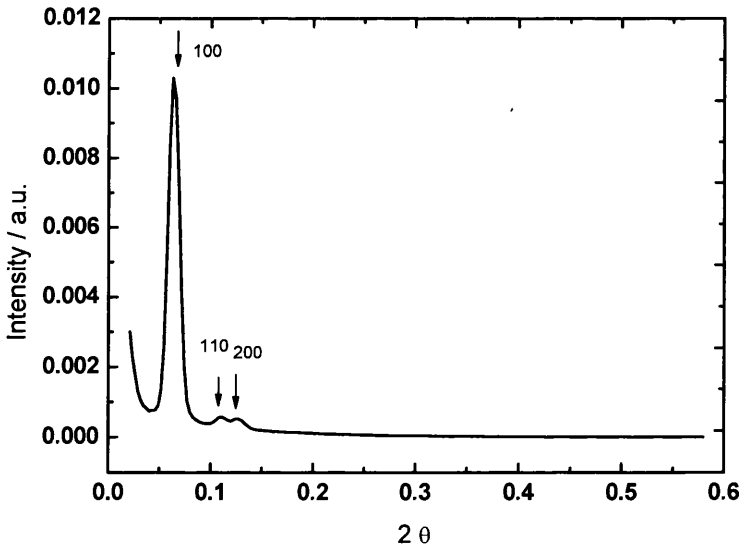

Figure 3.20: X-ray pattern of SBA-15.

Figure 3.20 shows the X-ray pattern of the synthesized material. One can see three peaks which correspond to 100, 110 and 200 planes respectively, indicating the correct 2D hexagonal structure for SBA-15.

Figure 3.21 shows the isotherm of adsorption of N_2 at 77 K. It corresponds to a typically type IV isotherm in the IUPAC classification. The nitrogen adsorbed at

low relative pressure values correspond to the saturation of the microporous which connect the hexagonal mesoporous channels in the SBA-15 structure.

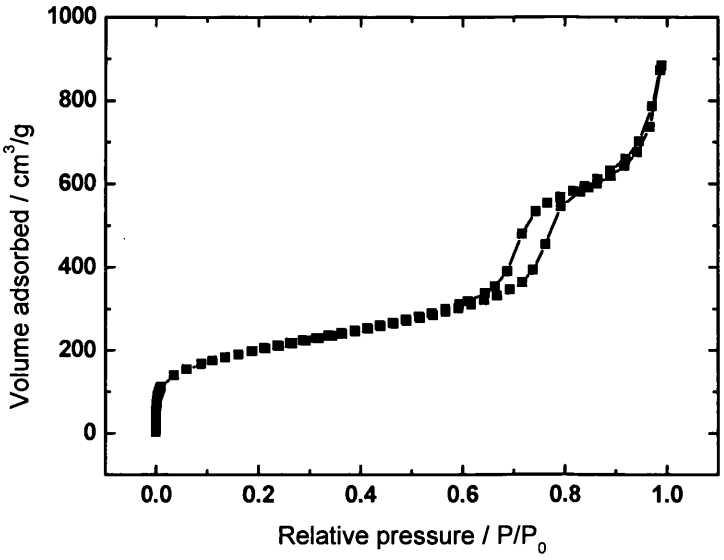

Figure 3.21: Isotherm of adsorption of N_2 on SBA-15 at 77K.

SBA-15 material shows a BET surface area of 685.76 ± 4.73 m^2/g. Figure 3.22 reveals its pore size distribution using the BJH method using desorption data. Mesoporous present an average size of 7 nm.

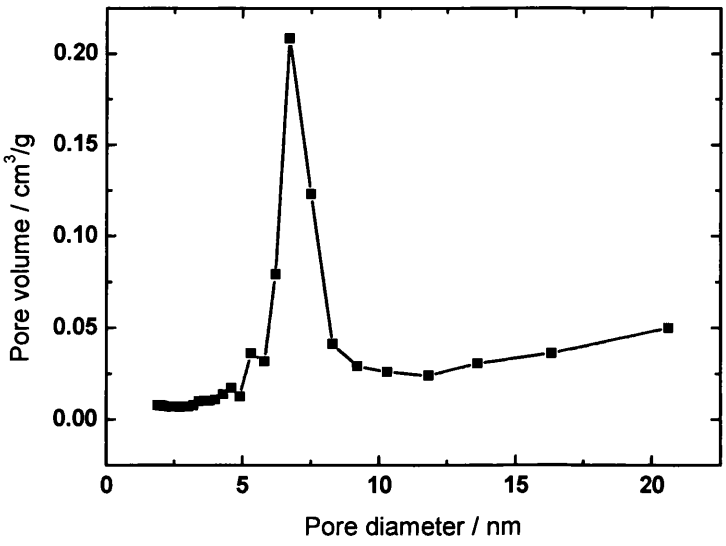

Figure 3.22: Pore size distribution of mesoporous material SBA-15.

Preparation of ZSM-5

Commercial ZSM-5 pellets were obtained from BHD limited. The material was used after grounding the pellets to powder without any further treatment. ZSM-5 is an aluminosilicate zeolite with a high silica and low aluminium content. Its structure is based on channels with intersecting tunnels as shown in Figure 3.23.

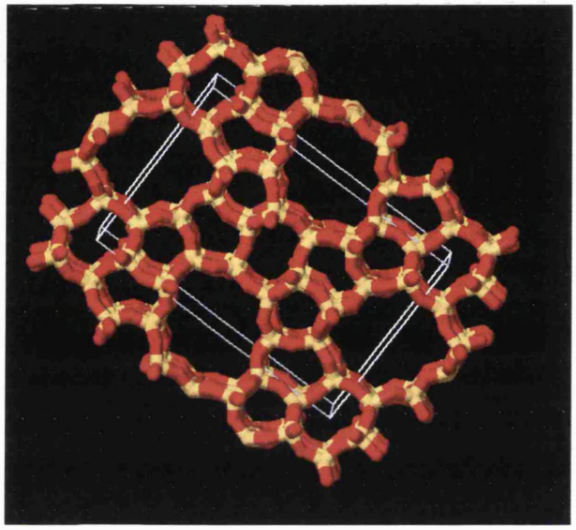

Figure 3.23: Structure of the zeolite ZSM-5 [20].

ZSM-5 has a BET surface area of 338.12 ± 2.81 cm^2/g. Figure 3.24 shows the isotherm of adsorption and desorption of N_2 at 77 K which reveals the presence of microporous and mesoporous. Pore size distribution using desorption data by the BJH method is shown in Figure 3.25. The average mesoporous size is 10.7 nm.

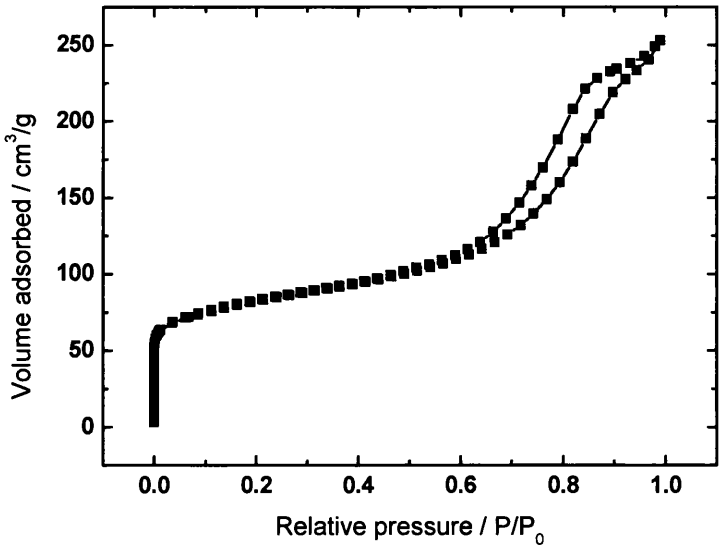

Figure 3.24: Isotherm of adsorption of N_2 on zeolite ZSM-5 at 77K.

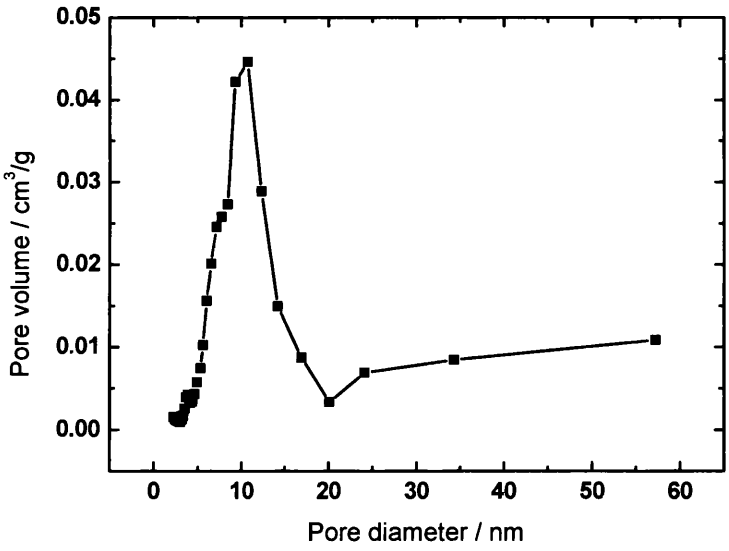

Figure 3.25: Pore size distribution of zeolite ZSM-5.

Deposition of ruthenium on silica supports

Ruthenium was supported onto SBA-15 and ZSM-5. For this purpose, aqueous solutions of solid of $RuCl_3$ were prepared in a concentration of 5%wt with respect to the solid used. The solutions were stirred with a determined quantity of silica

solid at room temperature for 3 hours. After this time, the catalysts were filtered using a 0.2 μm filter, washed with distilled water and dried overnight at 120°C.

The remaining solutions after the filtrations were collected and analyzed by atomic absorption spectroscopy (AAS) to determine the total quantity of metal deposited obtaining a loading of 0.8 %wt Ru on SBA-15 and 2.7 %wt Ru on ZSM-5.

3.1.2.3 DVB resins

PPh_3-resin (0.483 mmol, 1.25 mmol PPh_3/g, 0.385 g), $RuCl_3$ ($18.9 \cdot 10^{-3}$ mmol, 4.94 mg) and 7 mL of MeOH were stirred at 140°C for 19 hours in a sealed tube according to Figure 3.26. The mixture was cooled to room temperature. Then, the yellowish catalysts was filtered and washed gently with methanol. Finally, the catalyst was dried at 80°C under vacuum during 30 minutes. This catalyst was synthesised based on a known procedure [21].

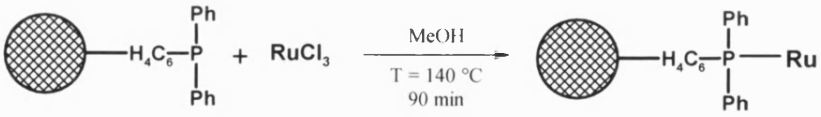

Figure 3.26: Synthesis of DVB-resin-PPh_3 – Ru.

The remained solution after synthesis was collected and analysed by AAS. 86.11% of ruthenium was deposited in the resin which has 0.53% wt Ru.

The same procedure was followed in order to support palladium and rhodium onto the PPh_3-resin. $PdCl_2$ ($23.8 \cdot 10^{-3}$ mmol, 4.22 mg) and $RhCl_3$ ($23.8 \cdot 10^{-3}$ mmol, 4.98 mg) were used respectively. The final content of metal was determined analyzing the remaining solutions after the syntheses by AAS, obtaining that 99.4% of the palladium was deposited with a 0.65% wt Pd-PPh_3-resin and 99.7% of the rhodium was deposited with a 0.63% wt Rh-PPh_3-resin.

3.2 CATALYSTS FOR THE TELOMERIZATION REACTIONS

3.2.1 HOMOGENEOUS CATALYSTS

Palladium homogeneous telomerization catalysts based on carbene ligands have been used for the reaction with isoprene, 1,3-pentadiene and 1,3-hexadiene. The advantages of these ligands versus the classical phosphorus ones are discussed in Chapter 5. However, in order to be able to compare them, both have been used in our studies. Different sources of palladium have also been screened. In Figure 3.27, the chemical structures of the commercial compounds are shown.

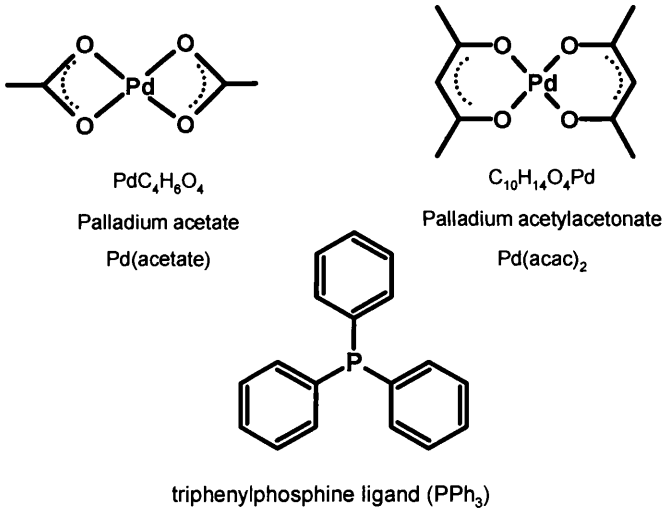

Figure 3.27: Palladium salts and triphenylphosphine ligand used for homogeneous telomerization reactions.

3.2.1.1 Palladium - carbene ligands complexes

As part of the project, different carbene ligands and complexes were synthesised in the University of Cardiff by Dr. David Nielsen (Kingsley Cavell's group).

The complex (1,3-dimesitylimidazol-2-ylidene)-palladium(0)-η^2,η^2-1,1,3,3-tetramethyl-1,3-divinyl-disiloxane (Pd(Imes)(dvds)) was synthesised by reacting

the palladium (0) diallylether complex $[Pd_2(dae)_3]$ (dae = diallylether) with 1,3-dimesitylimidazol-2-yline carbene (Imes) in 1,1,3,3-tetramethyl-1,3-divinyl-disiloxane (dvds) at -30°C in THF. Suitable crystals for X-ray crystallography were obtained by crystallization from pentane at low temperatures (< 0°C).

{1,3-bis-(2,6-diisopropylphenyl)-4,5-dimethylimidazol-2-ylidine} - palladium (0)-η^2,η^2-1,1,3,3-tetramethyl-1,3-divinyl-disiloxane (Pd(MeIPr)(dvds)) and (1,3,4-imidazol-2-ylidene) palladium (0)- η^2,η^2-1,1,3,3-tetramethyl-1,3-divinyl-disiloxane (Pd carbene complex 2) were obtained by reacting stoichiometric amounts of the corresponding free carbene with a Pd^0/dvds solution (8 %) in THF and subsequent crystallization from n-pentane at -30°C.

Characterization and crystallography data can be obtained in [22].

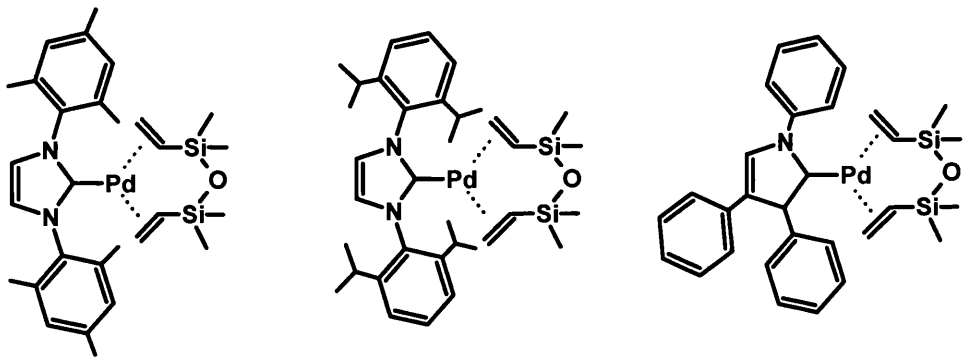

Pd(IMes)(dvds) Pd(MeIPr)(dvds) Pd carbene complex 2

Figure 3.28: Homogeneous palladium –carbene ligands complexes.

3.2.2 HETEROGENEOUS CATALYSTS

Different heterogeneous catalysts for telomerization reactions were synthesised based on DVB resins. According to the literature, different options for heterogenization of telomerization catalysts have been investigated recently [23-25] in order to avoid contamination with toxic transition metal complexes and ligands with the aim of developing more environmentally friendly systems. Triphenylphosphine-DVB-resin, Merrifield's peptide and Merrifield's resin have been used with the purpose of having different palladium complexes attached to the resins.

3.2.2.1 DVB-resin-PPh_3-Pd-dvds (Resin 1)

1.94 g of commercial triphenylphosphine resin, (1% DVB, 1-1.5 mmol/g, 100-200 mesh) was stirred with 3.25 mL of Pd-dvds solution (2.43 mmol Pd) overnight in dry THF under nitrogen (Figure 3.29). Fast stirring tends to break the resin. After that, resin was filtered and washed with a total of 40 mL of dry THF before drying briefly under vacuum. The remaining solution was analysed by AAS determining that 96.6 % of the palladium was adsorbed, with a concentration of 12.9 %wt Pd in the resin. The DVB-resin-PPh_3-Pd-dvds (resin 1) is stable under air at room temperature.

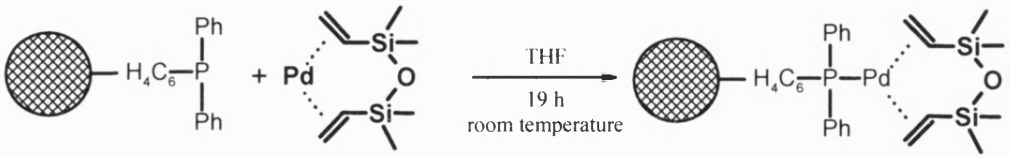

Figure 3.29: Synthesis of DVB-resin-PPh_3-Pd-dvds (resin 1).

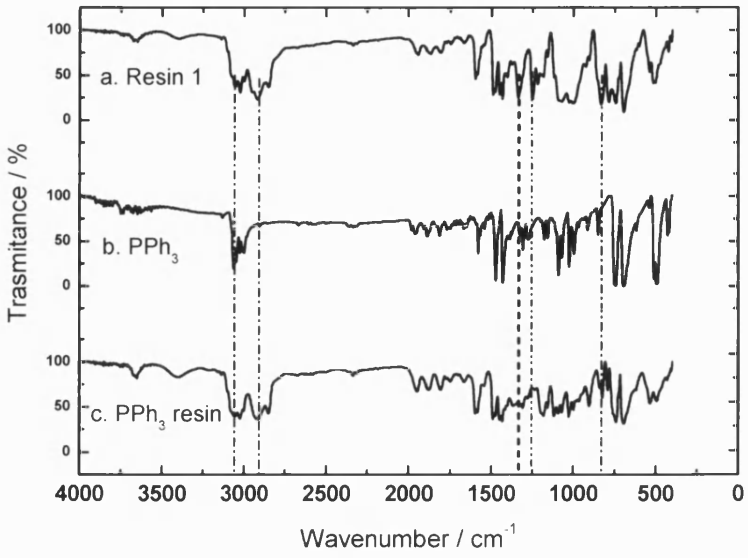

Figure 3.30: IR spectra of a. Resin 1, b. PPh_3 and c. PPh_3-resin.

In Figure 3.30, the infra-red spectra of Resin 1, triphenylphosphine and triphenylphosphine DVB-resin are shown for comparison. The bands between 2800 and 3100 cm^{-1} correspond to the PPh_3-DVB resin, bands at 1200 cm^{-1} and below are due to triphenylphosphine. The only bands which do not appear either on the resin or the ligand spectrum are the 1325 cm^{-1} and 1242 cm^{-1} peaks which might be due to the C-Si, C=C or Si-O bonds. Figure 3.35 shows the IR spectra of resin 2, where only palladium has been attached to the triphenylphosphine resin. The lack of peaks at 1325 cm^{-1} and 1242 cm^{-1} supports the idea that they are due to the coordinated dvds ligand.

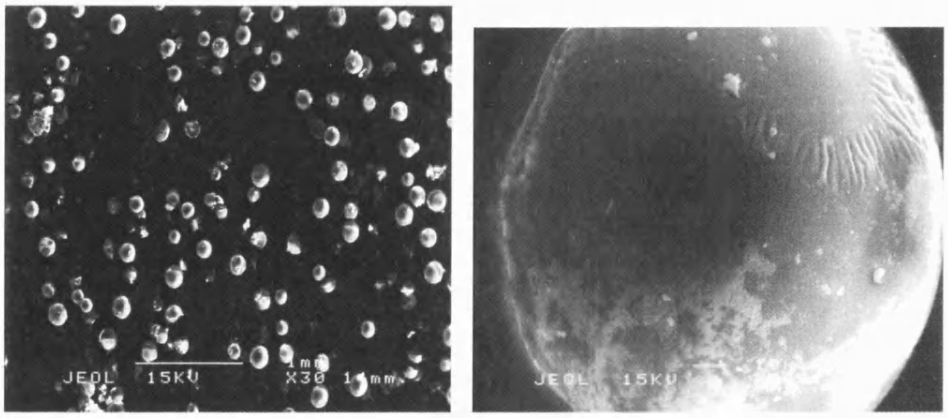

Figure 3.31: SEM images of resin 1.

Figure 3.31 shows scanning electron microscope (SEM) images of resin 1. The first image illustrates an overview of the sample where one can observe that some resin particles were broken during the palladium attachment step due to effects of mechanical stirring. The second image shows one of the unbroken particles where different details can be distinguished. Figure 3.32 shows the X-ray analysis of the resin where palladium, phosphorus and silica peaks can be easily distinguished.

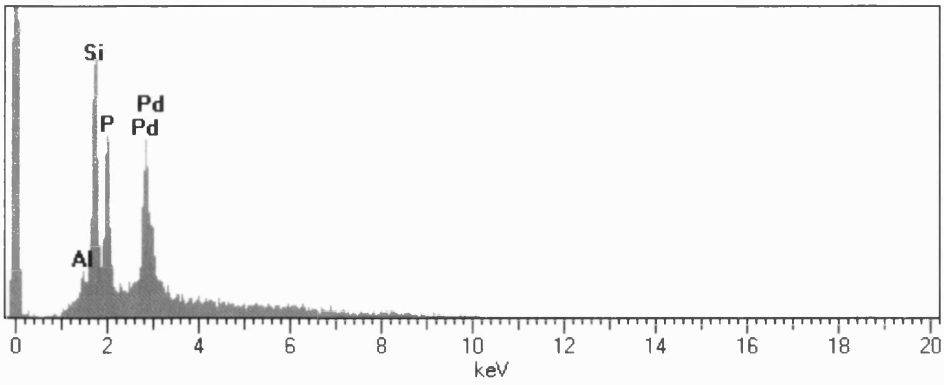

Figure 3.32: X-ray analysis of resin 1.

The second SEM image of Figure 3.31 suggests an uneven resin surface. In order to confirm the distribution of palladium, phosphorus and silica all over the resin, a higher magnification picture of the detail was taken and the presence of these elements was mapped by X-ray. The results are shown Figure 3.33.

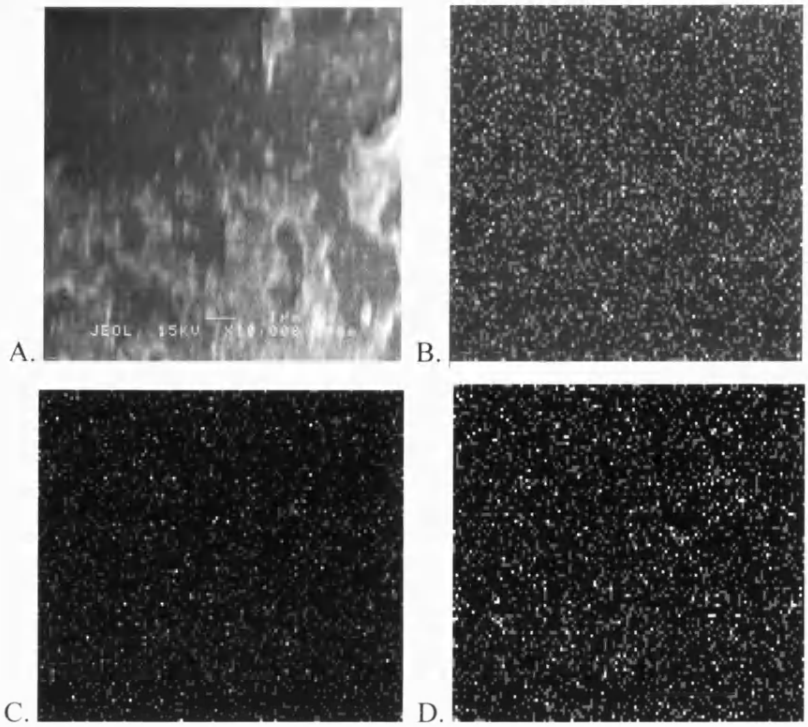

Figure 3.33: SEM and X-ray mapping of a detail of resin 1 (A. SEM image, B. Si, C. P and D. Pd presence by X-ray).

X-ray analysis and mapping around the resin confirm the uniform distribution of phosphorus, silica and palladium over the DVB resin. The surface details observed in Figure 3.31 must be due to the heterogeneous surface of the resin itself and not to a heterogeneous chemical composition.

3.2.2.2 DVB-resin-PPh_3-Pd (Resin 2)

This catalyst was synthesised based on a known procedure [21]. PPh_3-resin (0.483 mmol, 1.25 mmol PPh_3/g, 0.385 g), $Pd(acac)_2$ ($3.4 \cdot 10^{-3}$ mmol, 7.25 mg) and 7 mL of MeOH were stirred at 140°C for 90 minutes in a sealed tube according to Figure 3.34. The mixture was cooled to room temperature. Then, the yellowish catalyst was filtered and washed gently with methanol. Finally, the catalyst was dried at 120°C for 2 hours.

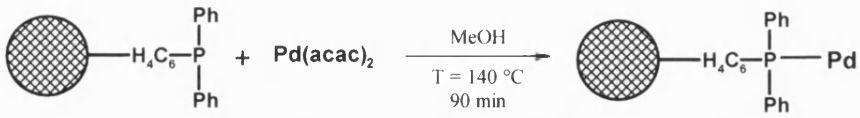

Figure 3.34: Synthesis of DVB-resin-PPh_3-Pd (resin 2).

The palladium loading was determined by ICP analysis of the resin, quantifying that resin 2 has 2.22 % wt Pd.

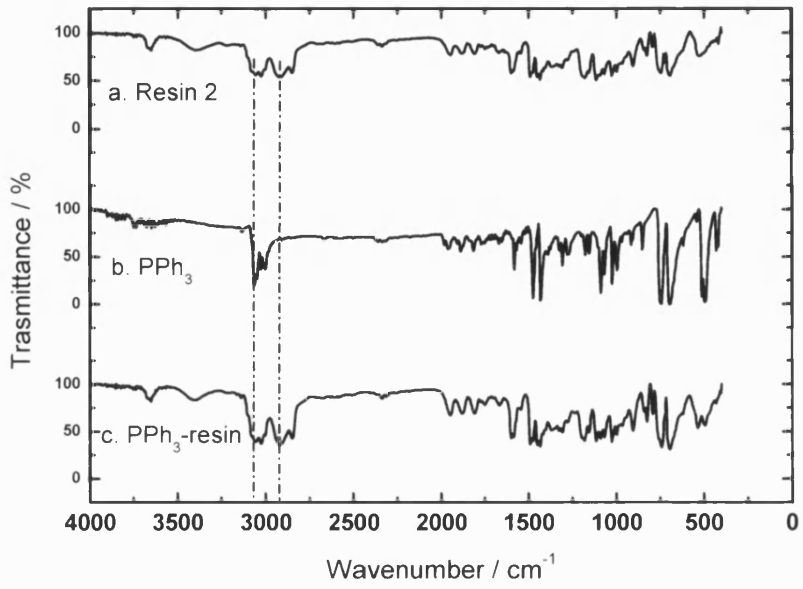

Figure 3.35: IR spectrum of a. Resin 2, b. PPh_3 and c. PPh_3-resin.

Figure 3.35 shows the IR spectra of resin 2, PPh_3 ligand and PPh_3-resin. The bands between 2800 and 3100 cm^{-1} correspond to the DVB resin. However, there is not distinction between the resin 2 and the resin itself. Pd-P bonds cannot be identified by IR.

3.2.2.3 Resin 3.a/.b

Merrifield's resin (0.2 g, 1% DVB-cross linked, 4 mmol Cl^-/g), the equivalent quantity of IMes·HCl (0.8 mmol, 0.1045 g) and 5 mL of methanol were stirred at 90°C during 15 hours in a sealed tube (Figure 3.36).

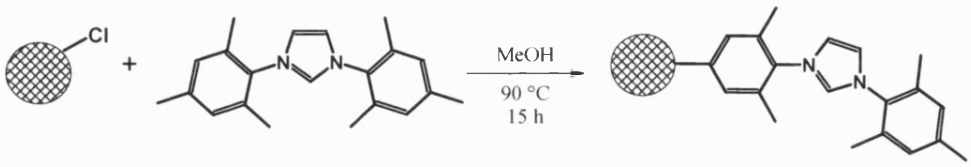

Figure 3.36: Step 1 in the synthesis of the resin 3.

The mixture was cooled down to room temperature. The resin was filtered, washed with methanol and dried at 80°C under vacuum during 1 hour. Palladium was incorporated into the resin by ion-exchange with (3.a.) 100 mL of aqueous solution of palladium chloride at room temperature over 15 hours and (3.b) 150 mL of DMF/H_2O (1:1 vol) solution of palladium acetate at 50°C over 4 hours (Figure 3.37).

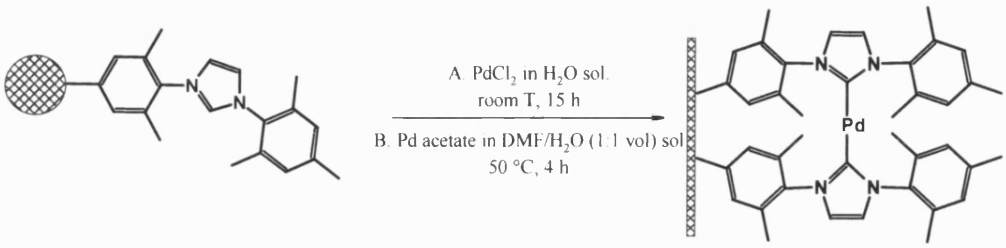

Figure 3.37: Step 2 in the synthesis of the resin 3.a/.b.

Palladium loading was determined by ICP analysis of the solid resin, quantifying a 0.396 % wt Pd, very low loading.

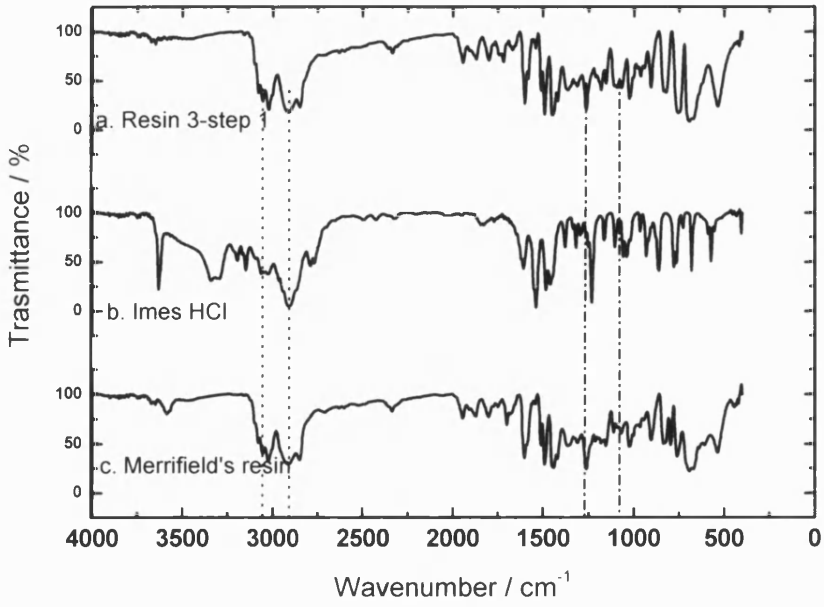

Figure 3.38: IR spectrum of a. Resin 3, b. Imes·HCl and c. Merrifield's resin.

Figure 3.38.c shows the IR spectrum of the commercial Merrifield's resin. A triple band can be observed at 3000 – 3100 cm^{-1} due to the C_{sp2} – H stretching vibrations and a small band at 1265 cm^{-1} corresponding to the C – Cl bond vibration [26]. Figure 3.38.a shows the IR spectrum of the Resin 3 after the step 1 when the incorporation of the Imes ligand might take place. However, no disappearance of the band at 1265 cm^{-1} corresponding to the C – Cl bond is observed, which suggest that most of the ligand has not been incorporated. Another possible explanation is the formation of another bond with similar vibration energy.

3.2.2.4 Resin 4.a/.b

Merrifield's peptide resin (0.5 g, 1% DVB-cross linked, 3.5-4.5 mmol Cl^-/g), 10 equivalents (considering an average of 4 mmol Cl^-/g) of 1-methylimidazole (20 mmol, 1.59 mL) and 5 mL of methanol were stirred at 90°C for 1 hour in a sealed tube according to Figure 3.39. The mixture was cooled to room temperature. The resin was filtered, washed several times with methanol and dried at 120°C overnight.

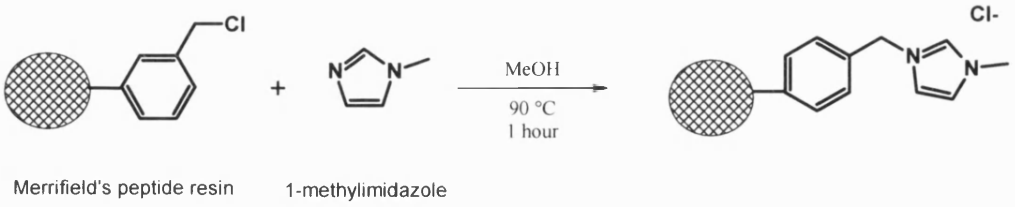

Figure 3.39: Step 1 in the synthesis of the resin 4.a/.b.

This first step can be easily followed by Raman spectroscopy. Figure 3.40.a shows the spectrum of the commercial Merrifield's peptide resin where one can observe a band at 1265 cm^{-1} due to the C – Cl vibration bond [26]. Figure 3.40.b shows the Raman spectrum of the Resin 4.a/.b after step 1. The peak at 1265 cm^{-1} has disappeared suggesting the incorporation of the methylimidazole group. Other peaks have also disappeared such as the triple one at 705 cm^{-1}.

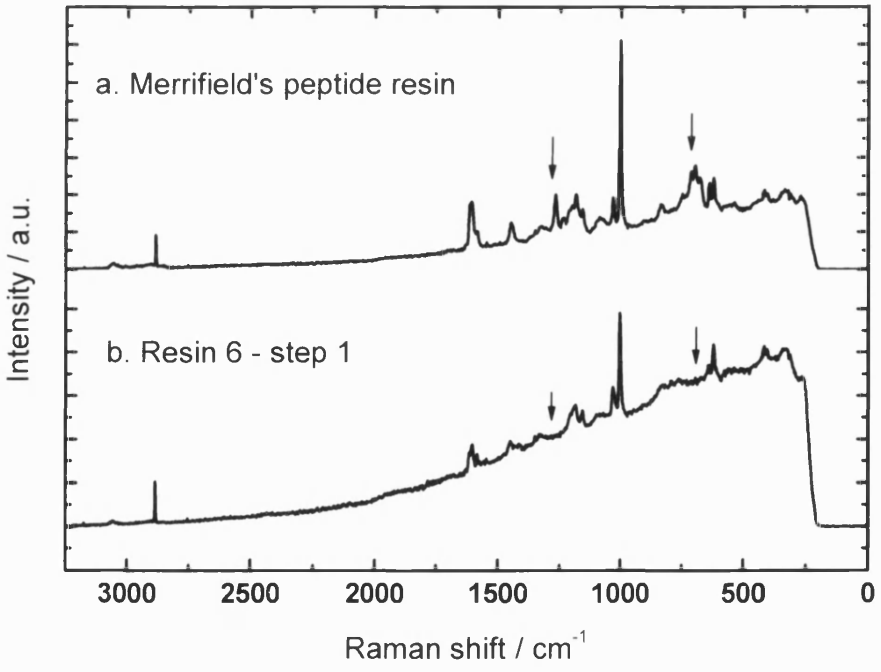

Figure 3.40: Raman spectra of Merrifield's peptide resin and resin 4.b after step 1.

The resin was suspended in 20 mL of acetone/H_2O (1:1) and $NaPF_6$ (4 mmol, 0.672 g) was added and stirred during 48 hours at room temperature. After this time, the resin was filtered again, washed with water and dried at 120°C (Figure 3.41).

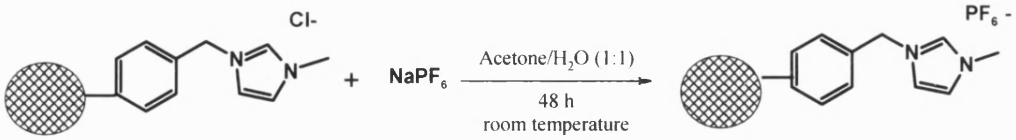

Figure 3.41: Step 2 of the synthesis of resin 4.a/.b.

Palladium was introduced into the resin by ion-exchange with (4.a) 100 mL $PdCl_2$ (4 mmol, 0.1418 g) aqueous solution over 20 hours at 50°C and (4.b) 150 mL of DMF/H_2O (1:1 vol) solution of palladium acetate at 50°C over 4 hours (Figure 3.42). Finally, the dark brown catalysts were filtered, washed with water and dried at 120°C during 2 hours.

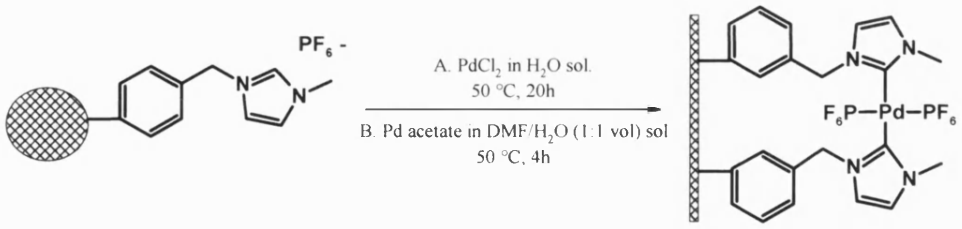

Figure 3.42: Step 3 of the synthesis of resin 4.a/.b.

A 0.864 %wt of Pd loading was determined by ICP analysis of the solid resin. Reduction of both resins 4.a and 4.b were done suspending the resins in 50 mL Acetone/H_2O (1:1) mixture and adding $NaBH_3$ under stirring. After 30 minutes, the reduced resins were filtered, washed with distillate water and dried at 80°C under vacuum for one hour. The initial brown resins became completely black.

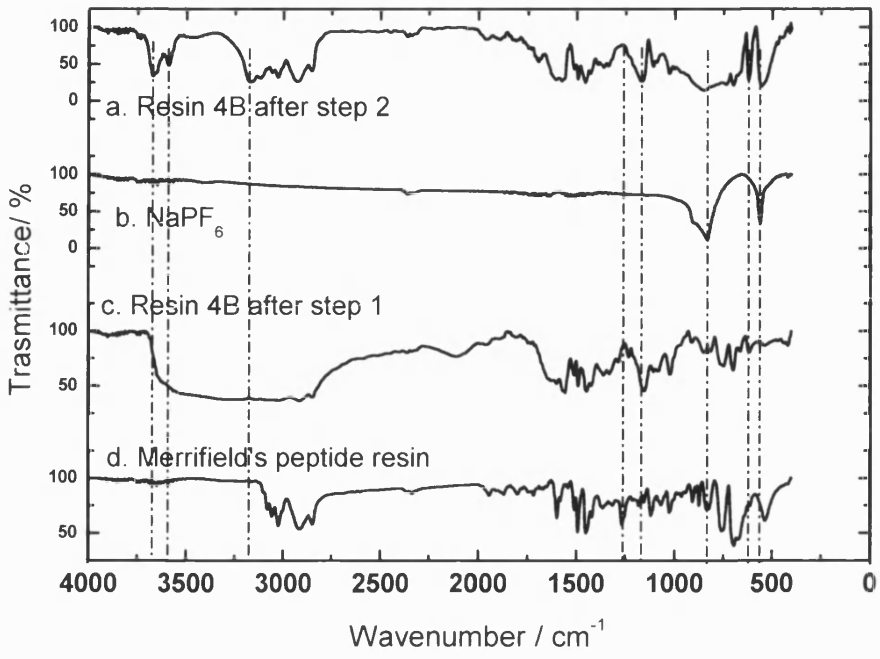

Figure 3.43: IR spectrum of a. Resin 4.b-step2, b. $NaPF_6$, c. Resin 4.b-step 1 and d. Merrifield's peptide resin.

Figure 3.43.d shows the IR spectrum of the commercial Merrifield's peptide resin. According to [26] the triple band at 3100 – 300 cm^{-1} corresponds to the C_{sp2} –H stretching vibrations and the double band at 2950 – 2800 cm^{-1} to the C_{sp3} – H stretching vibrations. The presence of the benzene group is represented by two bands at 1600 cm^{-1} and bands related to the benzene substitution are observed in the 1300 – 600 cm^{-1} region. Figure 3.43.c represents the IR spectrum of the resin 4 after the first step. All the bands observed in the Merrifield's peptide resin are presented except the small band at 1265 cm^{-1} which correspond to the C – Cl bond vibration. The same disappearance was previously observed by Raman spectroscopy (Figure 3.40). However, new bands appear due to the incorporation of the methylimidazole group. The more intensive ones are in the 3800 – 3100 cm^{-1} region although small ones at 1650 and 1160 cm^{-1} can also be observed. Figure 3.43.b corresponds to the IR spectrum of the $NaPF_6$ where only two intensive bands can be identified at 825 and 550 cm^{-1}. Finally, Figure 3.43.a shows the IR spectrum of the resin 4 after step 2 as a recompilation of all the bands

observed in the spectrum of the resin 4 after step 1 and the $NaPF_6$ which confirms the followed procedure.

3.2.2.5 Resin 5.a/.b

The first step in the synthesis of this catalyst is exactly the same as resin 4 (Figure 3.39), after the introduction of the imidazole group, palladium was incorporated by ion-exchange with (5.a) an aqueous solution of palladium dichloride at 50°C over 20 hours and (5.b) a DMF/H_2O (1:1 vol) solution of palladium acetate at 50°C for 4 hours, according to Figure 3.44.

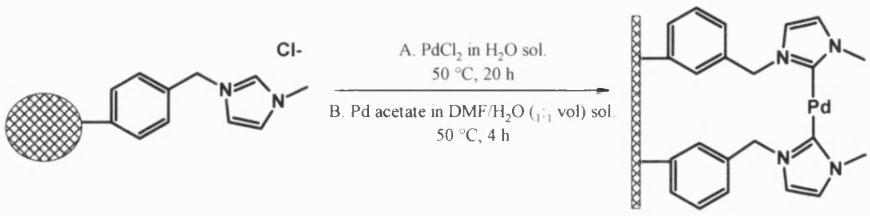

Figure 3.44: Step 2 in the synthesis of the resin 5.a./.b.

The catalyst was filtered, washed with water and dried overnight at 120°C. Resin was analysed by ICP in order to determine the palladium loading of 1.09 % wt Pd.

Reduction of both resins 5.a and 5.b was done suspending the resins in 50 mL Acetone/H_2O (1:1) mixture and adding $NaBH_3$ under stirring. After 30 minutes, the reduced resins were filtered, washed with distillate water and dried at 80°C under vacuum for 1 hour. The initial brown resins became completely black.

3.2.2.6 Resin 6.a/.b

Merrifield's resin (0.5 g, 1% DVB-cross linked, 3.5-4.5 mmol Cl^-/g), 10 equivalents (considering an average of 4 mmol Cl^-/g) of 1-methylimidazole (20 mmol, 1.59 mL) and 5 mL of methanol were stirred at 90°C for 1 hour in a sealed tube according to Figure 3.45. The mixture was then cooled to room temperature.

The resin was filtered, washed several times with methanol and dried at 120°C overnight.

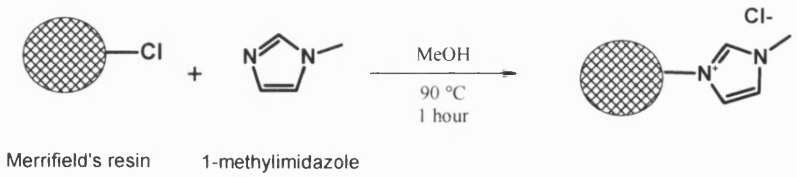

Figure 3.45: Step 1 of the synthesis of resin 6.a/.b.

This first step can be followed by Raman spectroscopy in a similar way as was done for resin 4. In the Figure 3.46, the Raman spectra of the Merrifield's resin and resin 6 after step 1 are shown. One can observed the disappearance of the band at 1265 cm^{-1} which corresponds to the C – Cl bond vibration. There are also other peaks such at the multiple bands at 705 cm^{-1} which also disappear.

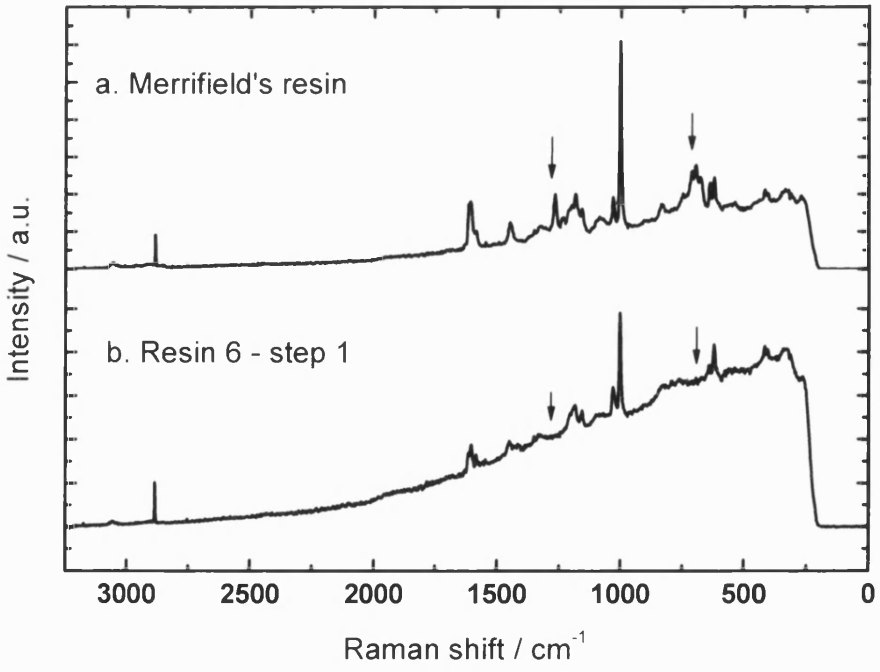

Figure 3.46: Raman spectra of Merrifield's resin and resin 6 after step 1.

The resin was suspended in 20 mL of acetone/H_2O (1:1) and $NaPF_6$ (4 mmol, 0.672 g) was added and stirred during 48 hours at room temperature. After this time, the resin was filtered again, washed with water and dried at 120°C (Figure 3.47).

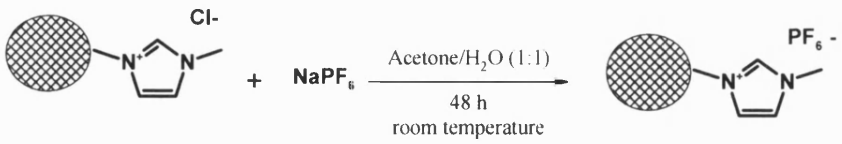

Figure 3.47: Step 2 of the synthesis of resin 6.a/.b.

Palladium was introduced into the resin by ion-exchange with (6.a) 100 mL $PdCl_2$ (4 mmol, 0.1418 g) aqueous solution during 20 hours at 50°C and (6.b) 150 mL DMF/H_2O (1:1 vol) solution of palladium acetate at 50°C for 4 hours (Figure 3.48). Finally, the catalysts were filtered, washed with water and dried at 120°C for 2 hours.

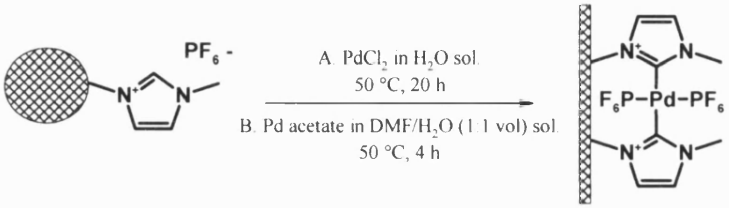

Figure 3.48: Step 3 of the synthesis of resin 6.a/.b.

The content of palladium in resin 6 is 0.428 % wt of Pd determined by ICP.

Reduction of both resins 6.a and 6.b was done suspending the resins in 50 mL Acetone/H_2O (1:1) mixture and adding $NaBH_3$ under stirring. After 30 minutes, the reduced resins were filtered, washed with distillate water and dried at 80°C under vacuum for 1 hour. The initial brown resins become completely black.

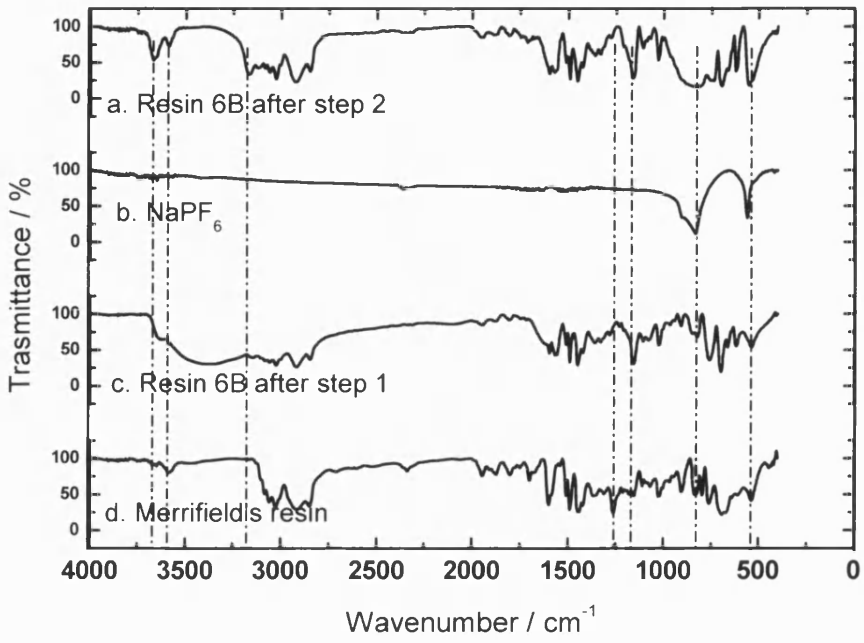

Figure 3.49: IR spectrum of a. Resin 6.b-step 2, b. $NaPF_6$, c. Resin 6.b-step 1 and d. Merrifield's resin.

Figure 3.49 shows the IR spectra of the commercial Merrifield's resin, Resin 6 after step 1 and 2 and $NaPF_6$. Although the initial resin is different than in the case of resin 4, exactly same bands are found during both steps and therefore, same discussion can be offered.

3.2.2.7 Resin 7.a/.b

The first step in the synthesis of this catalyst is exactly the same as that in the case of resin 6 (Figure 3.45), after the introduction of the imidazole group, palladium was incorporated by ion-exchange with (7.a) an aqueous solution of palladium dichloride at 50°C over 20 hours and (7.b) a DMF/H_2O (1:1 vol) solution of palladium acetate at 50°C over 4 hours, according to Figure 3.50.

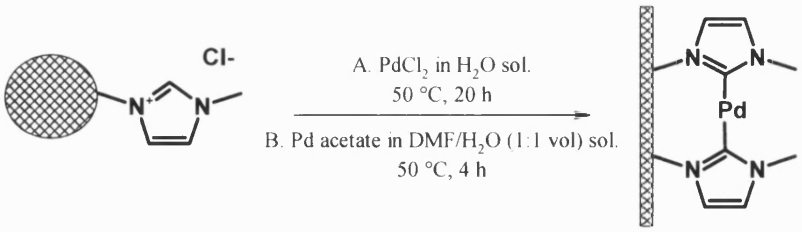

Figure 3.50: Step 2 of the synthesis of the resin 7.a/.b.

ICP analysis of the resin revealed that resin 7 has a 0.506 % wt of Pd. Reduction of both resins 7.a and 7.b was done suspending the resins in 50 mL Acetone/H_2O (1:1) mixture and adding $NaBH_3$ under stirring. After 30 minutes, the reduced resins were filtered, washed with distilled water and dried at 80°C under vacuum for one hour. The initial brown resins become completely black.

Chapter 4

STUDY OF THE ISOMERIZATION REACTION

4.1 INTRODUCTION

The first reaction that occurs in the tandem described previously is the isomerization reaction. This chapter begins with a literature review of this reaction, focusing on the proposed mechanisms and the different homogeneous and heterogeneous catalysts that have been used in the past. The second part consists of presentation and discussion of catalytic results for the use of palladium and rhodium supported on novel titanate nanotubes in the allylbenzene isomerization. This reaction is widely used to test catalysts due to its simplicity and narrow distribution of products. Finally, homogeneous and heterogeneous catalysts were tested for the isomerization of linear diolefins (initial reactants in the tandem reaction). Different metals (Pd, Rh and Ru) and heterogeneous supports (titanate

nanotubes, carbon, silica supports such as SBA-15 and ZSM-5 and DBV resins) have been tried in order to maximize the activity and, more importantly, selectivity.

The double bond migration reaction is fairly labile and is known to be catalysed by both liquid and solid acids and bases, transition metal salts and organometallic complexes of transition metals, as well as supported transition metals, especially Pd, Ru and Rh. Amongst many examples of double bond migration catalysis, the most active, selective and well researched catalysts are almost exclusively homogeneous transition metal salts and organometallic compounds, such as $PdCl_2$, $PdCl_2{\cdot}2C_6H_5CN$ [27], $RhCl_3{\cdot}3H_2O$ [28], $Ni[P(OEt)_3]_4$ [29] and $RuClH(CO)(PPh_3)_3$ [30].

A number of heterogeneous catalysts with double bond migration activity have been reported. The non-transition metal catalysts are either solid bases or acids. Thus, the earlier literature describes supported alkali metals [31] and a dispersed alkali hydroxide [32] as isomerisation catalysts. The double bond migration reaction was used to determine the number of acid sites in alumina catalysts [33] and to test the activity of magnesium mixed oxide catalysts [34]. It was found to be catalysed by strong Brønsted sites of some zeolites [35, 36]; silylated large pore acidic zeolites were reported to be more selective towards double bond migration rather than dimerisation [37]. Keggin type polyoxometalate salts were found to be active in gas phase double bond migration reactions [38]. More recently, hydrotalcites were found to be efficient in the synthetic application of double bond migration reactions for the production of high-value speciality molecules [39].

Double bond migration is often cited as an undesirable side reaction, for example in the case of Wacker-type oxidation by Pd (II)-polyoxometalate catalytic pairs [40], or in the hydrogenation of olefins [41-45]. However, there are also reports of synthetically important double bond migration reactions. Thus, rhodium supported on alumina or carbon catalysts were shown to selectively promote double bond migration towards a more stable higher substituted unsaturated carbon position in quinine and quinidine, whereas a commercial Pd (0)/C catalyst was inactive [46]. In a series of papers, Murzin et al [47-49] have reported conjugation of linoleic acid catalysed by supported transition metals, aiming to obtain the two specific

isomers known for their beneficial health effects. Supported ruthenium catalysts were found to be most active, stable and selective [50].

4.2 LITERATURE REVIEW

4.2.1 TYPES OF ISOMERIZATION

Unsaturated hydrocarbons of the olefin and cycloolefin types may undergo the following isomeric conversion:

1. cis – trans isomerization

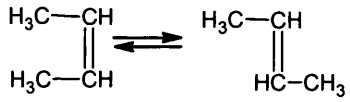

2. double bond shift at a chain branch

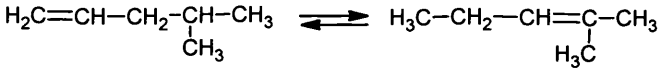

3. double bond shift in a branchless chain

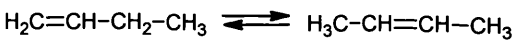

4. skeletal isomerization without change in maximum chain length

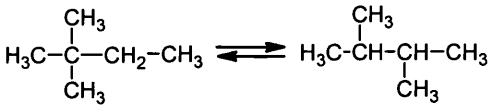

5. skeletal isomerization with change in maximum chain length

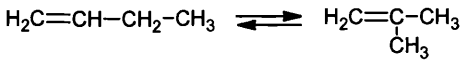

The second and third types of isomerization (shift of the multiple bond) take place most readily and are characterized by the rupture and the formation of a C-H bond, while a change in the carbon skeleton of the hydrocarbons is always associated with the rupture and also the formation of a carbon – carbon bond.

The fourth and fifth types of isomerization based on the rupture of the C – C bond are more varied. Reactions of this type include, for example, conversion of

straight-chain into branched-chain hydrocarbons and reactions of cyclization leading to the formation of cyclic parafins.

While the migration of a multiple bond may take place during a short contact time with a catalyst and even on compounds such as silica gel or pure aluminium oxide, the conversion of the carbon skeleton of a hydrocarbon molecule needs a more active catalyst [51, 52].

In olefin isomerization, thermodynamic driving forces favour formation of the trans-olefin rather than their cis isomers (in this study no distinction will be made between them), internal olefins rather than terminal olefins (being the main reason for the necessity of the tandem reaction to displace the equilibrium) and isomers exhibiting the highest degree of branching.

In the isomerization of α-olefins, it is the cis- isomer of the resulting β-olefins that is often formed, in preference to the trans-isomer as a result of the reaction kinetics. The preference for cis- isomers can be determined by the catalyst used or the presence of certain functional groups in the olefin [53].

The migration of double bonds in long chains takes place in a stepwise manner [54].

In this work, the focus will be on the double bond migration isomerization.

4.2.2 MECHANISMS OF ISOMERIZATION

4.2.2.1 Acid catalysts

The isomerization of olefins with acid catalysts is generally interpreted as a **carbenium ion intermediate mechanism** with the following steps, as shown in Figure 4.1 [52]. First, the alkene must be adsorbed on the surface of the catalyst. Then, a proton is added to one carbon of the double bond of the alkene to form an

adsorbed carbenium ion, where the C=C character is lost [50]. Next, loss of a different proton from the same carbon may result in cis – trans isomerization and loss of a proton from the adjacent carbon may result in double bond migration.

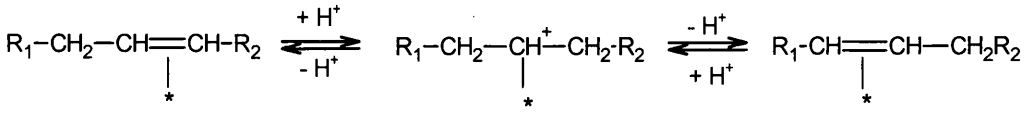

Figure 4.1: Carbenium ion intermediate mechanism of double bond migration on heterogeneous acid catalysts.

The proton needs to be supplied by the catalyst or pre-adsorbed H_2; thus, the catalyst must possess Brønsted acid sites. Practically all acidic catalysts that possess Brønsted acid sites can catalyze isomerization by this mechanism.

The cis/trans ratios obtained in reactions that proceed by this mechanism are around unity.

4.2.2.2 Base catalysts

Many metal oxides are active isomerization catalysts. Isomerization proceeds without extensive side reactions; no skeletal isomerization is observed and, in general, metal oxides are not very active hydrogenation catalysts.

The transition metal oxides are built by metallic cations and oxygen anions. The ionic radii of transition metals are smaller than that of O^{2-}. Thus, the oxygen atoms are usually close-packed with the smaller metal ions situated in the octahedral and tetrahedral spaces between the oxide ions.

On the surface of metal oxides, it is possible for cations and anions to form acidic and basic sites as well as acid-base pair sites. The surface composition of an oxide is determined by the surface anion to cation ratio, which, in the ideal case, depends on the stoichiometry of the oxide and the orientation of the crystal structure. It is important to know the surface electronic structure in order to understand the chemisorptive and catalytic properties of the metal oxides. Surface electron states

are usually partially filled so that the catalyst can both donate and accept electrons from the molecules interacting with the surface. The nature and energy of any surface state depend mainly on the ionicity of the oxides and the position of the ions. Surface electronic properties determine the mode of bonding of the adsorbates.

Double bond migration takes also place through the **carbanion intermediate mechanism**. This mechanism is known as Houriuti – Polanyi mechanism. The adsorbed olefin forms π-allyl species with a C=C bond coordinated to a Lewis acid site [50], a process which is accompanied by the formation of surface OH groups. Then, the addition of hydrogen back to the molecule but at the opposite end of the allylic bond results in isomerization. This mechanism is described in Figure 4.2.

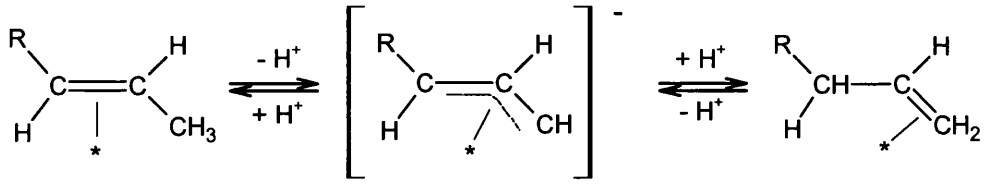

Figure 4.2: Carbanion intermediate mechanism.

This mechanism may proceed either by intramolecular or intermolecular H-transfer and results in cis – trans ratios with values of around ten. Hence, the cis/trans ratio can be an indicator of the mechanism.

4.2.2.3 Transition metals and organometallic compounds

The transition metals have partly filled d or f shells, which permit the formation of hybrid molecular orbitals in bonding. They are able to form sigma (σ-) and pi (π-) bonds with other atoms or ligands. This characteristic gives catalytic properties to the transition metals and their complexes.

The unoccupied antibonding π-orbital of the olefins forms a π-bond with the metal by interaction with its filled d_{yz} orbital and the filled π-orbital of the olefin forms

σ-bond with the empty metal orbitals (Figure 4.3). In the σ-component, the electron density flows from the olefin bonding orbital to the metal and in the π-component, the electron density is transferred from the metal to the olefin antibonding orbital.

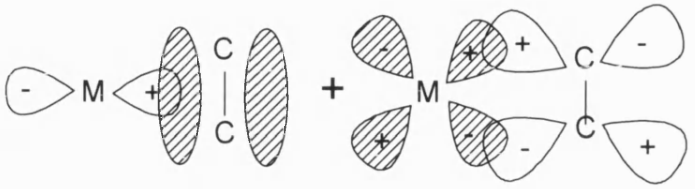

σ – component π – component

Figure 4.3: Molecular orbital representation of a transition metal-olefin bonding.

The transition metals can form bonds with a variety of organic molecules to form organometallics compounds. It is possible to distinguish basically two types of ligands:

- ionic, e.g. Cl^-, H^-, OH^-, CN^-, $alkyl^-$, $aryl^-$, $COCH_3^-$.
- neutral, e.g. CO, alkene, phosphine, arsine, H_2O, amine.

Some of these ligands play an important role in determining the activity and selectivity of the catalysts. Ligands can influence the behaviour of the transition metals by modifying the steric or electronic environment of the active site. Transition-metal complexes can contain as many as nine ligands. More commonly, co-ordination numbers of between four and six are encountered.

In theory, transition metals can have access to many oxidation states since they have valence d and s electrons, although not all elements form stable complexes for all of their available oxidation states. They have the ability to interchange between oxidation states during a catalytic reaction. This permits them to participate in redox cycles (mainly group VIII metals) and it is the major factor contributing to the wide range of catalytic activity of transition metals.

During a reaction catalyzed by transition metals or their complexes, activation of certain bonds in a reactant molecule takes place. There are two different types of activation:

- Activation by co-ordination; where the substrate interacts with the catalytic centre maintaining its integrity, although the distribution of the electrons over the bonds between substrate and catalyst is altered.
- Activation by addition; where the substrate interacts with the catalyst centre and its integrity is destroyed.

It is the latter mechanism that is responsible for the movement of the double bond, which involves the movement of a hydrogen atom from the alkyl group adjacent to the double bond to the α-carbon of the double bond.

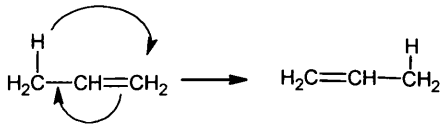

Figure 4.4: Migration of the hydrogen atom in the hydrocarbon chain.

Depending on the nature of the olefin and the metal (or complex) in question, two mechanisms can be distinguished, the π-allyl and the alkyl mechanisms. The coordination chemistry of the metal species in many cases determines the path of the olefin isomerization.

The π-allyl mechanism (1,3-hydrogen shift)

This mechanism can be described by consecutive steps. First, the co-ordination of the alkene and the metal occurs. Consequently, hydrogen abstraction or activation of the $C_\gamma H$ bond with the formation of a 3-carbon arrangement in a π-bonding with the metal to form hydrido metal-allyl species takes place. There is an increase of two units in both the oxidation state and co-ordination number of the metal centre. The next step consists of the addition of H from the metal-attached hydrido to the allyl unit. There are two possible positions to which it may be transferred: α-position (path A) and γ-position (path B).

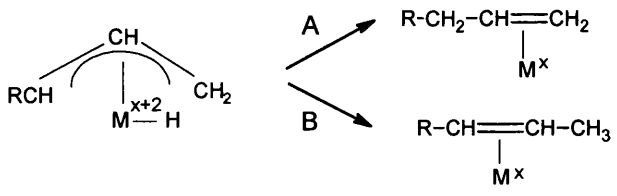

In the path A, the re-addition of the hydrogen takes place at the site of the abstraction what results in no movement of the double bond. In path B, the re-addition occurs at the γ-carbon, causing the double bond to move one position along the carbon skeleton. Finally, the alkene co-ordinated to the metal can exchange with other alkenes in the reaction medium.

The isomerization catalytic cycle involving π-allyl metal species includes a redox sequence; therefore, this mechanism only occurs in the case of metal complexes in low oxidation states and with x+2 states available.

$$M^x \rightarrow M^{x+2} \rightarrow M^x$$

This sequence of reactions creates to a catalytic isomerization cycle (Figure 4.5).

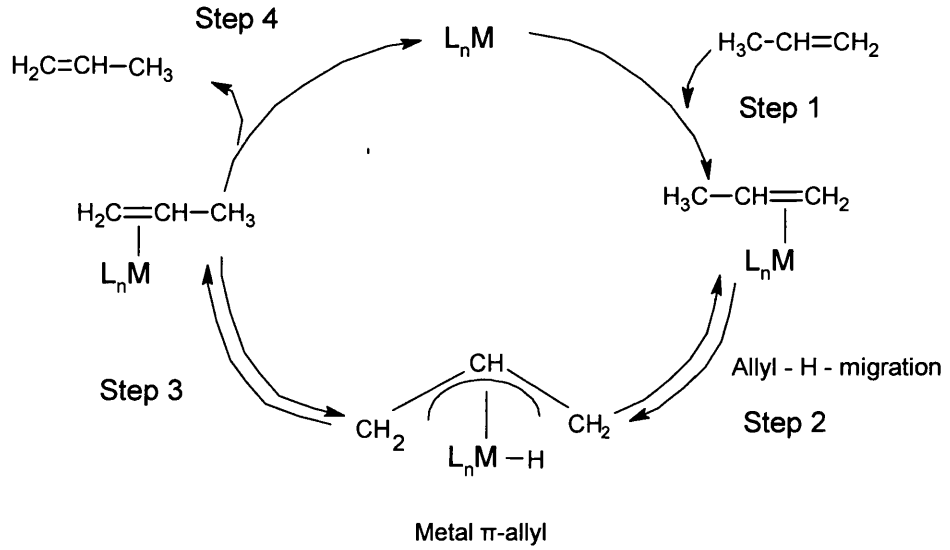

Figure 4.5: Scheme of the π-allyl mechanism of double bond migration on transition metal complexes.

This mechanism presents high cis/trans ratios of the isomerised olefin formed at the early stage in the reaction and little or no deuterium substitution on the 2-position (β) when deuterated olefins are being used.

The alkyl mechanism (1,2- Hydrogen shift)

The "alkyl mechanism" is the preferred pathway of isomerization if the catalytic species contain a metal-bonded hydride. The mechanisms can be described by the successive steps, starting with the co-ordination of the alkene and the metal hydride to form a metal alkyl species. The metal-hydrido complex can either be added to the reaction medium or formed in situ from a metal complex and a suitable hydride source such as gaseous hydrogen or aqueous acid. This is followed by the addition of hydrogen from the metal hydride to the hydrocarbon chain to form the metal σ-alkyl species. Next, γ-H elimination takes place, either by path A or path B.

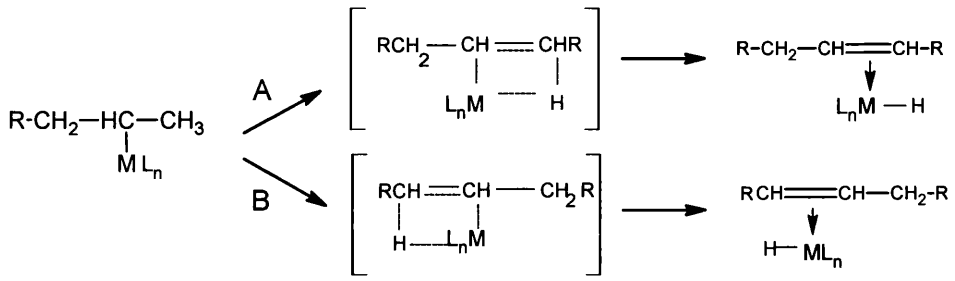

Path A is the reverse of the initial process and results in no migration of the double bond. It results in a hydrogen exchange reaction; in the presence of metal deuteride, deuterium can be incorporated into the non-isomerised olefins. In path B, the γ—H elimination takes place at the carbon next to the one where the H-addition occurred. This results in a migration of the double bond one position along the chain. In both paths A and B, either cis- or trans- alkenes can be formed.

Finally, the alkene co-ordinated to the metal can exchange with other alkenes in the reaction medium. This sequence of reactions constitutes a catalytic isomerization cycle shown in Figure 4.6.

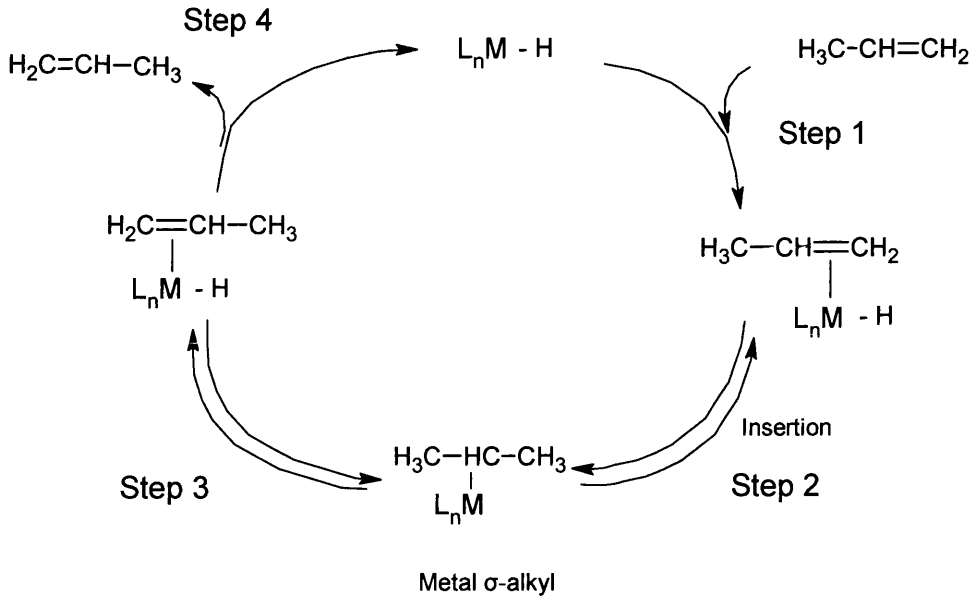

Figure 4.6: Scheme of the σ-alkyl mechanism of the double bond migration on transition metal complexes.

The hydride ion may originate from the co-catalyst, its anion or a nucleophilic attack. A variety of hydride – generating reactions are available such as [55]:

- oxidation of a carbon compound,

$$CH_3CH_2OH + OH^- + ClPt^{II} \rightarrow CH_3CHO + HPt^{II} + Cl^- + H_2O$$

- disproportionation of hydrogen

$$H_2 + ClRh^{III} \rightarrow HRh^{III} + Cl^-H^+$$

- oxidation of a metal with hydrogen

$$H_2 + Rh^I \rightarrow (H)_2 Rh^{III}$$

- oxidation of a metal with a proton

$$HCl + Rh^I \rightarrow HRh^{III}Cl$$

- displacement of hydrogen from co-ordinated olefin

However, in almost all cases the hydride is regenerated from the solvent proton, and this is confirmed by the inhibiting effect of added base.

The overall reaction is a complicated function of the different rates of each of the reversible reactions that constitutes the catalytic cycle, and these rates are influenced by the structure of the co-ordinated olefin, the metal and its ligands.

In the π-allyl mechanism, a substrate hydrogen moves between C_1 and C_3 of the C-3 units, and this process involves a 1,3-hydrogen shift. In the metal-alkyl mechanism, a 1,2-hydrogen shift is involved. This difference allows the two mechanisms to be distinguished by using deuterated olefins.

Cis/trans ratios

In the isomerization of olefins, the less stable cis-isomer is preferentially formed in the early stages of the reaction, giving high cis/trans ratios at low conversions [27, 55-57]. Which isomer is formed is governed by the orientation of the carbon-carbon bond at the time of formation of the allylic species (i.e. syn or anti configuration). The addition of a hydrogen atom to a carbon with anti-configuration yields a cis-2-olefin and the addition to a syn-configuration forms the trans-2-olefin. The π-species have preference for a more compact syn configuration. The initial trans/cis ratio is controlled by kinetic rather than thermodynamic factors [27].

If we consider that the equilibrium ratio cis/trans is close to but under one [56] after the initial period of the reaction, different theories explain how the equilibrium composition is reached. Bond and Hellier [27] postulated that cis-trans isomerization could occur by the mechanism shown in Figure 4.7, due to the fact that the rate of isomerization of cis-2-penten is slower than that of 1-pentene under equivalent conditions, and its rate only reaches its maximum after an induction period, during which 1-penten achieves its equilibrium concentration.

Cis-2-olefin ↔ 1-olefin → trans-2-olefin

Figure 4.7: Reaction scheme.

Another possibility is the reaction sequence (shown in Figure 4.8) postulated by Cramer and Lydsey [55], where the rate constant of 1-olefin to the cis-isomer is much higher than that to the trans-isomer and in the cis-trans isomerization, the

reaction constant from cis-isomer to trans-isomer is also much higher than the reverse reaction. This can explain the high cis/trans ratios at low conversions of isomerization of 1-olefins.

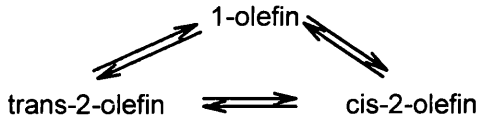

Figure 4.8: Reaction scheme.

Induction time

In some isomerization reactions, it is possible to distinguish an induction period that have been attributed to the formation of the olefin-metal complex [56]. This induction period depends on the catalyst concentration and the reaction temperature.

4.2.3 APPLICATIONS OF ISOMERIZATION

Olefins as reactants in many industrial applications

Some industrial processes that involve interactions between an olefin and a catalyst are, for example, the hydroformylation of olefins, the polymerization of ethylene by a one-site organometallic catalyst, the stereospecific polymerization of propene, metathesis of olefins, Wacker–Hoechst oxidation of ethylene, and many others, as shown in Figure 4.9 [58].

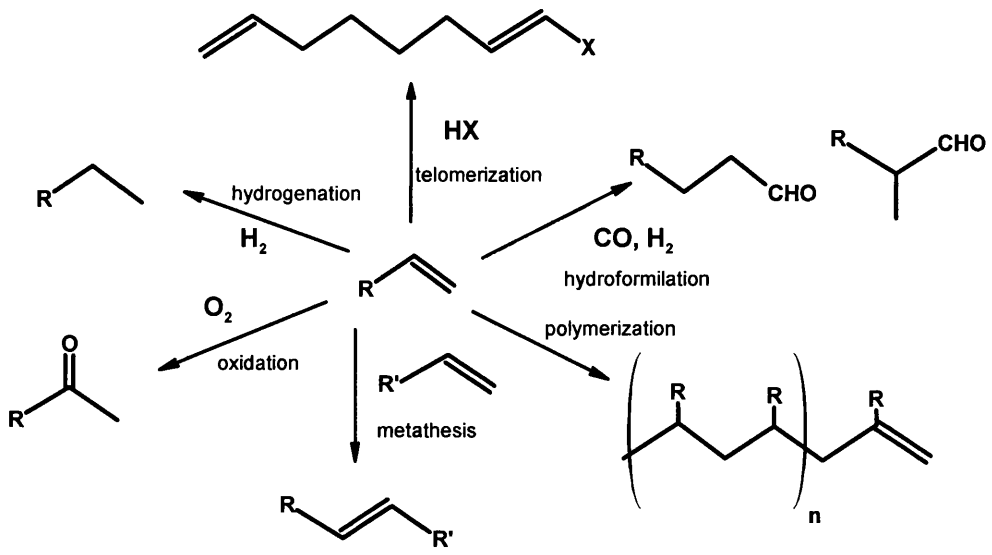

Figure 4.9: Olefins as raw materials in the synthesis of chemicals [58].

The skeletal isomerization plays an important part in the petroleum industry, owing to the higher octane number of branched-chain to straight-chain isomers in gasoline, the many isomers present in the naphthalene fractions and the possibility of making available many hydrocarbons from their less desirable isomers.

Specifically, the double bond migration is of great interest for the chemical industry because mixtures of internal aliphatic olefins, such as butanes, hexenes, and octenes, are substantially cheaper and more easily available than pure terminal isomers. In many reactions, terminal alkenes and branched products are required, both present in low concentration in the primary products of cracking.

Nowadays, double bond migration reactions have a significant synthetic importance including the transformation of allylic alcohols into carbonyls and the isomerization of eugenol, flavonoids and linoleic acid.

The synthesis of carbonyl compounds consists of a two step reaction, which is used in industry on a large scale (i.e. Mton per year). Starting with 1,3-butadiene, butanone and butanal are obtained in the first step. These allylic alcohols are then

isomerized to the carbonyl compounds as it is shown in Figure 4.10. Ruthenium and rhodium catalysts show the best results for the isomerization step [59, 60].

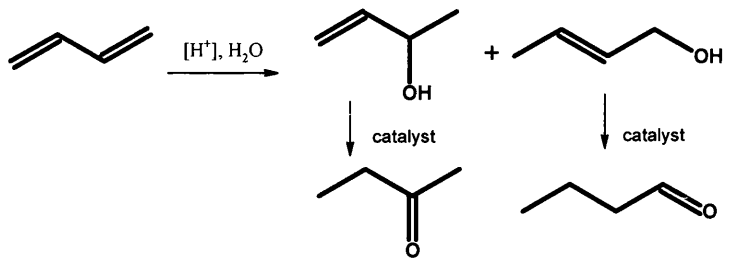

Figure 4.10: Isomerization of allylic alcohols to carbonyl compounds.

Isoeugenol is obtained from the migration of the double bond in the eugenol to a position conjugated with the benzene ring, as shown in Figure 4.11. The main applications of this product are in the pharmaceutical and fragrances industry. The most common catalyst for this reaction is formed by KOH in alcohol solution, although hydrotalcites have also shown good results [61].

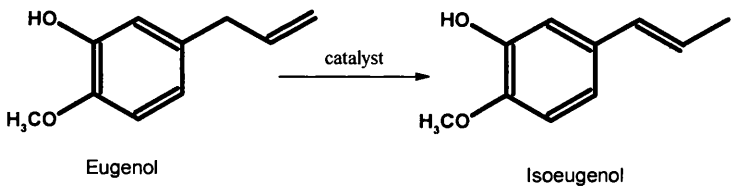

Figure 4.11: Isomerization of eugenol to isoeugenol.

Isomerization of linoleic acid into conjugated linoleic acid (CLA) has been of great interest during the last year in the functional food industry due to its ability to reduce or even eliminate cancer, improve immune function, prevent heart diseases and prevent atherosclerosis, among others. The classic catalysts are based on supported transition metals, especially Ru/C [49].

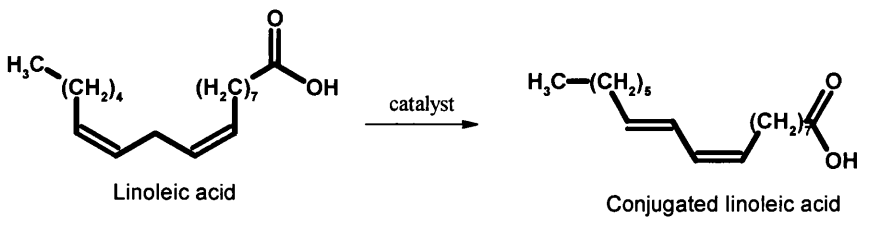

Figure 4.12: Isomerization of linoleic acid.

As it has been seen, there are several processes for which double bond migration is an important step in obtaining the desired products, but it could be the first stage in any process starting with a terminal olefin in tandem reactions, as it will be seen in Chapter 6.

4.2.4 HOMOGENEOUS ISOMERIZATION

4.2.4.1 Transition metal catalysts

Basic and metallic catalysts cause cis-trans isomerization or a double-bond shift [57]. The transition metal catalyzed reaction systems are characterized by the general necessity of co-catalysts [55] and by the formation of deuterated products when deuterated solvents are used.

The palladium catalyst system

The probable oxidation states of active palladium isomerization catalysts are Pd^0 and Pd^{II}. Although elemental palladium precipitates from some isomerization systems, complexes of Pd^0 are stabilized by appropriate coordination. The potential required to oxidize Pd^{II} to Pd^{IV} is so high that hydride formation is unlikely.

$$Pd^{II} + H^+ \xrightarrow{unlikely} Pd^{IV}H$$

Reactions carried out by palladium complexes seem to follow the σ-alkyl mechanism [28, 55, 56, 62] for which the presence of a hydride complex is necessary. Mirza-Aghayan et al. [63] studied isomerization reaction with $PdCl_2$ in the presence of triethylsilane Et_3SiH, proposing the reduction of palladium chloride before the formation of the hydride.

$$2\ Et_3SiH + PdCl_2 \rightarrow 2\ Et_3SiCl + Pd^0 + H_2$$

$$Pd^0 + Et_3SiH \rightarrow Et_3Si - PdH$$

Other authors support the idea of the π-allyl mechanism [27, 56, 57, 64, 65] in palladium systems where the presence of co-catalysts is not required. The hydride ion can be formed from the olefin, although some authors [28] suggest that the probability of a C-H bond being broken under mild conditions is low.

Isomerization catalyzed by palladium is susceptible to inhibition by competing ligands, such as Cl^- or $SnCl_3^-$, and selective co-ordination. For example, 1-hexene inhibits isomerization of 4-methyl-1-pentene.

In most of the reactions with Pd (II), the palladium is reduced to Pd^0. This can be avoided by the presence of a reoxidant such as $CuCl_2$, bezoquinone, $BiCl_3$, air, perchloric acid or $FeCl_3$. At very high concentration of reoxidant, the isomerization rate is retarded [64].

Some authors [56, 57, 62] have postulated the presence of olefin-palladium complexes as the real catalyst for the double bond migration, but the species suggested are different for all of them. For example, Conti et al [56] suggest that the true catalytic complex could be a monobridged dimeric π-complex, a $PdCl_2$(olefin)(base) or a $PdCl_2$(olefin)$_2$, the last of these being supported by some infrared evidence. They support the idea that the formation of π-complexes causes the olefin isomerization either in aprotic or protic solvents without the direct intervention of any external reagent.

In the case of isomerization with palladium (II) chloride using ethanol as cocatalyst, the true catalyst is formed by the reaction shown in Figure 4.13, where catalytic activity increases with the basicity of the donor atom.

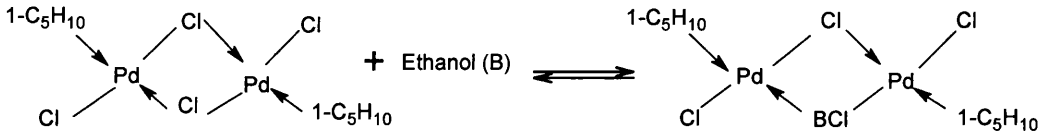

Figure 4.13: Formation of the catalytic species from $PdCl_2$ and ethanol.

Sparke et al [57] used palladium chloride bis(benzonitrile) as a catalyst, postulating that the true catalytic species is the olefin complex $(C_nH_{2n}\ PdCl_2)_2$, the presence of

which was confirmed by the brown colour of the solution. This idea is supported by the fact that palladium chloride complexes with ethylene, cyclohexene or benzonitrile as ligands are equally effective because all of them are converted into the mentioned complex.

The cis/trans ratio during the reactions is higher than one at low conversion and reach a value <1 in equilibrium [55-57].

There are not many kinetic studies of this reaction in the literature; however, conclusions can be extracted from the study of Conti et al [56] about the isomerization of 1-pentene with palladium (II) chloride using ethanol as co-catalyst. The kinetic of this reaction is first order with respect to both the complex and the alcohol concentration. Although linearity seems to be quite satisfactory in this concentration range, first order kinetic constants do not satisfy the Arrenhius law in the temperature range 0-35°C. Therefore, the isomerization mechanism is complex and the observed rate constants do not correspond to the true kinetic constants of the rate-determining step.

On the other hand, by increasing the ethanol concentration, a considerable increase in the isomerization rate is observed; however, palladium reduction takes place simultaneously with separation of the metal. The overall rate of olefin isomerization could be written as follows:

$$r = k_1 \cdot [C] + k_2 \cdot [C] \cdot [B] = k_{obs} \cdot [C]$$

where [C] represents the $[PdCl_2(1\text{-pentene})]_2$, [B] is the ethanol concentration and $k_{obs} = k_1 + k_2 [B]$. The first term (k_1) corresponds to a slow double bond migration in the absence of a "co-catalyst". The second term (k_2 [B]) can be explained by the breaking of a chloride bridge and the formation of a species that is active in the isomerization. Therefore, the role of the alcohol could be interpreted simply as that of a base that splits the halogen bridges, indeed a similar co-catalyst action was observed with different bases and the catalytic activity increased with the basicity of the donor atom.

Table 4.1: Literature data: Isomerization of 1-butene by palladium compounds [65].

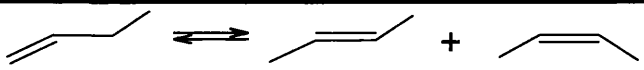

Thermodynamic equilibrium: 6:27:67

Catalyst	Solvent	T (°C)	Conversion (%)	Selectivity (%)	
				cis	trans
$[Pd(CH_3CN)_4][BF_4]_2$	CH_3CN	25	94	29.8	70.2
$[Pd(CH_3CN)_3(PPh_3)][BF_4]_2$	$CHCl_3$	25	96	29.1	71.8
$[Pd(CH_3CN)_2(PPh_3)_2][BF_4]_2$	$CHCl_3$	25	77	26	74
$[Pd(CH_3CN)(PPh_3)_3][BF_4]_2$	$CHCl_3$	25	0	-	-

Conditions: Catalyst concentration: $1.5 \cdot 10^{-2}$ M, Solution saturated with 1-butene. Time = 10 h.

Table 4.2: Literature data: Isomerization of 2,3-dimetyl-1-butene by palladium compounds [65].

Thermodynamic equilibrium: 12:88

Catalyst	Solvent	T (°C)	Conversion (%)	Selectivity (%)	TOF (h^{-1})
$[Pd(CH_3CN)_4][BF_4]_2$	CH_3CN	25	86	100	25.8
$[Pd(CH_3CN)_3(PPh_3)][BF_4]_2$	$CHCl_3$	25	88	100	5.9
$[Pd(CH_3CN)_2(PPh_3)_2][BF_4]_2$	$CHCl_3$	25	20	100	0.33
$[Pd(CH_3CN)(PPh_3)_3][BF_4]_2$	$CHCl_3$	25	0	-	-
$[Pd(CH_3CN)_3(PPh_2Me)][BF_4]_2$	$CHCl_3$	25	87	100	2.9
$[Pd(CH_3CN)_2(PPh_2Me)_2][BF_4]_2$	$CHCl_3$	25	17	100	0.28
$[Pd(CH_3CN)(PPh_2Me)_3][BF_4]_2$	$CHCl_3$	25	0	-	-
$Pd(PhCN)_2Cl_2$	$CHCl_3$	25	0	-	-

Conditions: Catalyst concentration: $9 \cdot 10^{-2}$M, Olefin/catalyst ratio = 10, different reaction times.

Table 4.3: Literature data: Isomerization of 1-pentene by palladium compounds [27, 56].

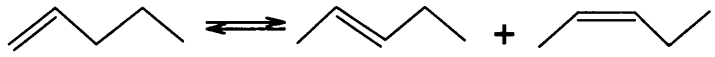

Catalyst	Cocatalyst	Solvent	T (°C)	Conversion (%)	Selectivity (%)		TON
					cis	trans	
$[PdCl_2(1\text{-}C_5H_{10})]_2$	-	chloroform	25	96	28	72	7.98
$[PdCl_2(1\text{-}C_5H_{10})]_2$	Ethanol	chloroform	25	98	28	72	8.15
$[PdCl_2(1\text{-}C_5H_{10})]_2$	C_6H_5OH	chloroform	25	-			-
$[PdCl_2(1\text{-}C_5H_{10})]_2$	$(CH_3)_3COH$	chloroform	25	-			-
$[PdCl_2(1\text{-}C_5H_{10})]_2$	2-hexene	chloroform	25				0.2
$[PdCl_2(1\text{-}C_5H_{10})]_2$	$C_6H_5CH_2OH$	chloroform	25				0.34
$[PdCl_2(1\text{-}C_5H_{10})]_2$	$(CH_3)_2CHOH$	chloroform	25				0.37
$[PdCl_2(1\text{-}C_5H_{10})]_2$	CH_3CH_2OH	chloroform	25				0.71
$[PdCl_2(1\text{-}C_5H_{10})]_2$	C_5H_5N	chloroform	25				1.45
$PdCl_2$ $2C_6H_5CN$[b]		C_6H_6	70	97	22	78	341.36

Conditions: Catalyst concentration: 0.055M, [b]0.22M.

Table 4.4: Literature data: Isomerization of cis-2-pentene by palladium compounds [27].

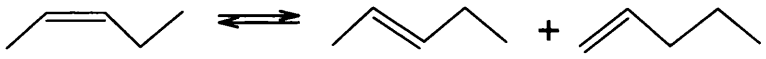

Thermodynamic equilibrium: 3:78:19

Catalyst	Solvent	T (°C)	Conversion (%)	Selectivity (%)		TON
				2-	1-	
$PdCl_2$	C_6H_6	70	97	71	29	8.06
$PdCl_2$ $2C_6H_5CN$	C_6H_6	70	97			341.36

Conditions: T = 70°C, catalyst: 0.4 g $PdCl_2$ and 0.02 g PdCl2 2C6H5CN.

Table 4.5: Literature data: Isomerization of 4-methyl-1-pentene by palladium compounds [57].

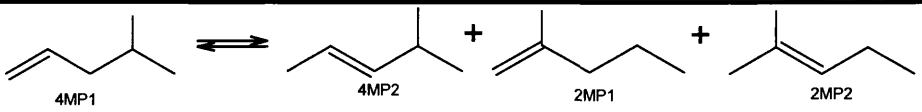

Thermodynamic equilibrium: 0.35:10.6:14.1:75

Catalyst	T	Conversion (%)	Selectivity (%)			TOF (h^{-1})
			4MP2	2MP1	2MP2	
$PdCl_2$	T_{reflux}	99.5	14	13.8	69.6	28.42
(Cyclo-C_6H_{10} $PdCl_2)_2$	T_{reflux}	99.4	11.9	11.6	75.0	28.40
(C_2H_4 $PdCl_2)_2$	T_{reflux}	99.4	11.4	12.0	75.0	28.39

Conditions: T = 60°C, catalyst: 3.5 mol % respect to olefin for $PdCl_2$ and 0.1 mol % for the rest.

The rhodium catalytic system

Different authors postulate that the double bond shift reaction with rhodium catalysts follows the σ-alkyl mechanism [28, 55, 62], where the rate of the olefin displacement step is comparable to the isomerization of the complexed olefin step.

Complexes of Rh^{III} can be active catalysts by themselves; as for example, $RhCl_3 \cdot 3H_2O$ has been found to be a potent catalyst for isomerization (although not potent enough for the induction time necessary for the formation of the rhodium hydride species [54]) and the possibility of its reduction to the simple olefin-chloro complex is excluded. This reaction involves a nucleophilic attack of the olefin and the reduction occurs due to the instability if the resulting metal alkyl.

It has been observed that Rh^{I} complexes by themselves are inactive, and the formation of a catalytically active intermediate in necessary [28].

$$2RhCl_3 \cdot 3H_2O + 6C_2H_4 \rightarrow (C_2H_4)Rh_2Cl_2 + 2CH_3CHO + 4HCl + 4H_2O$$

T.C. Morrill et al [54] added as hydroborating reagent "(BH_3)" (sic) to the $RhCl_3 \cdot 3H_2O$. The hydroborating reagent is apparently responsible for the in situ

generation of a metal hydride species. However, an excess of BH_3 reduces the catalyst into its elemental state.

Different types of co-catalysts have been used, such as secondary and tertiary alcohols, ethers, ketones and carboxylic acids. In this case, the function of the co-catalyst is to act as a co-solvent for the catalyst and the substrate. Thus, water is ineffective because it is not an adequate solvent for the olefins.

Some of the Rh^{III} complexes are inactive as catalyst, as for example the complex $[Py_4Rh^{III}HCl]Cl$ [55]. This can be explained in one of two ways. First, it is possible that the olefin may not displace the pyridine ligands to form an olefin-hydride complex, or alternatively, it could be possible that the initial isomerization occurs but not enough protons are available to regenerate the rhodium (III) hydride from rhodium (I).

The rhodium-phosphine complexes have shown considerable activity towards catalyzing olefin hydrogenation and isomerization reactions. The activity/selectivity of these catalysts may often be controlled by the choice of phosphine ligands bound to the metal [66].

The relative amounts of the cis- and trans- isomers may vary with the auxiliary ligands of the complexes, but in general, for the rhodium catalytic systems, the cis/trans ratio is very high mainly in the early stages of the reaction [28, 55]. The formation of products is particularly marked by the stereospecificity of formation of the most stable isomer during these stages of the reaction, which in this case is the cis isomer.

Table 4.6: Literature data: Isomerization of 1-hexene by rhodium compounds [28].

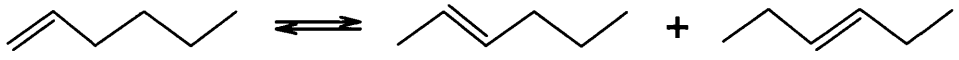

Thermodynamic equilibrium: 21% 1-hexene+trans-3, 16% cis-2, 63% trans-2+cis-3

Catalyst	Co-Solvent	T (°C)	Conversion (%)	Selectivity (%)		TON
				Trans-2+cis-3	Cis-2	
$RhCl_3 \cdot 3H_2O$	C_2H_5OH	65	87	62	38	1008.69

Conditions: Catalyst: 13 mg, Co-catalyst: 1 mL, 9 mL olefin, under N_2.

Table 4.7: Literature data: Isomerization of 1-butene by rhodium compounds [55].

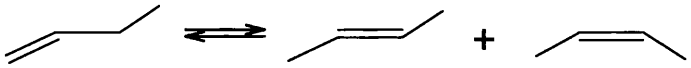

Catalyst	Cocatalyst	Solvent	T (°C)	Conversion (%)	Selectivity (%)		TOF (h^{-1})
					cis	trans	
$((C_2H_4)_2\ RhCl)_2$	HCl	CH_3OH	0	40.1	52.8	47.2	16.4
$((C_2H_4)_2\ RhCl)_2$	$SnCl_2{\cdot}2H_2O$ HCl	CH_3OH	0	66.6	32	68	27.32
$RhCl_3{\cdot}3H_2O$	H_2	CH_3OH	0	27.6	49.6	50.4	5.88
$RhCl_3{\cdot}3H_2O$	$SnCl_2{\cdot}2H_2O$ (0.5 mmol) H_2	CH_3OH	0	61.1	57.4	42.6	13.03
$RhCl_3{\cdot}3H_2O$	$SnCl_2{\cdot}2H_2O$ (0.75 mmol) H_2	CH_3OH	0	35	45.7	54.3	7.4

Conditions: Solvent: 2 mL, 1-butene: 8 mmoles, under N_2.

The ruthenium catalytic systems

It possible to find in the literature different ruthenium complexes used in the isomerization of olefins. Depending on the ligands and solvent used, the reaction takes place by either the π-allylic or σ-alkyl mechanism.

The nature of the solvent greatly affects the isomerization rate and conversion. With coordinating solvents, the reaction occurs by the π-allyl mechanism and, in general, lower conversions are reached because there is a competition between the solvent and the substrate for coordination places available on the catalyst. However, with hydrogen donor solvents, the reaction takes place by the σ-alkyl mechanism and the conversions are higher. Using aprotic solvents or solvents having lower polarity, the conversion increases. Complexes with more bulky ligands make the coordination of the olefin into the complex more difficult, which decreases the conversion. More basic ligands increase the stability of the complex such that it is less prone to form the carbonyl ligand to start the catalytic cycle.

With ruthenium trichloride trihydrate catalyst, an induction period is observed. The colour of the reaction solution changes due to the presence of ruthenium (II) species [67]. In the case of $RuCl_2(PPh_3)_3$ and $RuHCl(PPh_3)_3$ in benzene, the reaction occurs by the σ-alkyl mechanism [62, 68], with the conversion of the complex into a hydride in solution.

Edwing et al [68] proposed the same scheme as that shown in Figure 4.8 for the isomerization of 1-pentene, where the rate to form the cis isomer is double that to form the trans-2 isomer. All the reactions that take place are first order.

Terminal olefins isomerize faster than internal ones due to the steric hindrance around the double bond to form the π-olefin ruthenium complex with the catalyst.

If an additional gas, such as N_2, Ar, He or CO, is introduced into the reaction medium, the conversion generally decreases. In the case of CO, the isomerization is suppressed. The CO gas interacts with the ruthenium complex, forming an intermediate that blocks the activation of the olefin.

Table 4.8: Literature data: Isomerization of 1-pentene by ruthenium compounds [68].

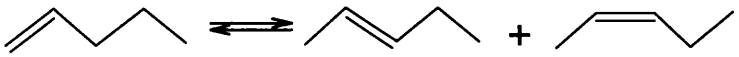

Catalyst	Co-Solvent	T (°C)	Conversion (%)	Selectivity (%)		TON
				cis	trans	
$[RuHCl(PPh_3)_3]$	benzene	50	97	67	33	41.7

Conditions: 1-pentene: 0.61 M, Catalyst: 1.7 mM.

Table 4.9: Literature data: Isomerization of 1-hexene by ruthenium compounds [58].

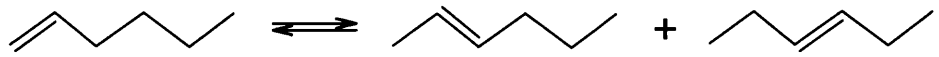

Catalyst	Co-Solvent	T (°C)	Conversion (%)	Selectivity (%)		TOF (h^{-1})
				2-hexene	3-hexene	
$Ru(CO)_3(PBu_3)_2$	toluene	80	5.9	-	-	1.96
$Ru(CO)_3(PBu_3)_2$	toluene	100	34.8	-	-	11.6
$Ru(CO)_3(PBu_3)_2$	toluene	120	94.9	-	-	31.6
$Ru_3(CO)_9(PBu_3)_3$	toluene	80	19.1	-	-	6.3
$Ru_3(CO)_9(PBu_3)_3$	toluene	100	69.4	-	-	23.1
$Ru_3(CO)_9(PBu_3)_3$	toluene	120	97.1	-	-	32.3
$Ru(CO)_3(PPh_3)_2$	toluene	80	25.1	75.7	24.3	11.7
$Ru(CO)_3(PPh_3)_2$	toluene	100	53.4	77.3	22.7	17.8
$Ru(CO)_3(PPh_3)_2$	toluene	120	91.7	76.0	24.0	30.6
$Ru(CO)_3(PPh_3)_2$	CF_3CHOH	120	8.4	92.8	7.2	2.8
$Ru(CO)_3(PPh_3)_2$	Acetone	120	9.5	80	20	3.2
$Ru(CO)_3(PPh_3)_2$	THF	120	11.0	75.5	24.5	3.7
$Ru(CO)_3(PPh_3)_2$	1,4-dioxane	120	23.7	91.5	8.5	7.9
$Ru(CO)_3(PPh_3)_2$	Toluene	120	34.6	73.7	26.3	11.5
$Ru(CO)_3(PPh_3)_2$	1-butanol	120	39.3	72.7	27.3	13.1
$Ru(CO)_3(PPh_3)_2$	1-propanol	120	46.1	73.1	26.9	15.4
$Ru(CO)_3(PPh_3)_2$	Ethanol	120	46.5	77.8	22.2	15.5
$Ru(CO)_3(PPh_3)_2$	2-propanol	120	87.6	74.2	25.8	29.2
$Ru_3(CO)_9(PPh_3)_3$	toluene	80	0	-	-	-
$Ru_3(CO)_9(PPh_3)_3$	toluene	100	97.0	-	-	32.3
$Ru_3(CO)_9(PPh_3)_3$	toluene	120	97.6	-	-	32.5
$Ru(CO)_2(OAc)_2(PBu_3)_2$	toluene	80	0	-	-	-
$Ru(CO)_2(OAc)_2(PBu_3)_2$	toluene	100	0	-	-	-
$Ru(CO)_2(OAc)_2(PBu_3)_2$	toluene	120	6.5	-	-	2.1

Conditions: under He, Catalyst: 0.040 mmol, hexane: 4 mmol, time: 3h.

The platinum catalytic systems

Platinum can be found in various oxidation states: Pt^0, Pt^{II}, and Pt^{IV}. Some authors [28, 55, 69, 70] have studied the double bond isomerization of olefins with different platinum compounds under different conditions. All of them consider that

the reaction takes place by the σ-alkyl mechanism with the hydride species acting as the catalyst.

The presence of a co-catalyst is necessary for the formation of the metal hydride. In the case of an alcohol as co-catalyst [28], the metal hydride is formed when it reacts with platinum complexes. Composition profiles are identical, but for different co-catalysts, the rate of isomerization decreases in the order C_2H_5OH > $(CH_3)_2CHOH$ > $(CH_3)_3COH \approx CH_3COOH$. The isomerization reaction in the presence of an alcohol as co-catalyst, is accompanied by the oxidation of the alcohol to aldehyde or ketone.

Tayim et al. [69] used different salts as co-catalysts and concluded that the $SnCl_2$ is the best one. Similar results were obtained by Cramer and Lidsey [55]. Other halides of groups III, IV and V are not as good co-catalysts as $SnCl_2$. $SnCl_2$ utilizes strong π-accepting and weak σ-donation properties to reduce the electron density on the platinum atom, making it more susceptible to be attacked by nucleophiles such as a hydride ion or the carbon-carbon double bond of an olefin. The strong π-accepting property stabilizes hydrido and metal-olefin complexes once they are formed and prevents reduction of the platinum (II) atom.

Platinum catalysts produce more trans-isomer, thus resulting in a trans/cis ratio near three [55], following the reaction scheme shown in Figure 4.8 with reversible firs-order reactions. The presence of $SnCl_2$ affects this ratio, increasing the amount of trans-isomer. However, Harrod and Chalk [28] found preferential formation of cis-isomer in the early stages of the reaction.

Other authors have studied the isomerization of olefins by platinum (II) complexes in acidic media, proposing that the presence of a carbonium ion attached to Pt^{n+} or $Pt^{(n+2)+}$ as the active isomerization species. Acid co-catalysts may produce the hydride by olefin oxidation rather than by oxidation of Pt^{II} to a Pt^{IV} hydride.

Table 4.10: Literature data: Isomerization of 1-hexene by platinum compounds [28].

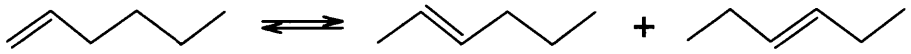

Catalyst	Solvent	T (°C)	Conversion (%)	Selectivity (%)		TOF (h^{-1})
				Trans-2 + cis-3	Cis -2	
Dichlorobis(ethylene) dichlorodiplatinum (II)	C_2H_5OH	100	81	72.8	27.2	-

Conditions: Catalyst: 0.001M, 1-hexene: 1mL.

Table 4.11: Literature data: Isomerization of 1-butene by platinum compounds [55].

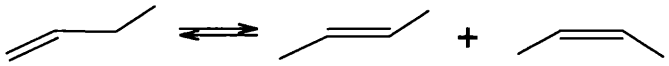

Catalyst	Co-catalyst	Solvent	T (°C)	Conversion (%)	Selectivity (%)			TOF (h^{-1})
					cis-2	trans-2	n-butene	
H_2PtCl_6	$SnCl_2$-H_2	CH_3OH	- 24	21.5	16	54.1	29.5	0.40
H_2PtCl_6	$SnCl_2$-H_2	CH_3OH	0	33.6	26.2	67.8	6	1.43

Conditions: Catalyst: 0.032 g, Co-catalyst: 0.093 g.

Table 4.12: Literature data: Isomerization of 1,5-cyclooctadiene by platinum [69].

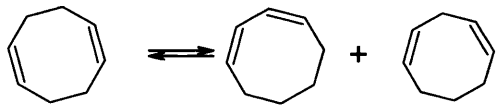

Catalyst	Cocatalyst	Solvent	T (°C)	Conversion (%)	Selectivity (%)		TOF (h^{-1})
					1,3	1,4	
$PtCl_2(PPh_3)_2$	$SnCl_2 \cdot 2H_2O$	CH_2Cl_2	50	77	41.5	58.5	21.73
$PtCl_2(PPh_3)_2$	$GeCl_2$	CH_2Cl_2	50	15	-	100	4.16
$PtCl_2(PPh_3)_2$	$PbCl_2$	CH_2Cl_2	50	6	-	100	1.66
$PtCl_2(PPh_3)_2$	PCl_3	CH_2Cl_2	50	1	-	100	0.27
$PtCl_2(PPh_3)_2$	$AsCl_3$	CH_2Cl_2	50	2	-	100	0.55
$PtCl_2(PPh_3)_2$	$SbCl_3$	CH_2Cl_2	50	35	14.3	85.7	9.7
$PtCl_2(PPh_3)_2$	$BiCl_3$	CH_2Cl_2	50	4	-	100	1.1
$PtCl_2(PPh_3)_2$	GaCl	CH_2Cl_2	50	7	-	100	1.94
$PtCl_2(PPh_3)_2$	InCl	CH_2Cl_2	50	13	23	77	3.6
$PtCl_2(PPh_3)_2$	TlCl	CH_2Cl_2	50	3	-	100	0.83
$PtCl_2(PPh_3)_2$	$SnCl_4 \cdot 5H_2O$	CH_2Cl_2	50	59	20.4	79.6	16.3
$PtCl_2(PPh_3)_2$	PF_3	CH_2Cl_2	50	23	13.1	34	6.38
$PtCl_2(PPh_3)_2$	CO	CH_2Cl_2	50	9	-	100	2.49

Conditions: under 500 psi of H_2, solvent: 50 mL, time: 2h.

The nickel catalytic systems

Nickel can be present in the oxidation states Ni^0, Ni^{II} and Ni^{III}. It is generally agreed [29, 55, 71] that the isomerization of olefins with nickel complexes goes by the σ-alkyl mechanism. However, in some specific cases, such as the isomerization with 1,3-bis(diphenylphosphino)propane nickel with HCN in benzene [29], there are no detectable amounts of Ni-hydride complexes, which may suggest a π-allylic mechanism.

Cramer and Lindsey [55] studied isomerization in acidic media and discovered that, in the absence of acid, the conversion is near zero, which means that the acid solvent is the source of hydrogen for the formation of the hydride species. Corain and Bingham [29, 71] used different acid co-catalysts with the same purpose, proposing the formation of a catalytically active species by protonation.

$$Ni[P(OEt)_3]_4 + CF_3CO_2H \leftrightarrow NiH[P(OEt)_3]_4^+ + CF_3CO_2^-$$

With nickel complexes, the catalysts do not require an activating ligand such as halide (as with rhodium catalysts) or $SnCl_3^-$ (as with platinum catalysts).

A kinetically controlled cis/trans ratio during the early stages of the reaction is observed, with values varying in the range of 2.3 – 3 in different reports. A possible reaction is shown in Figure 4.8 where the interconversion cis-trans 2-olefins is very fast [55, 71], nearly ten times faster than isomerization.

Table 4.13: Literature data: Isomerization of 1-pentene by nickel compounds [29, 71].

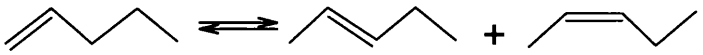

(dpb) = 1,4-bis(diphenylphosphino)butane

Catalyst	Cocatalyst	Solvent	T (°C)	Conversion (%)	Selectivity (%)		TOF (h^{-1})
					cis-2	trans-2	
$Ni(dpb)_2$	HCN	Benzene	70	97.8	23.2	76.8	
$Ni(dpb)_2$	CF_3COOH	Benzene	70	97.8	23.9	76.1	
$Ni(dpb)_2$	H_2SO_4	Benzene	70	97.2	30.6	64.4	
$Ni(dpb)_2$	CCl_3COOH	Benzene	70	0	-	-	
$Ni(dpb)_2$	HCN	Benzene	70	89.3	48.6	51.4	
$Ni(dpb)_2$	CF_3COOH	Benzene	70	0	-	-	
$Ni(dpb)_2$	-	Benzene	70	0	-	-	
$Ni_2(CN)_2(dpb)_3$	HCN	Benzene	70	97.4	22.7	77.3	
$Ni[P(OEt)_3]_4$	CF_3CO_2H	Benzene	35	75	26.6	73.4	600

Conditions: Catalyst: 10^{-2}M, co-catalyst: $7 \cdot 10^{-2}$M, 1-pentene: 1.5M, argon atmosphere.

Table 4.14: Literature data: Isomerization of allylbenzene by a nickel compound [29].

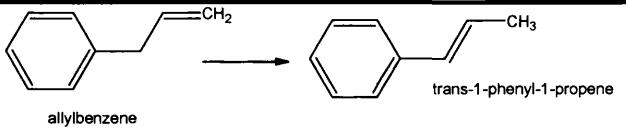

Catalyst	Cocatalyst	Solvent	T (°C)	Conversion (%)	Selectivity (%)		TOF (h^{-1})
					trans	cis	
$Ni(dpb)_2$	HCN	Benzene	70	100	100	-	60.25
$Ni(dpb)_2$	CF_3COOH	Benzene	70	100	100	-	60.25

Conditions: Catalyst: $3.9 \cdot 10^{-3}$M, co-catalyst: $1.5 \cdot 10^{-2}$M, allylbenzene: 0.5M, argon.

Table 4.15: Literature data: Isomerization of 1-butene by nickel compounds [55].

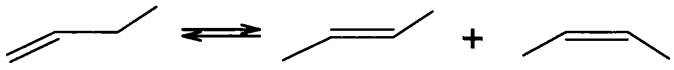

Catalyst	Cocatalyst	Solvent	T (°C)	Conversion (%)	Selectivity (%)		TOF (h^{-1})
					cis	trans	
$Ni[P(OC_2H_5)_3]_4$	HCl	CH_3OH	0	84.6	26.6	73.4	-

Other transition metal catalytic system

Other transition metal complexes such as osmium, iron, iridium and cobalt have also been studied in the isomerization of olefins.

Cobalt complexes such as $CoHN_2(PPh_3)$ isomerize olefins by the σ-alkyl mechanism, with similar results to those obtained with ruthenium hydrides [62].

Iron complexes follow the σ-alkyl mechanism, exhibiting slower rates of reaction than rhodium, platinum or palladium complexes [55].

Table 4.16: Literature data: Isomerization of 1-butene by an iron compound [55].

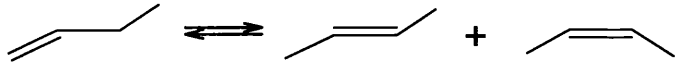

Catalyst	Solvent	T (°C)	Conversion (%)	Selectivity (%) cis -2	Selectivity (%) trans -2	time
$[HFe(CO)_4]^-$	D_2O	25	30.2	26.2	73.8	5 days

Conditions: Catalyst: 1.4 mmol, gas 1-butene: 200 mL.

Studies carried out with osmium complexes such as $OsHCl(CO)(PPh_3)_3$, show that the isomerization takes place according to the σ-alkyl mechanism with a very rapid cis-trans interconversion [71]. The active catalyst species are formed by dissociation of at least one phosphine ligand.

$$OsHCl(CO)(PPh_3)_3 \leftrightarrow OsHCl(CO)(PPh_3)_2 + PPh_3$$

Table 4.17: Literature data: Isomerization of 1-pentene by an osmium compound [71].

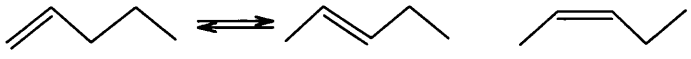

Catalyst	Solvent	T (°C)	Conversion (%)	Selectivity (%) cis -2	Selectivity (%) trans-2	TOF (h^{-1})
$[OsHCl(CO)(PPh_3)_3]$	benzene	85	70	28.6	71.4	21

Conditions: Catalyst: 2.3 mM, 1-pentene: 1M, Total volume: 11 mL.

4.2.5 HETEROGENEOUS ISOMERIZATION

4.2.5.1 SUPPORTED TRANSITION METAL COMPOUNDS

Isomerization and hydrogenation over transition metal supported catalysts are two competing parallel reactions. By varying reaction conditions, it is possible to achieve high isomerization activity and selectivity.

Influence of hydrogen concentration

The activity and selectivity of isomerization and hydrogenation reactions are sensitive to the surface structure and hydrogen adsorption capacity of the metal–support combination [47, 72]. Metals with high hydrogen storage capacity such as Pd show high activity and selectivity for hydrogenation. Others, including Ru, Ni and Pt, favour double bond migration. However, it is not only the metal involved in hydrogen storage, but also the support material.

When the hydrogen availability is high (e.g. for solvents with high hydrogen concentration, in the presence of a hydrogen atmosphere or for catalysts preactivated under hydrogen), the hydrogenation rate is increased. For the double bond migration [47, 48, 73], the Horiuty-Polanyi mechanism with hydrogen addition is favoured, in which the probability of double bond migration is equal to the probability of cis – trans isomerization [72].

At low hydrogen concentration (e.g. when the hydrogen is consumed during the reaction under a nitrogen atmosphere), isomerization is preferred over hydrogenation [47] and the carbenium ion intermediate mechanism is favoured, with the formation of π-allyl complexes resulting from the hydrogen abstraction as the primary step, where the cis – trans isomerization is not allowed [72, 74].

Thus, double bond migration also occurs in the absence of hydrogen. In this case, Bernas et al [47] assume that chemisorbed hydrogen sites are generated by the solvent. Hydrogenation can also takes place with the solvent as the hydrogen

source and therefore the rate is influenced by the nature of the solvent. Heertje et al [72] affirm that catalysts that cannot activate hydrogen by themselves can react by hydrogen abstraction from the olefin with the formation of π-allyl complexes by a carbenium ion intermediate mechanism. Accordingly, the overall reaction rate under a nitrogen atmosphere is lower than in a hydrogen atmosphere, but the isomerization selectivity is higher [47, 50]. The isomerization selectivity increases with conversion and the hydrogenation selectivity decreases with conversion since hydrogen is being consumed.

Influence of temperature

Cis – trans isomerization takes placed by the Horiuty –Ponalyi mechanism and dominates at low temperatures, whereas, at high temperatures, the double bond migration is the favoured reaction. This can probably be attributed to the concentration of adsorbed hydrogen, which is lower at high temperatures [74]. An increase in the reaction temperature results in an increase in the isomerization selectivity [50].

Influence of the solvent

In general, protic solvents generate more hydrogen chemisorbed sites on the catalyst surface than nonpolar solvents. Highly protic solvents, such as methanol or isopropyl alcohol, show high activity and high hydrogenation selectivity [48-50, 73]. Nonpolar solvents, such as hexane, cyclohexane, n-nonane or n-decane, show high isomerization selectivity [50, 73].

Between different protic solvents, the selectivity is affected by the reaction rates and the adsorption strength of the solvent [48]. As the competitive adsorption of the solvent on the catalyst surface increases, the fractional coverage of the olefin decreases. A low ratio of intermediate/hydrogen surface coverage favours the hydrogenation reaction. The conversion can be increased by the use of solvents with a high boiling point, which allow a higher reaction temperature.

Influence of the catalyst support

From studies of different supports, it has been concluded that external diffusion does not affect the catalytic activity or selectivity [50], but, internal diffusion does have an effect. In supports with wide pores, most of the metal particles are located inside the pores and conversion and selectivity are low [47]. As the particle diameter decreases, the initial rate of reaction increases until reaching a constant value which depends on the particle diameter [50].

Bernas et al [49, 50] studied double bond migration with ruthenium on different supports. Ru/C showed the highest conversion, followed in decreasing order by Ru/Al_2O_3 > Ru/H-Y > Ru/H-MCM-41, which is the same order as the hydrogen storage capacity of the supports.

Muskesh et al [75] concluded that, as the support is changed from acidic to basic, the selectivity for isomerization increases due to the absence of hydride transfer reactions taking place on the acid sites.

R. J. Grau et al [42] studied the isomerization over Pd/C and Pd/Al_2O_3. They found that isomerization takes place at the same time as hydrogenation. In the first case, over Pd/C, the involvement of π-allyl adsorbed species explains the isomerization process. In the second case, the alumina-supported catalyst exhibited higher initial activity under comparable conditions. The enhancement of the catalytic activity could be explained by the effects of the support. Two mechanisms take place at the same time, one involving a π-allylic route on palladium and the other, Lewis acid via induced on alumina. Another variable is the pre-treatment of the catalyst. A low temperature reduction of Pd/Al_2O_3 favours the "metallic" character while a high temperature reduction gives an "acidic" character to the catalyst due to an increment in the strong Lewis acidity of the Al_2O_3 [76]. The alumina support appears to be an essential constituent of the isomerization catalyst, following an addition-abstraction mechanism, where the exchanged hydrogen atoms are originally present in the hydroxyl groups bonded to the alumina. Migration of hydrogen atoms from support to metal and vice versa (known as spillover) proceeds at an appreciable rate, and this must be taken into account when

consideration is given to the role of adsorbed hydrogen in reactions catalyzed by supported metals [77].

Influence of the metal

Ru, Ni and Pt have good properties for isomerization. Metals with high hydrogen storage capacity, such as Pd, show high activity and high selectivity for the hydrogenation, whereas other metals, especially Ru, favour double bond migration. The high activity of ruthenium for isomerization is to be expected from the fact that it has vacant d-orbitals, which can interact with σ bonds of olefins as well as activating an adjacent C-H bond, which is a necessary step for double bond migration [50].

Catalysts based on supported Pd, Os, Ir and Pt-Rh show high hydrogenation selectivity [50]. Os/C shows high selectivity for isomerization but very low conversion [49]. Homogeneous Pd has a tendency to cause double bond migration, but this is considerably reduced when Pd is supported [49, 73]. It is commonly believed that the role of the supported Pd is to catalyze the dissociation of H_2 to supply H atoms required for the hydrogenation [76].

The study of different metals shows that, in general, the metals of the third transition series are significantly worse catalysts of isomerization reactions than those of the second transition series and nickel [77]. Other transition metal elements of group VI, Mo(IV), W(IV) and Cr(IV) supported onto silica (a relatively inert support) were studied by Ramani et al [78]. Mo(IV)/SiO_2 and Cr(VI)/SiO_2 catalysts contain well-dispersed cations in the isolated and fully oxidized (6^+) state. On W(VI)/SiO_2, both crystallites of WO_3 and isolated cations of W are present. In all cases, the presence of Brønsted acid sites is detectable. Isomerization through the carbenium mechanism (typically for Brønsted acid sites) is inversely related to cation reducibility (Cr>Mo>W). Both the acidity of the catalyst surface and the cation reducibility are important factors in determining activity and selectivity.

In the case of iron films studied by Tourdoude et al [79], two mechanisms can be responsible for the double bond migration, carbenium intermediate and Houriuti – Polanyi mechanisms, due to the wide heterogeneity of the surface. Apparently, the mechanism differs mostly in the nature and the strength of the olefin adsorption.

In summary, the total conversion is increased by [47]:

i. Increasing the reaction temperature,
ii. Increasing the catalyst metal loading,
iii. Increasing the catalyst quantity,
iv. Decreasing the initial reactive concentration,
v. Decreasing the catalyst particle size and
vi. Changing the nature of the solvent.

Isomerization selectivity is increased by [47]:

i. Decreasing the catalyst quantity,
ii. Increasing the initial reactive concentration and
iii. Changing the nature of the solvent.

Conversion and selectivity are influenced by:

i. the total amount of hydrogen,
ii. reaction conditions,
iii. deactivation of the catalyst (blocking of pores and coke formation),
iv. availability of active vacant sites on the catalyst surface and
v. competitive adsorption between olefin, solvent and reactions products.

Table 4.18: Literature data: Isomerization of linoleic acid by supported transition metals compounds [49].

Catalyst	Solvent	T (°C)	Conversion (%)	Selectivity (%)		TOF (h^{-1})
				Isomerization	Hydrogenation	
Ru/C[a]	1-octanol	120	78	42.3	57.7	1.56
Ru/Al_2O_3[a]	n-decane	120	44	63.6	36.4	0.88
Ru/H-MCM-41[a]	n-decane	120	30	70	30	0.60
Ru/H-Y[a]	n-decane	120	31	77.4	22.6	0.62
Ru/H-β[a]	n-decane	120	47	76.6	23.4	0.94
Ni/H-MCM-41[a]	n-decane	120	51	72.5	27.4	0.36
Ni/MCM-22[a]	n-decane	120	51	66.7	33.3	0.36
Ni/H-Y[a]	n-decane	120	27	74.1	25.9	0.19
Ni/H-β[a]	n-decane	120	37	67.6	32.4	0.25
Ni/Al_2O_3[a]	1-octanol	120	11	54.5	45.5	0.03
$Ni/SiO_2Al_2O_3$[a]	1-octanol	120	43	30.2	69.8	0.15
Pd/Al_2O_3[a]	n-decane	120	91	17.6	82.4	1.15
Pd/H-MCM-41[a]	n-decane	120	100	4	96	1.26
Pd/H-Y[a]	n-decane	120	78	21.7	78.3	0.98
Pt/Al_2O_3[a]	n-decane	120	14	21.4	78.6	0.32
Pt/H-Y[a]	n-decane	120	40	72.5	27.5	0.93
Pt/H-MCM-41[a]	n-decane	120	85	30.6	69.4	0.98
Pt-Rh/C[a]	1-octanol	120	63	58.7	41.3	1.46
Ir/C[a]	1-octanol	120	55	50.9	49.1	1.25
Rh/C[a]	1-octanol	120	31	51.6	48.4	0.38
Os/C[a]	1-octanol	120	14	57.1	42.8	0.32
Ru/C[b]	free	165	85	96	4	4.36
Ru/Al_2O_3[b]	free	165	3	-	-	0.1
Pd/C[b]	free	165	61	68	32	2.6
Os/C[b]	free	165	24	68	32	1.82
Ir/C[b]	free	165	65	46	54	5.59
Pt-Rh/C[b]	free	165	52	66	44	3.9

Conditions: [a] Linoleic acid: 200 mg, solvent: 70 mL, 1 atm of N_2, time: 6h.
[b] Linoleic acid: 70 mL, 1 atm of N_2, time: 24h.

4.2.5.2 ANCHORED TRANSITION METAL COMPLEXES

Another possible way to heterogeneize transition metal complexes is to entrap them in sol-gel matrices. Sertchook et al [80] anchored the Stephenson ($RuCl_2(PPh_3)_3$), Wilkinson ($RhCl(PPh_3)_3$) and Vaska ($IrCl(CO)(PPh_3)_3$) complexes onto silica, alumina, and polystyrene resin. The advantages of this approach are that the catalysts become recyclable over several runs and the air sensitivity of these complexes can be reduced substantially. The disadvantage is that the catalytic activity decreases compared to the homogeneous catalysts due to a partial blockage of the pores during the catalytic process or a slow reduction of the metal.

Zoran et al [81] anchored the same catalysts onto a polystyrene matrix (styryldiphenylphosphine resin). The activity of the rhodium catalyst dropped after the first run due to extensive leaching. However, the ruthenium catalyst became particularly efficient due to a chemical modification leading to the formation of immobilized ruthenium hydride. It was found that mixtures of good swelling solvents and potent hydrogen donors enhance catalytic efficiency and due to the differences between the activation energy in the homogeneous and heterogeneous cases, they suggest that the heterogeneous reaction is diffusion controlled.

4.2.5.3 ZEOLITES

Double bond migration on zeolite catalysts can proceed by the carbenium intermediate mechanism, as in many acid-catalyzed reactions over the Brønsted acid sites or, to a lesser degree, by a π-allylic carbanion intermediate formed by abstraction of H^+ [36].

Kondo et al [35, 36] studied double bond migration over different zeolites. The reaction is not observed on zeolites with very weak Brønsted acid sites as Y type zeolites nor on Na-exchanged ZSM-5. On weak Brønsted acid sites, such as those found in faujasite zeolites, the adsorption of the olefin is weak due to the weak acidity, but the reaction does takes place. Strong acidity of Brønsted acid sites was found to be important for double bond migration to occur in the experiments

carried out with ZSM-5 zeolites (Si/Al = 50) where each Brønsted acid site is well separated and each adsorbed olefin molecule forms a 1:1 complex with an isolated Brønsted acid site.

On mordenite zeolites, the reaction takes place also without proton transfer. This zeolite structure has stronger Brønsted acidity and a larger pore size than ZSM-5. This means that with small pore size, as in the case of ZSM-5, the secondary interaction of the adsorbed molecules with lattice oxygens is not the cause of the reaction.

Shell Oil Co has patented other zeolitic structures with 8 to 10 member ring channels as ZSM-35, ZSM-12, ZSM-22, ZSM-23 and ZSM-48 [82]. They select a channel size sufficient to permit the double bond migration and prohibit side reactions such as aromatization or alkylation. These aluminosilicates can be modified with metals as palladium, platinum, ruthenium, nickel, cobalt, molybdenum, osmium in quantities up to 25 wt%.

4.2.5.4 BASE CATALYSTS

There are some cases where basic oxides have been used for the double bond migration reaction, which does not require a strong basicity [83]. The isomerization takes place by the carbenium intermediates mechanism [83, 84]. The olefins adsorb associatively to the catalyst to form π-complexes. The hydrogen transfer step necessary for the double bond migration occurs by an intramolecular mechanism rather than an intermolecular one. At the same time as the double bond migration, the cis – trans isomerization also occurs via a σ-allyl intermediate but to a very low extent.

Rosynek at al [84, 85] studied the reaction over lanthanum oxide (La_2O_3) and observed very high rates of double bond migration and very slow cis – trans isomerization due to the absence of sites on La_2O_3 that permit the required anti-π-allyl ↔ syn-π-allyl rotation to occur. For this oxide, increasing the calcination temperature increases the catalytic activity due to the removal of trace surface

contaminants, such as carbonate ions, hydroxyl species or adsorbed water and generation of stoichiometric and/or structural defects, such as anion vacancies or disorders and exposed metal ions, which serve as catalytic sites.

Aranmendía and Na [83, 86] used various solids, including magnesium oxide, several mixed magnesium-titanium oxides and magnesium-zirconium oxide, obtaining a trans/cis ratio of about six for all catalysts. The conversion increases with increasing basicity of the catalyst.

Table 4.19: Literature data: Isomerization of 1-butene by a basic catalyst [85].

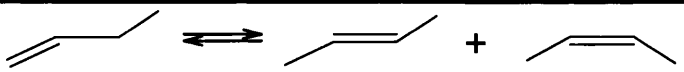

Catalyst	T (°C)	Conversion (%)	Selectivity (%) cis -2	Selectivity (%) trans -2	time
La_2O_3	20	90	70	20	70 min

Table 4.20: Literature data: Isomerization of allylbenze by basic catalysts [34].

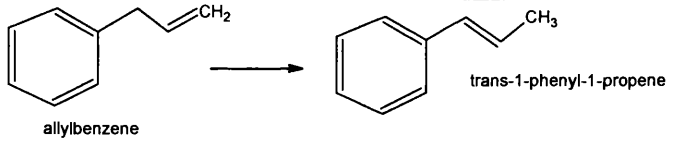

Catalyst	Solvent	T (°C)	Conversion (mole/g cat)
Mg-AIR	free	250	2.15
Mg-OX	free	250	3.07
MgZr27-OX	free	250	3.32
MgTi5-OX	free	250	4.24
MgTi19-OX	free	250	4.14
MgTi31-OX	free	250	3.08

4.2.5.5 HETEROPOLY SALTS AND OXOMETALATES

Metal-oxygen cluster compounds (also known as heteropoly oxometalates) can be synthesized with different structures. The Keggin anion, $(XM_{12}O_{40})^{n-}$, is the most

interesting due to its catalytic properties. Its approximately spherical structure is formed by a central atom (X) bonded tetrahedrally to four oxygen atoms. This tetrahedron is surrounded by twelve interconnecting octahedra, each consisting of a peripheral metal atom (M) with six oxygen atoms at their vertices. The resulting charge of the Keggin anion depends on the oxidation states of the central and peripherical metal atoms.

When the Keggin anion is balanced with protons, solid acids are formed, such as $H_3PW_{12}O_{40}$, $H_3PMo_{12}O_{40}$, $H_4SiW_{12}O_{40}$, which are good skeletal isomerization catalysts [86]. Substitution of the protons by certain of the monovalent cations from Group 1 of the periodic table produces salts with microporous structures and relatively high surface areas, in which rotation and translation of the Keggin anions in the lattice structure is possible, causing changes in the chemical environment [38].

Parent et al [38, 87] studied double bond migration over different thallium salts of $H_3PW_{12}O_{40}$. Strong Brønsted acid sites and elevated temperature are required to facilitate the skeletal isomerization but none of the catalysts investigated possessed sites of sufficient strength. As the cation to proton ratio with a given anion increases, the conversion decreases, regardless of the temperature. For different salts, the ratio of cis/trans isomers increases with an increase in the cation to proton ratio, for all temperatures.

Table 4.21: Literature data: Isomerization of 1-butene by heteropoly salts [38].

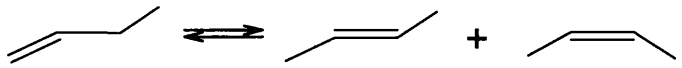

Catalyst	Diluent	T (°C)	Conversion (%)	Selectivity (%)	
				cis -2	trans-2
$H_3PW_{12}O_{40}$	helium	100	70	26.5	73.5
$H_3PW_{12}O_{40}$	helium	200	86	33.2	66.8
$H_3PW_{12}O_{40}$	helium	300	82	38	62
$H_3PMo_{12}O_{40}$	helium	100	5	55.2	48.2
$H_3PMo_{12}O_{40}$	helium	200	9	53.2	46.8
$H_3PMo_{12}O_{40}$	helium	300	4	49.4	50.6
$H_4SiW_{12}O_{40}$	helium	100	85	27.1	72.9
$H_4SiW_{12}O_{40}$	helium	200	85	35.9	64.1
$H_4SiW_{12}O_{40}$	helium	300	81	38	62
$Tl_3PW_{12}O_{40}$	helium	100	88	26.8	73.2
$Tl_3PW_{12}O_{40}$	helium	200	87	32.3	64.7
$Tl_3PW_{12}O_{40}$	helium	300	82	39.5	60.5
$Tl_3MoW_{12}O_{40}$	helium	100	28	49.1	50.9
$Tl_3MoW_{12}O_{40}$	helium	200	59	51.6	48.4
$Tl_3MoW_{12}O_{40}$	helium	300	57	51.4	48.6
$Tl_4SiW_{12}O_{40}$	helium	100	34	65.4	34.6
$Tl_4SiW_{12}O_{40}$	helium	200	67	44.7	55.2
$Tl_4SiW_{12}O_{40}$	helium	300	82	39.6	60.4

Conditions: time: 10 min, catalyst: 150 mg. Gas phase.

4.2.5.6 HYDROTALCITES

The general formula of the hydrotalcites is M(II)M(III)-xHT with carbonate as the interlayer anion where M(II) = Mg, Ni, Co, Zn, Cu and M(III) = Al, Cr, Fe, La, V with varying M(II)/M(III) ratio (denoted by x). By changing the nature of the cations in the layers, M^{2+}/M^{3+} ratio, the nature of the compensating anions or the activation methodology, it is possible to modify the acid-base properties of these catalysts.

Kishore et al [61] studied the influence of different parameters for the isomerization of isoeugenol. Solvents with high polarity, such as dimethyl sulfoxide (DMSO) or N,N-dimethyl formamide (DMF), show higher activity than solvents with lower polarity such as tetrahydrofuran (THF) or toluene. They investigated the effect of varying the bivalent and trivalent metal ions, concluding that the best combination was MgNiAl-15HT. In these structures, the structural hydroxyl groups act as Brønsted basic sites, particularly those present at the edges and surface, which are accessible for the reactant molecules, which suggest that the reaction mechanism involves hydroxyl groups.

Table 4.22: Literature data: Isomerization of eugenol by hidrotalcites [61].

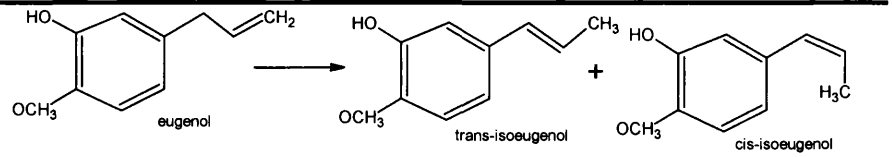

Catalyst	Solvent	T (°C)	Conversion (%)	Selectivity (%)	
				cis	trans
MgAl-4HT	DMF	200	73	16	84
NiAl-4HT	DMF	200	75	15	85
ZnAl-4HT	DMF	200	6	-	100
CuAl-4HT	DMF	200	-	-	-
CoAl-4HT	DMF	200	-	-	-
MgNiAl-51HT	DMF	200	59	20	80
MgNiAl-31HT	DMF	200	65	17	83
MgNiAl-11HT	DMF	200	53	21	85
MgNiAl-13HT	DMF	200	85	15	85
MgNiAl-15HT	DMF	200	94	16	84

DMF: N,N-dimethyl formamide
Reaction conditions: Eugenol: 0.5g, solvent: 20 mL, catalyst: 250 mg, time: 6h.

4.3 RESULTS AND DISCUSION: ISOMERIZATION OF ALLYLBENZENE

The isomerization of allylbenzene reaction was chosen to test the efficacy of novel catalysts, composed of metals supported on titanate nanotubes, for the double bond migration reaction (first reaction in the tandem system purposed). This reaction is a simple reaction with a narrow distribution of products. The double bond migration of allylbenzene produces trans-phenyl propene as the desired product (the unfavourable cis-isomer is less than 5% of the product in equilibrium [88]). The skeletal isomerization produces α-methyl styrene and hydrogenation of the double bond gives propyl-benzene and cumene. A scheme with all of these possible reactions is shown in the Figure 4.14.

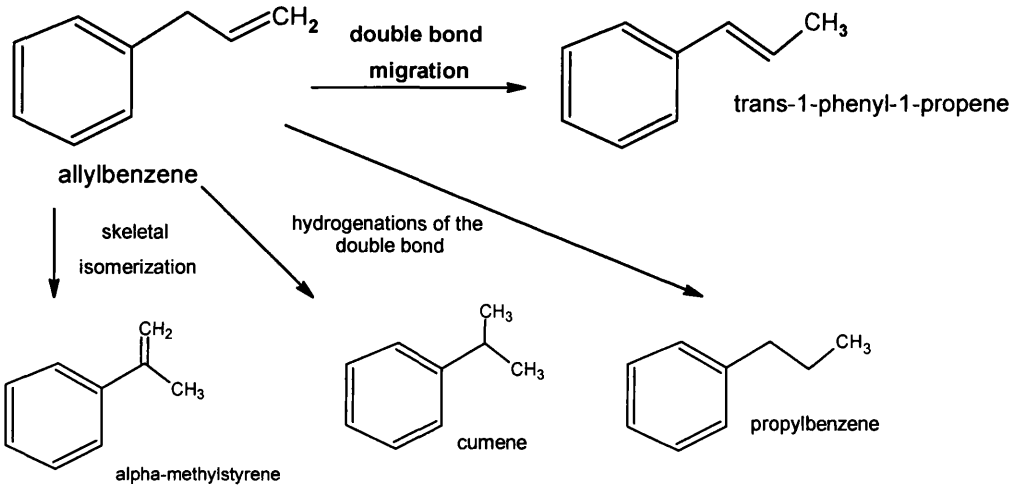

Figure 4.14: Scheme of potential reactions with allylbenzene as reactant.

4.3.1 HOMOGENEOUS ISOMERIZATION

In order to compare the synthesised heterogeneous catalysts and homogeneous ones under same conditions, some reactions were carried out with palladium chloride ($PdCl_2$), bis(benzonitrile) dichloropalladium (II) ($PdCl_2(PhCN)_2$),

rhodium(I) tris(triphenylphosphine) chloride ($ClRh(PPh_3)_3$), Rh(acac)(CO) and palladium acetate.

The procedure followed to assess the performance of these reactions consists on a reflux reactor described in Chapter 2. In all cases, the catalyst concentration was $5 \cdot 10^{-4}$ M. When $PdCl_2$ or $PdCl_2(PhCN)_2$ were used as a catalyst, some HCl was added to the solution to stabilize the catalyst.

The reaction profiles of all these reactions are shown in Figure 4.15.

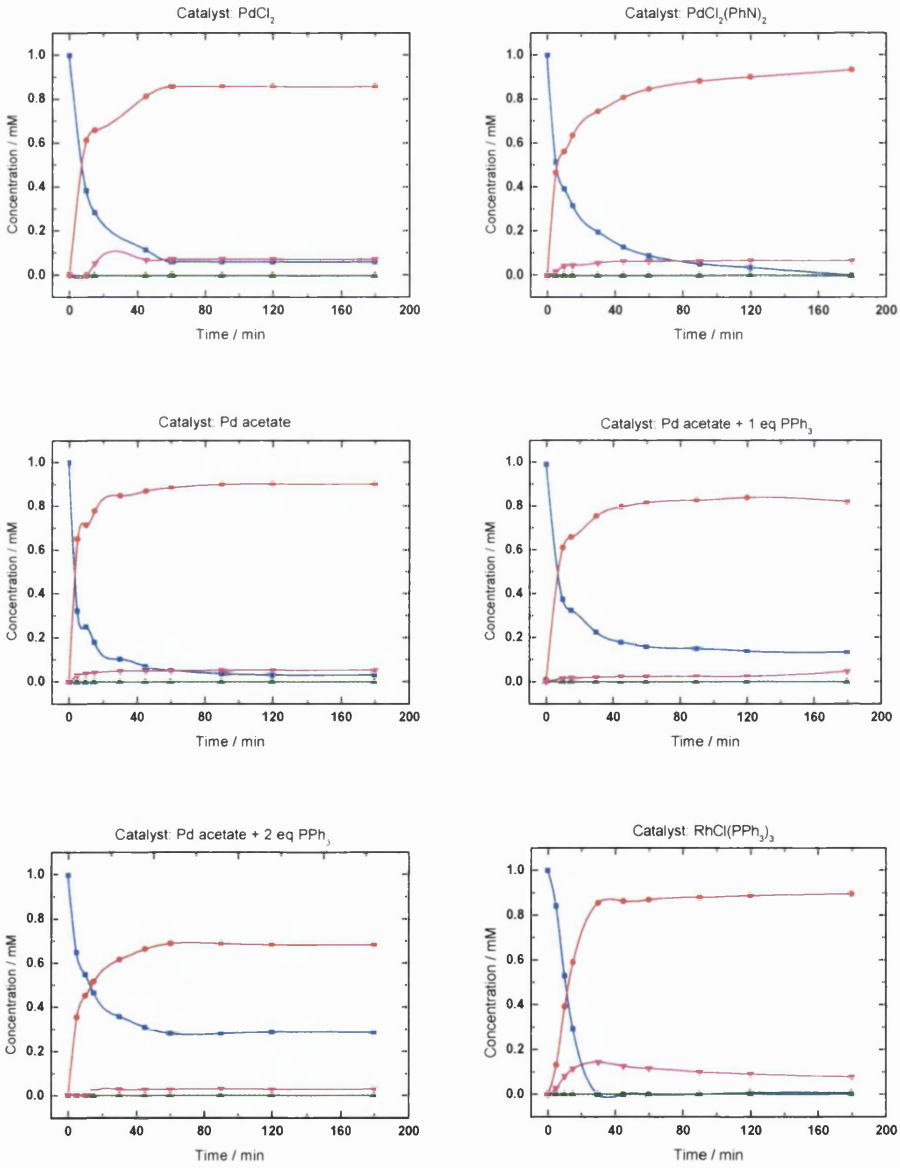

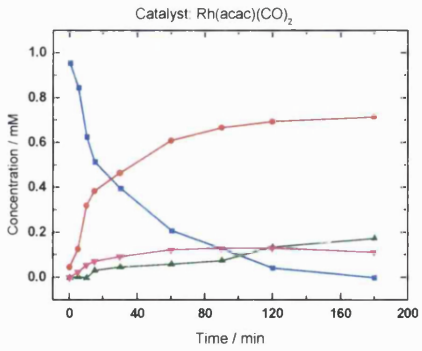

Figure 4.15: Reaction profiles of homogeneous catalysed isomerization of allylbenzene. Chemical components legend: ■ allylbenzene, ● trans-phenyl propene, ▲ propyl benzene ▼ unidentified.

These homogeneous catalysts show very good conversion in the isomerization of allylbenzene, with very high selectivities except in the case of Rh(acac)(CO), when hydrogenation products (propylbenzene) appeared. However, in all of these reactions, the homogeneous catalyst decomposes in the reaction medium forming metal nanoparticles which agglomerate and precipitate. Not all of the catalysts showed the same stability, with the time before decomposition was observed varying between five minutes to one hour. In order to stabilize the palladium atom in solution, when palladium acetate was used as catalyst, one and two equivalents of triphenylphosphine (PPh_3) ligand were added. When the ligand was presented, the catalyst was more stable; however, the conversions were lower. If the triphenylphosphine is bound to the palladium atom, the stability is higher, thus making the access of the reactant molecule to the palladium atom more difficult. In Table 4.23, conversions, selectivities, initial rates of reaction and times when the first sign of decomposition was observed are shown.

Table 4.23: Conversions, selectivities, initial rate of reaction and decomposition time obtained with different homogeneous catalysts in the isomerization of allylbenzene.

Catalyst	Conversion at 30 min (%)	Conversion at 3h (%)	Selectivity (%)	Initial rate ($mol \cdot s^{-1} \cdot g^{-1}$)	TON at 30 min	time to decompose (min)
$PdCl_2$	80.1	95.1	91.3	$8.36 \cdot 10^{-4}$	160.2	within 5
$PdCl_2(PhCN)_2$	80.2	100	93.3	$8.37 \cdot 10^{-4}$	160.4	within 5
Pd acetate	89.6	97.8	92.1	$9.35 \cdot 10^{-4}$	179.2	within 5
Pd acetate + 1 eq. PPh_3	78.2	87.5	94.5	$8.16 \cdot 10^{-4}$	156.4	within 10
Pd acetate + 2 eq. PPh_3	64.2	71.3	95.8	$6.70 \cdot 10^{-4}$	128.4	30
$RhCl(PPh_3)_3$	100	100	88.1	$1.08 \cdot 10^{-3}$	200	
Rh(acac)(CO)	63.2	100	71.2	$6.82 \cdot 10^{-4}$	126.4	60

Conditions: Allylbenzene: 10^{-3}M, solvent: EtOH 100mL, Catalyst: $5 \cdot 10^{-4}$M, T = 75°C.

4.3.2 HETEROGENEOUS ISOMERIZATION

4.3.2.1 Palladium on titanate nanotubes

The results presented in this section have already been published [89] (Appendix III).

It is interesting to investigate the activity of Pd/titanate nanotubes catalysts in the double bond migration reaction. In most previous studies of heterogeneous Pd catalysts for double bond migration reactions, the metal deposited from a salt solution was reduced by hydrogen or formic acid prior to catalytic tests, generating a Pd (0) catalytic species. However, it was also shown that supported Pd catalysts, in which the palladium was not reduced, exhibited higher selectivity towards double bond migration than reduced catalysts, which tend to be more selective towards hydrogenation [90]. The nature of the titanate support and the ion-exchange preparation mechanism may allow stabilisation of the ionic metal species, and therefore it could give high selectivity towards double bond migration

reaction. There is only one report in the literature of a Pd/titanate nanotubes catalyst, prepared by reduction of $PdCl_2$ by glycol [91].

Catalytic tests were performed following the procedure described in Chapter 2. Reactions performed at 50°C showed no conversion, so the following reactions were carried out at 75°C. In order to study the influence of palladium loading, a set of reactions were firstly done with the percentage of palladium supported on titanate nanotubes being varied from 2.9 to 10.1% wt. The reaction profiles are shown in Figure 4.16.

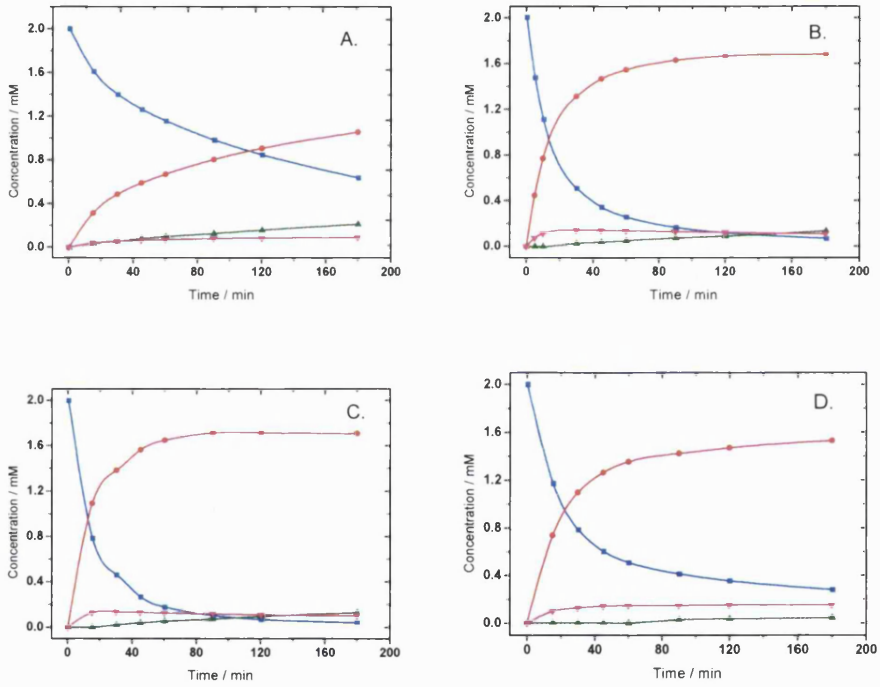

Figure 4.16: Isomerisation reaction profiles in EtOH at T = 75°C by Pd (II)/titanate nanotubes, (A) 2.9% (B) 6.9% (C) 8.8% (D) 10.1% wt of Pd. Chemical components legend: ■ allylbenzene, ● trans-phenyl propene, ▲ propyl benzene ▼ unidentified.

In all reactions with Pd(II)/titanate nanotubes as the catalyst, the main reaction was the double bond migration to trans-phenyl propene. However, dimerization (based on the assumption that the unidentified product is a dimer due to its retention time) and hydrogenation also occurred, although in much smaller quantities. In Table 4.24, conversions, selectivities, TOF numbers and initial rate of reaction are summarized.

Table 4.24: Activity and selectivity data on Pd (II)/titanate nanotubes for isomerisation reaction.

Pd species	Pd (%wt)	Conversion @ 0.5h (%)	Conversion @ 3 h (%)	Selectivity (%)	TOF @ 0.5h (h^{-1})	Initial rate ($mol \cdot s^{-1} \cdot g^{-1}$)
Pd(II)	2.9	28.9	68.0	77.1	2.18	$5.7 \cdot 10^{-6}$
Pd(II)	6.9	74.4	96.4	87.1	2.27	$5.9 \cdot 10^{-6}$
Pd(II)	8.8	77.01	98.9	86.2	1.85	$4.8 \cdot 10^{-6}$
Pd(II)	10.1	61.0	86.1	88.6	1.28	$3.3 \cdot 10^{-6}$

Reaction conditions: T = 75°C, solvent: ethanol 100mL, allylbenzene: 0.002 M.

The conversion as a function of Pd(II) loading follows a "volcano" plot shown in Figure 4.17. The conversion values increase with the loading of supported palladium (II) and then decrease with the highest loading, showing a maximum conversion at 8-9 wt% Pd. Selectivity was found to be a weak function of metal loading and varied between 80-90 %. This can be explained by the similarity in the particle size of the metal observed by TEM for catalysts with 4-9 %wt metal loading (see Chapter 3).

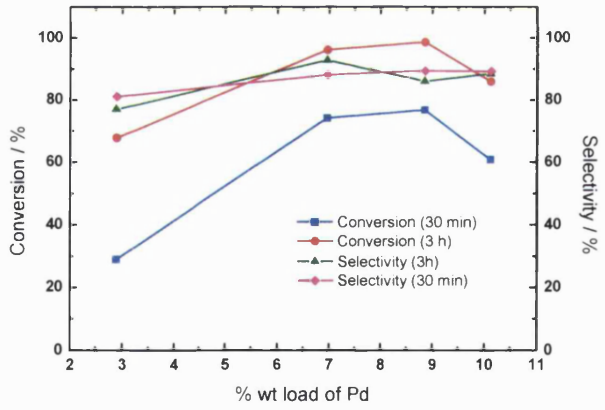

Figure 4.17: Conversion and selectivity at different loadings of palladium on titanate nanotubes. Reaction conditions: T = 75°C; solvent ethanol; initial concentration of reactant 0.002 M.

In all reactions, the orange-brown catalysts become completely black within first five minutes. This change of colour is due to the reduction of palladium (II) to palladium (0) as confirmed by XPS. XPS analysis of the fresh catalyst, after blank reaction (using ethanol as the solvent) and after double bond migration reactions were performed to determine the oxidation state of palladium in all the cases.

Figure 4.18 shows the Pd 3d region which reveals that, in the fresh catalysts, a mixture of Pd (II) and Pd (0) is present as indicated by the Pd $3d_{5/2}$ components at 337.1 and 335.5 eV respectively. The initial catalyst starts off with ~56 % of the Pd present as Pd (II), however, following exposure to EtOH or after the isomerisation reaction, the Pd (II) component decreases to 12.5 and 18.3 % respectively. The corresponding increase in the relative intensity of the 335.5 eV component was attributed to Pd (0), indicating that reduction of the catalysts has occurred.

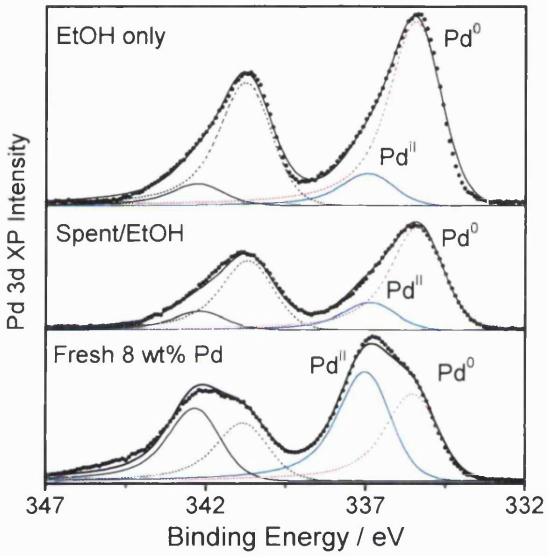

Figure 4.18: XPS analysis of Pd (II)/titanate nanotubes catalyst with 6.97 wt% Pd loading: equilibrated in EtOH at reaction conditions, after reaction and fresh "as prepared" catalyst.

A second set of reactions were done with Pd(0)/titanate nanotubes as the catalyst. The Pd(II) catalysts were pre-reduced before the reaction with $NaBH_3$ in aqueous, ethanolic and phosphine solutions. The reaction profiles are shown in Figure 4.19.

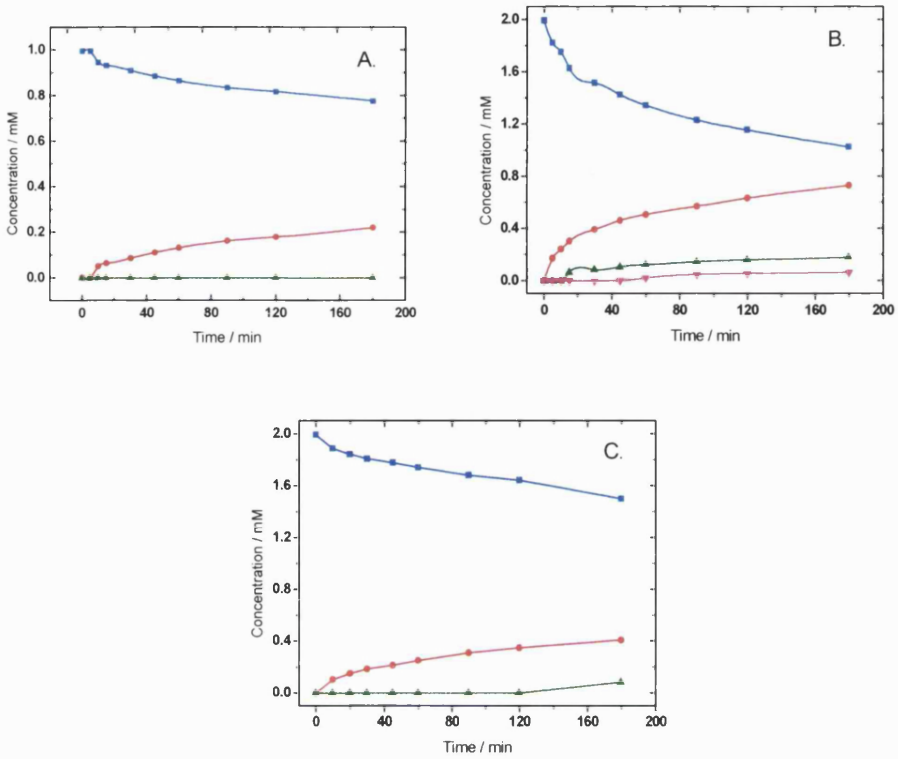

Figure 4.19: Isomerisation reaction profiles in MeOH at T = 60°C by pre-reduced 7.3 wt% Pd (0)/titanate nanotubes, (A) in H_2O (B) in EtOH and (C) in an aqueous PPh_3. Chemical components legend: ■ allylbenzene, ● trans-phenyl propene, ▲ propyl benzene.

In all reactions carried out with Pd(0)/titanate nanotubes as catalysts, the main product formed is the desired trans-phenyl propene, although other by-products are also presented in very low quantities. The conversions and selectivities are summarized in Table 4.25. The conversion values obtained in these cases are much lower compared with the Pd(II) catalyst, which indicates that Pd(II) species are much more active for the double bond migration than Pd(0) species. The selectivity values are in the same range which indicates that both Pd(II) and Pd(0) are responsible for the hydrogenation reaction. The medium in which the catalyst is pre-reduced also influences on its activity, suggesting that the ligand attached to the palladium(0) nanoparticle might have a role in the accessibility of the reactant molecule.

Table 4.25: Influence of ligands used in the preparation of Pd (0)/titanate nanotubes catalyst on activity and selectivity in double bond migration.

Pd species	Reduced in	Pd (%wt)	Initial cc (M)	Conversion @ 0.5h (%)	Conversion @ 3 h (%)	Selectivity (%)
Pd^0	H_2O	7.3	0.001	8.6	22.1	100
Pd^0	Ethanol	7.3	0.002	24.1	48.6	75.2
Pd^0	PPh_3	6.9	0.002	9.32	24.7	83.0

Conditions: Reactions in Methanol, T = 60° C.

By varying the initial concentration of reactant (allylbenzene) between 1 and 10 mM, different conversions and selectivities were obtained (see Table 4.26). In all cases, a high selectivity (around 90 %) to the double bond migration product was obtained at high conversions, except for the reaction with the lowest initial reactant concentration. In the latter case, almost 100 % conversion of allylbenzene is achieved in two hours of reaction; the very high extent of hydrogenation reaction results in decreased selectivity. The reaction profile for the reaction with low initial concentration of allylbenzene is shown in Figure 4.20. The decrease in the main product concentration appears to coincide with an increase in the rate of formation of the hydrogenation by-product.

Table 4.26: Conversions and selectivities obtained with different reactant concentrations using 6.97 wt% Pd (II)/titanate nanotubes catalyst.

Pd species	Pd (wt%)	Initial cc (M)	Conversion @ 0.5h (%)	Conversion @ 3h (%)	Selectivity (%)	TOF @ 0.5h (h^{-1})	Initial rate ($mol \cdot s^{-1} \cdot g^{-1}$)
Pd(II)	6.9	0.001	68.4	100	69.3	1.04	$2.72 \cdot 10^{-6}$
Pd(II)	6.9	0.002	74.4	96.4	93.0	2.27	$5.93 \cdot 10^{-6}$
Pd(II)	6.9	0.005	13.9	33.7	86.9	1.06	$2.77 \cdot 10^{-6}$
Pd(II)	6.9	0.01	5.1	12.5	86.8	0.77	$2.03 \cdot 10^{-6}$

Reaction conditions: T = 75°C, solvent: ethanol 100 mL, reactant: allylbenzene.

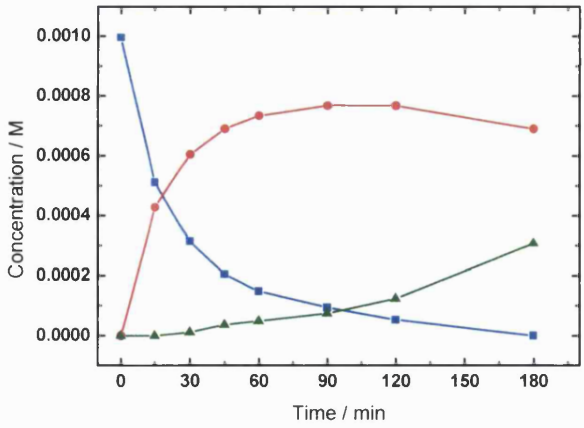

Figure 4.20: Isomerisation reaction profiles of 0.001M of allylbenzene in EtOH at T = 75°C using 6.9 wt% Pd(II)/ titanate nanotubes catalyst. Chemical components legend: ■ allylbenzene, ● trans-phenyl propene, ▲ propyl benzene.

It is known that palladium has a tendency to cause double bond migration [49]; however, all previous literature indicates that selectivity towards double bond migration is significantly reduced when supported palladium is used. Bernas et al [50] supported palladium on Al_2O_3, H-MCM-41 and H-Y, obtained less than 30% selectivity for the double bond migration versus hydrogenation of the olefin, except when the support was carbon when high selectivity (68%) was obtained. In our reactions, higher selectivity values are obtained. Nevertheless, it is difficult to compare the activity and selectivity of our catalysts with the literature data.

Influence of solvent

Different solvents were tested for the double bond migration reaction (Table 4.27). For the same palladium loading on titanate nanotubes (6.9 wt%), a high conversion was obtained when an alcohol was used as solvent (ethanol or methanol), with the highest conversion being obtained with ethanol. When non-polar solvents, n-hexane and NPM, were used the conversions obtained were much lower than in the case of the protic solvents or even zero.

The solvent clearly has an important effect on the rapid reduction of Pd (II), which can be monitored by the changes in the colour of the catalyst samples. Reduction of Pd (II) by the solvent has been proven in a blank experiment by XPS (Figure 4.18). With n-hexane or NMP as the solvent, the change in the colour of the catalyst due to the reduction of palladium, observed in almost all reactions, is much slower than in the case of alcohols solvents. In the case of reduced metal catalysts, the effect of the solvent has been attributed to the competitive sorption of solvent molecules on the active metal [42], with ethanol being treated as a special case.

Table 4.27: Influence of solvent on the activity and selectivity of Pd (II)/titanate nanotubes catalyst.

Pd species	Solvent	Pd (%wt)	Initial cc (M)	Conversion @ 0.5h (%)	Conversion @ 3 h (%)	Selectivity (%)
Pd(II)	Ethanol	6.9	0.002	74.4	96.4	93.0
Pd(II)	MeOH	6.9	0.002	16.9	60.1	82.6
Pd(II)	MeOH : EtOH	6.9	0.002	20.5	49.6	85.7
Pd(II)	NMP	6.9	0.002	0	0	0
Pd(II)	Hexane	6.9	0.002	3.6	16.6	100

Conditions: Temperature: 75°C when ethanol and NMP were used as solvent and 60°C for methanol and hexane.

Catalyst stability

Stability and re-usability of catalysts was tested by adding fresh reactant to the reaction mixture after completion of a reaction. The reaction profiles are shown in Figure 4.21. Taking into account dilution factor, the initial rates in the three consecutive reactions are $4.83 \cdot 10^{-6}$, $1.26 \cdot 10^{-6}$ and $7.19 \cdot 10^{-7}$ $mol \cdot s^{-1} \cdot g^{1}$. The apparent decrease in the rate of reaction is most likely due to the irreversible reduction of Pd (II) into less active Pd (0) species.

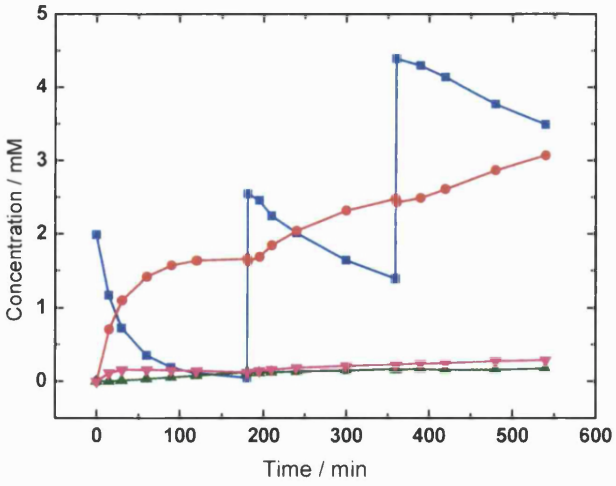

Figure 4.21: Concentration profiles in three consecutive runs. Reaction conditions: 0.2 g of 10.1 wt% Pd (II) /titanate nanotubes catalyst; initial concentration of allylbenzene: 0.002 M, solvent: ethanol, 75°C. Chemical components legend: ■ allylbenzene, ● trans-phenyl propene, ▲ propyl benzene, ▼ unidentified.

Direct oxidation of Pd (0) by oxygen has been suggested as a method of in-situ regeneration of the catalyst. The results obtained with and without air purge during a reaction are shown in Figure 4.22. A higher initial reaction rate was found when the reaction was performed in the presence of air. This is likely to be due to a temporary stabilisation of the active species by oxygen. Consecutive addition of fresh reagent after completion of the reaction resulted in the same reaction rate as that observed in the absence of oxygen.

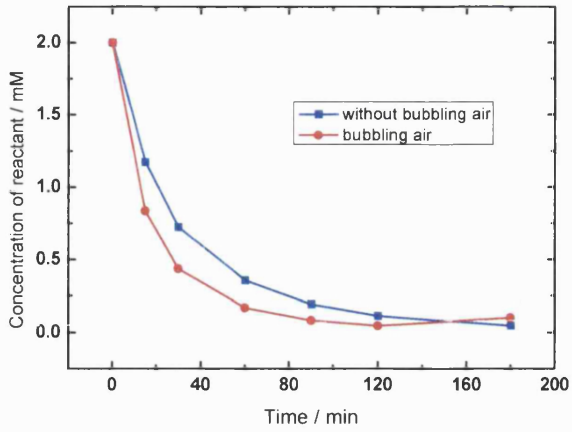

Figure 4.22: Reactant concentration profiles with and without bubbling air in the reaction medium. Reaction conditions: Catalyst: 0.2 g of 10.1 wt% Pd (II) /titanate nanotubes catalyst; initial concentration of allylbenzene: 2 mM, solvent: ethanol, temperature: 75°C.

In order to test the possible leaching of palladium into the reaction medium during the reactions, different blank reactions were carried out in methanol and in the presence of ligands such as triphenylphosphine (PPh_3) and an imidazolium salt (IMes·HCl), which are able to stabilize the palladium atom in solution at 60°C during 20 hours. None of the catalysts leached palladium in the presence of different ligands under these conditions.

4.3.2.2 Rhodium on titanate nanotubes

Similar tests were carried out using rhodium supported on titanate nanotubes rather than palladium. All catalytic tests were performed with methanol as the solvent at 60°C. In order to study the influence of the rhodium loading, a set of reactions were firstly done with the rhodium loading varying between 2.5 – 7 wt% Rh. The reaction profiles are shown in Figure 4.23.

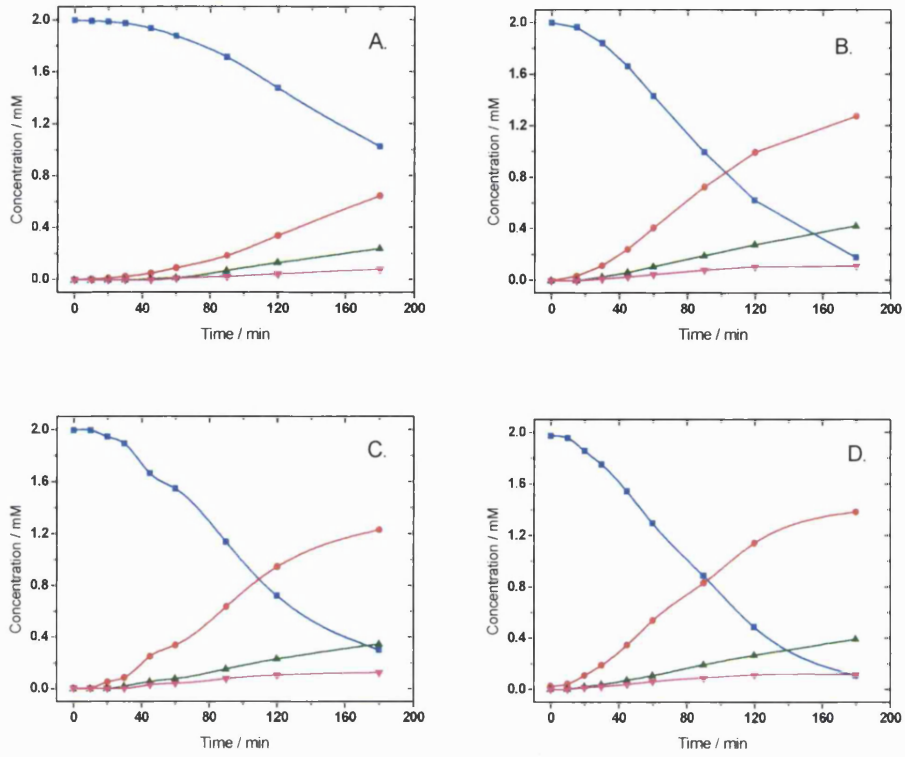

Figure 4.23: Isomerisation reaction profiles in MeOH at T = 60°C by Rh (III)/titanate nanotubes, (A) 2.3% (B) 4.5% (C) 5.1% (D) 6.3% wt of Rh. Chemical components legend: ■ allylbenzene, ● trans-phenyl propene, ▲ propyl benzene ▼ unidentified.

In all of these reactions, the main reaction is double bond migration, with trans-phenyl propene as desired product. However, hydrogenation products are also formed. In Table 4.28, conversions, selectivities, TOF number and initial rate of reaction are summarized.

Table 4.28: Activity and selectivity data on Rh (III)/titanate nanotubes for isomerisation reaction.

Rh species	Rh (%wt)	Initial cc (M)	Conversion @ 0.5h (%)	Conversion @ 3h (%)	Selectivity (%)	TOF @ 3 h (h^{-1})
Rh(III)	2.3	0.002	1.3	48.7	66.5	0.71
Rh(III)	4.5	0.002	7.9	90.8	70.2	0.68
Rh(III)	5.1	0.002	5.1	84.9	72.3	0.56
Rh(III)	6.3	0.002	12.5	95.7	73.2	0.52
Rh (0)	4.5	0.002	20.1	91.3	70.0	0.68
Rh(III)	4.5	0.004	3.5	42.1	86.4	0.63

Reaction conditions: T = 60°C, solvent: methanol.

The conversion and selectivity values as a function of Rh(III) loading are shown in Figure 4.24. At low rhodium loading, the conversion value is lower compared with higher rhodium loadings where the conversion apparently reaching a plateau (around 90%) for loadings greater than 5% wt. Selectivity is independent of the rhodium loading, remaining constant at approximately 70%. However, if a higher initial concentration of reactant is used, the selectivity increased to approximately 90%. This suggests again that both isomerization and hydrogenation reactions are consecutive reactions.

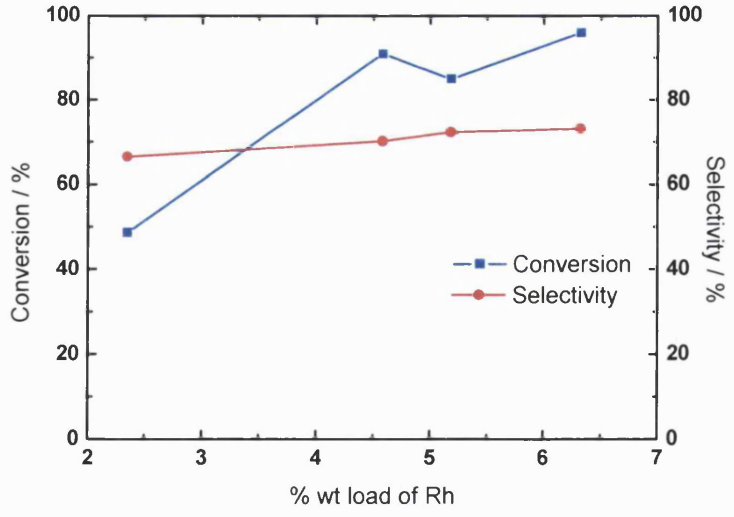

Figure 4.24: Conversion and selectivity at different loadings of rhodium on titanate nanotubes. Reaction conditions: T = 60°C; solvent methanol; initial concentration of reactant 0.002 M.

In all reactions, the colour of the catalyst, which was orange when the catalyst was fresh, became darker during the reaction but contrary to that on the palladium case, the change of colour is not complete in three hours and takes place very slowly. XPS analyses of the fresh and pre-reduced catalysts, both before and after reaction were done in order to determine the oxidation state of rhodium. The results are shown in Figure 4.25, which shows the Rh 3d region. The spectra can be deconvoluted into three components, for Rh 3d binding energies of 310.9, 308.9 and 307.5 eV, corresponding to Rh (III), Rh (I) and Rh(0) respectively. As an example, the fresh catalyst with 5.2% wt Rh is a mixture of only 62% Rh(III) and 37% of Rh(I). After the reaction, part of the Rh(III) is reduced to Rh(I) and Rh(I) to Rh(0) resulting in a mixture of 40% Rh(III), 46% Rh(I) and 14% Rh(0), this can explain the induction time observed in all of the reaction profiles. The low conversions obtained after only 30 minutes of reaction suggest that the active species is not Rh (III) but Rh(I).

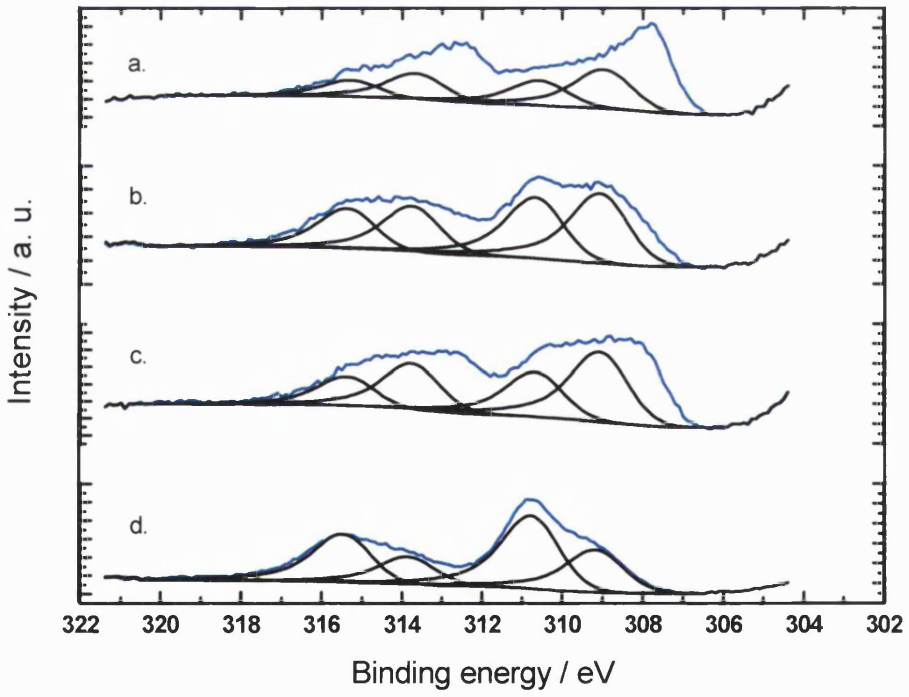

Figure 4.25: XPS analysis of a. pre-reduced 4.6%wt Rh/titanate nanotubes, b. 4.6%wt Rh/titanate nanotubes after reaction, c. pre-reduced 4.6%wt Rh/titanate nanotubes after reaction and d. "as-prepared" 5.2 %wt Rh/titanate nanotubes.

The reaction profile obtained when a catalyst of Rh/titanate nanotubes was reduced before the reaction in an aqueous solution of $NaBH_3$, is shown in Figure 4.26. In this case, no induction time is observed but the conversion and selectivity after three hours of reaction is the same as those obtained with Rh(III)/titanate nanotubes (Table 4.28). According to the XPS analyses (Figure 4.25 a. and c.), the pre-reduced catalyst with 4.6 % wt Rh consists of 28% Rh(III), 44% Rh(I) and 28% Rh(0); the higher conversion obtained with this catalyst after 30 minutes of reaction confirms that the most active species is Rh(I). After the reaction with this catalyst, the distribution of rhodium species is 20% Rh(III), 33% Rh(I) and 47% Rh(0).

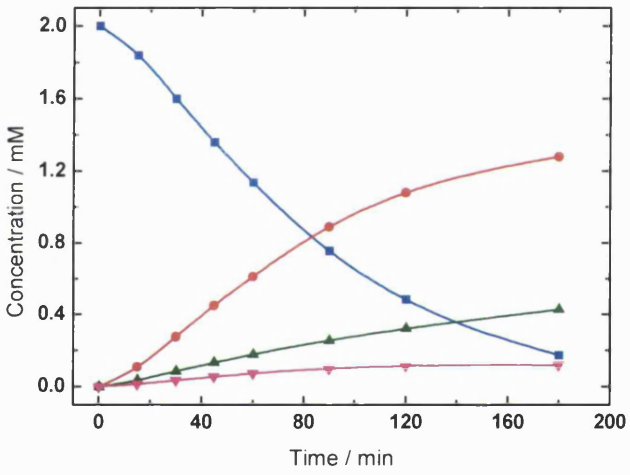

Figure 4.26: Isomerisation reaction profiles in MeOH at T = 60°C by pre-reduced 4.6 wt% Rh (0)/titanate nanotubes. Chemical components legend: ■ allylbenzene, ● trans-phenyl propene, ▲ propyl benzene ▼ unidentified.

Catalyst stability

In order to study the re-usability of Rh/titanate nanotubes catalysts, fresh reactant was added to the reaction mixture every three hours. Both Rh(III) and Rh(0) catalysts were tested. The reaction profiles are shown in Figure 4.27 and the initial rates for each reaction are summarized in Table 4.29.

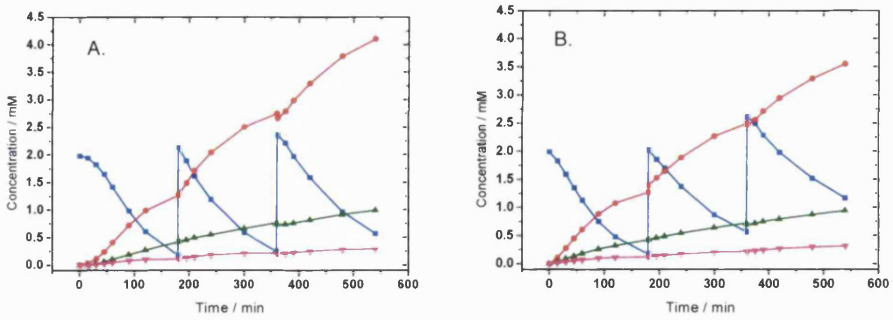

Figure 4.27: Concentration profiles in three consecutive runs. Reaction conditions: 0.2 g of (a) 4.5 wt% Rh (III) and (b) 4.5 wt% Rh(0) /titanate nanotubes catalyst; initial concentration of allylbenzene: 2 mM, solvent: methanol, 60°C. Chemical components legend: ■ allylbenzene, ● trans-phenyl propene, ▲ propyl benzene, ▼ unidentified.

The reactions profiles for both catalysts are very similar although an induction time is observed in the first run when Rh(III) is used as catalyst,. The initial rates of the consecutive reactions are very similar with values one order of magnitude higher than those obtained with Pd(II)/titanate nanotubes catalysts, although the selectivity is lower. The loss of activity can be attributed to the reduction of oxidized rhodium to rhodium (0).

Table 4.29: Initial rates, conversions and selectivities of three consecutive reactions with Rh(III) and Rh(0) over titanate nanotubes.

Rh species	Run	Initial rate ($mol \cdot s^{-1} \cdot g^{-1}$)	Conversion @ 3h (%)	Selectivity (%)
Rh(III)	1	$9.66 \cdot 10^{-6}$	90.8	70.1
Rh(III)	2	$3.15 \cdot 10^{-5}$	93.6	73.7
Rh(III)	3	$2.35 \cdot 10^{-5}$	90.3	75.9
Rh(0)	1	$2.46 \cdot 10^{-5}$	91.2	70.1
Rh(0)	2	$1.99 \cdot 10^{-5}$	85.9	72.7
Rh(0)	3	$1.97 \cdot 10^{-5}$	80.5	73.7

4.4 RESULTS AND DISCUSION: ISOMERIZATION OF LINEAR DIOLEFINS: C_5 AND C_6

In the previous section, isomerization of allylbenzene was studied where one double bond is moved along a hydrocarbon chain attached to a benzene ring. However, in order to set the proposed tandem reaction, study of the isomerization of linear diolefins is needed. In this case, two conjugated or non-conjugated double bonds are moved along a hydrocarbon chain. There is not much literature data about this specific reaction except in the case of the isomerization of linoleic acid [90].

First step in the studied tandem reaction (Chapter 6) consists of the isomerization of 1,4-pentadiene into 1,3-pentadiene (Figure 4.28). Starting with a non-conjugated molecule, one double bond moves one position along the hydrocarbon chain to obtain an external conjugated product.

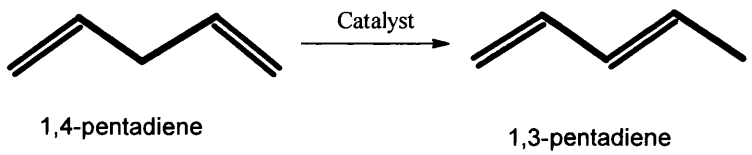

Figure 4.28: Isomerization reaction of 1,4-pentadiene.

However, selectivity of this reaction versus hydrogenation could not be studied due to the overlapping of the peak of hydrogenation products in the gas chromatograms. In order to study the selectivity of different catalysts, isomerization of 1,5-hexadiene (Figure 4.29) was considered. Starting with a non-conjugated reactant, an internal conjugated product is obtained. However, in this case, both double bonds migrate one position along the hydrocarbon chain.

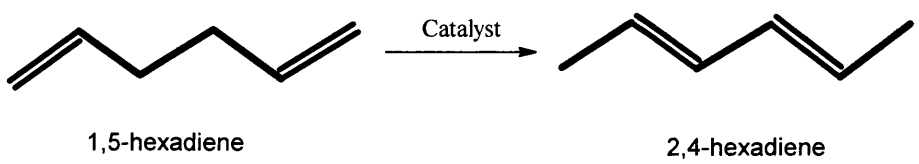

Figure 4.29: Isomerization reaction of 1,5-hexadiene.

Considering that double bond migration reaction takes place in a stepwise manner [54], it should be expected to obtain double conversion values for the isomerization of 1,4-pentadiene than for 1,5-hexadiene. However, the results obtained for both reactions cannot be compared between them because according to the mechanisms, during each double bond movement, cis-trans isomerization can take place in different extension depending if the double bond has an internal or external position in the hydrocarbon chain.

4.4.1 HOMOGENEOUS ISOMERIZATION

Different palladium, rhodium and ruthenium homogenous complexes were tested for both isomerization of 1,4-pentadiene (Table 4.30) and 1,5-hexadiene (Table 4.31). The procedure followed to assess the performance of these reactions consisted on a pressure tube described in Chapter 2. Reactions were carried out at 110°C.

Table 4.30: Isomerization of 1,4-pentadiene with homogeneous catalysts.

Catalyst	Solvent	T (°C)	Conversion @ 0.5h (%)	Conversion @ 3h (%)	TON
$PdCl_2$	MeOH	110	0	0	-
Pd acetate	MeOH	110	0	0	-
Pd acetate + $3PPh_3$	MeOH	110	0	0	-
Pd acetate+$10PPh_3$	MeOH	110	0	0	-
$PdCl(PPh_3)_3$	MeOH	110	0	0	-
$Pd(acac)_2$+PPh_3	MeOH	110	0	0	-
$RhCl_3$	MeOH	110	4.5	8.7	17.4
$RhCl(PPh_3)_3$	MeOH	110	5.2	8.8	17.5
Rh(acac)(CO)	MeOH	110	0	0	-
$RuCl_3$	MeOH	110	6.5	100	199.3
$RuHCl(CO)(PPh_3)_3$	MeOH	110	29.0	63.1	125.9
$RuHCl(PPh_3)_3$	MeOH	110	78.9	100	199.6
$Ni[P(OEt)_3]_4$	MeOH	110	0	0	-

Reaction conditions: 0.5 mL 1,4-pentadiene (0.8 M). Solvent: 5 mL dry MeOH, 0.5 mL decane as internal standard. Catalyst: $2.5 \cdot 10^{-5}$ moles.

None of the palladium complexes tested for the isomerization reaction of 1,4-pentadiene exhibited any conversion at 110°C, regardless whether free ligand triphenylphosphine was added into the solution. The addition of several equivalents of ligand had shown to have influence on the stability of the palladium complexes in the isomerization of allylbenzene. Rhodium complexes such as $RhCl_3$ and $RhCl(PPh_3)_3$ showed very low activity. However, high conversion values were obtained with ruthenium complexes. Chloride ligand does not show steric constrictions due to its small volume however, it does not contribute to a high stability to the metal atom. This can have critical effects in long time reactions such as the proposed tandem. Improvements on stability can be obtained with triphenylphosphine ligand which, in spite of being bulky, is very labile. Ruthenium complexes with triphenylphosphine ligand such as $RuHCl(CO)(PPh_3)_3$ and $RuHCl(PPh_3)_3$ exhibited high conversion values as triphenylphosphine group moved out from the ruthenium atom allowing the incorporation of the reactant to the metal.

Table 4.31: Isomerization of 1,5-hexadiene with homogeneous catalysts.

Catalyst	Solvent	T (°C)	Conversion @ 0.5h (%)	Conversion @ 3h (%)	Selectivity @ 3h (%)	TON
$Pd(acac)_2$	MeOH	110	0	0	0	-
$RhCl_3$	MeOH	110	0	0	0	-
$RhCl(PPh_3)_3$	MeOH	110	0	0	0	-
$RuCl_3$	MeOH	110	5.6	11.3	61.2	19.0
$RuHCl(CO)(PPh_3)_3$	MeOH	110	42.8	67.7	55.4	114.1
$RuHCl(PPh_3)_3$	MeOH	110	35.7	52.8	98.6	88.9

Reaction conditions: 0.5 mL 1,5-hexadiene (0.7 M). Solvent: 5 mL dry MeOH, 0.5 mL decane as internal standard. Catalyst: $2.5 \cdot 10^{-5}$ moles.

Very similar conclusions can be obtained for the isomerization reaction of 1,5-hexadiene (Table 4.31). Neither palladium nor rhodium complexes showed any activity under these conditions. However, ruthenium catalysts exhibited good conversion values.

In this case, selectivity of isomerization versus hydrogenation was also studied. Very high selectivity values were obtained with $RuHCl(PPh_3)_3$ as a catalyst. However, hydrogenation was observed to be very competitive reaction with $RuCl_3$ and $RuHCl(CO)(PPh_3)_3$ as catalysts, exhibiting low selectivity values.

4.4.2 HETEROGENEOUS ISOMERIZATION

Palladium, rhodium and ruthenium were supported onto different materials in order to study activity and selectivity for the isomerization reaction of 1,4-pentadiene and 1,5-hexadiene.

4.4.2.1 Titanate nanotubes

Titanate nanotubes (Ti-NT) were used as a catalytic support for the isomerization of allylbenzene obtaining high selectivity values versus hydrogenation reaction. Different metals such as palladium, rhodium and ruthenium were supported on this material and tested for the isomerization reaction of 1,4-pentadiene (Table 4.32) and 1,5-hexadiene (Table 4.33).

Table 4.32: Isomerization of 1,4-pentadiene with metals on titanate nanotubes as catalysts.

Catalyst	Metal content (% wt)	Solvent	Conversion @ 0.5h (%)	Conversion @ 3h (%)	Selectivity @ 3h (%)	TON
Pd^{2+}/Ti-NT	4.75	MeOH	-	18.1	na	10.1
Pd^{0}/Ti-NT	4.75	MeOH	-	10.9	na	6.1
Rh^{3+}/Ti-NT	4.58	MeOH	14.4	58.7	na	32.9
Rh^{0}/Ti-NT	4.58	MeOH	1.4	5.6	na	3.2
Ru^{3+}/Ti-NT	4.90	MeOH	-	36.4	na	18.7
Ru^{0}/Ti-NT	4.90	MeOH	-	36.5	na	18.8

Reaction conditions: 0.5 mL 1,4-pentadiene (0.8 M). Solvent: 5 mL, 0.5 mL decane as internal standard. T = 130°C. Catalyst: 0.2 g.

In both cases, higher conversion values were obtained with Pd^{2+}/Ti-NT than with pre-reduced Pd^{0}/Ti-NT. As it was previously concluded from XPS analysis, during the reaction, palladium (II) is reduced to palladium (0), which is much less active specie for the isomerization reaction. Rhodium (III) showed good performance in both reactions although rhodium (0) was found to be almost inactive. However, in the isomerization of allylbenzene reaction, both rhodium species showed very similar activity. Same difference in activity was observed between Ru^{3+}/Ti-NT and Ru^{0}/Ti-NT catalysts in the isomerization of 1,5-hexadiene with methanol.

There are two main differences comparing isomerization of diolefins with isomerization of allylbenzene reactions. On one hand, a much higher initial concentration of reactant was used in the case of diolefins (0.7 – 0.8 M) than in allylbenzene reactions (0.001 M). This variation could explain the low selectivity values obtained for the isomerization of 1,5-hexadiene comparing with almost 100% selectivity obtained in the isomerization of allylbenzene. On the other hand, diolefin reactions were carried out at 130°C versus 60°C used for the isomerization of allylbenzene. Higher temperatures favour isomerization versus hydrogenation due to lower solubility of hydrogen. However, isomerization of 1,5-hexadiene reactions were carried out in a closed system, with the solvent as hydrogen source. This explains the differences observed not only in selectivity but also in conversion values when reaction was carried out in different alcohols.

Table 4.33: Isomerization of 1,5-hexadiene with metals on titanate nanotubes as catalyst.

Catalyst	Metal content (% wt)	Solvent	Conversion @ 0.5h (%)	Conversion @ 3h (%)	Selectivity @ 3h (%)	TON
Pd^{2+}/Ti-NT	4.75	MeOH	-	10.3	36.2	4.9
Pd^{2+}/Ti-NT	4.75	Butanol	-	24.2	100	11.4
Pd^{0}/Ti-NT	4.75	MeOH	5.8	6.5	17.3	3.2
Rh^{3+}/Ti-NT	4.58	MeOH	16.3	46.6	57.6	22.0
Rh^{3+}/Ti-NT	4.58	Butanol	-	38.9	39.4	18.4
Rh^{0}/Ti-NT	4.58	MeOH	-	-	-	-
Ru^{3+}/Ti-NT	4.90	MeOH	8.7	42.5	67.4	18.6
Ru^{3+}/Ti-NT	4.90	Propanol	38.0	79.4	88.8	34.5
Ru^{3+}/Ti-NT	4.90	Butanol	12.8	49.0	68.6	21.3
Ru^{0}/Ti-NT	4.90	MeOH	-	2.6	41.0	1.1
Ru^{0}/Ti-NT	4.90	Butanol	18.2	55.6	90.2	26.7

Reaction conditions: 0.5 mL 1,5-hexadiene (0.7 M). Solvent: 5 mL, 0.5 mL decane as internal standard. T = 130°C. Catalyst: 0.2 g.

4.4.2.2 Carbon

Commercial palladium, rhodium and ruthenium on carbon catalysts (5% weight) were tested for the isomerization of 1,4-pentadiene and 1,5-hexadiene (Table 4.34) in order to compare the influence of different supports. Ru/C catalysts was shown as the best heterogeneous catalyst for the isomerization of linoleic acid [90].

Table 4.34: Isomerization of 1,4-pentadiene and 1,5-hexadiene with metals on carbon as catalysts.

Reactant	Catalyst	Solvent	Conversion @ 0.5h (%)	Conversion @ 3h (%)	Selectivity @ 3h (%)	TON
1,4-pentadiene	5% Pd/C	MeOH	9.2	20.9	na	11.1
1,4-pentadiene	5% Rh/C	MeOH	6.1	6.4	na	6.4
1,4-pentadiene	5% Ru/C	MeOH	15.9	51.7	na	33.6
1,5-hexadiene	5% Pd/C	MeOH	-	-	-	-
1,5-hexadiene	5% Rh/C	MeOH	-	3	53.1	1.3
1,5-hexadiene	5% Ru/C	MeOH	17.5	40.1	71.2	17.1
1,5-hexadiene	5% Ru/C	Butanol	14.8	71.2	90.3	30.3

Reaction conditions: 0.5 mL 1,4-pentadiene (0.8 M) or 0.5 mL 1,5-hexadiene (0.7 M). Solvent: 5 mL, 0.5 mL decane as internal standard. T = 130°C. Catalyst: 0.2 g.

Metals on carbon catalysts showed slightly higher conversion values in the isomerization of 1,4-pentadiene than metals on titanate nanotubes. The difference can be attributed to different metal contents. However, palladium and rhodium on carbon showed no conversion for the isomerization of 1,5-hexadiene which highlight the differences between conjugated (1,4-pentadiene) and non-conjugated (1,5-hexadiene) systems. On the other hand, high conversion and selectivity values were obtained with Ru/C, especially when butanol was used as a solvent. These values are similar to the ones obtained with Ru^{3+}/Ti-NT catalyst but not with Ru^{0}/Ti-NT.

4.4.2.3 PPh_3-resin

PPh_3-DVB-resin was also used as a support for palladium, rhodium and ruthenium. These catalysts were tested in the isomerization reaction of 1,4-pentadiene and 1,5-hexadiene, results are shown in Table 4.35.

Table 4.35: Isomerization of 1,4-pentadiene and 1,5-hexadiene with metals on PPh_3-resin as catalysts.

Reactant	Catalyst	Solvent	Conversion @ 0.5h (%)	Conversion @ 3h (%)	Selectivity @ 3h (%)	TON
1,4-pentadiene	Ru-PPh_3-resin	MeOH	9.1	17.8	na	84.9
1,5-hexadiene	Pd-PPh_3-resin	MeOH	-	-	-	-
1,5-hexadiene	Rh-PPh_3-resin	MeOH	-	-	-	-
1,5-hexadiene	Ru-PPh_3-resin	MeOH	53.5	73.9	56.7	297.1
1,5-hexadiene	Ru-PPh_3-resin	Propanol	28.9	67.9	47.7	272.8
1,5-hexadiene	Ru-PPh_3-resin	Butanol	35.2	88.7	66.7	356.4

Reaction conditions: 0.5 mL 1,4-pentadiene (0.8 M) or 0.5 mL 1,5-hexadiene (0.7 M). Solvent: 5 mL, 0.5 mL decane as internal standard. T = 130°C. Catalyst: 0.2 g (0.53%wt Ru).

Similarly as with other supports, palladium and rhodium resins did not show catalytic activity. However, high conversion values were obtained in the case of ruthenium, especially in the isomerization of 1,5-hexadiene with TON values in the same order of magnitude than using homogenous ruthenium catalysts. During the reaction, the yellowish ruthenium resin did not change colour, suggesting that no reduction of the metal took place. In order to study the reusability of the resin, consecutive runs were carried out. After each run, more reactant was added into the reaction medium obtaining a reaction profile as the one shown in Figure 4.30.

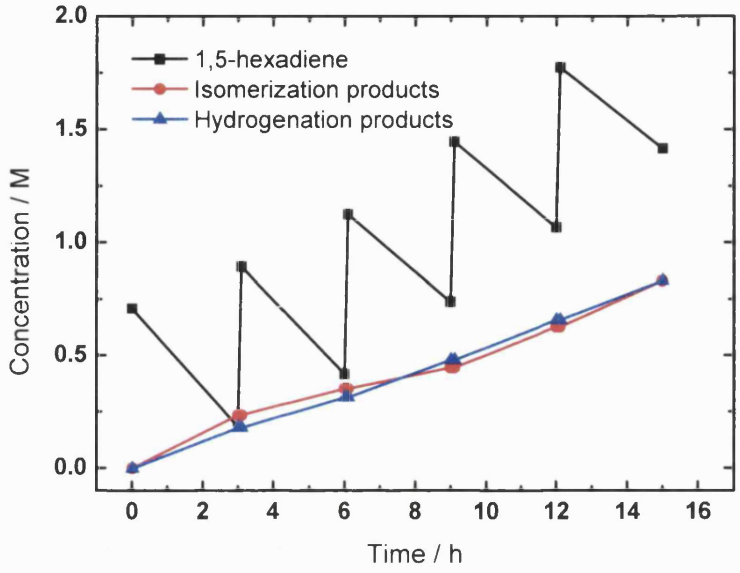

Figure 4.30: Reaction profile of five consecutive isomerization reactions with Ru-PPh_3-resin as catalyst.

Table 4.36 shows the conversion and selectivity values obtained during each run. Conversion decreases slightly in each run while selectivity keeps constant. However, the linear increment of products suggests that rate of reaction keeps constant through the different runs, changing the initial concentration of reactant in each run. Very high overall values of TON were obtained. Finally, the reaction medium was filtered and analysed by AAS in order to quantify leaching of ruthenium, determining that around 30% of initial content of ruthenium was leached. However, due to the high conversion values obtained, the activity cannot be attributed to the leached ruthenium which is ten times lower than the number of ruthenium moles used in the homogeneous reactions.

Table 4.36:Consecutive runs of isomerization of 1,5-hexadiene with Ru-PPh_3-resin.

Run	Conversion @ 3h (%)	Selectivity @ 3h (%)	Overall TON
1	73.9	56.7	297.1
2	67.2	54.5	566.9
3	54.8	48.7	786.8
4	53.6	49.4	1002
5	50.6	50.3	1205

Reaction conditions: 0.5 mL 1,5-hexadiene (0.7 M). Solvent: 5 mL, 0.5 mL decane as internal standard. T = 130°C. Catalyst: 0.2 g 0.53 %wt Ru-PPh_3-resin.

4.4.2.4 Silica supports

Silica supports such as commercial zeolite ZSM-5 and mesoporous material SBA-15 were used to deposit ruthenium. The catalysts were tested in the isomerization of 1,5-hexadiene reaction obtaining the results showed in Table 4.37.

Table 4.37: Isomerization of 1,5-hexadiene with ruthenium on silica supports.

Catalyst	Metal content	Solvent	Conversion @ 0.5h (%)	Conversion @ 3h (%)	Selectivity @ 3h (%)	TON
Ru/SBA-15	0.8 % wt	MeOH	-	-	-	
Ru/ZSM-5	2.7 % wt	MeOH	14.3	19.6	100	15.5

Reaction conditions: 0.5 mL 1,5-hexadiene (0.7 M). Solvent: 5 mL, 0.5 mL decane as internal standard. T = 130°C. Catalyst: 0.2 g.

No activity was observed with SBA-15 as support and very low conversion value was obtained with ZSM-5. This last support was previously claimed to be a good isomerization catalysts of 1-butene [35] which emphasizes the different systems formed by olefins and diolefins.

Another problem found during the preparation of these catalysts was the difficulty of supporting high loadings of metals. At low pH values, the supports surfaces present a positive charge which repeals the metal's cations. If a base is added into the ruthenium chloride aqueous solution in order to increase the pH, ruthenium black was precipitated. A different metal source would be recommended.

4.5 RESULTS AND DISCUSSION: ISOMERIZATION OF LINOLEIC ACID

In order to extend the isomerization study to longer diolefins than hexadienes, linoleic acid was chosen. This molecule consists in a C_{18} acid with two non-conjugated double bonds in positions C_9 and C_{12} (Figure 4.12). All literature data about isomerization of diolefins used this molecule as reactant [90]. This study will allow us to compare novel supports such as titanate nanotubes and resins with commercial and homogeneous catalysts.

Isomerization of linoleic acid reactions were carried out in pressure tubes (as described in Chapter 2) using methanol as solvent at 130°C for 7 hours. Best catalysts in the previous study of pentadienes and hexadienes were tested obtaining the results shown in Table 4.38.

Table 4.38: Isomerization of linoleic acid with different catalysts.

Catalyst	Metal content (% wt)	Solvent	T (°C)	Conversion @ 3h/7h (%)	Selectivity @ 3h/7h (%)	TON
$RuHCl(PPh_3)_3$	-	MeOH	130	79.7 / 89.7	56.8 / 65.9	57.4
Ru-PPh_3-resin	0.53	MeOH	130	60.9 / 84.1	37.6 / 53.8	128.9
Ru^{3+}/Ti-NT	4.9	MeOH	130	6.4 / 12.1	82.0 / 78.4	2.0
Ru/C	5	MeOH	130	3.9 / 4.3	87.2 / 89.0	0.7

Reaction conditions: 0.5 mL Linoleic acid (0.23 M). Solvent: 6.5 mL of MeOH, T = 130°C. Catalyst: $2.5 \cdot 10^{-5}$ moles for homogeneous and 0.2 g for heterogeneous.

High conversion values were obtained with homogeneous catalyst $RuHCl(PPh_3)_3$ and with the heterogeneous Ru-PPh_3-resin. Figure 4.31 shows the reaction profiles obtained with different tested catalysts. One can observe that the formation of hydrogenation products is favoured in the first three hours of reaction with both catalysts, $RuHCl(PPh_3)_3$ and Ru-PPh_3-resin giving low selectivity values. Same tendency is observed with $RuHCl(PPh_3)_3$ catalyst during seven hours. However, isomerization products are favoured versus hydrogenation products in the last hours of reaction when Ru-PPh_3-resin was used as a catalyst. It can be concluded

that the heterogeneous Ru-PPh_3-resin catalysts has a very similar performance that homogeneous catalyst $RuHCl(PPh_3)_3$.

Lower conversion value was obtained with Ru^{3+}/Ti-NT as a catalyst, although higher selectivity was achieved. Ru/C is the catalyst which showed the lowest activity from the tested ones.

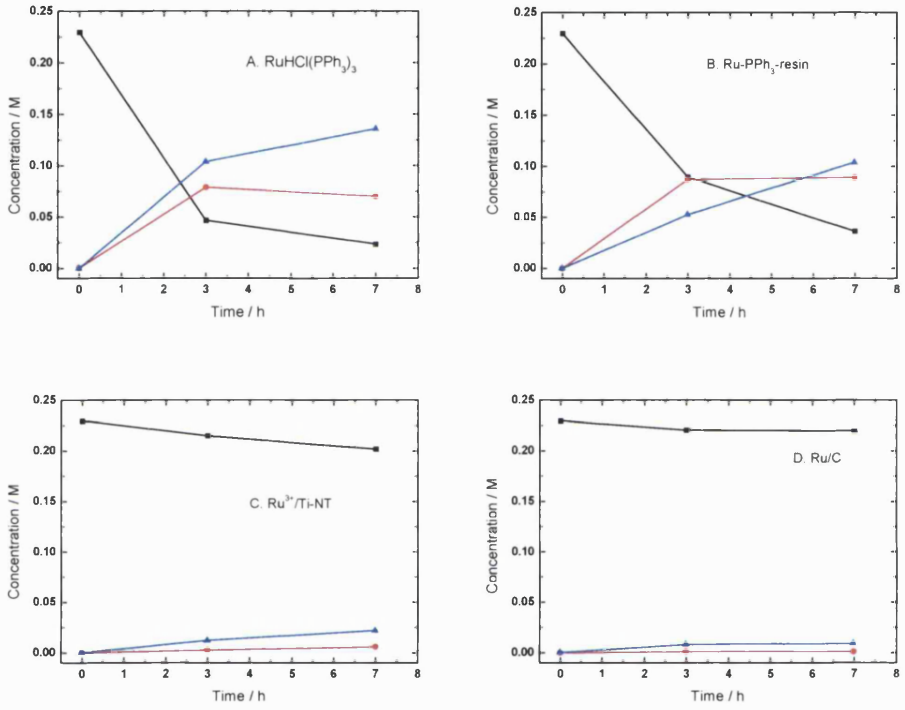

Figure 4.31: Reaction profiles of isomerization of linoleic acid with different catalysts. Chemical components legend: ■ linoleic acid, ● hydrogenation products, ▲CLA.

A similar study was carried out by Bernas et al [90] with different supported metals catalysts finding the best catalyst Ru/C. Their experiments were carried out at 120°C for 6 hours with similar quantities of reactant and catalysts. According to our results, very low conversion was obtained with Ru/C. However, conversion increased substantially if the catalyst was pre-activated under hydrogen at 100°C during one hour. Using pre-activated Ru/C and an alcohol (1-octanol) as a solvent, 78% of conversion and 43% of selectivity was obtained. Selectivity values were increased using n-decane as a solvent (77% conversion and 68% selectivity).

Better conversion and selectivity values were obtained with Ru-PPh_3-resin catalyst when alcohols are used as a solvent, without the necessity of pre-activation. Selectivity value might be increased if a different solvent is used such as n-decane.

4.5 CONCLUSIONS

Isomerization of allylbenzene was chosen as a model reaction in order to study the double bond migration due to its simplicity and narrow distribution of products. Screening of homogeneous catalysts based on transition metal complexes was done with the aim of comparing catalytic results with novel palladium and rhodium supported on multilayered titanate nanotubes catalysts.

Pd (II) on titanate nanotubes catalysts show high selectivity towards double bond migration reaction vs. hydrogenation of the double bond in linear olefins. The catalytic activity exhibits the volcano-type dependence on the metal loading, with the maximum activity observed at ca. 8 %wt while selectivity is independent of the metal content. Pd (II) was rapidly reduced to Pd (0) active species by the solvent. However, pre-reduced Pd (0) catalysts were found to be not as active towards double bond migration.

Rh (III) and pre-reduced Rh on titanate nanotubes catalysts show higher conversion values than their analogous palladium catalysts; however, lower selectivity values were obtained. Rh (I) was shown to be the active species, observing an induction time when initial Rh (III) catalysts were reduced to Rh (I) by the solvent. Further reductions to Rh (0) decrease the catalytic activity of the catalysts. Rh on titanate nanotubes catalysts can be reused at least three times without high lost of activity or leaching of metal.

In order to set the proposed tandem reaction, isomerization of linear diolefins reactions was studied. There is not much literature data about this reaction which differs from isomerization of monolefins. Higher temperatures of reaction

(> 110°C) and longer reaction times are needed with diolefins than with monolefins.

Screening of homogeneous and heterogeneous catalysts was done for the isomerization of 1,4-pentadiene, 1,5-hexadiene and linoleic acid. These molecules form completely different systems due to the position of their double bonds along the hydrocarbon chain (internal or external positions, conjugated or non conjugated).

Different palladium, rhodium and ruthenium homogeneous complexes were tested with the different reactants. Palladium and rhodium compounds showed no catalytic activity. However, high conversion, sensible selectivity values and TON in the order of 100 – 150 were obtained with ruthenium complexes, obtaining the best results with $RuHCl(PPh_3)_3$.

In order to heterogenize the system, transition metals (Pd, Rh and Ru) were supported, studying the influence of different solids on the conversion and selectivity. Heterogeneous palladium and rhodium show activity only when titanate nanotubes are used as a support. The decrease in selectivity values compared to same catalysts in the isomerization of allylbenzene is believed to be due to higher initial concentration of reactant. Ru (III) on titanate nanotubes catalysts show very similar activity to commercial ruthenium on carbon, while having bigger particle size and therefore being easier to remove from the reaction medium. Best selectivity values towards hydrogenation were obtained with ruthenium (0) (around 90 %) with TON in the order of 15 – 30 in both cases.

Silica supports ZSM-5 and SBA-15 present difficulties supporting metals, obtaining very low loadings and consequently, very low catalytic activity. An alternative metal source other than chloride salts should be used in order to obtain higher loadings.

DVB resin funzionalized with triphenylphosphine ligand were used in order to support metals. Palladium and rhodium attached to the triphenylphosphine resin are completely inactive for this reaction. Only ruthenium show catalytic activity. Very

high conversion and acceptable selectivity values were obtained with TON around 300 – 350, twice the values that were obtained with the homogeneous catalysts. Ru-PPh_3-resin catalyst can be reused a minimum of five times with a slight decrease in conversion due to metal leaching showing an overall TON of 1200.

Similar conclusions are obtained screening the tested catalysts for the isomerization of linoleic acid, the only diolefin used in the literature for the double bond migration reaction. Ru-PPh_3-resin catalyst show high conversion in the same order than homogenous catalyst $RuHCl(PPh_3)_3$, without the necessity of pre-activation under a hydrogen atmosphere as it is needed for the best literature catalyst, Ru/C [90]. Based on literature data, enhancement of selectivity would be possible using a different solvent, such as n-decane.

Chapter 5

STUDY OF THE TELOMERIZATION REACTION

5.1 INTRODUCTION

The second reaction in the proposed tandem is the telomerization reaction. In this chapter, the results of the study of this reaction are shown. Firstly, there is a review of the state of the art of this reaction, focussing on the telomerization reaction with alcohols. Next, the results obtained in the telomerization reaction of isoprene and 1,3-pentadiene with methanol are shown. Both homogeneous and heterogeneous catalysts have been screened. In the homogeneous part, the study has been focused on palladium complexes with phosphorus and carbene ligands. In the heterogeneous part, different palladium catalysts based on DVB resins have been tested. The influence of different parameters such as temperature, initial concentration of reactant and nucleophile on conversion and selectivity has been investigated.

5.2 LITERATURE REVIEW

5.2.1 INTRODUCTION

The telomerization reaction was reported in 1967 simultaneously by Smutny at Shell and Takahashi at Osaka University. Telomerization is defined as a dimerization of conjugated diolefins together with the addition of a nucleophilic molecule (telogen) leading to the formation of carbon – carbon and carbon – heteroatom bonds. 1,3-butadiene is the olefin most often used for telomerization due to its low price and high reactivity; isoprene (2-methyl-buta-1,3-diene) has also been studied extensively. Different nucleophilic molecules have been studied such as carbon dioxide, water, ammonia, alcohols, amines, acetic acid, water, etc. (Figure 5.1). If the nucleophile used is water, the telomerization is usually designated as hydromerization.

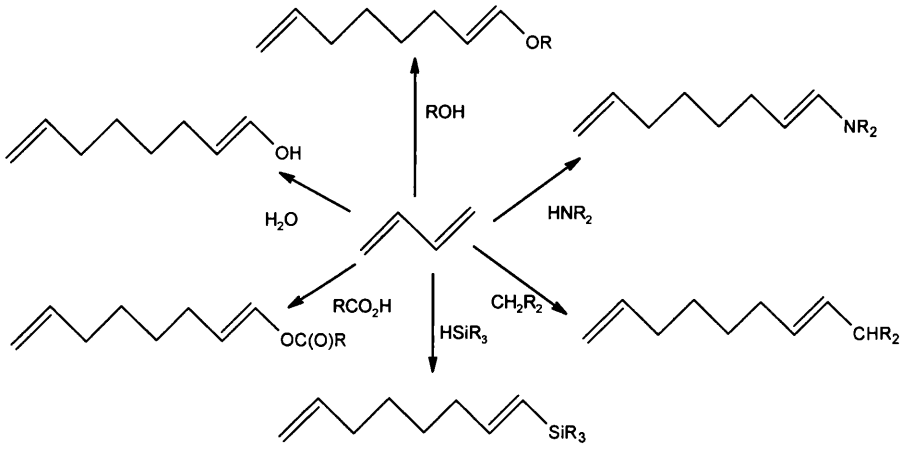

Figure 5.1: Telomerization of butadiene with different nucleophiles.

In all these reactions linear products are formed preferentially. The linear telomer is the thermodynamically more stable product due to the internal double bond, whereas the branched telomer with the terminal double bond is less stable. The telomerization reaction does not proceed under thermodynamic control since product formation is irreversible [92]. The trans isomer is favoured and the trans:cis ratio (typically greater than 5:1) remains roughly constant over the course of the reaction [93].

Thus, telomerization is one of the most versatile reactions in organometallic chemistry due to the great variability of dienes and nucleophiles that can be used. Telomerization is an atom efficient reaction. Starting from simple and inexpensive feedstocks, the reaction can be 100% atom efficient and valuable products can be obtained.

However, the only current industrial application of the telomerization reaction is the production of 2,7-octadiene-1-ol from butadiene with water. The commercialization of the process founds several problems:

- The need for expensive palladium catalysts and in most of the cases these catalysts are not thermally stable. In the homogeneous case, the catalysts are, at least in part, lost and in the heterogeneous case no satisfactory results were achieved.
- Sufficiently high reaction rates to satisfy industrial needs have not been obtained.
- Low selectivity to the desired products.
- Separation of products and unreacted molecules by distillation causes formation of polymeric products.

All these factors are an important challenge in Green Chemistry; the desired product should be synthesized from cheap available raw materials with high selectivity and avoiding waste or by-products.

5.2.2 APPLICATIONS

According to Figure 5.1, the range of possible products in the telomerization reaction is very wide, depending on the telomer and nucleophile used. The resulting compounds in the telomerization reaction with alcohols are used as intermediates for several products. The compounds obtained after hydrogenation of the remaining double bond in the olefinic products, can be used as fuel additives or plasticizers for polymers such as PVC [94-96]. Other applications are as

monomers, solvents, corrosion inhibitors, non-volatile herbicides [97], surfactants and in cosmetics products [95].

The telomerization of butadiene with water has been studied by industrial research groups such as Kuraray, BASF, Elf Atochem and Mitsubishi [98]. However, the only industrial process of this reaction is the telomerization of butadiene with water into 2,7-octadien-1-ol developed by Kurary Company in Japan on a scale of 5000 T/year. The product of telomerization is hydrogenated into octanol, a key intermediate for the synthesis of the most important plasticizer raw material.

The telomerization using amines as nucleophile is a technologically attractive reaction allowing the synthesis of long-chain amines, useful as detergent additives and as intermediates for a variety of products [99].

5.2.3 MECHANISM OF REACTION

The mechanism of the palladium catalyzed telomerization reaction is not completely proven. Two main mechanisms were proposed: a bis-allyl monometallic mechanism and the monometallic Pd-hydride mechanism.

The bis-allyl monometallic mechanism was proposed by Jolly [100] and it is shown in Figure 5.2. Starting from the active species PdL_n, two butadiene molecules are coordinated forming the complex **A.** Coupling of the two coordinated butadiene molecules gives the formation of the bis(η^3-allyl) complex (complex **B**). Further attack of a nucleophile on the C_8 chain leads to the formation of the bis-allylic complex **C**. If the attack occurred at a terminal carbon atom, the linear telomer is formed. Otherwise, attack at carbon atom 3, results in the formation of a branched product. If no nucleophilic attack takes place, the dimer 1,3,7-octadiene leaves the complex as a by-product of the telomerization. In all palladium species, at least one ligand stays coordinated to the metal centre [92].

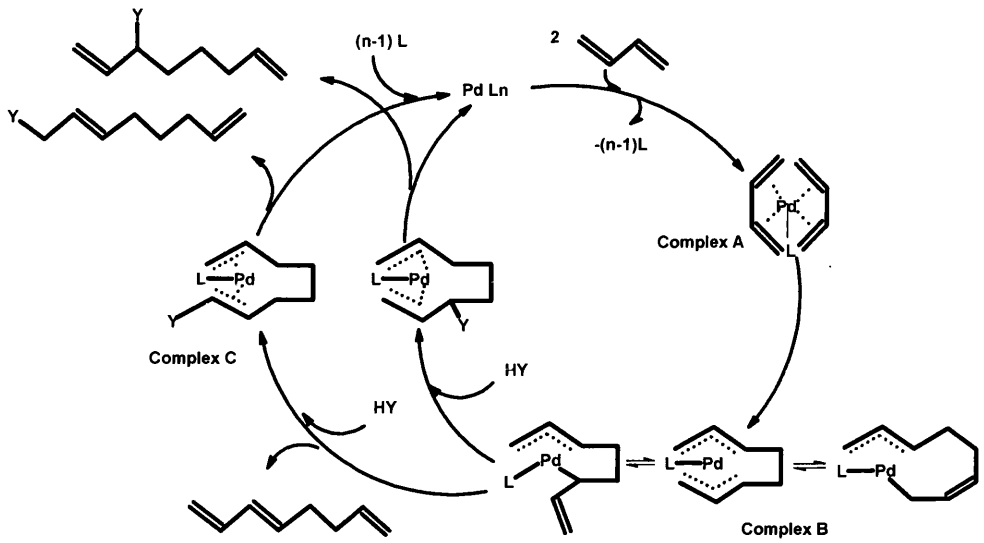

Figure 5.2: Bis-allyl monometallic mechanism for telomerization reaction [101].

The nucleophilic attack at complex **B** is the regioselective-determining step. The nucleophilic attack at carbon atom 1 in the C_8-chain is favoured for steric reasons. The selective formation of the linear telomer may also be explained by the energetically favoured structure of a trigonal planar (1,6-diene)palladium complex. The branched telomer shows a 1,7-diene structure which has much lower stability [92].

The second monometallic mechanism was proposed by Maitlis [100]. It explains the telomerization as a step by step reaction. Starting from a Pd(0) complex, the oxidative addition of the nucleophile forms the active Pd(II)-hydride complex. Subsequent additions of butadiene molecules to the hydride complex lead to telomer products or the dimer by-product. This mechanism is shown schematically in Figure 5.3.

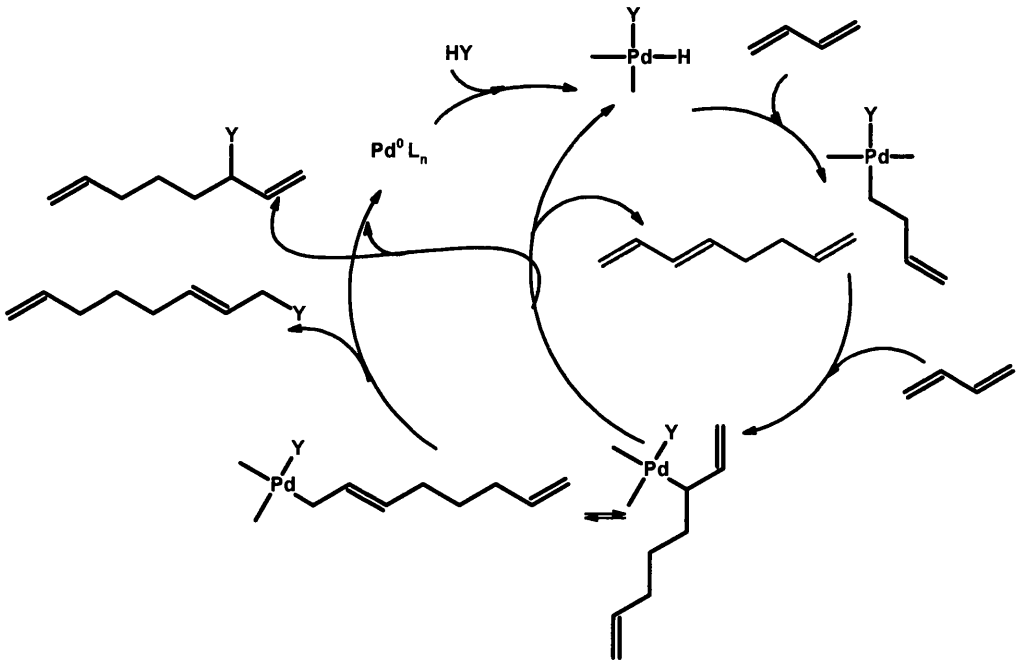

Figure 5.3: Monometallic hydride mechanism of telomerization reaction.

However, the latter mechanism is generally not accepted today [101], and different modifications of the monometallic mechanism proposed by Jolly have been proposed. Behr et al [92] explain the formation of ditelomers with some nucleophiles by adding a second catalytic cycle to the above monometallic mechanism. This mechanism is shown in Figure 5.4 where the formation of branched products is omitted for clarity. A further butadiene molecule can be added to the complex **C** in the first cycle, forming complex **D** which is analogous to the complex **A**. The same steps as take place in the first cycle occur in the second one. The coupling of the butadiene molecules gives the formation of the complex **E** and the nucleophilic attack forms the complex **F**, leading to the ditelomer products and regenerating the catalytic species. If no nucleophilic attack takes place, the trimerization products are formed. Thus, the telomers and ditelomers are produced in parallel at the same time.

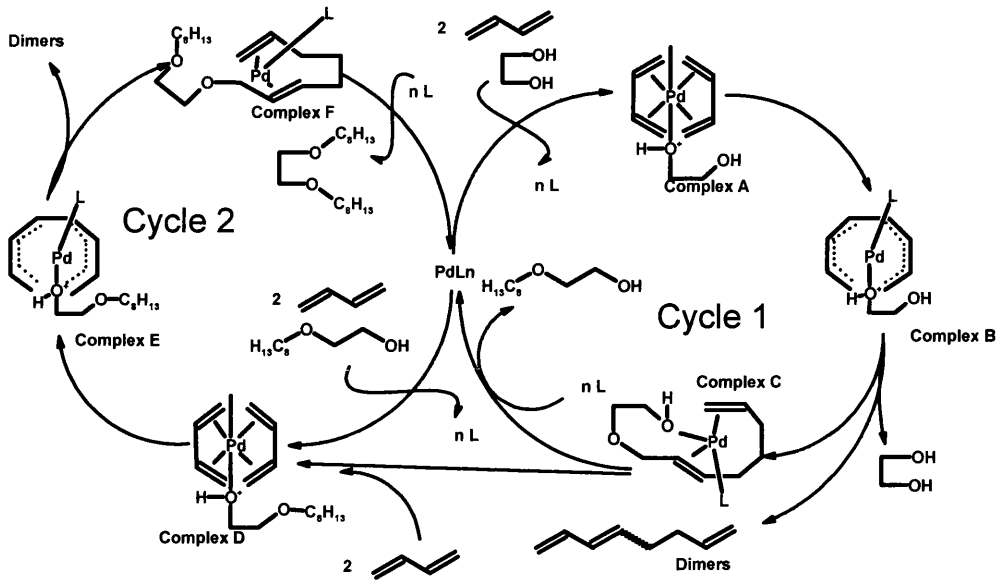

Figure 5.4: Proposed mechanism for the telomerization of butadiene with ethylene glycol [92].

Increasing the steric bulk in the coordination sphere of the metal (Figure 5.4) favours the elimination of the telomer products from complex **C**, suppressing the cycle 2. When very stable catalytic complexes are used, the nucleophile attack on the C_8 chain of intermediate **B** is harder and thus, more dimers are formed.

In a series of papers [96, 97, 102, 103], Matthias Beller's group developed an extended mechanism based on the one proposed by Jolly. By adding a second catalytic cycle the large influences of the P/Pd and butadiene/nucleophile ratios were explained. The two cycles are shown in Figure 5.5.

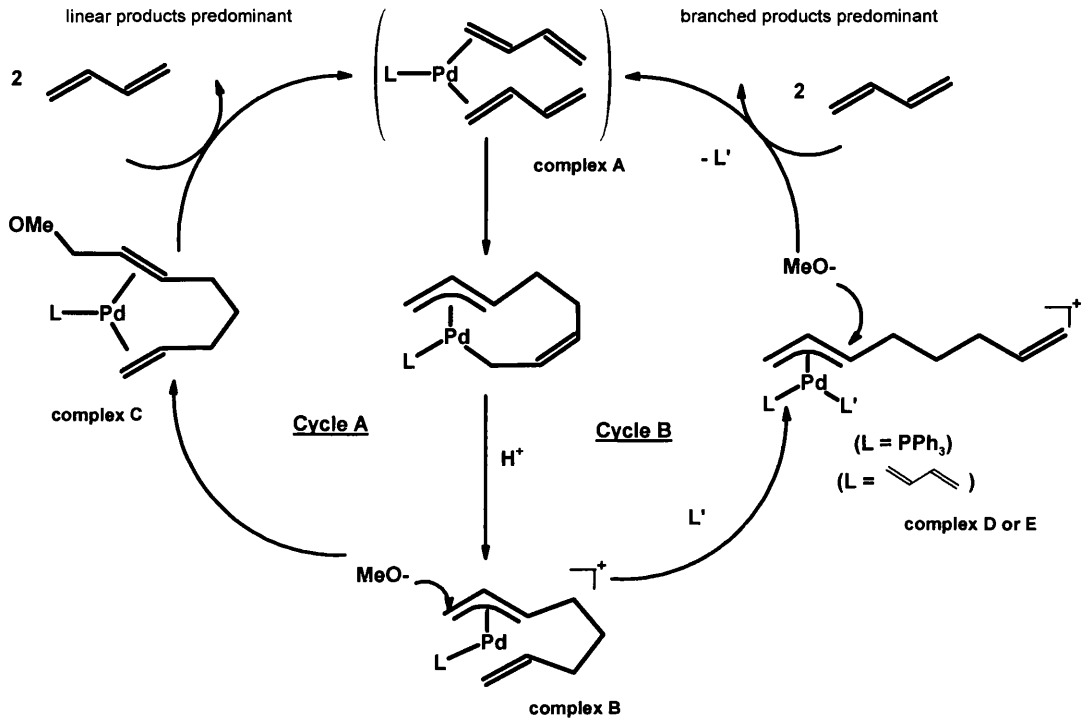

Figure 5.5: Proposed mechanism for the telomerization of butadiene with alcohols [96, 97].

An excess of ligand in the medium of reaction leads to the formation of allylbis(phosphine)palladium complex **D** and the excess of butadiene in the medium favours the formation of an intermediate complex **E**. Both complexes are formed from the complex **B**. Thus, an excess of butadiene has an analogous effect to an excess of phosphine being responsible for a lower linear/branched ratio in the telomer products.

The butadiene/alcohol ratio not only affects regioselectivity, but also the chemoselectivity of the reaction. At low alcohol concentrations, the nucleophile attack on the complex **B** to form complex **C** is more difficult, leading to the formation of dimerization by-products.

This mechanism was proposed for telomerization of butadiene with alcohols but it might be extended to other oxygen nucleophiles or amines [103].

Most of the mechanistic studies were done with phosphine ligand catalytic systems, but the same mechanisms apply for the carbene ligand systems if one takes into account some differences. Carbenes are good σ-donors and poor π-acceptors compared to phosphines. This results in a more favoured nucleophilic attack at carbon atom 1 and the predominant formation of linear telomers. In other words, when carbenes are used as ligands, the cycle A (Figure 5.5) is favoured against cycle B [104].

5.2.4 TELOMERIZATION CATALYSTS

The catalysts for telomerization reactions may be formed by any transition metal compound. Preferably, a compound of an element of the group VIIIB of the Periodic Table, but more preferred are cobalt, rhodium, nickel, platinum and palladium [94].

5.2.4.1 Homogeneous catalysts

Palladium catalysts for telomerization reaction

The classical catalyst is formed from a palladium salt in the presence of a phosphorus compound producing a catalyst in situ where the phosphorus acts as a ligand for the palladium atom. The most used palladium precursors are palladium acetate, palladium acetylacetonate and palladium bis-benzylidene-acetone $Pd(dba)_2$. Inorganic precursors such as palladium nitrate, palladium oxide and palladium chloride give lower activities than the organic ones. Inorganic ions (especially chloride) block free coordination sites of palladium, inhibiting its coordination with the phosphine [98, 105].

Some authors suggest that there is no general advantage in starting either with Pd(II) or Pd(0) precursor complexes [97]. However others believe that palladium metal does not seem to form the active palladium – phosphine complex, thus giving very low conversions [98]. In contrast, the brief induction time observed with some

systems is sometimes explained by the in situ formation of the catalytically active species $L_nPd(0)$ complex from the Pd(II) precursor [93].

Ligands and P/Pd ratio

The type of ligand and the P/Pd molar ratio influence catalytic efficiency [101, 102, 106-108], distribution of products and chemioselectivity [102, 103, 106, 109, 110] and regioselectivity [103].

The **monodentated** phosphine or phosphates ligands used are triphenylphosphine $(PPh)_3$ [92, 101, 103, 111], triethylphosphine (PEt_3) [101], tricyclohexylphosphine (PCy_3) [101, 111], triisopropylphosphine (P^iPr_3) [101], tri-n-butylphosphine (PBu_3) [101, 111], tri-n-hexylphosphine ($PHex_3$) [101], n-butyl-diphenylphosphine (PPh_2Bu) [101], di-n-butyl-phenylphosphine ($PPhBu_2$) [101], ethyl-di-n-dodecylphosphine ($PEtDod_2$) [101].

The Pd(II) precursors are rapidly reduced into the catalytically active Pd(0) species [103, 108] For this to occur, it is necessary that an excess of phosphine ligand, acting as a reducing agent [92] or a reducing agent such as $AlEt_3$ [92] or NEt_3 [103], is added. Alkaline alkoxides such as MeONa are also used to favour the reduction of Pd(II) to Pd(0), but also may act as nucleophiles in the catalytic cycle [112].

The steric and electronic properties of the phosphine ligands can be evaluated by the cone angle υ (Figure 5.6) and the χ parameter related to the donor/acceptor properties. A high value of the parameter χ means low basic properties of the ligand. Increasing the acid character of the phosphines, a linear decrease in the activity of the resulting catalyst is observed [101, 109].

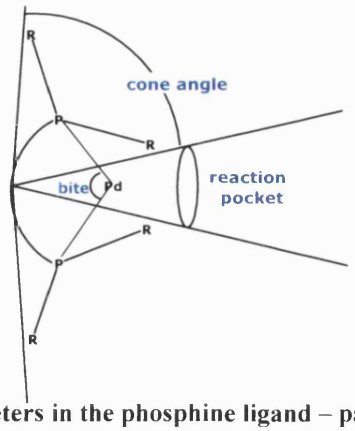

Figure 5.6: Steric parameters in the phosphine ligand – palladium complex.

Steric hindrance of the phosphine ligand also influences the activity of the resulting palladium catalysts. Very bulky ligands show low tendency to telomerization with respect to less hindered phosphines [101, 106]. Phosphine ligands characterized by a large cone angle υ parameter have low selectivity to telomers [101].

Table 5.1: Telomerization of 1,3-butadiene with methanol. Influence of different phosphorus ligands [101].

Phosphine ligand	Conversion (%)	υ (°)	χ (cm^{-1})	Selectivity (%)	
				telomers	dimers
PPh_3	76	145	12.9	93.7	6.1
PPh_2Bu	83	141	10.0	95.7	4.2
$PPhBu_2$	89	136	7.1	96.8	3.1
PBu_3	96	134	4.2	97.2	2.6
PEt_3	99	132	5.4	97.9	2.0
PPr_3	100	160	3.1	76.0	22.5
PCy_3	95	170	0.3	81.6	17.9
$PHex_3$	89	135	3.8	97.3	2.0
$PDod_2Et$	98	134	4.0	96.7	2.2

Reaction conditions: Catalyst system: $Pd(dba)_2$ = 0.1 mmol; solvent: hexane = 20 mL; $Pd/PR_3/MeOH/C_4H_6$ = 1/2/3000/2000 mol/mol; time = 0.5 hours, T = 60°C.

The optimal P/Pd molar ratio depends on the nature of a phosphine ligand. More basic ligands require a ratio near one, whereas a ratio close to two is necessary for the less basic phosphines [101]. Low ligand concentrations result in the deactivation of the palladium catalyst, whereas an excess of phosphine ligand leads

to the inhibition of catalytic activity [102] due to the formation of stable $Pd(PPh_3)_2$ complexes [107].

$$[Pd] \overset{L}{\longleftrightarrow} [PdL] \overset{L}{\longleftrightarrow} [PdL_2]$$
$$\textit{inactive} \quad \textit{active} \quad \textit{inactive}$$

Figure 5.7: Influence of the P/Pd molar ratio in the formation of active catalytic species.

A maximum of two ligands are bound to the palladium (0) atom in the catalytic cycle of telomerization, although only one phosphorus atom is bound to palladium during the C-C bond forming step. However, the second phosphorus atom is crucial in the early stages of the cycle and for the elimination of the product [108]. The two coordinated phosphine – palladium complexes are only stable for very bulky ligands, whereas coordination numbers of three and four are preferred for stabilization of the complexes. This decreases the catalytic activity according to Figure 5.7. In general, strongly basic monodentate with low steric hindrance phosphines show the best results in terms of activity and selectivity of the telomerization reaction, because of their ability to stabilize palladium at a low P/Pd molar ratios [101, 109].

The sulfonate ligands, tris(m-sulfonatophenyl)phosphine (TPPTS), bis(p-sulfonatophenyl) phenylphosphine dehydrate dipotassium salt (TPPDS) and diphenylphosphinobenzene-3-sulfonic acid sodium salt (TPPMS) can be used instead of the neutral ligands to stabilize the Pd(0) complex in the reaction mixture. These phosphines increase considerably the selectivity toward the linear telomers [113].

Table 5.2: Telomerization of 1,3-butadiene with β-naphthol. Influence of ligand and ratio ligand/Pd [102].

Ligand	Ratio ligand : Pd	Conversion (%)	T (°C)	Selectivity to the C-allylated product
PPh_3	1:1	75	90	33
PPh_3	3:1	82	90	93
PPh_3	10:1	94	90	80
PPh_3	50:1	75	90	42
PCy_3	3:1	73	90	52
$P(C_6H_2(OMe)_3)_3$	3:1	0	90	-
$P(tBu))_3$	3:1	0	90	-
$P(OC_6H_3(C_4H_9)_3)_3$	3:1	57	90	29
PPh_3	3:1	90	60	9
PPh_3	3:1	88	120	78
PPh_3 + 1% mol NEt_3	3:1	91	90	92

Reaction conditions: 100 mmol β-naphthol; 200 mmol 1,3-butadiene; 0.1% mol $Pd(acac)_2$; 50 mL THF, 16 hours.

Table 5.3: Telomerization of 1,3-butadiene (BDi) with ethylenglycol (EG). Influence of catalyst concentration, ratio telomer/nucleophile and ratio Pd/Ph [92].

Catalyst concentration (%mol)	T (°C)	Time (h)	Ratio BDi/EG	Ratio Ph/Pd	Product yield (%)			TON
					Mono-telomers	Di-telomers	Oligomers	
0.12	120	2	2.5	4	60	20	22	675
0.12	80	2	2.5	4	56	22	5	655
0.06	80	2	2.5	4	53	18	6	1204
0.03	80	2	2.5	4	45	10	8	1945
0.03	80	2	2.5	4	50	9	11	2071
0.06	80	2	2.5	2	60	23	11	1389
0.06	80	2	2.5	1	59	21	17	1354
0.06	80	2	2.5	0.25	-	-	-	-
0.06	80	2	2.5	8	-	-	-	-
0.06	80	4	4.2	2	64	26	27	1501

Reaction conditions: $Pd(acac)_2$ + PPh_3, THF (5 mL).

Table 5.4: Telomerization of 1,3-butadiene with methanol. Influence of P/Ph ratio [101].

Ratio P/Pd (mol/mol)	Conversion (%)	Selectivity (%)		
		Linear telomer	Branched telomer	Dimers
0.5	51.6	71.8	9.2	17.4
1	80.7	92.4	3.9	3.3
2	93.3	90.4	4.1	5.3
4	10.4	82.2	12.5	5.3

Reaction conditions: Catalyst system: $Pd(dba)_2$ (0.1 mmol)/ DPPB system; $Pd/P/MeOH/C_4H_6$ = 1/2/3000/2000; solvent: n-hexane = 20 mL; time = 4 hours; T = 60°C.

Table 5.5: Telomerization of 1,3-butadiene with methanol [103].

Ratio C_4H_6 / ROH	Catalyst	[Catalyst] (% mol)	T (°C)	Time (h)	Conversion (%)	Selectivity (%)	TON
2:1	[a]	0.07	-10	6	64	98	914
2:1	[a]:1PPh_3	0.05	-10	6	29	97	560
1:2	[a]	0.004	50	2	35	97	8500
1:2	$Pd(OAc)_2$+3PPh_3[b]	0.01	50	2.5	63	97	6200
1:2	$Pd(OAc)_2$+ 3PPh_3[b]	0.0018	90	2.5	58	85	30280
2:1	$Pd(OAc)_2$+3PPh_3[b]	0.002	50	16	43	95	21500
2:1	$Pd(OAc)_2$+3PPh_3[b]	0.0005	90	16	27	75	48000
1:6	$Pd(OAc)_2$+3PPh_3[b]	0.001	90	16	43	84	39000
1:2	$Pd(OAc)_2$+10PPh_3[b]	0.01	50	16	23	>99	23000
1:2	$Pd(OAc)_2$+10PPh_3[b]	0.0018	90	2.5	73	85	38890
2:1	$Pd(OAc)_2$+10PPh_3[b]	0.002	50	16	34	97	17000
2:1	$Pd(OAc)_2$+10PPh_3[b]	0.0005	90	16	35	66	70000
2:1	$Pd(OAc)_2$+50PPh_3[b]	0.0005	50	16	14	>99	28000
2:1	$Pd(OAc)_2$+50PPh_3[b]	0.0005	90	16	40	75	70000

[a] Catalyst: (diallyl ether)(triphenylphosphine)palladium (0).
[b] 100 equiv of NEt_3 were added.

The active phosphine – palladium complex can also be formed with bidentate phosphine ligands according to Figure 5.8.

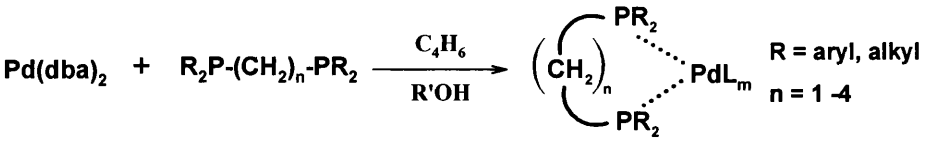

Figure 5.8: Formation of the active phosphine – palladium complex with bidentate ligands.

Diphosphine chelating ligands provide strong stabilization of the palladium metal atom which implies a decrease in activity. This decrement is increased as the basicity of the ligand increases [114]. The stabilization effect strongly depends on the size of the ring, for example, diphsophines with n equal to 2 or 3 are the most stable [101]. Some diphosphine ligands, such as 1,4-bis(diphenylphosphino)butane (DPPB), with a large coordination flexibility, can show an analogous activity to the corresponding monophosphine ligands [101]. The chemoselectivity in telomerization reaction is strongly affected by the nature of the chelating ligand; an increase of steric hindrance causes a drop in chemoselectivity [101].

The P/Pd molar ratio also has an important influence in the diphosphine systems. The maximum activity is found when the ratio has a value of 2, which means one diphosphine ligand anchored to each palladium atom. At lower values the stabilization of palladium is low, resulting in the deposition of metallic palladium [101, 114], whereas an excess of P$^{\cap}$P ligands favours the formation of non-catalytic species, as shown in Figure 5.8.

Table 5.6: Telomerization of 1,3-butadiene with methanol. Influence of chelating diphosphine ligands [101].

Chelating ligand		Conversion	Selectivity (%)			TOF
R	n	(%)	Linear telomer	Branched telomer	Dimers	(h^{-1})
PPh_3	1	93.3	90.4	4.1	5.3	467
PPh_3	2	64.2	91.5	6.2	2.1	326
PPh_3	3	46.0	85.7	7.1	6.8	230
PPh_3	4	99.9	93.4	4.1	2.5	500
Et	2	37.2	86.6	4.4	7.3	186
Cy	2	11.1	65.4	4.5	24.3	56

Reaction conditions: $Pd(dba)_2$ (0.1 mmol) with different $R_2P-(CH_2)_n-PR_2$ chelating diphosphine ligands; $Pd/P/MeOH/C_4H_6$ = 1/2/3000/2000; solvent: n-hexane = 20 mL; time = 4 hours; T = 60°C.

To achieve a compromise between stability and activity, other chelating ligands formed by a strong phosphorus donor centre (to assure permanent coordination to palladium atoms, which gives stability) and a labile donor centre (O, N), have been used. The P∩O ligands do not appear to be suitable for the telomerization reaction, probably due to excessive stabilization of the metal species at high oxidation states [114]. In the case of N∩N chelate ligands, it has been observed that the amino groups are not able to stabilize the palladium species at low oxidation states as they have low tendency to accept electrons from the electron-rich metal [114].

The phosphinoamine P∩N ligands (Figure 5.9) are able to stabilize the palladium centre and behave as very active and selective catalysts for telomerization reaction [106]. This type of ligands form palladium species characterized by both high stability and low oxidation state, which give high activity. These results can be explained considering that the phosphino group is tightly bound to the palladium atom and the amino group may exist both as a metal-bound and as a free ligand assisting the insertion of the nucleophile [114] or the coordination of the substrate and further product elimination [109]. In these cases, the steric hindrance of the nucleophile would not be so critical. In particular, the 2-diethyl-phosphino-1-methylpyrrole ($MePyPEt_2$) ligand shows the best results (Table 5.8) [114].

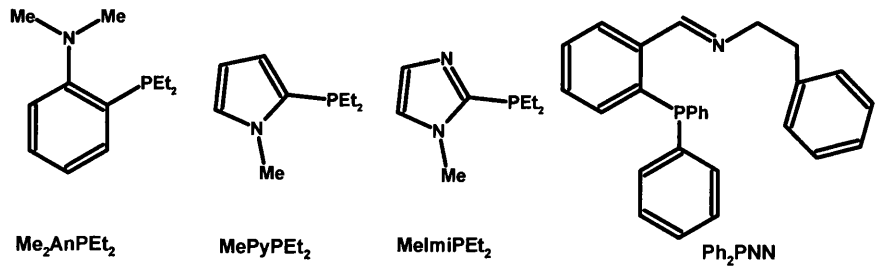

Figure 5.9: P∩N chelate ligands for telomerization reaction [114].

Camargo et al [115] used cationic cyclopalladated complexes (Figure 5.10) for the telomerization reaction observing that conversion is not influenced by the nature of the cyclopalladated ligand. However, selectivity is dramatically influenced by the nature of the palladium catalyst precursor. If triphenylphosphine or tri(n-butyl)phosphine are added, the conversion is decreased due to the competition

between phosphines and reactants for the vacant coordination sites on the palladium centre.

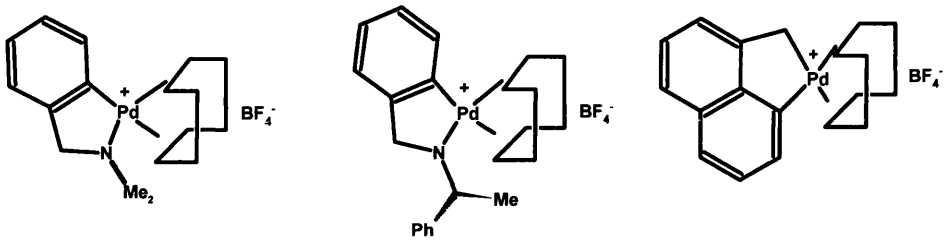

(N,N-dimethylbenzylamine) (N-benzylidene-(S)-α-methylbenzylamine) 8-methyl quinoline

Figure 5.10: Cyclopalladated complexes.

Table 5.7: Telomerization of 1,3-butadiene with methanol. Influence of P∩O chelating ligands [114].

Precursor	T (°C)	Butadiene conversion (%)	Selectivity (%)		
			Linear telomer	Branched telomer	Dimers
Pd(P∩O)	60	<1	42.4	2.0	46.6
Pd(P∩O)	80	22.3	88.0	5.1	7.5
$Pd(P^{\cap}O)_2$	60	traces	-	-	-
$Pd(P^{\cap}O)_2$	80	7.6	85.4	6.5	4.8
$Pd(P^{\cap}O)_2$	100	3.0	61.7	6.0	30.2

Reaction conditions: Pd = 0.1 mmol; Pd/MeONa//MeOH/C_4H_6 = 1/10/6000/4000; solvent: n-hexane = 20 mL, time = 4 hours.

Table 5.8: Telomerization of 1,3-butadiene with methanol. Influence of P^N chelating ligands [114].

Chelating ligand	ROH	T (°C)	Butadiene conversion (%)	TON (h^{-1})	Selectivity (%)		
					Linear telomer	Branched telomer	Dimers
Me_2AnPEt_2	CH_3OH	60	56.6	283	90.4	6.6	2.9
Me_2AnPEt_2	CH_3OH	80	57.7	289	80.4	13.1	6.3
DEPE	CH_3OH	60	37.2	186	86.6	4.4	7.3
Me_2AnPEt_2	n-C_3H_7OH	60	32.8	164	83.0	3.6	13.0
$MePyPEt_2$	CH_3OH	60	54.6	273	86.2	10.0	3.7
$MePyPEt_2$	CH_3OH	80	51.3	257	91.0	8.1	0.9
$MePyPEt_2$	CH_3OH	100	61.3	306	89.0	9.1	1.7
$MePyPEt_2$	C_2H_5OH	60	69.6	348	88.8	3.4	7.6
$MePyPEt_2$	n-C_3H_7OH	60	61.0	305	87.5	3.6	8.6
$MePyPEt_2$	n-$C_5H_{11}OH$	60	77.5	387	83.8	2.9	12.9
$MePyPEt_2$	n-$C_8H_{17}OH$	60	71.9	360	82.2	2.2	14.9

Reaction conditions: $Pd(dba)_2$ = 0.15 mmol; $Pd/ROH/C_4H_6$ = 1/3000/2000 mol/mol; P^N/Pd = 1 solvent: n-hexane = 20 mL, time = 4 hours.
DEPE: 1,2-bis(diethylphosphino)ethane.

Another catalytic system tested for telomerization reaction is formed by a palladium(0) complex of 15-membered macrocyclic triolefins (Pd-Ma) represented in Figure 5.11. This catalyst requires the presence of phosphine compounds to show activity and can be recycled several times by distillation, recovering its activity by adding new phosphine compounds in each run. It is believed that soluble catalytic species are formed and, after the reaction, palladium(0) is redeposited into the macrocycle [116]. These systems were supported and the results obtained are reviewed in the heterogeneous part below.

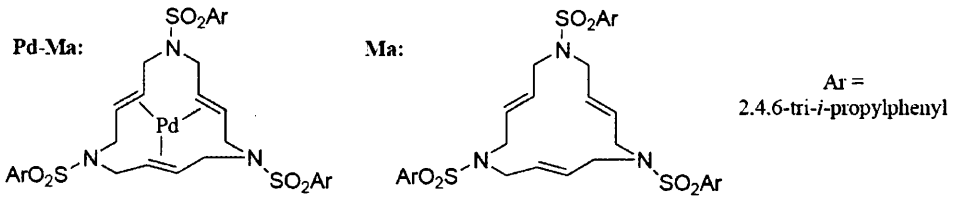

Figure 5.11: Structures of Pd-catalyst and macrocyclic ligand.

Table 5.9: Telomerization of 1,3-butadiene with methanol with Pd-macrocyclic ligand [116].

Run	Catalyst system	equiv PPh_3	Conversion (%)	TOF (h^{-1})	Selectivity (%)		
					Linear telomer	Branched telomer	Dimers
1	Pd-Ma	-	3	60	16	0	84
1	Pd-Ma-PPh_3	-	49	980	81	8	11
1	Pd-Ma-2PPh_3	-	59	1180	76	14	10
1	Pd-Ma-3PPh_3	-	68	1360	72	16	12
2	Pd-Ma-3PPh_3	-	41	820	85	7	8
2	Pd-Ma-3PPh_3	3	87	1740	80	14	6
3	Pd-Ma-3PPh_3	3	70	1400	79	14	7
4	Pd-Ma-3PPh_3	3	75	1500	81	14	5

Reaction conditions: Pd/MeOH/C_4H_6 = 1/6000/4000; 0.025 mmol Pd, T = 60°C; time =1h. Catalyst system: See Figure 5.11.

The N-heterocyclic carbenes (NHCs) were first synthesized and characterized by Arduengo in 1991. They have been used in organometallic chemistry (in reactions such as the Heck, Suzuki and Sonogashira) to replace the electron rich phosphine ligands to produce metal complexes showing high catalytic activity and stability. A more strongly bound and sterically hindered ligand on the palladium centre gives a productive and more selective catalyst system [97]. The NHCs are superior to phosphine in terms of higher thermal stability, tighter coordination to the metal which reduces dissociation, relative inertness toward oxidation and reduced toxicity [117]. However, the isolation of N-heterocyclic carbenes is complicated because they are extremely air and moisture sensitive.

Carbenes can be synthesised with a considerable diversity of structures (Figure 5.12) by varying the heteroatom in the ring (X = N or S), the steric arrangement and electronics of the groups attached to the imidazole ring ($R_{4,5}$) and the nitrogen(s) ($R_{1,3}$), and the ethylene backbone (saturated vs unsaturated) [118].

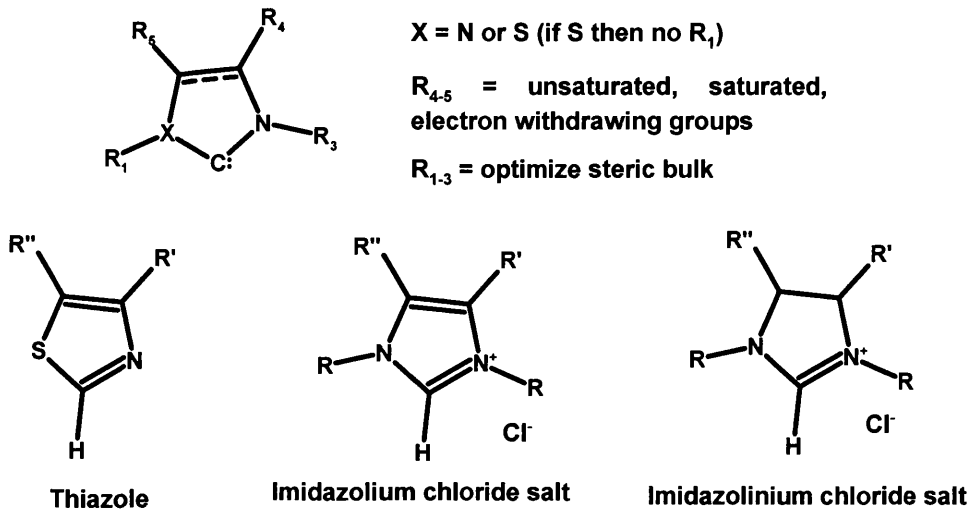

Figure 5.12: Carbene structures and nomenclature [118].

The use of carbene ligands in the telomerization reaction avoids the need for high ligand:Pd molar ratios necessary to stabilize the palladium catalysts. The strongly bound and sterically hindered carbene ligands on the palladium centre have been proven successfully for other palladium catalyzed reactions [97].

Beller's group and collaborators [96, 97] studied the activity and selectivity of different imidazolium salts for the telomerization reaction. Apparently, unsymmetrical substituted carbenes are especially suited to give high regioselectivities. A set of carbene complexes was synthesized where the central palladium atom is coordinated by the olefin unit $H_2C{=}CHSiMe_2OSiMe_2HC{=}CH_2$ (dvds), and the corresponding carbene ligand is in a trigonal planar coordination (Figure 5.13). In order to obtain good yields and selectivities in the telomerization reaction, the presence of N,N-diarylcarbene ligand is crucial.

The effect of substitution in the backbone of the carbene ligand (positions 4 and 5, Figure 5.12) has influence on the stability of the complexes and their activity. The substitution with an electron donating methyl group (Figure 5.13, complex b) stabilizes the complexes and reduces the reactivity. By contrast, an electron withdrawing chlorine substitution (Figure 5.13, complex c) destabilizes the complexes and promotes the reactivity. In order to study the steric effects on the

stabilization and reactivity of the different complexes, substitutions in benzene rings were performed. The bulky isopropyl substitutes (Figure 5.13, complex e) were found to destabilize the catalysts and at the same time reduce their catalytic activity.

For these palladium-carbene complexes, it was found that addition of imidazolium salts improved the yield of reactions without any change in the regioselectivity, which is contradictory to the observed behaviour of the palladium/phosphine ligands catalysts described above.

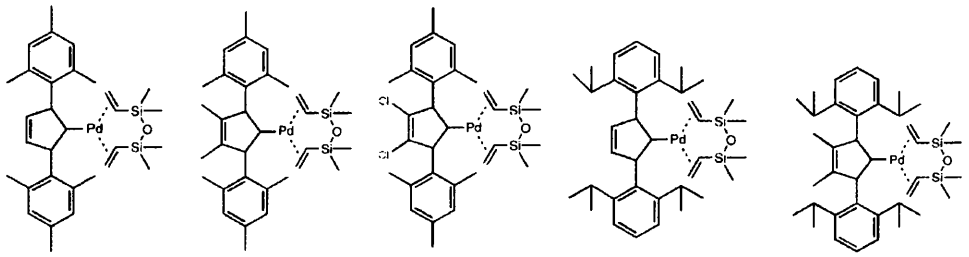

Pd(Imes)(dvds) Pd(IPr)(dvds) Pd(MeIPr)(dvds)

complex a complex b complex c complex d complex e

Figure 5.13: Monocarbenepalladium (0)-dvds complexes.

Table 5.10: Telomerization of 1,3-butadiene with ethylenglycol. Influence of di-phosphine and carbene ligands [92].

[Catalyst] (%mol)	Ligand	Time (h)	Ratio Bu/EG	Volume THF (mL)	Product yield (%)			TON
					Mono-telomers	Ditelomers	Oligomers	
0.06	DPPM	2	2.5	5	57	25	7	1388
0.06	DPPE	2	2.5	20	56	16	18	1223
0.06	DPPP	2	2.5	15	44	5	4	820
0.06	DPPB	2	2.5	15	22	1	2	389
0.06	DPPP	4	2.5	15	60	27	13	1467
0.06	DPPB	4	2.5	15	60	21	7	1367
0.02	carbene[a]	2	2.5	0	51	41	1	4299
0.02	carbene[a]	2	4.2	0	25	75	6	5226

Reaction conditions: $Pd(acac)_2$, ratio P/Pd = 2:1 or carbene/Pd = 2:1; T = 80°C.
[a]. N-heterocyclic carbene 1,3-dimesityl-imidazolin-2-ylidene.

Table 5.11: Telomerization of 1,3 butadiene with methanol. Different carbenes used as ligands [97].

a. different imidazolium salts (carbenes)

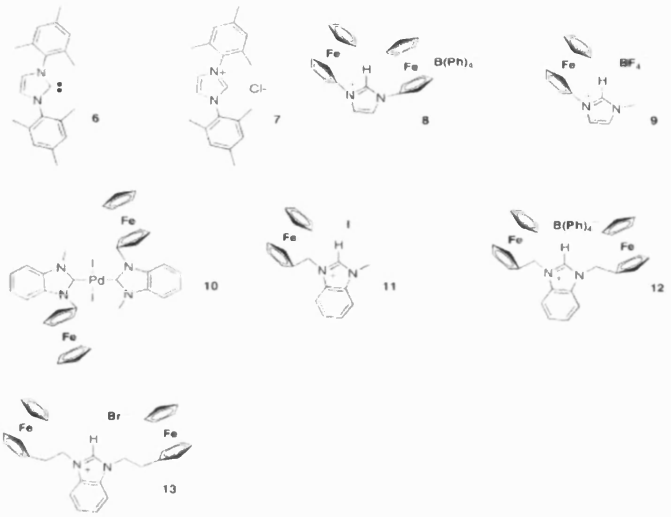

Pd source	Pd (%mol)	Ligand	Pd:ligand ratio	Telomer yield (%)	Selectivity (%)	Linear: branched telomer	TON
$Pd(dba)_2$	0.001	PPh_3	1:2	86	92	14:1	86000
$Pd(dba)_2$	0.0003	PPh_3	1:2	69	92	14:1	230000
$Pd(dba)_2$	0.001	a 6	1:2	92	98	35:1	92000
$Pd(OAc)_2$	0.001	a 6	1:2	93	98	35:1	93000
$Pd(dba)_2$	0.001	a 7	1:2	95	98	35:1	95000
$Pd(OAc)_2$	0.001	a 7	1:2	87	98	36:1	87000
$Pd(dba)_2$	0.0003	a 6	1:2	83	97	39:1	278000
$Pd(dba)_2$	0.0003	a 6	1:4	89	98	39:1	296000
$Pd(dba)_2$	0.0003	a 7	1:4	92	98	39:1	308000
$Pd(OAc)_2$	0.0003	a 7	1:4	94	98	39:1	314000
$Pd(dba)_2$	0.001	a 8	1:2	0	0	0	0
$Pd(dba)_2$	0.001	a 9	1:2	73	96	61:1	73000
$Pd(dba)_2$	0.001	a 11	1:2	8	75	99:1	8000
$Pd(dba)_2$	0.001	a 12	1:2	88	97	42:1	88000
$Pd(dba)_2$	0.0003	a 12	1:4	41	94	25:1	137000
$Pd(dba)_2$	0.001	a 13	1:2	82	97	36:1	82000

Reaction conditions: 16 h; 90°C; 1%mol NaOH, MeOH:Bu = 2:1.

Table 5.12: Telomerization of 1,3-butadiene with methanol with carbene-palladium (0) complexes [96].

Catalyst	[Catalyst] (% mol)	Ligand [% mol]	Telomer yield (%)	Selectivity (%)	linear: branched telomer	TON
-	0	0.004	0	0	-	0
[a] complex a	0.001	0	96	>99	98:2	96000
[a] complex b	0.001	0	93	99	98:2	93000
[a] complex c	0.001	0	96	>99	98:2	96000
[a] complex d	0.001	0	90	97	92:8	90000
[a] complex e	0.001	0	2	-	91:9	2000
complex f	0.001	0	94	99	98:2	94000
complex g	0.001	0	46	96	92:8	46000
[a] complex a	0.0001	-	20	89	98:2	200000
[a] complex f	0.0001	-	19	90	98:2	190000
[a] complex a	0.0001	0.0002	17	88	98:2	170000
[a] complex a	0.0001	0.0004	40	95	98:2	400000
[a] complex a	0.0001	0.001	69	97	98:2	690000
[a] complex a	0.0001	0.002	87	98	98:2	870000
[a] complex a	0.0001	0.004	91	99	98:2	910000
[a] complex f	0.0001	0.004	89	98	98:2	890000
[a] complex a	0.00005	0.004	77	99	98:2	1540000

Reaction conditions: 16 h; 70°C; 1%mol NaOH, MeOH:Bu = 2:1, L = IMes·HCl
a. See Figure 5.13.
Complex f = [(IMes)Pd(allyl)Cl] Imes = 1,3-bis(2,4,6-trimethylphenyl)imidazol-2-ylidene.
Complex g = [(IPr)Pd(allyl)Cl] IPr = 1,3-bis(2,6-diisopropylphenyl)imidazol-2-ylidene.

5.2.4.2 Heterogeneous catalysts

Benvenutti et al [112, 119] have been working towards heterogenizing palladium catalysts for the telomerization reaction of 1,3-butadiene with methanol. Different supports have been used, resulting in different interactions with the palladium complexes. Palladium (II) complexes anchored on activated silica do not display any activity in this reaction (Figure 5.14b).

The use of crosslinked styrenedivinylbenzene resins with acetylacetone (Figure 5.14c) results in an active telomerization catalysts in the presence of phosphine ligands, although it is believed that activity is due to the leaching of palladium into solution, leading to homogeneous catalysis. The same resin was used as a support of palladium linked via bis(diphenylphosphino)methane (DPPM) (Figure 5.14a). This catalyst shows activity for the telomerization reaction but activity decreases after several runs due to superficial erosion caused by mechanical stirring. This system is more active than its analogous, synthesised with 1,3-bis(diphenylphosphino)propane (DPPP) chelating ligands (Figure 5.14d). These last two catalytic systems do not show appreciable leaching of metal species into the reaction medium. The improved performance of the catalysts during the first recycle suggests that the system is characterized by a certain induction period. Catalysts show similar activity and selectivity as the analogous homogeneous catalysts, which suggests that these parameters are not affected by diffusion and steric hindrance in the support [112].

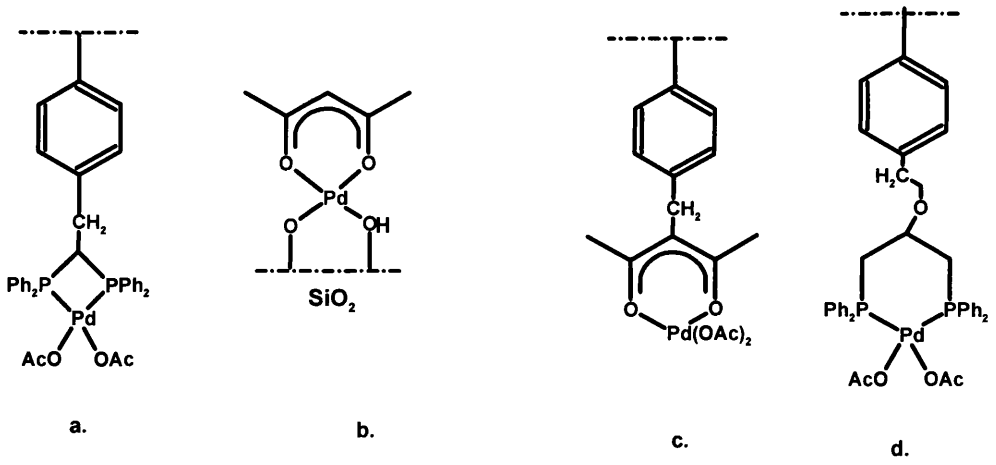

Figure 5.14: Different heterogeneized palladium complexes.

Other heterogeneous catalysts have been screened for the telomerization reaction with water. Pd/C and Pd/Al_2O_3 show activity but during the reaction they are deactivated by the formation of high molecular weight carbon products, necessitating in the oxidative treatment for reactivation [105].

Different montmorillonite supports were tested to anchor a number of palladium precursors, exhibiting high catalytic activity and selectivity in telomerization with water. No intraparticle mass transfer limitations of reactant were observed between liquid phase and palladium located in the interlayer space of the clay. Same activity and selectivity were shown upon reused of catalyst as with the fresh ones [105].

The macrocyclic triolefin 15-membered palladium(0) complexes discussed in the homogeneous part (Figure 5.11) were supported by Muzart et al into silica-based inorganic polymers [120] and into KF/Alumina [121]. The SBA-15 fails as a support for the telomerization reaction but an alternative silica material was used (Figure 5.15). No reaction occurred without added phosphine and it is believed that the palladium species are dissolved in the medium of reaction and redeposit into the supported macrocycle when the reaction is completed.

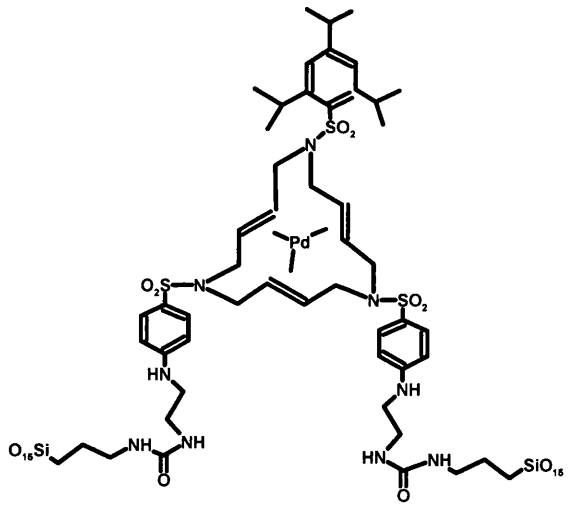

Figure 5.15: Supported Pd-macrocyclic system into silica polymer.

Table 5.13: Telomerization of 1,3 butadiene with phenol over heterogeneous catalysts [121].

Run	Time (min)	Pd: PhOH: butadiene	Phenol conversion (%)	Selectivity (%)			TON
				Linear telomer	Branched telomer	Dimers	
1	120	1:88:176	29.5	51	3	34	26
2	128	1:88:176	100	92	4	4	88
3	124	1:88:176	97	86	7	7	86
4	120	1:88:176	95.5	84	8	8	84
5	120	1:88:176	96.5	94	3	3	85
6	125	1:88:176	80.5	94	3	3	71
7	118	1:88:176	100	92	4	4	88
8	123	1:88:176	93	96	3	1	82
1	125	1:176:352	28.5	91	2	6	50
2	121	1:176:352	58	91	4	5	102
3	120	1:176:352	95.8	92	5	3	169
4	120	1:176:352	94	95	3	2	165

Reaction conditions: Catalyst system: $Pd(TPPTS)_n$-KF/Al_2O_3; Pd = 0.25 mmol; acetone = 5 mL; T = 60°C.

Table 5.14: Efficiency of various $Pd(TPPTS)_n$/supports in telomerization of 1,3-butadiene with methanol [121].

Support	Run	Butadiene conversion (%)	Selectivity (%)			TON
			Linear telomer	Branched telomer	Dimers	
montmorillonite	1	36	78	4	18	720
	2	16	82	6	12	320
	3	2	71	1	28	40
silica	1	23	70	10	20	460
	2	31	75	20	5	620
	3	0	-	-	-	0
KF/Al_2O_3	1	18	70	4	26	360
	2	22	68	6	26	440
	3	16	73	4	23	320
	4	18	71	5	24	360

Reaction conditions: Catalyst system: $Pd(TPPTS)_n$-KF/Al_2O_3; Pd = 0.25 mmol; acetone = 5 mL; T = 60°C; Pd:MeOH:butadiene = 1:6000:4000; 1 hour.

Table 5.15: Telomerization of 1,3-butadiene with methanol and phenol with Pd-macrocyclic complexes supported on silica [120].

Alcohol	$Pd/PPh_3/C_4H_6/ROH$	Butadiene conversion (%)	Selectivity (%)		
			Linear telomer	Branched telomer	Dimers
MeOH	1/3/4000/6000	18	38	4	58
MeOH	1/2/4000/6000	14	0	0	100
MeOH	1/4/4000/6000	8	5	0	95
MeOH	1/3/4444/10000	28	0	0	100
PhOH	1/3/24100/129	67.7	78	22	-
PhOH	1/3/19900/96	100	67	33	-
PhOH[b]	1/3/20300/105	100	74	26	-
PhOH	1/3/13900/58[c]	100	68	32	-
PhOH[b]	1/3/19850/65[c]	100	78	22	-

Reaction conditions: butadiene = 1mL; time: 2 hours whit MeOH and 3hours with PhOH, T = 60°C. [b]. Recycling experiments [c]. 150 equiv of Pd are added of Et_3N.

Table 5.16: Telomerization of 1,3-butadiene with methanol by heterogenized palladium complexes [112].

Catalyst precursor	T (°C)	Conversion (%)	Selectivity (%)		
			Linear telomer	Branched telomer	Dimers
Dow-DPPM-$Pd(OAc)_2$	60	32.8	74.7	13.7	11.5
2nd cycle	60	18.4	76.1	16.2	7.7
3rd cycle	60	18.2	75.5	16.0	8.5
Dow-DPPM-$Pd(OAc)_2$	80	48.8	68.1	15.3	16.6
2nd cycle	80	33.5	70.3	14.9	14.8
3rd cycle	80	27.7	70.6	14.7	14.7
4th cycle	80	17.2	64.9	14.1	21.0
5th cycle	80	16.5	70.2	12.4	17.4
Dow-DPPM-$Pd(OAc)_2$[a]	60	100	67.5	9.7	20.1
2nd cycle[a]	60	92.0	68.9	8.9	19.5
3rd cycle[a]	60	67.6	65.6	11.9	22.1
4th cycle[a]	60	65.6	68.1	9.6	22.0
5th cycle[a]	60	51.6	70.4	7.7	21.7

Reaction conditions: Catalyst: Palladium(II) complexes anchored to polymer-bound diphenylphosphine by their homogeneous analogues; n-hexane = 20 mL; P = 0.05 mol; P/Pd = 2 mol/mol; $MeOH/C_4H_6$ = 1.5 mol/mol; C_4H_6/Pd = 2000 mol/mol; 18 hours. [a] In the presence of NaOMe as promoter.

Table 5.17: Telomerization of 1,3 butadiene with methanol by heterogeneized catalysts [119].

Catalyst precursor	T (°C)	Conversion (%)	Selectivity (%)		
			Linear telomer	Branched telomer	Dimers
Dow-DPPP-Pd(0)	60	0.2	0.9	traces	99.1
Dow-DPPP-Pd(0)	80	0.4	2.3	2.6	95.2
Dow-DPPP-Pd(0)	100	1.6	0.4	1.0	98.6
Dow-DPPP-Pd(II)	60	1.7	0.7	0.3	99.0
Dow-DPPP-Pd(II)	80	0.1	7.5	23.5	69.0
Dow-DPPP-Pd(II)[a]	60	0.7	9.9	3.8	86.0
Pst-DPPP-Pd(II)	60	0.3	0	0	100
Dow-DPPP-Pd(II)[b]	60	87.0	80.1	6.0	7.9
Dow-DPPP-Pd(II)[b, c]	60	97.0	87.5	5.5	7.0
Pst-DPPP-Pd(II)[b,d]	60	83.1	82.0	7.2	10.2
Pst-DPPP-Pd(II)[b, e]	60	66.2	73.2	8.9	16.6
Pst-DPPP-Pd(II)[b,f]	60	24.3	29.7	2.9	66.0
Dow-DPPP-Pd(0)[b]	60	68.0	87.0	7.0	6.0
Dow-DPPP-Pd(0)[b,g]	60	98.0	86.5	6.8	6.8

Reaction conditions: Catalyst: Palladium(II) complexes anchored to polymer-bound diphenylphosphine. (Figure 5.14.d); P = 0.05 mol; P/Pd = 2 mol/mol; C_4H_6/Pd = 6500 mol/mol; MeOH/C_4H_6 = 1.5 mol/mol; 18 hours. [a] In the presence of 15 mL of toluene. [b]. In the presence of MeONa as promoter MeONa/Pd = 10 mol/mol [c]. Pd = 0.08 mmol [d]. In the presence of 20 mL of n C_6H_{14} [e]. In the presence of 20 mL of toluene [f]. In the presence of 20 mL of THF [g]. MeOH/C_4H_6 = 3.0 mol/mol.

Table 5.18: Telomerization of 1,3-butadiene with methanol by fresh and recycled catalysts [119].

Precursor	Released Pd (%)	Conversion (%)	Selectivity (%)	
			Telomers	Dimers
Dow-DPPP-Pd(II)	1.6	13.4	76.1	22.1
1st recycle	1.4	19.9	94.1	4.9
2nd recycle	1.1	11.3	91.7	7.6
3rd recycle	0.6	11.4	88.8	10.2
4th recycle	0.3	10.5	86.8	12.1

Reaction conditions: Dow-DPPP-Pd(II) complex; Pd = 0.08 mmol; C_4H_6/Pd = 6500 mol/mol; MeOH/C_4H_6 = 1.5 mol/mol; MeONa/ Pd = 10 mol/mol; time = 3 hours; 20 mL of n-hexane; T = 60°C.

Table 5.19: Telomerization of butadiene with alcohols by polymer-bound Pd(0) complexes [122].

P/Pd ratio	ROH	T (°C)	Time (h)	TON (h^{-1})	Selectivity (%)		
					Linear telomer	Branched telomer	Dimers
4.0	MeOH	80	5	98	85	8	7
4.0	MeOH	80	0.5	90	87	6	7
4.0	EtOH	90	18	99	74	11	14
4.0	EtOH	90	2	23	83	4	13
2.0	EtOH	90	1	34	91	6	3
4.0	i-PrOH	95	2	99	73	22	5
4.0	HOC_2H_4OH	95	18	72	89	7	4

Reaction conditions: Polystyrene-bound palladium (0) catalyst = 0.1 mmol, alcohol = 16 mL; solvent: benzene = 4 mL; butadiene = 120 mmol.

5.2.5 REACTION CONDITIONS

5.2.5.1 Telomer / nucleophile ratio

The concentration of telomer affects the regioselectivity of the attack of the nucleophile on the (allyl)palladium complex. An increase in telomer concentration favours loss of coordination of the internal olefin in the complex B (Figure 5.5 and Figure 5.16), producing the intermediate complex F (Figure 5.16), analogous to complex D (Figure 5.5). Thus, an excess of butadiene has an analogous effect as an excess of phosphine [103].

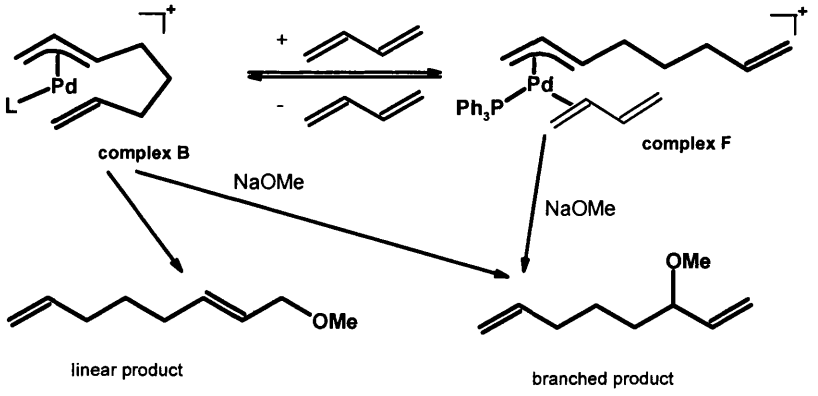

Figure 5.16: Influence of telomer / nucleophile ratio on selectivity [103].

The ratio of telomer to nucleophile also influences the chemoselectivity of the reaction. At low nucleophile (methanol) concentrations, the dimer products are favoured [103]. A decrease in the telomer/nucleophile ratio results not only in an increase in the diene conversion, but also allows to improve the chemoselectivity to telomers and the regioselectivity to the linear telomers [101, 112]. In Table 5.20 the ratios telomer/nucleophile used in different references are shown.

Table 5.20: List of ratios telomer/nucleophile used in different references.

Telomer	Nucleophile	Ratio telomer/nucleophile	Reference
butadiene	methanol	0.2 - 2	[94]
butadiene	methanol	0.66	[101]
butadiene	methanol	0.33 – 1.8	[119]

Table 5.21: Telomerization of 1,3 butadiene with methanol. Influence of nucleophile/telomer ratio [101].

$MeOH/C_4H_6$ (mol/mol)	Conversion (%)	Selectivity (%)		
		Linear telomer	Branched telomer	Dimers
3.0	95.1	89.0	5.8	4.8
1.5	93.3	90.5	4.1	5.4
1.0	59.4	82.3	7.9	9.3

Reaction conditions: Catalyst system: $Pd(dba)_2$ (0.1 mmol)/ DPPM system; Pd/P/MeOH = 1/2/3000; solvent: n-hexane = 20 mL; time = 4 hours; T = 60°C.

5.2.5.2 Temperature of reaction

By variation of the reaction temperature, it is possible to obtain different products selectively [102]. The reaction rate increases at the expense of selectivity at elevated temperature favouring the formation of dimers [101, 107].

Table 5.22: Telomerization of 1,3-butadiene with methanol. Influence of temperature [101].

T (°C)	Conversion (%)		Selectivity (%) @ 0.5h		Selectivity (%) @ 4h	
	0.5 h	4 h.	Telomers	Dimers	Telomers	Dimers
60	26.6	46.0	95.3	4.5	92.8	6.8
80	39.2	75.1	85.5	14.4	83.4	16.3
100	59.0	100	77.0	22.8	72.1	27.3

Reaction conditions: $Pd(dba)_2$/ DPPP system; $Pd(dba)_2$ = 0.1 mmol; Pd/P/MeOH/ C_4H_6 = 1/2/3000/2000; solvent: n-hexane = 20 mL.

Table 5.23: Telomerization of 1,3-butadiene with methanol. Influence of the reaction temperature on the product selectivity [103].

Ratio butadiene / methanol	[catalyst] (%mol)	T (°C)	Time (h)	Conversion (%)	Selectivity (%)	TON
2:1	0.07	-10	6	64	98	914
1:2	0.025	30	2.5	36	95	1376
2:1	0.004	50	2	27	96	6750
2:1	0.001	90	0.5	11	77	10500

Catalyst: (diallyl ether)(triphenylphosphine)palladium (0).

5.2.5.3 Solvent

In most cases, the alcohol used as a nucleophile is also acting as a solvent for the telomers and the catalyst. But, if hydrocarbon solvents, such as toluene or n-hexane, are used, higher activities are obtained compared to other solvents such as tetrahydrofuran or dioxane, when the activity decreases due to their electron donating character. These solvents compete with the reagents in the coordination to the palladium species through their oxygen electron pairs, decreasing the activity and complicating the nucleophile attack, favouring the formation of dimers, and therefore, decreasing the chemoselectivity [112].

When organic polymer-bound complexes are used as catalysts, the degree of swelling should be taken into account when the solvent is selected to favour the diffusion rate of substrates into the polymer matrix [122].

Basset et al [113] used ionic liquids for the telomerization of butadiene with methanol finding that 1,3-dialkyllimidazolium ionic liquids show activity for the reaction. However, the formation of carbene-Pd complexes deactivates the catalyst. Using biphasic systems formed by ionic liquids which do not deactivate the catalyst, such as [BMMI][TF_2N] or [BMMI][BF_4] and a cosolvent such as heptane, it was observed that the catalyst is immobilized in the ionic liquid phase and the products are recovered in the organic phase [113].

Behr et al [95] studied an aqueous biphasic system observing a high selectivity towards telomers and high conversions. The triphenylphosphinetrisulfonate (TPPTS) ligand was used to make the catalyst system water-soluble. High selectivity could be explained by the ligand effect and by in situ extraction of the product monotelomers, which are poorly soluble in the catalytic aqueous phase. The whole process is slower than the monophasic one, but permits effective catalyst recycling due to the easy separation of the catalyst and product phases. In each recycle run, an appropriate quantity of TPPTS ligand has to be added to compensate its oxidation and about 1% of the initial Pd is lost by leaching into the product phase.

Table 5.24: Telomerization of 1,3-butadiene with methanol. Influence of different ionic liquids [94].

Catalyst	Ionic liquid	Conversion (%)	Ratio l/b	Time (h)	Selectivity (%)	TON
$Pd(acac)_2 + PPh_3$	[BuPy][PF_6]	100	18.2	5	56.8	2403
$Pd(acac)_2 + PPh_3$	[BMMI][BF_4]	100	8.1	1	81.8	2619
$Pd(acac)_2 + PPh_3$	[BMMI][TF_2N]	100	8.5	1	84	2537

Reaction conditions: $Pd(acac)_2$ = 30 g.(0.134 mol); PPh_3 = 105 g. (0.400 mol); ionic liquid (4 mL); MeOH = 15 mL (370 mol); C_4H_6 = 20 g (370 mmol), T = 85°C.

Table 5.25: Telomerization of 1,3-butadien with methanol in ionic liquids. Influence of Pd concentration [94].

Catalyst $Pd(acac)_2$ (mmol)	T (°C)	Conversion (%)	Ratio l/b	Time (h)	Selectivity (%)	TON
0.134	85	100	13.7	1	77.9	2769
0.028	85	85	16.0	5.75	77.7	11092
0.025	110	89	11.7	5.75	50.4	11953

Reaction conditions: TPPMS = 3eq/Pd; ionic liquid: [BMMI][TF2N] (4 mL); MeOH = 15 mL (370 mol); C_4H_6 = 20 g (370 mmol).

Table 5.26: Telomerization of 1,3-butadiene with methanol in biphasic systems. Influence of phosphine ligand [94].

Phosphine	Time (h)	Conversion (%)	Ratio l/b	% Pd leaching	Selectivity (%)	TON
TPP	3	82	14.6	14.2	53.3	2127
TPPMS	3	74	1.9	1.9	70.3	1816
TPPDS	3	56	1.8	1.8	58.6	1373

Reaction conditions: $Pd(acac)_2$ = 30 mg (0.134 mmol); Phosphine = 3eq/Pd; ionic liquid: [BMMI][TF2N] (4 mL); heptane = 10 mL; MeOH = 7.5 mL (185 mol); C_4H_6 = 20 g (370 mmol), T = 85°C.

Table 5.27: Telomerization of 1,3-butadiene with ethylenglycol in two phases [92].

Recycle	[Catalyst] (%mol)	Ligand	Ratio BUi/EG	Ratio ligand/Pd	Product yield %			TON
					Mono-telomers	Ditelomers	Oligomers	
Start	0.06	TPPTS	2.5	5	80	<0.5	<1	1356
1	0.06	TPPTS	2.5	5	74	<0.5	1	1253
2	0.06	TPPTS	2.5	5	23	<0.5	2	384
Start[b]	0.06	TPPTS	2.5	5	74	<0.5	<1	1249
1[b]	0.06	TPPTS	2.5	5	84	<1	<1	1418
2[b]	0.06	TPPTS	2.5	5	83	<1	<1	1393
3[b]	0.06	TPPTS	2.5	5	79	<1	<1	1324
4[b]	0.06	TPPTS	2.5	5	76	<1	<1	1278
5[b]	0.06	TPPTS	2.5	5	68	<1	<1	1145
6[b]	0.06	TPPTS	2.5	5	56	<0.5	<1	936
Start[c]	0.02	Carbene[a]	2.5	2	14	48	2	2889
start	0.02	Carbene[a]	4.2	2	15	73	5	4135

Reaction conditions: $Pd(acac)_2$ + ligand; 10 mL H_2O; 4 h; T = 80°C. [a]. N-heterocyclic carbene 1,3-dimesityl-imidazolin-2-ylidene [b].2.5 equivalents of TPPTS are added per recycle [c]. time = 3 hours.

Table 5.28: Telomerization of 1,3-butadiene with methanol with different promoters [114].

Alkoxide	Alk/Pd (mol/mol)	T (°C)	Butadiene conversion (%)	Selectivity (%)		
				Linear telomer	Branched telomer	Dimers
MeONa	10	50	35.5	74.6	0.5	22.6
MeONa	10	60	51.0	78.1	2.8	18.1
MeONa	10	70	34.6	68.2	3.0	28.3
MeONa	10	80	33.9	72.0	3.0	25.0
MeONa	4	60	13.4	55.4	0.6	38.9
MeONa	20	60	51.2	70.0	2.2	26.6
^{t}BuOK	5	60	18.1	49.7	1.2	46.4
^{t}BuOK	10	60	28.0	62.8	2.7	33.0
^{t}BuOK	20	60	44.3	59.0	4.4	35.0
^{t}BuOK	50	60	53.3	68.2	1.5	28.6

Reaction conditions: $PdCl_2Y_2$ = 0.1 mmol; Pd/P/MeOH/C_4H_6 = 1/2/3000/2000; solvent: n-hexane = 20 mL, time = 5 hours.

Table 5.29: Telomerization of 1,3-butadiene with methanol in ionic liquids [113].

Ionic liquid	Time (h)	Conversion (%)	Selectivity (%)			TON
			Telomers	VCH	Dimers	
[EMI][TF_2N]	22	7	27.5	44.7	0.6	271
[BuPy][PF_6]	5	100	56.8	1.0	28.1	2403
[BMMI][BF_4]	1	100	81.8	0.2	15.1	2619
[BMMI][TF_2N]	1	100	84.0	0.2	13.7	2537

Reaction conditions: $Pd(OAc)_2$ = 30 mg (0.134 mmol); PPh_3 = 105 mg (0.400 mmol); ionic liquid = 4mL, MeOH = 15 mL (370 mmol); C_4H_6 = 20 g (370 mmol); T = 85°C.

Table 5.30: Telomerization of 1,3-butadiene with EG in an aqueous biphasic system [95].

Run	Yield to monotelomers (%)	Total TON
1	73	1249
2	84	2667
3	84	4060
4	78	5384
5	76	6662
6	69	7807
7	55	8743

Aqueous biphasic system. Bu:EG = 2.5:1; $Pd(acac)_2$ = 0.006 %mol (based on EG) + 5 equiv. NaTPPTS ligand; ligand supplementation: 2.5 equiv. per recycle; 10 mL H_2O; 20 mL EG; 4 hours; T = 80°C.

5.2.5.4 Influence of nucleophile

Conversion and chemoselectivity to telomers in the telomerization with alcohols depend also on the length of the alcohols used as nucleophiles. The conversion decreases drastically from methanol to 1-propanol and then it reaches almost a steady value. Similar behaviour is observed with the chemoselectivity to telomers [101].

Table 5.31: Telomerization of 1,3 butadiene with different alcohols [102].

Nucleophile	Ligand	Conversion (%)	Time (h)	Ratio C:O allylated product
α-naphthol	PCy_3	47	12	> 98 : 2
β-naphthol	PPh_3	84	16	> 98 : 2
Resorcinol monomethyl ether	PCy_3	63	16	> 98 : 2
Phloroglucinol dimethyl ether	PPh_3	72	12	> 98 : 2
3-dimethyllaminophenol	PPh_3	41	16	> 98 : 2
3,4- methyl enedioxyphenol	PCy_3	46	16	> 98 : 2
β-naphthol	PCy_3	55	16	> 98 : 2

Reaction conditions: 100 mmol ROH; 200 mmol 1,3-butadiene; 0.5% mol $Pd(acac)_2$; ratio Pd:Ligand = 1:3; THF; NEt_3; T = 90°C.

Table 5.32: Telomerization of 1,3-butadiene and different alcohols [97].

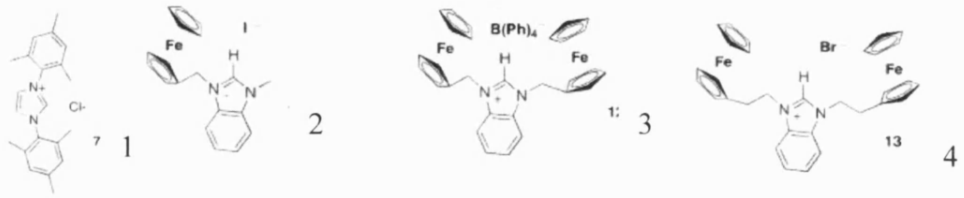

1 2 3 4

a. different imidazolium salts (carbenes).

ROH	Pd (%mol)	Ligand	Pd:ligand ratio	Telomer yield (%)	Selectivity (%)	Linear: branched telomer	TON
$n\text{-}C_4H_9OH$	0.001	PPh_3	1:4	20	36	16:1	20000
$i\text{-}C_3H_7OH$	0.005	PPh_3	1:4	3	29	-	600
$n\text{-}C_4H_9OH$	0.001	1[a]	1:4	90	93	44:1	90000
$n\text{-}C_4H_9OH$	0.001	2[a]	1:4	15	90	99:1	15000
$n\text{-}C_4H_9OH$	0.001	3[a]	1:4	85	86	70:1	85000
$n\text{-}C_4H_9OH$	0.001	4[a]	1:4	79	84	70:1	79000
$i\text{-}C_3H_7OH$	0.005	1[a]	1:4	71	75	52:1	14200
$i\text{-}C_3H_7OH$	0.005	2[a]	1:4	2	29	-	400
$i\text{-}C_3H_7OH$	0.005	3[a]	1:4	35	40	99:1	7000
$i\text{-}C_3H_7OH$	0.005	4[a]	1:4	27	32	99:1	5400

Reaction conditions: 16 h; 90°C; 1%mol NaOH, ROH:Bu = 2:1; $Pd(dba)_2$

Table 5.33: Telomerization of 1,3-butadiene with different primary alcohols [101].

Alcohol	Conversion (%)	Selectivity (%)		
		Linear telomer	Branched telomer	Dimers
CH_3OH	93.3	90.4	4.1	5.3
C_2H_5OH	46.0	79.4	3.6	17.0
n-C_3H_7OH	37.8	70.6	2.4	25.9
n-C_4H_9OH	36.9	69.3	2.5	28.2
n-$C_5H_{11}OH$	33.2	60.2	4.3	35.5
n-$C_6H_{13}OH$	40.5	70.3	0.7	29.0

Reaction conditions: Catalyst system: $Pd(dba)_2$ (0.1 mmol)/ DPPM system; $Pd/P/ROH/C_4H_6$ = 1/2/3000/2000; solvent: n-hexane = 20 mL; time = 4 hours; T = 60°C.

Table 5.34: Telomerization of 1,3-butadiene with different primary alcohols [101].

P^P ligand	Alcohol	Conversion (%)	Selectivity (%)	
			Telomers	Dimers
DPPE	CH_3OH	64.2	97.7	2.1
DPPE	C_2H_5OH	30.1	74.9	24.3
DPPE	n-C_3H_7OH	39.7	30.6	68.8
DPPE	n-$C_6H_{13}OH$	22.1	23.2	76.5
DPPB	CH_3OH	99.9	97.5	2.5
DPPB	C_2H_5OH	83.0	84.2	13.6
DPPB	n-C_3H_7OH	78.4	73.3	26.2
DPPB	n-$C_6H_{13}OH$	36.0	66.3	33.1

Reaction conditions: Catalyst system: $Pd(dba)_2$ = 0.1 mmol; Ph_2P-$(CH_2)_n$-PPh_2 ligands solvent: hexane = 20 mL; $Pd/P/ROH/C_4H_6$ = 1/2/3000/2000 mol/mol; time = 4 hours; T = 60°C.

Table 5.35: Telomerization of 1,3-butadiene with different alcohols with carbene-Pd(0) complexes [96].

ROH	Catalyst	Catalyst [%mol]	Telomer yield (%)	Selectivity (%)	Linear: branched telomer	TON
n-butanol	$Pd(OAc)_2$/ 3 equiv PPh_3	0.001	36	47	95:5	76000
n-butanol	[a] complex 8	0.001	97	97	98:2	99500
n-butanol	[a] complex 9	0.001	97	97	99:1	99500
n-butanol	[a] complex 10	0.001	63	86	96:4	73000
n-butanol	[a] complex 11	0.001	89	89	89:11	99500
n-butanol	[a] complex 12	0.001	34	43	89:11	78000
iso-propanol	$Pd(OAc)_2$/ 3 equiv PPh_3	0.005	3	16	97:3	3800
iso-propanol	[a] complex 8	0.005	82	82	98:2	20000
iso-propanol	[a] complex 9	0.005	85	85	99:1	20000
iso-propanol	[a] complex 10	0.005	68	68	98:2	20000
iso-propanol	[a] complex 11	0.005	37	37	99:1	19800
benzyl alcohol	[a] complex 8	0.005	96	96	97:3	19200
benzyl alcohol	[a] complex 9	0.005	96	96	98:2	20000
n-hexanol	[a] complex 8	0.001	90	95	97:3	95000
n-hexanol	[a] complex 9	0.001	93	93	98:2	99800
2-methoxyethanol	[a] complex 8	0.001	98	98	98:2	99800
2-methoxyethanol	[a] complex 9	0.001	95	98	99:1	96500
phenol	[a] complex 8	0.005	37	97	98:2	7600
2-metylphenol	[a] complex 8	0.005	56	97	84:16	11500
2,6-dimethylphenol	[a] complex 8	0.005	86	92	84:16	18600

Reaction conditions: 16 h; 70°C; 1%mol NaOH, ROH:Bu = 2:1.
a. See Figure 5.13.

5.3 RESULSTS AND DISCUSSION: TELOMERIZATION REACTION WITH HOMOGENEOUS CATALYSTS

Different homogeneous catalysts were tested in the telomerization reaction of isoprene and 1,3-pentadiene. Two main groups of catalysts were used, the classical combination of a palladium salt and a phosphorus compound acting as a ligand versus carbene ligands. The chemical structures of the ligands used in this study are shown in Figure 5.17.

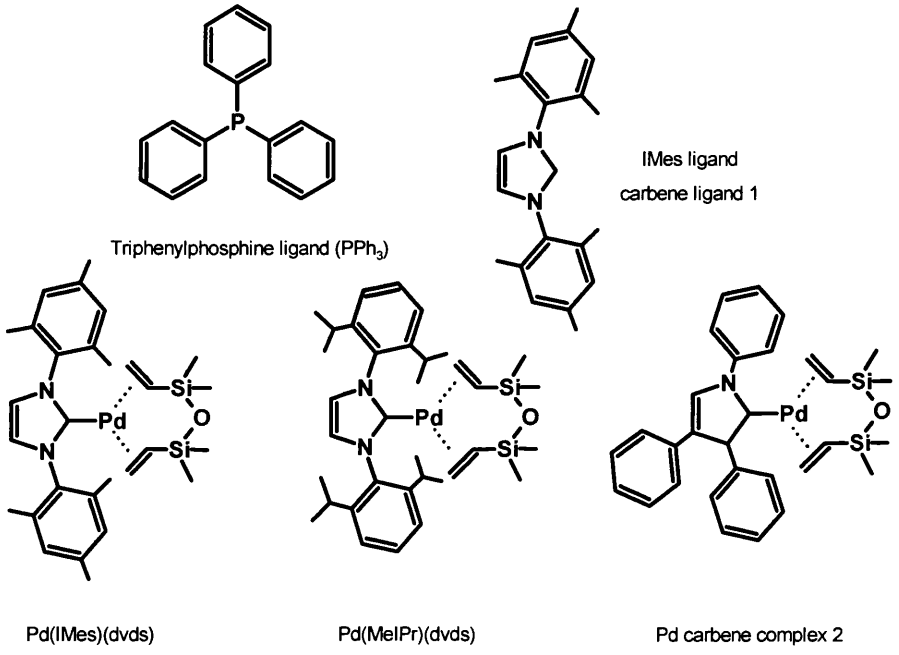

Figure 5.17: Homogeneous ligands and complexes for telomerization reaction.

The influence of different parameters such as initial concentrations of reactant and nucleophile were studied. Conversion and turn over numbers are calculated relative to the disappearance of reactant according to Equations (5.1) and (5.2). These values could not be calculated relative to the appearance of products because only products of the telomerization of isoprene with methanol were isolated (by Cardiff and Rostock Universities) and therefore only gas chromatography calibrations were done for them. The rest of products were identified by GC-MASS (Appendix I).

$$Conversion = \left(\frac{C_0 - C_i}{C_0} \right) \cdot 100 \qquad (5.1)$$

where C_i is the concentration of reactant at a determined time and C_0 is the initial concentration of reactant.

$$TON = \frac{moles\ of\ telomer\ reacted}{moles\ of\ catalyst\ (Pd)} \qquad (5.2)$$

Selectivity values were calculated for telomerization reaction versus side reactions such as dimerization and trimerization. Regioselectivity values were calculated for different telomerization isomers.

5.3.1 TELOMERIZATION OF ISOPRENE

The telomerization of isoprene with methanol as a nucleophile can potentially lead to tail-to-head, head-to-head and tail-to-tail telomerization products and dimers and trimers as by-products. The reaction scheme is shown in Figure 5.18.

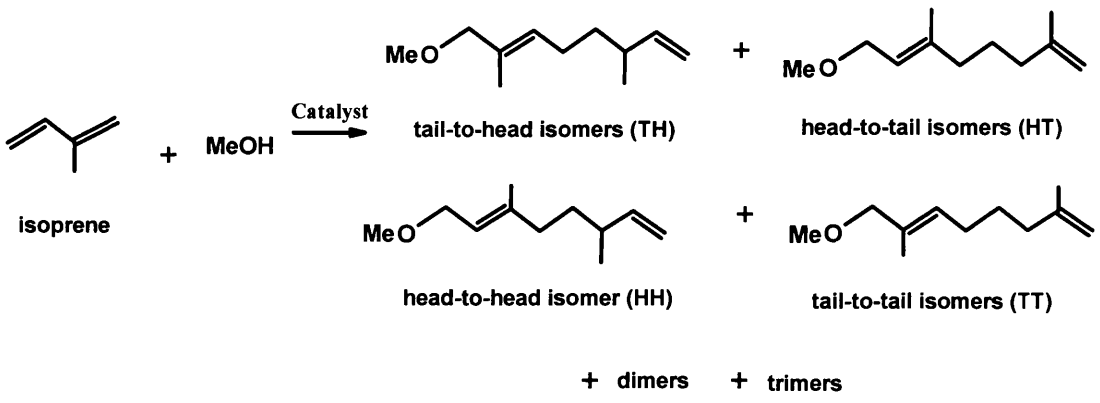

Figure 5.18: Scheme of potential products of isoprene telomerization with methanol.

As shown in the literature review, a typical catalyst for this reaction consists of a palladium salt and a phosphorus compound to form an active catalyst in-situ. However, better results have been obtained with carbene ligands instead of phosphorus compounds. In this study, several catalysts based on both the Pd/P and

the Pd/carbene ligands were tested for the telomerization of isoprene. The results obtained are summarized in Table 5.36.

Table 5.36: Telomerization of isoprene with different homogenous catalysts.

Catalyst	T (°C)	TON	Conversion (%) @7h	Selectivity (%) @7h	Regioselectivity (%) HT	HH	TT
$Pd(acetate)_2$ + 3 eq. PPh_3	70	1537	18.9	77.4	63.4	4.9	31.7
$Pd(acac)_2$ + 3 eq. PPh_3	70	862	10.6	73.5	67.5	5.5	26.9
Pd(MeIPr)(dvds)[b]	70	5.4	0.2	71.7	17.3	76.3	6.5
Pd carbene complex 2[b]	70	1740	42.9	98.6	23.2	74.6	2.1
Pd(Imes)(dvds)	70	3694	45.5	87.9	14.2	85.0	0.8

Reaction conditions: 3.25 mL Isoprene (4.35 M). Solvent: 3.25 mL dry 1%NaOMe MeOH, 1 mL decane as internal standard. Time: 7h. Catalyst: $4 \cdot 10^{-6}$ moles of Pd. ([b] $8 \cdot 10^{-6}$ moles of Pd).

High conversions were obtained with all tested palladium catalysts except with the complex Pd(MeIPr)(dvds) which almost does not show catalytic activity for this reaction. When triphenylphosphine is used as a ligand, different conversion values are obtained depending on the palladium salt. The best results are obtained with palladium acetate without any influence on selectivity. The reason for this observation might be the easy accessibility of the palladium atom to form active telomerization species in combination with the triphenylphosphine ligands. However, palladium complexes based on carbene ligands show much higher conversion in this reaction, especially the complex Pd(Imes)(dvds). The difference between the three tested carbene complexes is related to the electronic density around the palladium atom. Substitution with an electron donating methyl group in the backbone of the carbene stabilizes the complex and therefore reduces the reactivity [96], same effect is promoted by isopropyl substitutions in the benzene rings, reasons of the low activity obtained with Pd(MeIPr)(dvds) complex.

Comparing the catalysts, in some cases, the selectivity to telomerization decreases due to the formation of dimers. When the combination of a palladium salt and triphenylphosphine ligand is used as a catalyst, the main telomerization product obtained is the head-to-tail isomer, followed by the tail-to-tail one, in accord with previous observations [100]. However, when a carbene is used as a ligand, the

main telomerization product is the head-to-head isomer. The mechanism of the telomerization of isoprene is similar to 1,3-butadiene (Figure 5.5) and independent on the ligand used. Hence, the apparent differences are likely to be due to the high basicity and more planar structure of carbene ligands. According to the literature [104], cycle A is favoured over cycle B when carbenes are used as ligands, due to the electrochemical properties of carbene ligands, resulting in different regioselectivity. On the other hand, cycle B is predominant when phosphorus ligands are used. Carbene ligands exhibit poor π-acceptor properties which results in an electronically directed nucleophile attack at carbon atom 1. However, steric effects of carbene ligands can also play an important role in the regioselectivity compared to phosphorus ligands.

5.3.1.1 Influence of initial concentration of isoprene

An important parameter to study, focusing on the tandem reaction objective, is the initial concentration of reactant in the telomerization reaction. For this reason, different initial concentrations of isoprene between 2 and 7 M were tested under the same reaction conditions using Pd(Imes)(dvds) as a catalyst. The results are shown in Table 5.37.

Table 5.37: Influence of initial concentration of isoprene.

Initial concentration (M)	$(r_A)_{max}$ (mol/L·h)	TON	Conversion (%) @7h	Selectivity (%) @7h	Regioselectivity (%)		
					HT	HH	TT
6.3	- 0.4846	6363	53.7	93.0	31.0	67.8	1.2
5.0	- 0.3581	4700	50.2	90.6	22.8	76.3	0.9
4.3	- 0.2816	3694	45.5	87.9	14.2	85.0	0.8
3.3	- 0.2344	3077	49.3	88.7	19.6	79.6	0.8
2.3	- 0.1235	1621	37.1	89.9	19.1	80.2	0.7

Reaction conditions: Solvent: up to a total volume of 6.5 mL dry 1%NaOMe MeOH, 1 mL decane as internal standard. Time: 7h. Catalyst: $4 \cdot 10^{-6}$ moles Pd(Imes)(dvds).

Similar selectivity values are obtained when different initial concentrations of isoprene are used, which suggests that the formation of dimers is not affected by

the telomer/nucleophile ratio. However, it has influence on the regioselectivity of the telomerization products. When the initial concentration of isoprene is increased, the formation of head-to-tail products is favoured versus head-to-head ones, following the conclusions obtained previously by Benvenuti et al [101, 112] for the telomerization of 1,3-butadiene with methanol.

The initial rates of reaction were calculated in reactions with different initial concentrations of isoprene. The reaction profile obtained for an initial concentration of 4.35 M is shown in Figure 5.19, initial rate of reaction was calculated as the maximum rate obtained during the first hour of reaction. As it was expected, initial rate of reaction increased when the initial concentration of isoprene was increased.

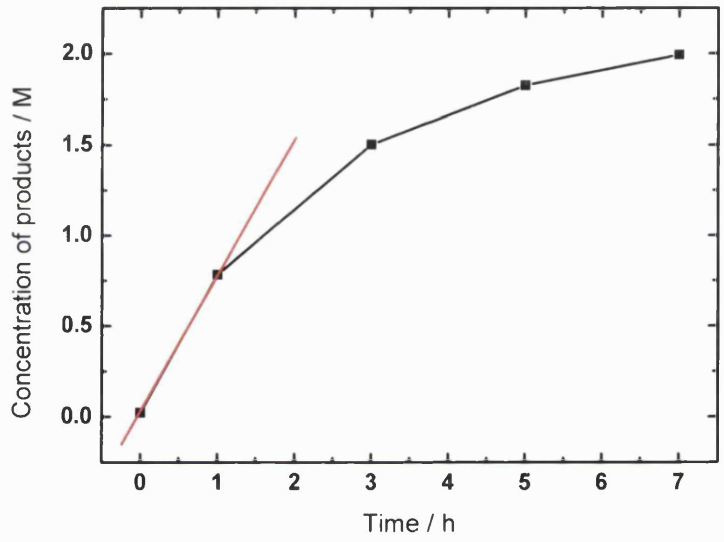

Figure 5.19: Reaction profile of telomerization of isoprene (4.35 M) with methanol and calculation of maximum rate of reaction.

In order to calculate kinetic constant and the order of reaction, Equation (5.3) was used.

$$(-r_A) = k \cdot C_A^n \cdot C_B^m \qquad \textbf{(5.3)}$$

Where the concentrations of the reactants isoprene and methanol are represented by C_A and C_B respectively.

Different orders of reactions were considered (first and second order for both reactants) with the best correlation obtained when second order for isoprene and first order for methanol were used, which is in accordance with the proposed mechanism, in which two molecules of isoprene and one molecule of methanol react together to form the telomerization products. In this case, the above Equation (5.3) is linearized to give the Equation (5.4).

$$\ln(-r_A) = \ln K + 2 \cdot \ln(C_A) + \ln(C_B) \tag{5.4}$$

Kinetic data are summarized in Table 5.38. Correlation of the data is shown in Figure 5.20.The kinetic constant for the telomerization of isoprene with methanol at 70°C was found $1.41 \cdot 10^{-3}$ $L^2 \cdot mol^{-2} \cdot h^{-1}$. Due to the decomposition of catalysts at higher temperatures than 70°C, it was impossible to calculate the activation energy for the telomerization of isoprene.

Table 5.38: Kinetic data for the telomerization of isoprene with methanol at 70°C.

Initial concentration of isoprene (M)	Initial concentration of MeOH (M)	$(r_A)_{max}$ (mol/L·h)	ln (r_A)	$2 \cdot \ln(C_A) + \ln(C_B)$
4.99	8.24	-0.3581	-1.0269	5.324
4.32	9.74	-0.2816	-1.2672	5.205
3.33	10.98	-0.2344	-1.4507	4.888
2.33	14.23	-0.1235	-2.0915	4.346

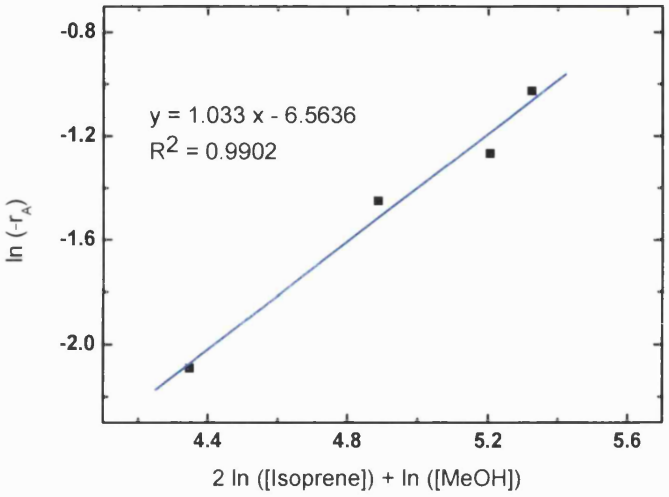

Figure 5.20: Correlation of kinetic data to calculate kinetic constant for the telomerization of isoprene with methanol at 70°C.

5.3.1.2 Influence of the nature of the nucleophile

The effect of the nucleophile on the telomerization of isoprene was studied, through homologous sequence of alcohols. The results are shown in Table 5.39.

Table 5.39: Influence of nucleophile in the telomerization of isoprene.

Catalyst	Nucleophile	T (°C)	TON	Conversion (%) @7h	Selectivity (%) @7h
Pd(Imes)(dvds)	MeOH	70	3694	45.5	87.9
Pd(Imes)(dvds)	EtOH	70	1433	17.7	100
Pd(Imes)(dvds)	1-propanol	70	6935	85.5	92.1
Pd(Imes)(dvds)	1-propanol	110	7345	90.6	84.1
Pd(Imes)(dvds)	1-butanol	70	6854	84.5	100
Pd(Imes)(dvds)	1-butanol	110	7675	94.6	85.6
$Pd(acac)_2$+3PPh_3[b]	MeOH	70	4055	100	83.5
$Pd(acac)_2$+3PPh_3[b]	EtOH	70	2203	54.3	27.0
$Pd(acac)_2$+3PPh_3[b]	1-propanol	70	1020	25.2	98.0

Reaction conditions: 3.25 mL Isoprene (4.35 M) Solvent: 3.25 mL 1%NaOMe solvent, 1 mL decane as internal standard. Time: 7h. Catalyst: $4 \cdot 10^{-6}$ moles Pd. [b] Catalyst: $8 \cdot 10^{-6}$ moles Pd.

When triphenylphosphine was used as a ligand in combination with a palladium salt, the conversion decreased significantly as the length of the alcohol used as a nucleophile increases. The same trend is followed by selectivity, with special mention to the value obtained when ethanol acts as nucleophile, only 27% of telomerization versus 73% of dimerization. These tendencies are in accordance with what has been previously observed for the telomerization of 1,3-butadiene [101].

Very different results were obtaining when the complex Pd(Imes)(dvds) was used as a catalyst. Conversion increases as longer alcohols were used as a nucleophile, although telomerization of isoprene with ethanol shows lower conversion compared with the value obtained with methanol. This observation could potentially be correlated with a higher solubility of isoprene in longer chain alcohols. However, in this case, the same tendency should be observed with both catalysts. Yet, conversion values decrease dramatically when longer alcohols were used as nucleophiles using a palladium salt and triphenylphosphine ligand as a catalyst. Therefore, the enhancement of conversion obtained with long alcohols as nucleophiles must be related to the catalyst. It could be due to higher solubility or higher stability of carbene ligands in longer chain alcohols.

Telomerization products of isoprene with ethanol, 1-propanol and 1-butanol as nucleophile were identified by their mass spectra (Appendix I)

5.3.2 TELOMERIZATION OF 1,3-PENTADIENE

Telomerization of 1,3-butadiene was studied in detail. Longer linear dienes, such as hexadienes or octadienes, exhibit much lower reactivity or even no reactivity at all with the known catalysts. In order to establish the tandem reaction, telomerization of 1,3-pentadiene was considered. Different catalysts and nucleophiles were screened and the influences of initial concentration of reactant and nucleophile

were studied. However, in this case, it was not possible to distinguish analytically between different telomerization products. Therefore, regioselectivity was not studied.

Telomerization of 1,3-pentadiene, also known as piperylene, with methanol leads to the potential product distribution shown in Figure 5.21. 1,3-pentadiene is an asymmetrical molecule and therefore it is possible to distinguish between head and tail of the molecule.

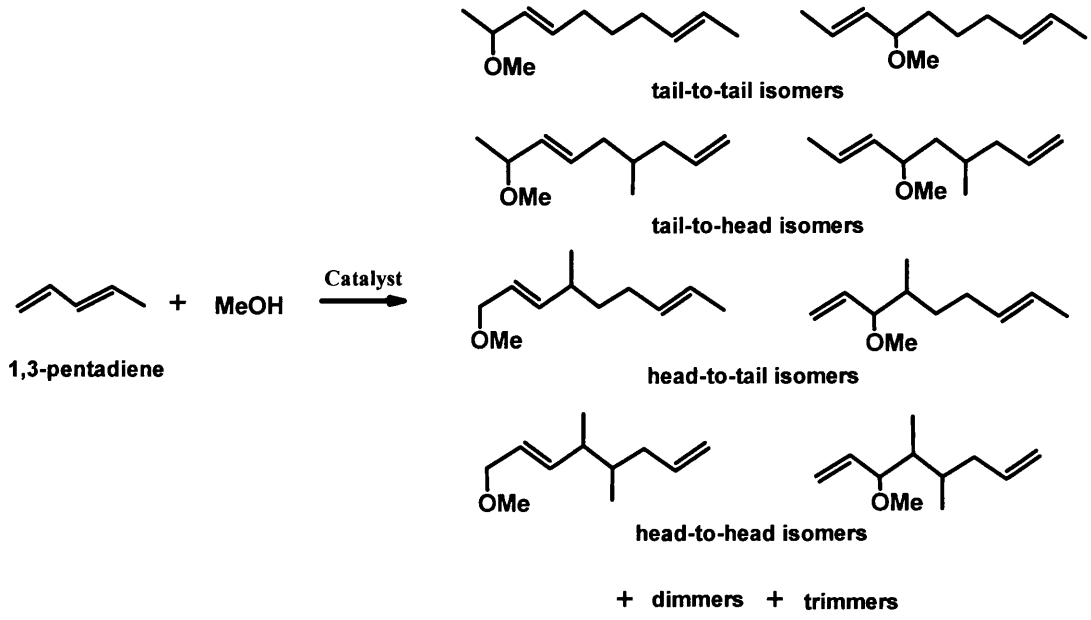

Figure 5.21: Scheme of potential products of 1,3-pentadiene telomerization.

Firstly, different catalysts were screened for the telomerization of 1,3-pentadiene (Table 5.40). Two sets of catalysts were used, both based on palladium catalysts, one with phosphine ligands and the other one with carbene ligands.

Table 5.40: Telomerization of 1,3-pentadiene with methanol and different catalysts.

Catalyst	T (°C)	TON	Conversion (%) @7h	Selectivity (%) @7h
$Pd(acetate)_2$ + 3 eq. PPh_3	70	46	2.4	100
$Pd(acac)_2$ + 3 eq. PPh_3	70	457	24.4	100
Pr(MeIPr)(dvds)	70	25	1.3	100
Pd carbene complex 2	70	91	4.8	91.8
Pd(Imes)(dvds)	70	157	8.4	97.9

Reaction conditions: 1.5 mL 1,3-pentadiene (2 M) Solvent: 5 mL dry 1%NaOMe MeOH, 1 mL decane as internal standard. Time: 7h. Catalyst: $8 \cdot 10^{-6}$ moles of Pd.

As it can be seen from the conversion values, 1,3-pentadiene is much less reactive in the telomerization reaction than isoprene. Based on the literature data, 1,3-pentadiene is also much less reactive than 1,3-butadiene [97, 103]. The only difference between 1,3-butadiene and 1,3-pentadiene molecules is an extra carbon. This might cause steric constrictions when two reactant molecules approach the catalyst, especially considering the bulky ligands attached to the palladium atom. If 1,3-pentadiene and isoprene molecules are compared, the same explanation can be applied. Both molecules have five carbons, however, the branch methyl group in the isoprene molecule could also have an electronic effect on the conjugated double bonds exhibiting more reactivity than 1,3-pentadiene.

Appreciable conversion values were only obtained with the combination of palladium acetylacetonate and triphenylphosphine and the complex Pd(Imes)(dvds). Influence of the palladium salt used in combination with triphenylphosphine ligand was observed, with better results in the case of palladium acetylacetonate. Between carbene based catalysts, only Pd(Imes)(dvds) showed a considerable conversion.

Very high selectivity towards telomerization products values were obtained with all tested catalysts. However, the regioselectivity was impossible to determine.

5.3.2.1 Influence of initial concentration of 1,3-pentadiene

In order to study the effect of the initial concentration of 1,3-pentadiene on conversion and selectivity, reactions were carried out with initial concentrations between 1 and 4.3 M. The results obtained are summarized in Table 5.41.

Table 5.41: Influence of initial concentration of 1,3-pentadiene.

Initial concentration (M)	$(r_A)_{max}$ (mol/h·L)	TON	Conversion (%) @7h	Selectivity (%) @7h
4.3	-0.093	608	14.9	95.9
3.3	-0.054	361	11.6	97.2
2.0	-0.024	157	8.4	98.2
1.0	-0.015	99	10.6	97.9

Reaction conditions: Solvent: up to a total volume of 6.5 mL dry 1%NaOMe MeOH, 1 mL decane as internal standard. Time: 7h. Catalyst: $8 \cdot 10^{-6}$ moles of Pd(Imes)(dvds).

Low conversion values were obtained in the range of initial concentration of 1,3-pentadiene studied. The differences between values are smaller than the error (Appendix II) being impossible to conclude about the influence of the initial concentration of 1,3-pentadiene on conversion. No influence on the selectivity was either observed which could mean that formation of dimers and trimers is not affected by the concentration of reactant in the medium. However, due to the low conversions obtained in all cases, it is difficult to determine if the formation of by-products is favoured versus telomerization at low concentrations of 1,3-pentadiene in the reaction medium.

Initial rate of reactions were calculated assuming that the rate of reaction is constant during the seven hours of reaction. In order to validate this assumption, different tests were carried out in a batch reactor system similar to the one described in Chapter 2 but using a cold finger with dry ice instead of a water reflux. The results showed almost constant rate of reaction due to the low conversion obtained. According to this, rates of reaction were calculated from the reactions carried out in pressure tubes as it was done for isoprene reactions.

Equations (5.3) and (5.4) were used to fit order of reaction and calculate kinetic constant. Kinetic data are shown in Table 5.42 and correlation of the data in Figure 5.22.

Table 5.42: Kinetic data for the telomerization of 1,3-pentadiene with methanol at 70°C.

Initial concentration of 1,3-pentadiene (M)	Initial concentration of MeOH (M)	$(r_A)_{max}$ (mol/L·h)	ln (r_A)	$2 \cdot \ln(C_A) + \ln(C_B)$
4.3	9.7	-0.093	-2.3752	5.205
3.3	12.0	-0.054	-2.9187	4.888
2.0	14.0	-0.024	-3.7339	4.089
1.0	17.2	-0.015	-4.1931	2.843

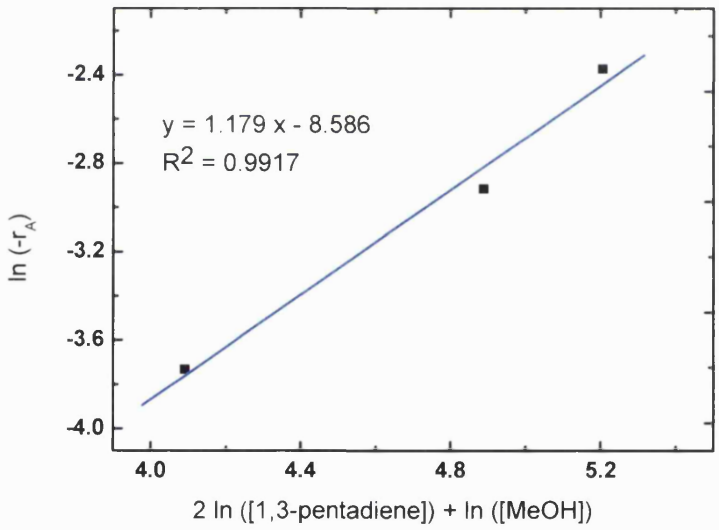

Figure 5.22: Correlation of kinetic data to calculate kinetic constant for the telomerization of 1,3-pentadiene with methanol at 70°C.

According to this, telomerization of 1,3-pentadiene with methanol shows second order respect to 1,3-pentadiene and first order respect to methanol, with a kinetic constant of $1.87 \cdot 10^{-4}$ $L^2 \cdot mol^{-2} \cdot h^{-1}$ at 70°C. The rate constant is almost ten times smaller than the value obtained for the same reaction with isoprene. Due to the

decomposition of catalysts at higher temperatures than 70°C, it was impossible to calculate the activation energy for the telomerization of 1,3-pentadiene.

5.3.2.2 Influence of the nature of nucleophile

Finally, the influence of a nucleophile was studied. Different alcohols such as methanol, ethanol, 1-propanol and 1-butanol have been used. The results obtained are shown in Table 5.43.

Table 5.43: Influence of the nucleophile in the telomerization of 1,3-pentadiene.

Catalyst	Nucleophile	T (°C)	TON	Conversion (%) @7h	Selectivity (%) @7h
Pd(Imes)(dvds)	MeOH	70	157	8.4	98.2
Pd(Imes)(dvds)	EtOH	70	409	21.8	100
Pd(Imes)(dvds)	1-Propanol	70	314	16.7	100
Pd(Imes)(dvds)	1-butanol	70	451	24.1	100
$Pd(acac)_2$+3PPh_3	MeOH	70	457	24.4	100
$Pd(acac)_2$+3PPh_3	EtOH	70	15	0.8	100
$Pd(acac)_2$+3PPh_3	1-Propanol	70	-	-	-

Reaction conditions: 1.5 mL 1,3-pentadiene (2 M) Solvent: 5 mL 1%NaOMe, 1 mL decane as internal standard. Catalyst: $8 \cdot 10^{-6}$ moles Pd(Imes)(dvds).

When the catalyst is formed by $Pd(acac)_2$ and triphenylphosphine as ligand, the increment in the length of the alcohol used as a nucleophile gives a decrease in the conversion obtained. Due to the low values of conversions, it is difficult to see the influence that the nature of nucleophile has on selectivity. These results are in agreement with the results obtained previously for the telomerization of 1,3-butadiene [101].

However, when the carbene complex Pd(Imes)(dvds) was used as a catalyst, the conversion increases when the length of the alcohol used as nucleophile increases being necessary a primary alcohol. No conversion was observed when 2-propanol was used as nucleophile. Same discussion than in the case of isoprene applies. The

increment is not related to the solubility of 1,3-pentadiene but to an increment of stability or solubility of the catalyst.

It can be seen visually that the catalyst does not decompose over time when ethanol is used as a nucleophile which suggests a higher stability of this catalyst in ethanol than in methanol. Figure 5.23 shows the reaction mixture after seven hours when different alcohols were used as nucleophile. Only in the case of methanol, precipitated palladium black was observed. The turbidity of the solution disappears when higher alcohols were used.

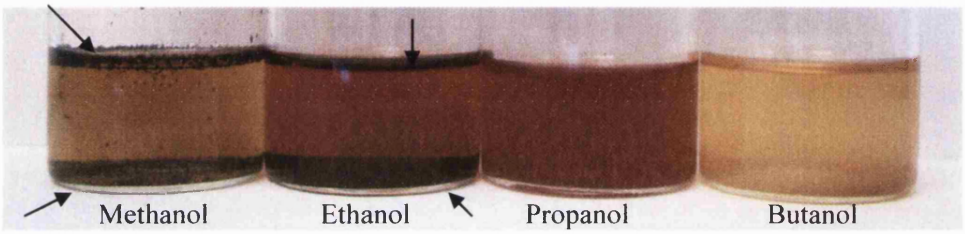

Figure 5.23: Visual decomposition of catalyst into Pd^0 in the telomerization of 1,3-pentadiene when methanol and ethanol are used as solvents.

Telomerization products of 1,3-pentadiene with different alcohols were identified by their mass spectra (Appendix I).

5.3.3 TELOMERIZATION OF 1,3-HEXADIENE

One of the main challenges of the present project is to extend the telomerization reaction to long molecules in order to obtain long chain functionalized products. It has already seen that activity decreases considerably when 1,3-pentadiene is used instead 1,3-butadiene as reactant. Therefore, increasing the length of the reactant one more carbon is expected to show much lower reactivity.

1,3-hexadiene did not show any conversion in the telomerization reaction with methanol with any of the catalysts previously tested with isoprene or 1,3-pentadiene neither palladium complexes based on carbene ligands or the combination of a palladium salt with a phosphorus ligands. Other reaction

conditions such as temperature of reaction or reaction time were also varied without any success.

Considering the improvement of activity found in the telomerization of isoprene and 1,3-pentadiene when a longer alcohol than methanol was used as nucleophile, same study was carried out with 1,3-hexadiene. The results obtained are shown in Table 5.44.

Table 5.44: Influence of the nucleophile in the telomerization of 1,3-hexadiene.

Catalyst	Nucleophile	T (°C)	TON @21h	Conversion (%) @7h	Conversion (%) @21h
Pd(Imes)(dvds)	MeOH	90	-	-	-
Pd(Imes)(dvds)	EtOH	90	78.1	-	14.3
Pd(Imes)(dvds)	1-Propanol	90	281.3	36.1	51.8
Pd(Imes)(dvds)	1-butanol	90	263.1	39.2	48.4

Reaction conditions: 0.5 mL 1,3-hexadiene (0.6 M) Solvent: 5 mL 1%NaOMe, 0.5 mL decane as internal standard. Catalyst: $8 \cdot 10^{-6}$ moles Pd(Imes)(dvds).

In order to compare these results with previous ones, it is important to highlight some differences. Firstly, in this case, a much lower initial concentration of reactant has been used due to the high cost of 1,3-hexediene. Secondly, trying to obtain maximum conversion, the temperature of reaction was optimized to 90°C.

As it was said above, no conversion was obtained when methanol was used as a nucleophile and very low conversion, in the case of ethanol. In both cases, when the reactant 1,3-hexadiene was added into the reaction medium, the solution became completely cloudy. Using longer alcohols as nucleophiles such as 1-propanol and 1-butanol, acceptable conversion values and TON numbers similar to those in the case of 1,3-pentadiene were obtained. In terms of catalytic activity, no difference between both alcohols was observed, similar than what was obtained in the telomerization reaction with isoprene.

As in the above results, the increment of conversion increasing the length of the alcohol using as nucleophile is associated with a higher stability of the catalyst in the reaction medium. Again, the main evidence to support this is that the

combination of a palladium salt and a phosphorus ligand as catalyst does not show any activity. However, in this case, the nucleophile used as a solvent, is believed to have also influence on the solubility of the reactant. When the reactant 1,3-hexadiene is added into the reaction solution on 1-propanol or 1-butanol much less turbidity is observed than in the case of methanol or ethanol.

Telomerization products of 1,3-hexadiene with ethanol, 1-propanol and 1-butanol were identified their mass spectra (Appendix I).

5.4 RESULSTS AND DISCUSSION: TELOMERIZATION REACTION WITH HETEROGENOUS CATALYSTS

One of the main problems found establishing a tandem reaction is the incompatibility of the catalysts due to their interactions during the reaction. A way to resolve this problem is by compartmentalization or immobilization of homogeneous catalysts. In this section, some heterogeneous catalysts based on DVB resins have been tested for the telomerization reaction of both isoprene and 1,3-pentadiene. In Chapter 3, the syntheses and characterizations of these heterogeneous catalysts (Figure 5.24) are described.

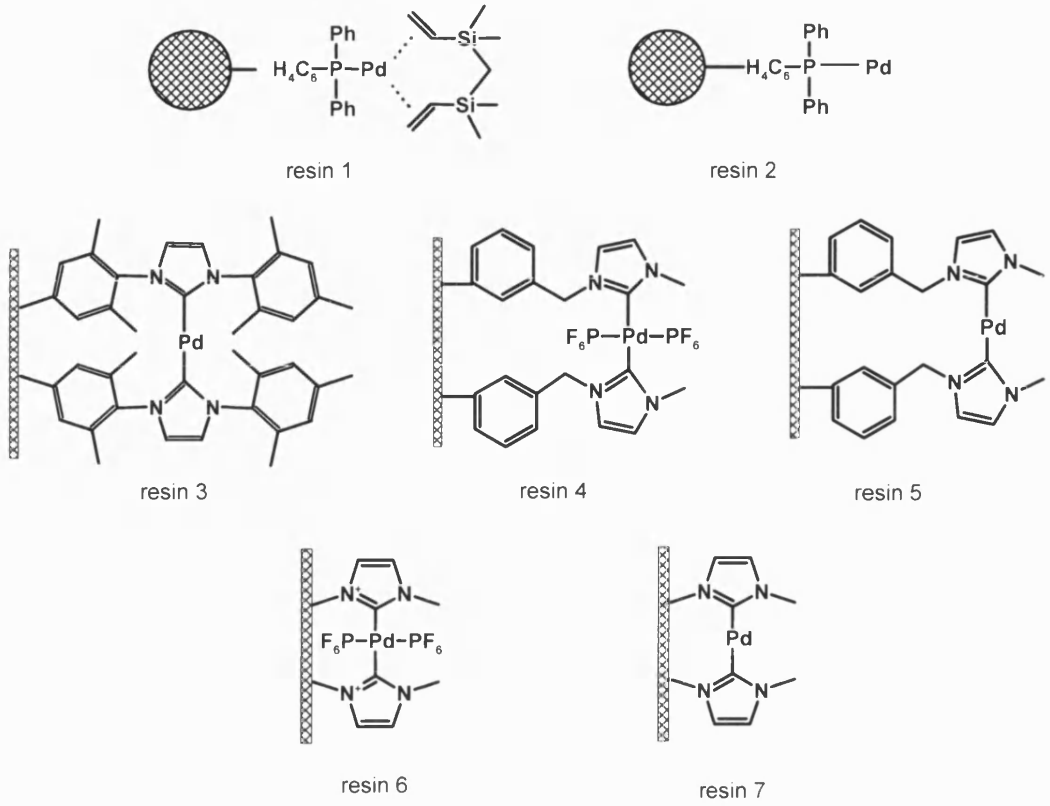

Figure 5.24: Heterogeneous catalysts for telomerization reaction based on DVB resins.

Firstly, catalysts based on triphenylphosphine resin (Resins 1 and 2) were tested in the telomerization of isoprene with methanol. Results are shown in Table 5.45.

Table 5.45: Telomerization of isoprene with catalysts based on triphenylphosphine resin.

Catalyst	T (°C)	TON	Conversion (%) 7h	Leaching (ppm)	Selectivity (%) 7h	Regioselectivity (%)			
						HT	HH	TT	TH
resin 1	70	906	84.7	127.5	57.8	31.6	5.7	0.9	61.8
resin 1	130	206	21.0	na	60.0	20.7	6.6	2.6	70.1
resin 2	130	448	7.4	10.5	16.8	45.2	5.2	49.6	-

Reaction conditions: 3.25 mL Isoprene (4.35 M). Solvent: 3.25 mL dry 1%NaOMe MeOH, 1 mL decane as internal standard. Time: 7h. Catalyst: 0.025 g of resin 1 and 0.05 g of resin 2.

Resin 1 exhibited the best performance with a conversion around 85% in 7 hours at 70°C with TON three times lower than best homogeneous catalyst

(Pd(Imes)(dvds)). However, the conversion decreased at a higher temperature probably due to decomposition of the resin. The main telomerization product obtained is the tail-to-head isomer which is not formed at all by any homogeneous catalysts tested using carbenes or phosphorus ligands. Higher temperatures than 70°C favoured even more the formation of the tail-to-head isomer. This leads us to the conclusion that this heterogeneous catalyst shows a highest selectivity to the tail-to-head product (which was identified by NMR at Rostock University) than any other tested catalysts.

In the case of resin 2, the conversion obtained was very low, and the distribution of products was completely different to that achieved in the case of resin 1 and very similar to the values obtained by the combination of a palladium salt and triphenylphosphine ligand as a catalyst in the homogeneous case (Table 5.36). This suggests that the regioselectivity obtained by resin 1 is not due to the triphenylphosphine group or the resin itself but due to the combination of the (dvds) group and the triphenylphosphine ligand attached to the palladium atom.

Although, during the reaction with resin 1, some leaching of palladium was observed, catalytic activity cannot be attributed to it as the regioselectivity to telomerization products is different than the one obtained with homogeneous catalyst.

Recycling of resin 1 (DVB resin-PPh_3-Pd-Imes)

In order to study the recyclability of the resin 1, different runs using the same catalyst under the same reaction conditions were carried out over a period of seven days. After each run, solvent, reactants and products were removed and the catalyst was stored under solvent and recharged the next day with fresh reactants. The conversion and selectivity obtained for each run are shown in Table 5.46. If a different method of recycling was used, removing the catalyst from the medium of reaction and drying it overnight at 120°C, the activity obtained in the following run was very low due to decomposition of the resin.

Table 5.46: Consecutive runs with resin 1. Telomerization of isoprene with methanol.

Run	Overall TON	Conversion (%) 7h	Leaching (ppm)	Selectivity (%) 7h	Regioselectivity (%) HT	HH	TT	TH
1	906	84.7	127.5	57.8	31.6	5.7	0.9	61.8
2	1510	56.4	48	67.3	28.0	5.5	1.4	65.1
3	1868	33.7	15	70.5	29.0	5.4	0.4	65.1
4	2022	14.4	11.5	76.0	27.8	5.1	2.4	64.7
5	2149	11.8	5.7	74.3	33.6	4.9	2.6	58.9
6	2186	3.5	-	76.4	34.4	5.8	3.2	56.7

Reaction conditions: 3.25 mL Isoprene (4.35 M). Solvent: 3.25 mL dry 1%NaOMe MeOH, 1 mL decane as internal standard. Catalyst: 0.025g resin 1. T = 70°C. Time: 7h.

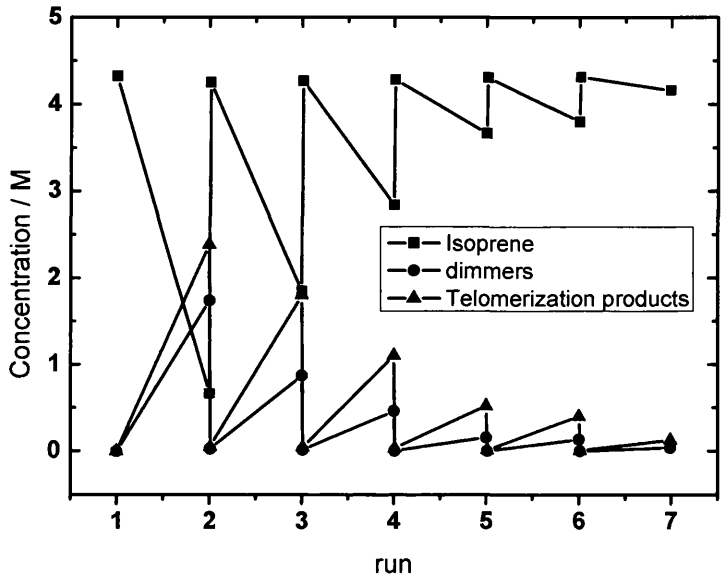

Figure 5.25: Reaction profile of consecutive telomerization reactions of isoprene with methanol using resin 1 as a catalyst.

The halving of conversion in subsequent runs is obvious from Figure 5.25 and it cannot be explained by simple losses of the resin due to manipulations, estimated at no more than 5% of the catalyst between each run. In spite of it, overall TON is obtained in the same order of magnitude than the ones obtained with homogeneous catalysts. The chemioselectivity and regioselectivity values across each run are largely unchanged which suggests that the same active palladium specie is

responsible for the activity across all runs. Again, the high regioselectivity for the tail-to-head product implies that the leaching of palladium is not responsible for activity.

The loss of activity upon recycling of the catalyst could be due to the erosion of the catalysts as it was claimed in previous heterogeneous telomerization reactions using polymeric supports [112]. Figure 5.26 shows SEM overview images of the fresh catalyst and of the Resin 1 beads recovered after six telomerization runs. It is immediately obvious that most of the resin particles were broken during the reaction, likely due to stirring of the reaction medium.

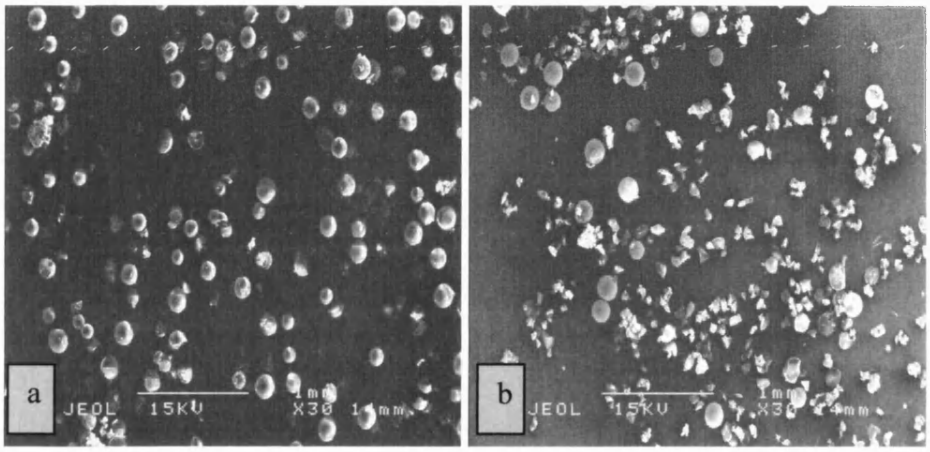

Figure 5.26: SEM images of a. fresh Resin 1 and b. Resin 1 after 6 runs.

Figure 5.27 shows SEM images and mapping of Si, P and Pd over the surface of an unbroken bead of Resin 1 after one telomerization run. Although the catalyst became completely black after just one run, comparison with fresh Resin 1 (Chapter 3), shows the same homogeneous distribution of Si, P and Pd across the bead. This suggests that there was little loss of metal or ligands from the surface of Resin 1 during the telomerization reaction. It also proves that, there is not accumulation of palladium nanoparticles on the resin surface.

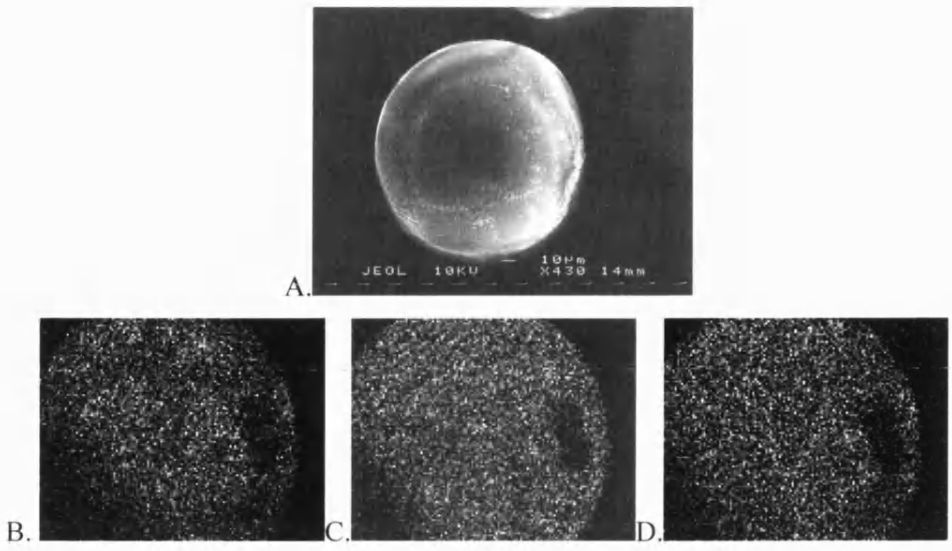

Figure 5.27: SEM and X-ray mapping of resin 1 after 1 run (A. SEM image, B. Si, C. P and D. Pd presence by X-ray).

When the same analysis was performed on an unbroken particle of Resin 1 after six recycling runs, no silicon was observed at the surface. Palladium and phosphorus distribution remained homogeneous as it can be observed Figure 5.28.

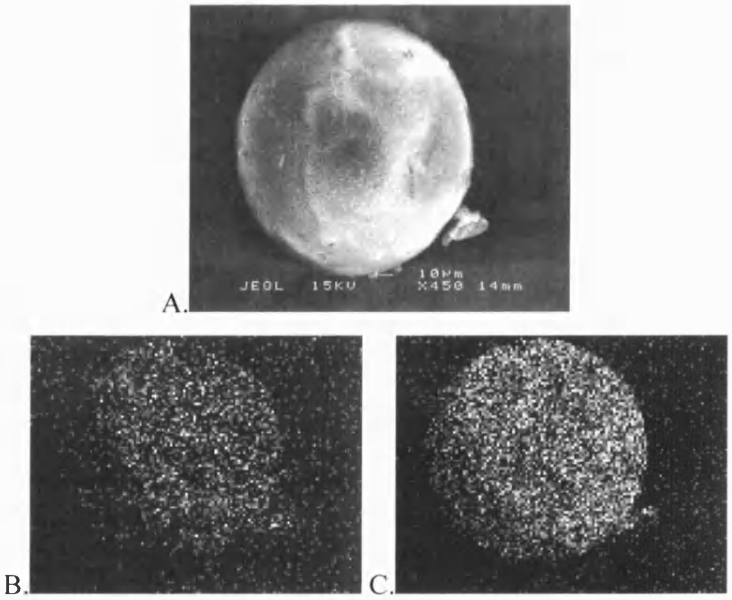

Figure 5.28: SEM and X-ray mapping of unbroken resin 1 after 6 runs (A. SEM image, B. P and C. Pd presence by X-ray).

Finally, Figure 5.29 shows the same SEM and X-ray study of a broken particle of resin 1 after six recycling runs. The internal and external surfaces of the resin can

be easily distinguished by the X-ray analysis, with the external surface retaining the homogeneous distribution of palladium. This suggests that broken resin particles should retain their catalytic activity and that the ongoing loss of activity in subsequent runs is likely due to chemical rather than the observed macroscopic physical changes in resin 1.

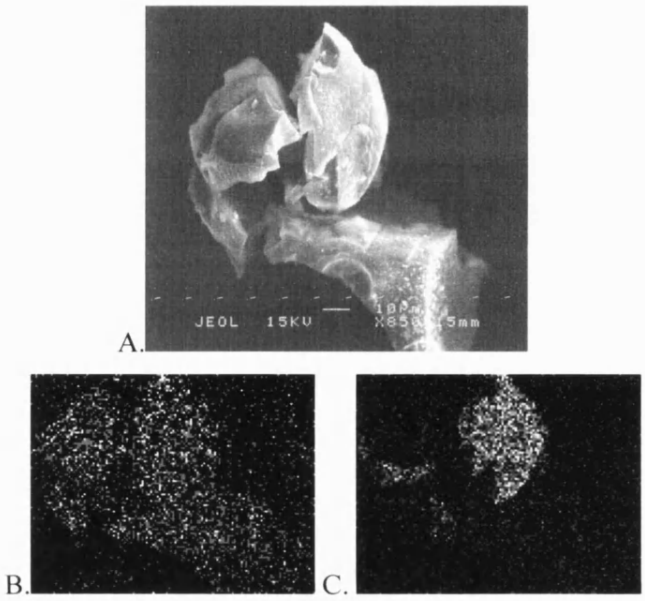

Figure 5.29: SEM and X-ray mapping of broken particle of resin 1 after 6 runs (A. SEM image, B. P and C. Pd presence by X-ray).

X-ray analyses of the fresh resin 1 after one and after six telomerization runs were performed, showing the results in Figure 5.30. Due to the rounded surface of the resin, these analyses cannot be used quantitatively; however, ratios of elements can be considered. The palladium/phosphorus ratio remained constant throughout the recycling runs, but the amount of silicon present on the resin is observed to decrease after the first run and has disappeared completely after six recycling runs. This suggests that loss of the Pd-dvds association is related to catalyst deactivation and it is in accordance with the very low activity shown by resin 2, which does not contain dvds. The low activity of the resin 1 at 130°C (Table 5.48) may also be explained by increased labilisation of the dvds ligand at high temperature.

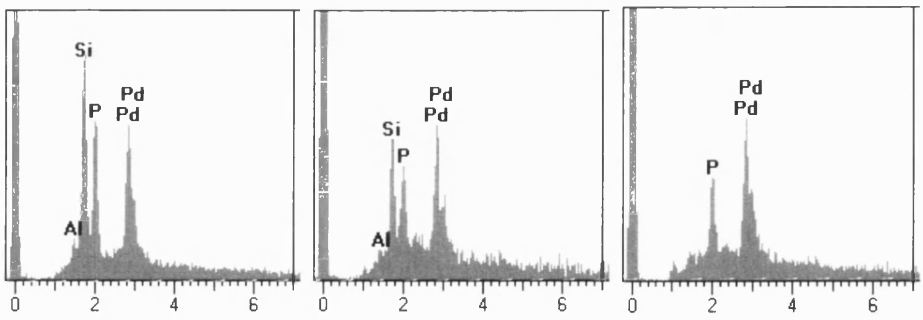

Figure 5.30: X-ray analysis of the resin 1: A. Fresh catalyst, B. After one recycling run and C. After six recycling runs.

The change of chemical composition of resin 1 following recycling is confirmed by IR analyses. Figure 5.31 shows the IR spectra of the fresh catalysts and after one and six recycling runs respectively. The bands corresponding to Si-O-Si bonds at 1082 and 800 cm^{-1} decreased considerably in intensity following the first run and are not present after six recycling runs.

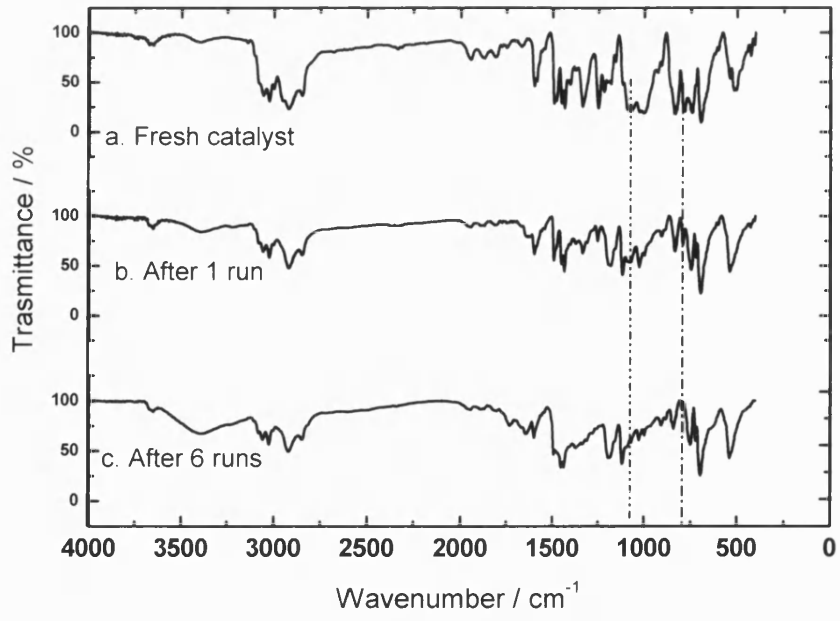

Figure 5.31: IR spectra of resin 1 a. fresh catalyst, b. after one recycling run and c. after six recycling runs.

A possible way of reactivating the resin 1 would be adding few equivalents of dvds related to the palladium content. Adding higher quantities could react under telomerization reactions.

Same resins were used in the telomerization of 1,3-pentadiene with methanol. The results are shown in Table 5.47.

Table 5.47: Telomerization of 1,3-pentadiene with catalysts based on triphenylphosphine resin.

Catalyst	T (°C)	TON	Conversion (%) 22h	Selectivity (%) 22h
resin 1	70	23	4.6	92.3
resin 2	130	-	-	-

Reaction conditions: 1.5 mL 1,3-pentadiene (2 M). Solvent: 5 mL dry 1%NaOMe MeOH, 1 mL decane as internal standard. Time: 22h. Catalyst: 0.025 g of resin 1 and 0.05 g of resin 2.

As it was observed in the homogeneous case, 1,3-pentadiene exhibits much less reactivity than isoprene and therefore, the conversion obtained is much lower, only 4.6 %. Resin 2 showed no conversion at all. The difference in reactivity between both molecules is even bigger than in the homogeneous case which might suggest that steric constrictions have an important role in the 1,3-pentadiene case.

Merrifield's resin and Merrifield's peptide resins were used in order to synthesise resins 3 to 7 (Chapter 3). Different versions of these resins (.a) and (.b) were tested in the telomerization of isoprene and 1,3-pentadiene with methanol. Results obtained in the first reaction are shown in Table 5.48.

Table 5.48: Telomerization of isoprene with different heterogeneous catalysts based on DVB resins.

Catalyst	Quantity	T (°C)	TON	Conversion (%) 22h	Selectivity (%) 22h	Regioselectivity (%)		
						HT	HH	TT
resin 3.a	0.025	70	-	-	-	-	-	-
resin 4.a	0.05	70	13	0.1	42.5	-	-	-
resin 5.a	0.05	70	433	6.8	36.2	48.1	19.3	32.5
resin 4.b	0.025	70	64	0.4	100	-	-	-
resin 5.b	0.025	70	916	7.2	79.6	30.6	62.6	6.7
resin 6.b	0.025	70	-	-	-	-	-	-
resin 7.b	0.025	70	1453	5.3	100	30.3	65.1	4.6
resin 4.b-red	0.025	70	32	0.2	100	-	-	-
resin 5.b-red	0.025	70	302	2.4	96.9	30.4	67.2	2.7
resin 6.b-red	0.025	70	-	-	-	-	-	-
resin 7.b-red	0.025	70	3367	12.3	100	31.7	65.3	2.9
Pd/C	0.15	130	-	-	-	-	-	-

Reaction conditions: 3.25 mL Isoprene (4.35 M). Solvent: 3.25 mL dry 1%NaOMe MeOH, 1 mL decane as internal standard, time = 22h.

Resin 3.a showed no conversion at all and very low values were obtained with the rest of tested catalysts although it is important to highlight the low palladium content of the resins (less than 1 % wt). In order to compare the regioselectivities obtained with resin 5, it is important to highlight that different palladium sources were used in the synthesis. Palladium chloride was used for the resin 5.a and palladium acetate for resin 5.b (Chapter 3). Using resin 5.a as catalyst, the main products obtained were the head-to-tail and the tail-to-tail isomers; however, there was a high presence (around 20%) of head-to-head isomer. This is a peculiar case if one compares it with the regioselectivity obtained with the homogeneous catalysts (Table 5.36) where head-to-head telomerization isomer was the main product with a presence of more than 75% when phosphorus ligands were used, or it was disfavoured with a selectivity to it of less than 5% when carbene ligands are used. Although different palladium sources did not influence regioselectivity in the homogeneous case, completely different distribution of products were obtained with resin 5.a and resin 5.b at the same values of conversion. With resin 5.b, majority product was the head-to-head isomer followed by the head-to-tail isomer

and very little presence of the tail-to-tail one. This distribution of products is similar to the one obtained with carbene ligands in the homogeneous case.

Similar regioselectivity values were obtained with all resins (.b) which showed reactivity which suggests that carbene ligands were formed in the resins 4.b to 7.b.

Although some leaching of palladium was observed during the reaction with most of the resins, the activity observed cannot be attributed only to it because other catalysts such as resin 4 which showed leaching, did not show any activity, which suggests that leached palladium has no activity for this reaction.

In the reactions which did not show any activity, the resins did not show visual reduction of palladium either. This could be the cause of their inactivity, according to what has been reported [103], the Pd^{II} precursor must be reduced to the catalytically active Pd^0 species. However, pre-reduced resins not always improved their reactivity. Resin 4.b and 6.b showed almost inactivity either pre-reduced or not which suggest that reaction is blocked by the presence of PF_6 attached to the palladium atom. Pre-reduced resin 5.b, exhibited much lower reactivity than without pre-reduction. On the other hand, resin 7.b improved its reactivity if it was reduced before the reaction obtaining similar TON than the ones obtained with homogeneous Pd(Imes)(dvds). Therefore, no conclusion can be obtained about the influence of pre-reduction of these resins before the reaction.

Finally, Pd/C did not show any activity either, however it had been claimed to be active for the telomerization reaction with water [105].

Same heterogeneous catalysts have been used for the telomerization of 1,3-pentadiene, and the results obtained are shown in Table 5.49.

Table 5.49: Telomerization of 1,3-pentadiene with different heterogeneous catalysts based on DVB resins.

Catalyst	Quantity (g)	T (°C)	TON	Conversion (%) @22h	Selectivity (%) @22h
resin 3.a	0.025	70	-	-	-
resin 4.a	0.05	70	-	-	-
resin 5.a	0.05	70	58	1.9	100
resin 4.b	0.025	70	-	-	-
resin 5.b	0.025	70	178	3.0	100
resin 5.b	0.025	130	261	4.5	100
resin 6.b	0.025	70	-	-	-
resin 7.b	0.025	70	353	2.8	100
resin 4.b-red	0.025	70	-	-	-
resin 5.b-red	0.025	70	210	3.6	100
resin 6.b-red	0.025	70	-	-	-
resin 7.b-red	0.025	70	369	2.9	100
resin 7.b-red	0.025	130	332	2.6	100
Pd/C	0.15	70	-	-	-

Reaction conditions: 1.5 mL 1,3-pentadiene (2 M) Solvent: 5 mL dry 1%NaOMe MeOH, 1 mL decane as internal standard, time = 22h.

As it has been observed in the homogeneous case, 1,3-pentadiene has much lower reactivity. Confirming this again, conversion values obtained with heterogeneous catalysts based on Merrifield's and Merrifield's peptide resins were very low or even null. Only resin 5 and resin 7 showed some activity. However, taking into account the low palladium loading of the catalysts, acceptable TON were obtained, similar to the ones obtained with homogeneous catalysts and much higher than other reported heterogeneous catalysts [121, 122]. In catalytic terms, it is not possible to distinguish between palladium sources or the influence of pre-reduction of the resin catalysts before starting the reaction.

5.5 CONCLUSIONS

In order to study the telomerization reaction with alcohols, isoprene and 1,3-pentadiene were chosen as reactants. Telomerization of 1,3-pentadiene is the second step of the proposed tandem reaction while products of telomerization of isoprene with methanol were already identified allowing the study of the influence of different parameters in the regioselectivity. 1,3-pentadiene was found to be much less reactive than isoprene for this reaction.

Two main groups of homogeneous palladium catalysts were screened based on carbene complexes and triphenylphosphine ligands showing different regioselectivities to telomerization products. At 70°C, Pd(Imes)(dvds) showed the best results for the isoprene reaction favouring the head-to-head product. On the other hand, phosphorus ligands promote principally the formation of head-to-tail products. In the telomerization reaction of 1,3-pentadiene with methanol at 70°C low conversion values are obtained in general; the combination of $Pd(acac)_2$ and triphenylphosphine as a ligand show best results.

The initial concentration of reactants have also influence in the regioselectivity. Decreasing the initial concentration of isoprene and increasing the concentration of methanol as nucleophile favours the selective formation of the head-to-head product versus head-to-tail one.

In both cases, reaction shows a second order respect to diolefin concentration and first order respect to the concentration of alcohol acting as a nucleophile which is in accord with the accepted mechanism.

Previously to this study, it was believed that increasing the length of the alcohol used as a nucleophile, the conversion to telomerization decreases. This was confirmed when the combination of a palladium salt and triphenylphosphine ligand is used as a catalyst. However, when the palladium carbene ligand Pd(Imes)(dvds)

is used as catalyst, conversion is significantly increased when 1-propanol or 1-butanol are used as nucleophiles. This enhancement of the catalytic activity is believed to be due to the higher solubility of the carbene complex in long primary alcohols.

One of the main aims of the project is the possibility of extending the telomerization reaction to long chain diolefins (longer than the typical 1,3-butadiene used in most of the literature studies). So far, nobody has obtained positive results in molecules longer than C_5. Applying previous results, 1,3-hexadiene was telomerised for first time using ethanol, 1-propanol and 1-butanol as nucleophiles and Pd(Imes)(dvds) as a catalyst. The use of methanol as nucleophile forms completely inactive systems.

A second part of the telomerization study consists of testing different novel heterogeneous catalysts based on resins were different ligands and palladium were attached. A high loading of palladium (12.9 %wt) was possible only in (dvds)-Pd-PPh_3-resin catalyst which showed for first time a very high selectivity to the tail-to-head telomerization product. The resin can be reused halving its catalytic activity in each run due to the loosing of the (dvds) attached to the palladium atom which form the active species. Therefore, Pd-PPh_3-resin shows very low activity.

When carbene ligands were tried to be attached to different resins, very low loadings of palladium were obtained. As a result, very low conversion values to telomerization of isoprene or 1,3-pentadiene were obtained however, very high selectivities and TON similar than the ones obtained for homogeneous catalysts were achieved.

Chapter 6

FEASIBILITY OF THE TANDEM REACTION

6.1 INTRODUCTION

This Chapter contains a study about the feasibility of a new tandem reaction comprising isomerization and telomerization steps. Non-conjugated diolefin 1,4-pentadiene was used as starting material to obtain telomerization isomers as final products, according to Figure 6.1.

The Chapter begins with a literature review of the main established tandem reactions which comprise a double bond migration step. To the best of my knowledge, none of the known tandem reactions contain a telomerization reaction step. Finally, the conclusions obtained in Chapter 4 about isomerization reaction and Chapter 5 about telomerization reaction were used in order to establish the new

tandem reaction. Several factors such as influence of temperature or presence of base in the reaction medium were studied.

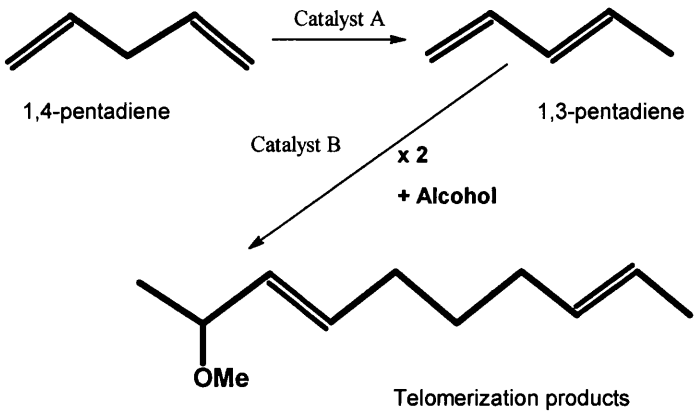

Figure 6.1: Tandem isomerization – telomerization reaction of 1,4-pentadiene.

6.2 LITERATURE REVIEW

Tandem reactions are defined as two or more reaction steps carried out in a single pot instead of sequentially. In these processes, the product of the first reactions becomes a substrate for the next one and consecutively until termination leads to a final product. This type of reactions allows a more environmentally friendly production of fine and bulk chemicals, due to an increment of their efficiency and economy in terms of reagent consumption and without the need to purify at each step.

This approach leads not only to the reduction in the number of unit operations, but also indirectly contributes towards improved safety, reduced energy consumption and reduced capital costs fulfilling some of the principles of Green Chemistry (Chapter 1).

Many processes require terminal alkenes as reactants. However, they are present in low concentrations in the primary products of cracking while internal olefins are cheaper and more available. Therefore, literature presents several examples of tandem reactions comprising an isomerization step, some of them are described below.

- The Shell Higher Olefin Process [123] is an efficient and flexible combination of three reactions: oligomerization, isomerization and methathesis [124]. It was designed to meet the market needs for linear α-olefins for detergents. The first commercial plant was built in 1977 and the actual production is 1190000 Tons/year under the trade name Neodene®. In the oligomerization step, linear α-olefins are produced from ethylene with a distribution of 96 – 98% terminal olefins over the rage from C_4 to C_{30+}. The olefins are isomerised to internal olefins. Isomerization is accomplished by an isomerization catalyst such as Na/K on Al_2O_3 or a MgO catalyst in the liquid phase at 80-140°C and 0.3-2 MPa, where about 90% of the α-olefins are converted to internal olefins. Finally, metathesis of the lower and higher internal olefins gives a mixture of α-olefins with odd and even carbon chain lengths (Figure 6.2).

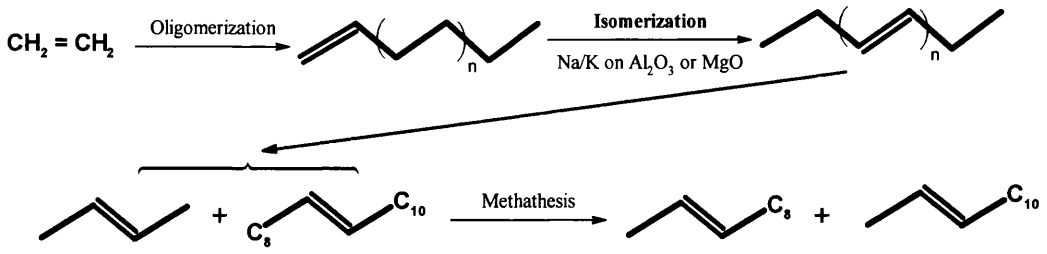

Figure 6.2: SHOP process comprising oligomerization, isomerization and methathesis.

- Domino reaction of internal olefin isomerization followed by hydroformylation and reductive amination with a rhodium based catalyst to obtain linear aliphatic amines used for production of solvents, fine chemicals, agrochemicals, pharmaceutical intermediates and vulcanization

accelerators. The overall reaction scheme can be represented by Figure 6.3 [125]:

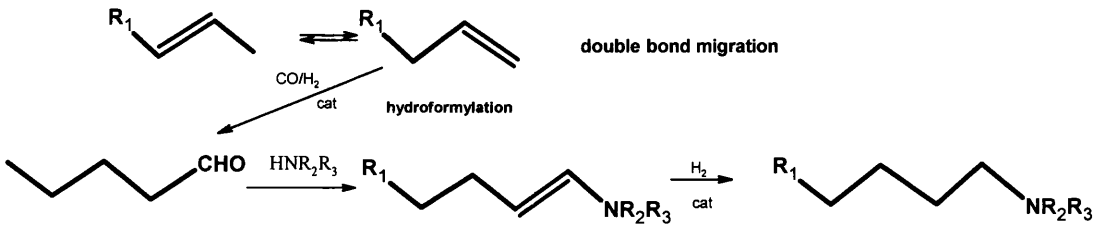

Figure 6.3: Tandem reaction comprising isomerization, hydroformilation and amination steps.

- A tandem reaction which generates cyclic enol ethers from acylic dienes through a ruthenium alyline catalyst in a ring-closing metathesis step followed by olefin isomerization of the resulting product by a ruthenium hydride catalyst (Figure 6.4).

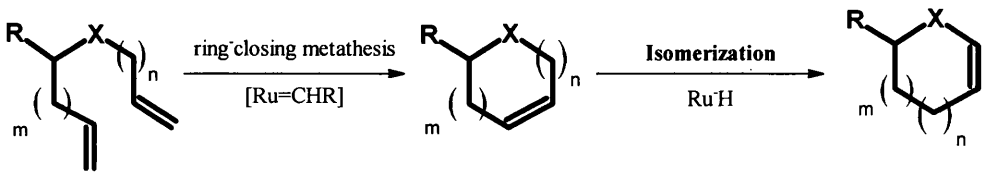

Figure 6.4: Tandem reaction comprising a ring-closing metathesis and isomerization steps.

- In the BASF synthesis of vitamin A the intermediate β-olefin is obtained from the isomerization of 6-methyl-6-hepten-2-one, with the latter resulting from condensation of acetone, isobutene and formaldehyde [126]:

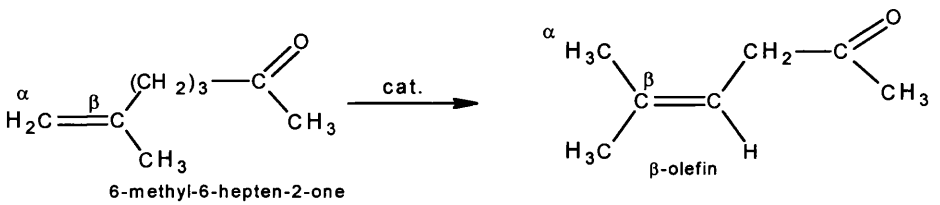

Figure 6.5: Tandem reaction for the BASF synthesis of vitamin A.

- The DuPont adiponitrile process consists in hydrocyanation of butadienes. The overall process is described as the addition of two HCN molecules to butadiene in the presence of a tetrakisphosphite-nickel(0) catalyst and a Lewis acid promoter. The overall reaction can be separated into three stages: synthesis of mononitriles by hydrocynation of butadiene, isomerization and synthesis of dinitriles. In the isomerization stage, a skeletal rearrangement is followed by a double –bond shift, yielding the terminal olefin. About 75% of the world's demand for adiponitrile is covered by this process.

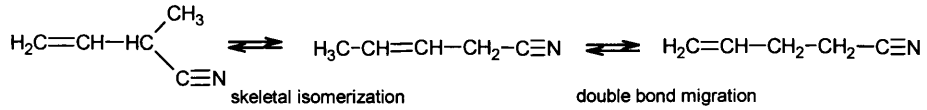

Figure 6.6: Tandem reaction of the DuPont adiponitrile process.

It is important to highlight the difference between the isomerization step in the previous tandem and the one proposed. In the first case, only one double bond is migrated while in this study, diolefins are isomerized.

6.3 RESULTS AND DISCUSSION: TANDEM REACTIONS

Accordingly with the results obtained for the isomerization and telomerization reactions (Chapter 4 and 5), homogeneous catalysts exhibited the best results for both reactions. A first set of tandem reactions was carried out using homogeneous ruthenium based catalysts for isomerization reaction and palladium based catalysts for telomerization reaction (using carbenes and phosphorus ligands). The results obtained are shown in Table 6.1.

Table 6.1: Tandem reactions with homogeneous isomerization and telomerization catalysts.

Isomerization catalyst	Telomerization catalyst	T (°C)	Conversion to isomerization (%) @ 19h	Conversion to telomerization (%) @ 19h
$RuCl_3$	Pd(Imes)(dvds)	150	96.9	1.12
$RuCl_3$	Pd(acetate) + PPh_3	130	94.2	3.5
$RuHCl(CO)(PPh_3)_3$	Pd(Imes)(dvds)	130	62.2	0.5
$RuCl_3$	$PdCl_2$ + PPh_3	130	100	2.5

Reaction conditions: 1 mL 1,4-pentadiene (1.4 M). Solvent: 5 mL dry 1%NaOMe MeOH, 1 mL decane as internal standard. Catalysts: $2.5 \cdot 10^{-5}$ moles for isomerization catalyst and $8 \cdot 10^{-6}$ moles for telomerization catalyst.

At temperatures of 130°C and 150°C, isomerization conversions were very high in most cases, as it was expected from results obtained in Chapter 4; however, the conversion values for the telomerization reaction were very low. There are different possible reasons for this fact which are going to be investigated and discussed in this Chapter:

- Does the presence of the isomerization catalyst deactivate the telomerization catalyst?
- Is the telomerization catalyst deactivated during the first minutes of reaction due to lack of telomerization reactant?
- Which is the influence of temperature on both catalysts?
- Which is the influence of NaOMe on both catalysts?

The presence of ruthenium complexes as isomerization catalysts might deactivate the telomerization catalyst. This applies especially in the case of a palladium carbene complex (Pd(Imes)(dvds)) used as telomerization catalyst. Ruthenium atoms might compete with palladium atoms for the carbene ligands. This effect might be less evident when the telomerization catalyst is formed by a palladium salt and triphenylphosphine ligand because triphenylphosphine ligands are very labile and could migrate between elements. In order to avoid these interferences, homogeneous ruthenium complexes were substituted by heterogeneous catalysts in tandem reactions. Results are shown in Table 6.2.

Table 6.2: Tandem reactions with heterogeneous isomerization catalysts and homogeneous telomerization catalysts.

Isomerization catalyst	Telomerization catalyst	T (°C)	Conversion to isomerization (%) @ 19h	Conversion to telomerization (%) @ 19h
10.1% Pd^{2+}/Ti-NT	Pd(Imes)(dvds)	130	67.5	0
6.3% Rh^{3+}/Ti-NT	Pd(Imes)(dvds)	130	37.4	0
19% Ru^{3+}/Ti-NT	Pd(Imes)(dvds)	130	79.4	0
19% Ru^{3+}/Ti-NT	$PdCl_2 + PPh_3$	130	86.9	0.2
2.7% Ru/ZSM-5	$Pd(acac)_2 + PPh_3$	130	26.2	0

Reaction conditions: 1 mL 1,4-pentadiene (1.4 M). Solvent: 5 mL dry 1%NaOMe MeOH, 1 mL decane as internal standard. Catalysts: 0.2 g for isomerization catalyst and $8 \cdot 10^{-6}$ moles for telomerization catalyst.

In tandem reactions carried out with a combination of homogeneous and heterogeneous catalysts, high conversions to isomerization reaction were obtained in most of the cases, but lower values as expected especially for 6.3% Rh^{3+}/Ti-NT and 2.7% Ru/ZSM-5 catalysts. However, no telomerization products were obtained in any of the tested combinations. Migration of telomerization ligands into isomerization catalysts might also apply to theses cases. Another possible reason might be the adsorption of the telomerization catalyst onto the heterogeneous support, being therefore, deactivated.

Two telomerization reactions of isoprene with methanol were carried out with Pd(Imes)(dvds) as a catalyst under the same conditions with the presence of titanate nanotubes in one of them. Same catalytic results were obtained in both cases. This discards the previously proposed idea of adsorption of homogeneous telomerization catalysts onto the surface of titanate nanotubes.

It has been observed during telomerization reactions that once that the reaction was completed; decomposition of the catalysts into palladium black was quicker than during the reaction. This enhancement of decomposition was also observed from the beginning during blank reactions where no reactant was present. These two observations suggest that the reason why no telomerization products were observed in tandem reactions could be due to the lack of telomerization reactant at the beginning followed by decomposition of the telomerization catalyst. This could be

especially evident if the isomerization reaction is not active enough or if it exhibits an induction time. In order to prove if this fact is the cause of the telomerization inactivity during tandem reactions, several tandem reactions were carried out using as starting material a mixture of 1,3-pentadiene and 1,4-pentadiene. The results are shown in Table 6.3.

Table 6.3: Tandem reactions starting with a mixture of 1,3-pentadiene and 1,4-pentadiene as reactants.

Reactant	Isomerization catalyst	Telomerization catalyst	T (°C)	Conversion to isomerization (%) @ 19h	Conversion to telomerization (%) @ 19h
1,4-pentadiene + 1,3-pentadiene	10.1% Pd^{2+}/Ti-NT	Pd(Imes)(dvds)	130	45.5	0.4
1,4-pentadiene + 1,3-pentadiene	6.3% Rh^{3+}/Ti-NT	Pd(Imes)(dvds)	130	20.7	1.2
1,4-pentadiene + 1,3-pentadiene	19% Ru^{3+}/Ti-NT	Pd(Imes)(dvds)	130	94.4	3.3

Reaction conditions: 1 mL 1,4-pentadiene (1.4 M) and 0.5 mL 1,3-pentadiene (0.7 M). Solvent: 4.5 mL dry 1%NaOMe MeOH, 1 mL decane as internal standard. Catalysts: 0.2 g for isomerization catalyst and $8 \cdot 10^{-6}$ moles for telomerization catalyst.

Comparing the results with the ones obtaining without the initial presence of 1,3-pentadiene (Table 6.2), the isomerization conversion decreased when palladium and rhodium on titanate nanotubes catalysts are used. However, in the case of ruthenium on titanate nanotubes as a catalyst, the isomerization conversion was higher when 1,3-pentadiene is present. A possible explanation could be that 1,3-pentadiene competes with 1,4-pentadiene for the palladium and rhodium sites for cis-trans isomerization. However, this does not take place with ruthenium catalysts.

In the case of the telomerization reaction, low conversions were obtained in all cases, but higher when the isomerization catalyst was supported ruthenium on titanate nanotubes. This could be either due to the higher isomerization conversion obtained with this catalyst or due to less interferences between both catalysts. Although telomerization conversion obtained was low, it is important to take into

account that high conversions were not obtained either in the telomerization of 1,3-pentadiene with methanol (Chapter 5).

In order to avoid all possible interferences between isomerization and telomerization catalysts during tandem reactions, heterogeneous catalysts were tested for both reactions obtaining the results shown in Table 6.4.

Table 6.4: Tandem reactions with heterogeneous isomerization and telomerization catalysts.

Isomerization catalyst	Telomerization catalyst	T (°C)	Conversion to isomerization (%) @ 19h	Conversion to telomerization (%) @ 19h
2.7% Ru/ZSM-5	resin 5.b	130	36.6	-

Reaction conditions: 1 mL 1,4-pentadiene (1.4 M). Solvent: 5 mL dry 1%NaOMe MeOH, 1 mL decane as internal standard. Catalysts: 0.2 g for isomerization and telomerization catalysts.

Due to the very low conversion values obtained with heterogeneous catalysts in the telomerization reaction of 1,3-pentadiene with methanol (Chapter 5), only resin 5.b was tested without positive results. No telomerization products were detected.

6.3.1 INFLUENCE OF THE PRESENCE OF BASE (NaOMe)

Table 6.2 and Table 6.4 have also shown that not only telomerization conversions were influenced by tandem conditions but also isomerization values. The reaction conditions used differed from the ones used in the isomerization tests (Chapter 4) by the presence of a base (1% NaOMe). The next step followed was to study the influence of the base in both telomerization and isomerization reactions, obtaining the results shown in Table 6.5.

Table 6.5: Influence of the presence of NaOMe in telomerization reactions with Pd(Imes)(dvds) as a catalyst.

Reactant	Telomerization catalyst	T (°C)	Presence of 1% base	Conversion (%) @7h	Selectivity (%) @ 7h
Isoprene	Pd(Imes)(dvds)	110	Yes	94.6	85.6
Isoprene	Pd(Imes)(dvds)	90	No	43.7	100
1,3-pentadiene	Pd(Imes)(dvds)	70	Yes	8.4	97.9
1,3-pentadiene	Pd(Imes)(dvds)	90	No	0	-

Reaction conditions: 3.25 mL isoprene (4.35 M) or 1 mL 1,3-pentadiene (2 M). Solvent: up to 6.5 mL butanol, 1 mL decane as internal standard. Catalysts: $4 \cdot 10^{-6}$ moles and $8 \cdot 10^{-6}$ moles for isoprene and 1,3-pentadiene respectively.

Although reactions were not carried out at the same temperatures, it is obvious that the presence of base (NaOMe) in telomerization reaction is crucial, especially in the case of 1,3-pentadiene where no reaction is observed if NaOMe is not present. The presence of NaOMe increases the concentration of MeO^- anions in solution which is crucial at the beginning of the reaction.

Best isomerization catalysts are also tested in the presence of NaOMe to study the influence of the base in their activity. In Table 6.6, the results are shown in pair, with and without base.

Table 6.6: Influence of the presence of NaOMe in the activity of isomerization catalysts.

Catalyst	Solvent	T (°C)	Presence of 1% base	Conversion (%) @ 0.5h	Conversion (%) @ 3h	Selectivity (%) @ 3h
$RuHCl(PPh_3)_3$	MeOH	110	No	35.7	52.8	98.6
$RuHCl(PPh_3)_3$	MeOH	110	Yes	2.5	4.4	79.2
4.9% Ru^{3+}/Ti-NT	MeOH	130	No	8.7	42.5	67.4
4.9% Ru^{3+}/Ti-NT	MeOH	130	Yes	1.2	6.6	100
5% Ru/C	MeOH	130	No	17.5	40.1	71.2
5% Ru/C	MeOH	130	Yes	5	11.1	80.6
0.5% Ru-PPh_3-resin	MeOH	130	No	53.5	91.6	71.9
0.5% Ru-PPh_3-resin	MeOH	130	Yes	0	3.8	87

Reaction conditions: 0.5 mL 1,5-hexadiene (0.7 M), Solvent:5 mL dry methanol, 1 mL decane as internal standard. Catalysts: $2.5 \cdot 10^{-5}$ moles Ru for homogeneous catalyst and 0.2 g for heterogeneous catalysts.

The presence of NaOMe in the reaction medium decreases the isomerization activity of all tested ruthenium catalysts, both homogeneous and heterogeneous. The base might capture the protons involved in the isomerization mechanisms decreasing the activity dramatically [127]. This fact would also have effects in the telomerization activity as the concentration of MeO^- anions is also decreased.

6.3.2 INFLUENCE OF TEMPERATURE

Another parameter which can have influence in tandem results is the effect of temperature of reaction in the catalyst. Isomerization study in Chapter 4 was done at high temperatures (110°C and 130°C). However, telomerization reactions in Chapter 5 were carried out at 70°C. In the first place, the influence of temperature on the telomerization reaction was studied. In Table 6.7, the results obtained are shown.

Table 6.7: Influence of temperature in the telomerization of isoprene.

Catalyst	T (°C)	TON	Conversion (%) @7h	Selectivity (%) @7h	Regioselectivity (%) HT	HH	TT
Pd(acetate) + 3 eq. PPh_3	70	1537	18.9	77.4	63.4	4.9	31.7
Pd(acetate) + 3 eq. PPh_3	130	2432	29.9	42.4	42.6	5.2	52.2
Pd(acac) + 3 eq. PPh_3	70	862	10.6	73.5	67.5	5.5	26.9
Pd(acac) + 3 eq. PPh_3	90	2105	25.9	67.0	60.5	6.1	33.4
Pd(acac) + 3 eq. PPh_3	110	2775	34.2	47.2	50.4	5.6	44.0
Pd(acac) + 3 eq. PPh_3	130	3060	37.7	42.2	42.3	6.1	51.6
Pd(Imes)(dvds)	70	3694	45.5	87.9	14.2	85.0	0.8
Pd(Imes)(dvds)	90	6696	82.5	85.0	24.4	74.6	0.9
Pd(Imes)(dvds)	110	6547	80.7	87.1	33.6	65.2	1.2
Pd(Imes)(dvds)	130	4861	57.7	91.7	40.5	58.2	1.3

Reaction conditions: 3.25 mL Isoprene (4.35 M). Solvent: 3.25 mL dry 1%NaOMe MeOH, 1 mL decane as internal standard. Time: 7h. Catalyst: $4 \cdot 10^{-6}$ moles of Pd.

Two different tendencies are observed. Firstly, when the combinations of a palladium salt and triphenylphosphine ligand are used as catalysts, the conversion increases as the temperature increases. However, this increment is not as high as it could be expected due to the decomposition of the catalyst. The selectivity is also much lower at high temperatures with a large amount of dimers formed. This is in accordance to earlier observations of telomerization of 1,3-butadiene [128, 129]. Temperature also influences on the regioselectivity to different telomerization products, decreasing the formation of head-to-tail and head-to-head products and increasing the formation of tail-to-tail products at higher temperatures. The same trend is observed independent on the palladium source. The possibility of obtaining different product selectively varying the temperature had already been observed by the Beller's group [130].

On the other hand, different behaviour is observed when Pd(Imes)(dvds) was used as a catalyst. In this case, conversion increases in the range of 70-90°C; it keeps constant until 110°C to decrease again at higher temperatures. Similar values of selectivity are obtained at temperatures between 70 to 130°C. However, it can be observed visually that the decomposition of the catalyst is more pronounced at elevated temperatures. This is the reason why conversion does not increase with temperature as it should do according to the Arrhenius' law. At 150°C, the instability of the catalysts is much higher, showing much lower activity. The effect of temperature on the regioselectivity of telomerization products is opposite to the one observed previously. The formation of head-to-tail telomerization products is favoured versus the head-to-head ones at higher temperatures.

During all reactions, visual observations of catalyst decomposition were made. In order to study thermal stability of both catalysts, samples were taken periodically during reactions carried out at different temperatures. The reaction profiles of disappearance of isoprene at different temperatures are shown in Figure 6.7.

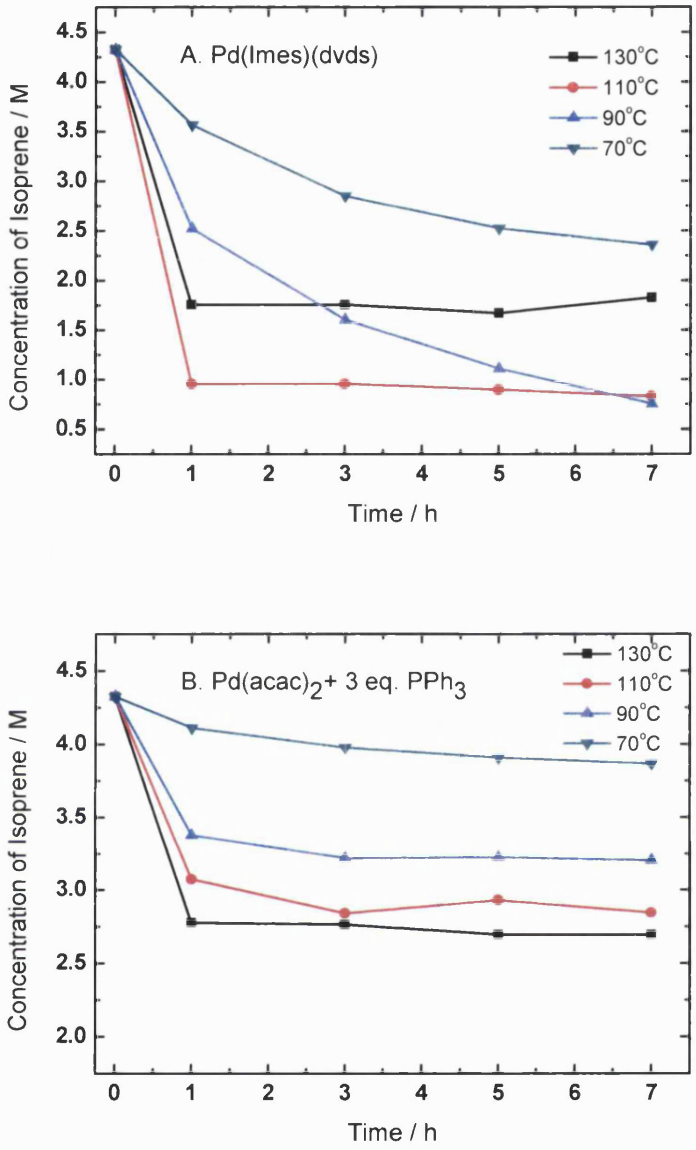

Figure 6.7: Reaction profiles of telomerization of isoprene (4.35 M) with methanol at different temperatures (range 70 - 130°C) with $4 \cdot 10^{-6}$ moles of A. Pd(Imes)(dvds) and B. $Pd(acac)_2$ + 3eq. PPh_3 as catalysts.

According to these results, the catalyst Pd(Imes)(dvds) is thermally stable for seven hours of reaction up to 90°C. At higher temperatures, decomposition of the catalyst is complete within the first hour of reaction and, therefore, no further reaction takes place. On the other hand, the combination of palladium acetylacetonate with triphenylphosphine as a catalyst is even less stable. At 70°C, the reaction takes

place. However, at higher temperatures, the catalyst is active for up to one hour, being completely decomposed within this time.

A similar study was carried out for the telomerization reaction of 1,3-pentadiene. The results are shown in Table 6.8.

Table 6.8: Influence of temperature in the telomerization of 1,3-pentadiene.

Catalyst	T (°C)	TON	Conversion (%) @7h	Selectivity (%) @7h
Pd(acetate) + 3 eq. PPh_3	70	46	2.4	100
Pd(acetate) + 3 eq. PPh_3	130	34	1.8	84.8
Pd(acac) + 3 eq. PPh_3	70	457	24.4	100
Pd(acac) + 3 eq. PPh_3	130	24	1.3	100
Pd(Imes)(dvds)	70	157	8.4	97.9
Pd(Imes)(dvds)	90	405	21.7	98.8
Pd(Imes)(dvds)	110	352	18.8	93.7
Pd(Imes)(dvds)	130	226	12.1	91.6
Pd(Imes)(dvds)	150	197	10.5	94.9

Reaction conditions: 1.5 mL 1,3-pentadiene (2 M) Solvent: 5 mL dry 1%NaOMe MeOH, 1 mL decane as internal standard. Time: 7h. Catalyst: $8 \cdot 10^{-6}$ moles of Pd.

The catalysts based on palladium salts and triphenylphosphine as a ligand show very poor stability in the telomerization of 1,3-pentadiene at high temperatures, showing almost no conversion at 130°C. In this case, the increment of temperature has no apparent influence on selectivity. However, this effect is difficult to determine due to the low conversions obtained. On the other hand, when the carbene based catalyst, Pd(Imes)(dvds), was used, conversion increases considerably in the range of 70-90°C; conversion is almost constant in the temperature range of 90-110°C and decreases again at higher temperatures. Higher decomposition of the catalyst is observed visually upon the increase in temperature. No influence on selectivity was observed, which suggests that dimerization was not especially favoured at high temperatures. Same tendency was observed during the telomerization of isoprene with methanol using Pd(Imes)(dvds) as a catalyst. Again, these results show the higher thermal stability of carbene ligands, versus

phosphorus ligands, although visual decomposition of Pd(Imes)(dvds) was observed, especially at higher temperatures.

According to previous results, the maximum temperature that can be used with the telomerization catalyst is 90°C. At higher temperatures, the catalyst decomposes within an hour. This explains why no telomerization conversion was observed in the previous tandem reactions as the telomerization catalyst had decomposed before the isomerization reaction took place. Therefore, it is necessary to perform the isomerization reactions at lower temperatures than these tested in Chapter 4. Results are shown in Table 6.9.

Table 6.9: Influence of temperature in the isomerization reaction.

Catalyst	Solvent	T (°C)	Conversion @ 0.5h (%)	Conversion @ 3h (%)	Selectivity @ 3h (%)
$RuCl_3$	MeOH	90	0	0	-
$RuHCl(PPh_3)_3$	MeOH	90	22.1	32.5	22.4
0.5% Ru-PPh_3-resin	MeOH	70	0	0	-
0.5% Ru-PPh_3-resin	MeOH	90	3.2	5.4	52.3
0.5% Ru-PPh_3-resin	MeOH	110	3.0	8.7	54.8
4.9% Ru^0/Ti-NT	MeOH	90	3.2	6.6	86.1
4.9% Ru^0/Ti-NT	MeOH	110	2.2	11.2	88.3
4.9% Ru^{3+}/Ti-NT	MeOH	110	1.4	21.9	73.2
5% Ru/C	MeOH	90	0	0	-
5% Ru/C	MeOH	110	0	0	-

Reaction conditions: 1 mL 1,5-hexadiene (0.7 M), Solvent: 5 mL dry methanol, 1 mL decane as internal standard. Catalysts: $2.5 \cdot 10^{-5}$ moles Ru for homogeneous catalyst and 0.2 g for heterogeneous catalysts.

Homogeneous isomerization catalysts were tested at 90°C showing much lower activity (if any) and very low selectivity. No better results were obtained with heterogeneous catalysts which activity decreased substantially at temperatures below 130°C.

Different tandem reactions were carried out at 90°C and 110°C using both homogenous and heterogeneous isomerization catalysts. Results are shown in Table 6.10.

Table 6.10: Tandem reactions at 90°C and 110°C.

Isomerization catalyst	Telomerization catalyst	Nucleophile	T (°C)	Conversion to isomerization (%) @ 19h	Conversion to telomerization (%) @ 19h
$RuHCl(PPh_3)_3$	Pd(Imes)(dvds)	MeOH	90	15.4@7h	-
$RuHCl(PPh_3)_3$	Pd(Imes)(dvds)	Butanol	90	42	-
0.5% Ru-PPh_3-resin	Pd(Imes)(dvds)	MeOH	90	-	-
0.5% Ru-PPh_3-resin	Pd(Imes)(dvds)	Butanol	90	-	-
4.9% Ru^{3+}/Ti-NT	Pd(Imes)(dvds)	MeOH	90	-	-
4.9% Ru^{3+}/Ti-NT	Pd(Imes)(dvds)	Butanol	90	-	-
5% Ru/C	Pd(Imes)(dvds)	MeOH	90	21.3	-
5% Ru/C	Pd(Imes)(dvds)	Butanol	90	33.5	-
$RuCl_3$	Pd(Imes)(dvds)	MeOH	110	98.1	1.73
$RuCl_3$ [b]	Pd(Imes)(dvds)	MeOH	110	100	2.27

Reaction conditions: 1 mL 1,4-pentadiene (1.4 M), [b] Added 0.5 mL 1,3-pentadiene (0.7 M). Solvent: 5 mL 1%NaOMe, 1 mL decane as internal standard. Catalysts: $2.5 \cdot 10^{-5}$ moles for homogeneous and 0.2 g for heterogeneous isomerization catalyst, $8 \cdot 10^{-6}$ moles for telomerization catalyst.

None of the heterogeneous isomerization catalysts tested showed conversion even after nineteen hours of reaction. When both isomerization and telomerization catalysts were homogeneous, good conversion values for isomerization were obtained, especially at 110°C. It is in this case when some telomerization products were detected but with low conversions.

It can be concluded that there is an incompatibility of working temperatures between isomerization and telomerization catalysts of at least 20°C. Telomerization catalysts decomposes very quickly at temperatures above 90°C and homogenous isomerization catalysts show very little activity at temperatures below 110°C or 130°C in the heterogeneous case.

6.3.3 IMPROVEMENT OF THERMAL STABILITY OF THE TELOMERIZATION CATALYST (Pd(Imes)(dvds))

As it has been seen in Chapter 5, using long chain alcohols such as butanol as nucleophile/solvent in telomerization reactions improved the activity of the catalyst Pd(Imes)(dvds) in respect to the values obtained with methanol. Following the discussion, it was believed to be due to the higher solubility of the catalysts in long chain alcohols. In order to study if long alcohols such as butanol have also influence on the thermal stability of the catalyst due to its better solubility, reactions with different alcohols as nucleophiles were carried out taking samples periodically in order to obtain reaction profiles. Results are shown in Table 6.11.

Table 6.11: Influence of the nucleophile in the thermal stability of Pd(Imes)(dvds).

Reactant	Catalyst	Nucleophile	T (°C)	Conversion @ 7h (%)	Selectivity @ 7h (%)
Isoprene	Pd(Imes)(dvds)	MeOH	110	22.3	92.4
Isoprene	Pd(Imes)(dvds)	Butanol	110	61.2	100

Reaction conditions: 3.25 mL Isoprene (4.35 M). Solvent: 3.25 mL 1%NaOMe, 1 mL decane as internal standard. Time: 7h. Catalyst: $2 \cdot 10^{-6}$ moles of Pd.

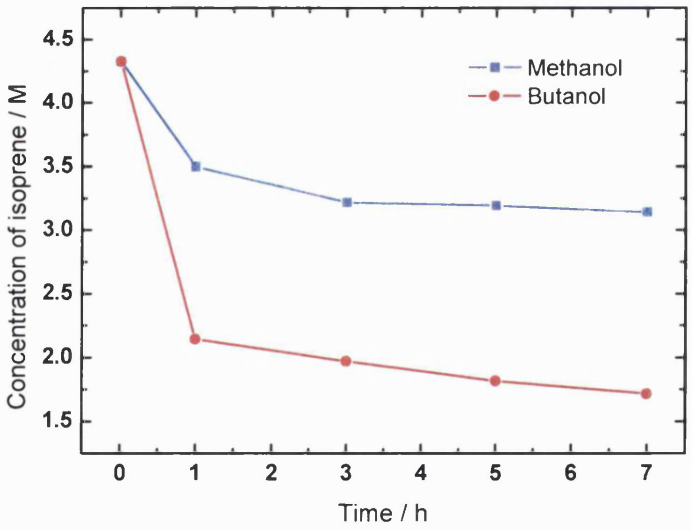

Figure 6.8: Reaction profiles of telomerization of isoprene with methanol and butanol.

As it can be observed in Figure 6.8 and as it was previously observed, higher conversion was obtained in the telomerization with butanol than with methanol. In both cases, most of the conversion of isoprene took place within the first hour of reaction. However, in the case of butanol, small conversion could be observed during the rest of the time which was not observed with methanol. Nevertheless, it cannot be concluded that the thermal stability of the catalyst Pd(Imes)(dvds) is enhanced by the use of butanol.

Beller's group [131] obtained high TON for the telomerization of 1,3-butadiene with alcohols with Pd(Imes)(dvds) as catalyst in the presence of free ligand (Imes) in the reaction medium. Based on these results, the influence of free (Imes) ligand on the thermal stability of the catalyst was studied obtaining the results shown in Table 6.12.

Table 6.12: Influence of the presence of free ligand Imes in the thermal stability of Pd(Imes)(dvds) catalyst.

Reactant	Catalyst	Nucleophile	T (°C)	TON	Conversion @ 7h (%)	Selectivity @ 7h (%)
Isoprene	Pd(Imes)(dvds)	MeOH	110	3618	22.3	92.4
Isoprene	Pd(Imes)(dvds) + 4eq (Imes) ligand	MeOH	110	10098	62.2	100
Isoprene	Pd(Imes)(dvds) + 4eq (Imes) ligand	MeOH	130	9080	55.9	93.1

Reaction conditions: 3.25 mL Isoprene (4.35 M). Solvent: 3.25 mL 1%NaOMe, 1 mL decane as internal standard. Time: 7h. Catalyst: $2 \cdot 10^{-6}$ moles of Pd.

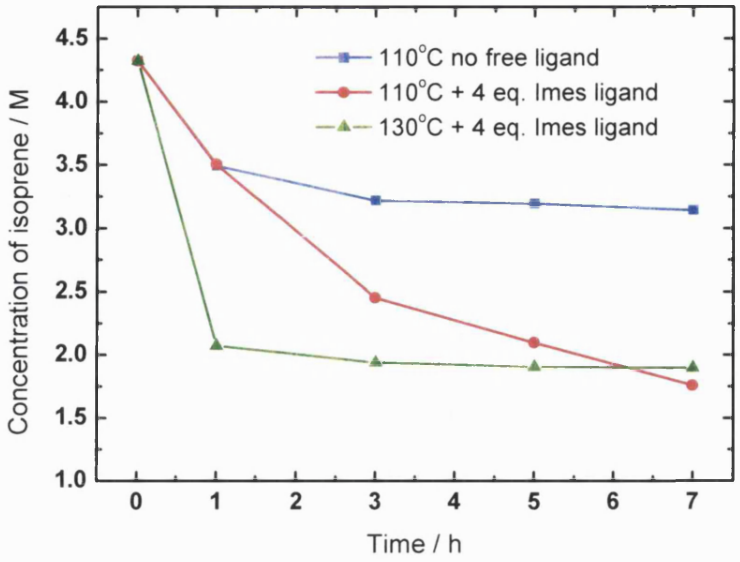

Figure 6.9: Reaction profiles of telomerization of isoprene with methanol with and without presence of free ligand.

As it can be observed in Figure 6.9, at 110°C, the presence of free ligand (Imes) in the reaction medium enhanced substantially the thermal stability of the catalyst Pd(Imes)(dvds). Same conversion values were obtained at this temperature after one hour of reaction however, after this time, catalyst decomposed very quickly when free ligand (Imes) was not present. On the other hand, reaction continued at least for seven hours in the presence of four equivalents of (Imes) ligand. At higher temperatures such as 130°C, the presence of free (Imes) ligand cannot prevent the decomposition of the catalyst Pd(Imes)(dvds) within the first hour of reaction. Nevertheless, the catalytic activity of the catalyst was improved in the presence of free (Imes) ligand. Table 6.13 compares results obtained in telomerization reactions with isoprene, 1,3-pentadiene and 1,3-hexadiene with different alcohols as nucleophiles.

Table 6.13: Influence of free ligand (Imes) in the telomerization reactions.

Reactant	Catalyst	Nucleophile	T (°C)	TON	Conversion @ 7h (%)	Selectivity @ 7h (%)
Isoprene	Pd(Imes)(dvds)	MeOH	110	3618	22.3	92.4
Isoprene	Pd(Imes)(dvds) + 4eq (Imes) ligand	MeOH	110	10098	62.2	100
1,3-pentadiene[a]	Pd(Imes)(dvds)	MeOH	110	352	18.8	93.7
1,3-pentadiene[b]	Pd(Imes)(dvds) + 4eq (Imes) ligand	MeOH	110	326	28.5	100
1,3-pentadiene[b]	Pd(Imes)(dvds) + 4eq (Imes) ligand	Butanol	110	829	66.3	100
1,3-pentadiene[a]	Pd(Imes)(dvds)	MeOH	130	226	12.1	91.6
1,3-pentadiene[b]	Pd(Imes)(dvds) + 4eq (Imes) ligand	MeOH	130	347	27.8	98.1
1,3-pentadiene[b]	Pd(Imes)(dvds) + 4eq (Imes) ligand	Butanol	130	869	69.6	100
1,3-hexadiene	Pd(Imes)(dvds)	Propanol	90	195.9	36.1	100
1,3-hexadiene	Pd(Imes)(dvds) + 4eq (Imes) ligand	Propanol	90	90.3	16.6	100
1,3-hexadiene	Pd(Imes)(dvds)	Butanol	90	213.1	39.2	100
1,3-hexadiene	Pd(Imes)(dvds) + 4eq (Imes) ligand	Butanol	90	163.2	30.1	100

Reaction conditions: Isoprene (4.35 M), 1,3-pentadiene [a](2 M) [b](1.3 M), 1,3-hexadiene (0.6 M). Solvent: 1%NaOMe, 1 mL decane as internal standard. Time: 7h. Catalyst: $2 \cdot 10^{-6}$ moles of Pd for isoprene and $8 \cdot 10^{-6}$ moles of Pd for 1,3-pentadiene.

The presence of free (Imes) ligand in telomerization reactions with methanol as nucleophile at higher temperatures than 90°C increased not only the thermal stability of the catalyst but also conversion values because catalyst was not decomposed within the first hour of reaction. An increment of activity was also observed in telomerization reactions with higher alcohols at temperatures higher than 90°C, but not at 90°C or lower, where catalyst is already stable without the necessity of free (Imes) ligand in the medium. In these cases, the presence of free (Imes) ligand slows down the activity although same values of conversion are obtained after 21 hours.

In accordance with all previous data, new tandem reactions were carried out using different isomerization catalysts (both homogeneous and heterogeneous) and Pd(Imes)(dvds) with free (Imes) ligand as telomerization catalyst. Results are shown in Table 6.14.

Table 6.14: Tandem reactions using Pd(Imes)(dvds) with free (Imes) ligand as telomerization catalyst.

Isomerization catalyst	Nucleophile	T (°C)	Conversion to isomerization (%) @ 19h	Conversion to telomerization (%) @ 19h	Selectivity to telomerization (%) @ 19h
$RuCl_3$	MeOH	130	95.8	11.3 (38%)	91.3
$RuCl_3$ [a]	MeOH	130	89.8	9.9 (33%)	91.2
$RuCl_3$	Butanol	110	58.7	9.3 (4%)	27.2
$RuCl_3$	Butanol	130	98.0	41.4 (11%)	19.2
$RuHCl(PPh_3)_3$	Butanol	110	98.0	28.3 (15%)	34.9
$RuHCl(PPh_3)_3$	Butanol	130	99.0	59.1 (23%)	27.2
10.1% Pd^{2+}/Ti-NT	MeOH	130	68.3	0.5	51.7
6.3% Rh^{3+}/Ti-NT	MeOH	130	85.3	1.5	71.3
19% Ru^{3+}/Ti-NT	MeOH	130	96.9	2.4 (1%)	71.4
4.9% Ru^{3+}/Ti-NT [a]	MeOH	130	88.9	4.1 (13%)	83
4.9% Ru^{3+}/Ti-NT	Butanol	110	25.6	-	-
4.9% Ru^{3+}/Ti-NT	Butanol	130	57.9	3.9 (6%)	100
5% Ru/C	Butanol	110	93.5	2.3 (1%)	16.6
5% Ru/C	Butanol	130	99.0	3.0 (1%)	18.2
0.5% Ru-PPh_3-resin	Butanol	110	33.8	2.9 (3%)	65.3
0.5% Ru-PPh_3-resin	Butanol	130	99.9	6.8 (3%)	24.5
2.7% Ru/ZSM-5	Butanol	130	50.8	-	-

Reaction conditions: 1 mL 1,4-pentadiene (1.3 M) [a] +1,3-pentadiene (0.7 M) . Solvent: 5 mL 1%NaOMe, 1 mL decane as internal standard. Time: 19h. Isomerization catalyst: $2.5 \cdot 10^{-5}$ moles for homogeneous and 0.2 g for heterogeneous. Telomerization catalyst: $8 \cdot 10^{-6}$ moles of Pd(Imes)(dvds) + 4 eq. (Imes) ligand.

Numbers between brackets in the conversion to telomerization column refer to the obtained percentage to telomerization reaction comparing to the values obtained for the telomerization reaction of 1,3-pentadiene in the same conditions. Calculations were done without taking into consideration dimerization reactions.

Very similar results for tandem reactions were obtained after seven and nineteen hours of reaction which suggests that both isomerization and telomerization catalysts are deactivated within the first ten hours.

Satisfactory results were obtained with homogeneous isomerization catalysts $RuCl_3$ and $RuHCl(PPh_3)_3$, especially using methanol as nucleophile when almost 40% of the total telomerization conversion was reached. However, it is important to highlight conclusions obtained in Chapter 5. The telomerization reaction is a second order reaction in respect to concentration of reactant, in this case, 1,3-pentadiene. During tandem reactions, concentration of 1,3-pentadiene is much smaller than in telomerization reactions because the first isomerization step is needed. This could explain the differences in conversion values.

Heterogeneous isomerization catalysts do not show good tandem results. On one hand, as it was seen in Chapter 4, all of them except Ru-PPh_3-resin, are much slower than homogeneous catalysts which can favour the decomposition of telomerization catalyst in the first hours of reaction due to the lack of reactant. On the other hand, telomerization catalyst can be chemically interfered by the heterogeneous isomerization catalysts as it is guessed from the null telomerization conversion obtained when high loadings of metals are used.

Very low selectivity values were obtained when butanol was used as nucleophile which decreases even more the concentration of 1,3-pentadiene as telomerization reactant.

6.4 CONCLUSIONS

Different tandem reactions of 1,4-pentadiene into telomerization products were carried out applying the results obtained in Chapters 4 and 5 without success, being necessary further studies of the influence of different parameters such as presence of base or temperature in both isomerization and telomerization reactions.

The presence of base (NaOMe) has resulted to be crucial in telomerization reactions due to the increment of MeO^- concentration in the reaction medium. Telomerization of isoprene conversion decreases extremely and no conversion is observed in the case of 1,3-pentadiene when no base is present. NaOMe presence has also an important role in the isomerization reaction decreasing the catalytic activity of all catalysts to isomerization due to the capture of protons involved in the isomerization mechanism.

Another important parameter is the reaction temperature. When telomerization catalysts are formed by the combination of a palladium salt and triphenylphosphine as a ligand, the catalyst is stable only up to 70°C. Better thermal stability is achieved with palladium carbene complex Pd(Imes)(dvds) which is stable up to 90°C. In both cases, at higher temperatures the catalysts decompose within one hour.

On the other hand, in the isomerization of diolefins, homogeneous catalysts show catalytic activity at temperatures above 110°C. 130°C is the minimum temperature value for heterogeneous catalysts.

In the telomerization of isoprene with methanol, regioselectivity is modified by the reaction temperature. With triphenylphosphine as a ligand, head-to-tail products are favoured versus tail-to-tail ones when the temperature is decreased. A different tendency is observed with Pd(Imes)(dvds) where as temperature decreases, the formation of head-to-head products are preferred versus head-to-tail ones.

The use of long chain primary alcohols such as 1-propanol or 1-butanol as nucleophiles in telomerization reactions was shown to increase the solubility of the Pd(Imes)(dvds) catalyst and therefore its activity. However, they do not have apparent influence on the thermal stability of the catalyst.

Adding free (Imes) ligand into the reaction medium improves the thermal stability of Pd(Imes)(dvds) catalyst in telomerization reactions, being stable for more than seven hours at 110°C. However, the catalyst is decomposed within one hour at 130°C. Free (Imes) ligand increases the stability of the catalyst decreasing its activity. However, as the catalyst is stable for longer times, higher overall conversion values are obtained in the presence of (Imes) ligand.

Different homogeneous and heterogeneous isomerization catalysts were screened in the tandem reaction of 1,4-pentadiene with alcohols using Pd(Imes)(dvds) and free (Imes) ligand as telomerization catalyst. Almost 40% of the total possible telomerization conversion is obtained with $RuCl_3$ as isomerization catalyst. This is judged a very high value considering that very low concentration of telomerization reactant is present, especially at the beginning of the tandem reaction. Although very high isomerization conversion values are obtained with almost all isomerization catalysts, lower telomerization conversions are achieved when heterogeneous isomerization catalysts are used. Chemical interferences are believed to be responsible for it as supported metals might capture the (Imes) ligands destabilizating the telomerization catalyst. No interferences of telomerization catalyst with heterogeneous supports were observed.

Chapter 7

CONCLUSIONS

The main aim of the project consists of proving the feasibility of a new tandem reaction comprising isomerization and telomerization steps starting with internal diolefin molecules. In addition, extending telomerization to long-chain molecules would open new opportunities for building high molecular weight functionalized molecules. Isomerization reaction leads to an isomer distribution where the external diolefins are taken by the telomerization step. By carrying out both reactions in the same pot, not only minimization of the number of step is achieved but also a shift of the chemical equilibrium towards the desired products. The whole process reduces energy, waste formation and capital costs comparing with a step-by-step process. Therefore, the whole process fulfils some of the main goals of the Green Chemistry principles which approach environmental protection by prevention of pollution.

7.2 RESEARCH ACHIEVEMENTS

In order to set the tandem reaction, both reaction steps, isomerization and telomerization, were studied independently focusing on screening commercial and novel catalysts as well as studying the influence of operating conditions.

In respect to isomerization reaction, the novel titanate nanotubes was found to be a suitable support for different metals such as palladium and rhodium for the isomerization of allylbenzene. Due to the physical properties of the titanate nanotubes, catalysts with a high loading of metal can be easily synthesised and recycled. In contrast to most supported metal catalysts, metals over titanate nanotubes show very high selectivity towards isomerization versus hydrogenation of the double bond.

Isomerization of diolefins such as 1,4-pentadiene and 1,5-hexadiene was studied for the first time. Screening of different homogeneous and heterogeneous catalysts based on transition metals was done. Heterogeneous palladium and rhodium only show catalytic activity when metals are supported on titanate nanotubes. Ruthenium on titanate nanotubes shows a similar catalytic activity as the commercial ruthenium on carbon. However, best results were obtained with the novel Ru-PPh_3-resin catalyst which show higher TON than the ones obtained with homogeneous catalysts and can be recycled a minimum of five times.

Novel isomerization catalysts were also tested versus homogeneous and commercial ones in the only isomerization of diolefins reported so far, the isomerization of linoleic acid. Ru-PPh_3-resin catalyst was found to be as active as homogeneous catalysts, with a rate of reaction almost ten times higher than the best reported heterogeneous catalyst (Ru/C) on the same conditions.

In order to get a better understanding of the telomerization of isoprene and 1,3-pentadiene with methanol, kinetic studies were carried out finding that both reactions are second order in respect to telomer and first order in respect to the nucleophile. Other parameters such as the influence of temperature were studied

discovering that palladium carbene complexes, especially Pd(Imes)(dvds), are more thermally stable than catalysts based on the combination of a palladium salt and phosphorous ligand triphenylphosphine. Pd(Imes)(dvds) catalyst is stable up to 90°C. However, the thermal stability can be enhanced by adding free carbene ligand (Imes) to the reaction medium.

Primary alcohols with different chain length were used as nucleophiles, finding out that increasing the length of the alcohol, the telomerization conversion increases significantly when carbene based catalysts are used. Exactly opposite tendency is found with phosphorous ligand (PPh_3). It is believed to be due to the higher solubility of the catalyst Pd(Imes)(dvds) as the length of the alcohol is increased. This allows high conversion in the telomerization of isoprene and 1,3-pentadiene to be achieved and extending the telomerization reaction to a longer molecule as 1,3-hexadiene for the first time, opening opportunities for long-chain reactants.

In order to overcome the drawbacks of homogeneous catalysts, especially the difficulties of removal from the reaction medium and potential interferences in tandem reactions, novel heterogeneous telomerization catalysts were synthesised and tested. Pd-(dvds)-PPh_3-resin shows to be a highly active catalyst in the telomerization of isoprene with methanol, giving a extremely high selectivity (the highest reported so far) to the tail-to-head isomer due to the combination of the (dvds) and PPh_3 ligands. The catalysts can be easily reused loosing its activity due to the realising of the (dvds) ligand into the solution.

The heterogenization of carbene ligands on different DVB resins were also tried obtaining very low loadings of palladium and therefore, low conversion values although high TON were obtained.

Finally, the study of tandem reactions was successful in meeting the main target of the project. Starting with 1,4-pentadiene, telomerization products are obtained. The best results are given by a combination of homogeneous catalysts for both reactions in methanol.

7.3 RESEARCH LIMITATIONS

The main limitations were found in the study of the telomerization reaction. Identification of telomerization products by isolation and NMR analyses was not possible due to the low quantity of reactants used, especially products of 1,3-hexadiene because of its extremely high price.

Restrictions were also found in the possibility of extending the telomerization reaction to longer chain molecules than 1,3-hexadiene caused by the absence of commercial reactants such as 1,3-heptadiene or 1,3-octadiene.

7.4 FUTURE WORK

Based on the different achievements along this thesis, further refinement of several aspects would be recommended in order to develop commercial processes not only for the proposed tandem reaction but also in the isomerization and telomerization reactions separately.

1. An increment of selectivity of Ru-PPh_3-resin in the isomerization reaction could be obtained by using different solvents other than methanol such as n-decane based on previous results. This achievement would allow the obtaining of not only a very active catalyst but also highly selective for the isomerization of diolefins versus hydrogenation. Especial interest would be found in the commercial isomerization of linoleic acid.

2. The success on the telomerization of 1,3-hexadiene with 1-propanol and 1-butanol encourages further investigation into the extension to longer molecules. Due to the absence of commercial 1,3-heptadiene or 1,3-octadiene, either synthesis of these molecules or the use of tandem reactions starting with internal diolefins are proposed.

3. In spite of the low palladium content in the heterogeneous carbenes on DVB resins, acceptable TON were obtained, which gives confidence in further investigation with these catalysts, especially increasing the ratio reactant/palladium ratio in telomerization reactions.

4. Finally, if previous targets are achieved, the success of tandem reactions using heterogeneous catalysts for both isomerization and telomerization reactions seems promising.

Chapter 8

REFERENCES

[1] P. T. Anastas and J. C. Williamson, Green Chemistry: An overview, **1996**, American Chemical Society.

[2] P. T. Anastas and J. C. Warner, Green Chemistry: Theory and Practice, **1998**, Oxford University Press.

[3] A. Seayad, M. Ahmed, H. Klein, R. Jackstell, T. Gross and M. Beller: Science. 297, 1676 - 1678, **2002**.

[4] P. Eilbracht, L. Barfacker, C. Buss, C. Hollmann, B. E. Kitsos-Rzychon, C. L. Kranemann, T. Rische, R. Roggenbuck and A. Schmidt: Chem. Rev. 99, 3329 - 3365, **1999**.

[5] B. Breita and S. K. Zahn: Tetrahedron. 61, 6171 - 6179, **2005**.

[6] A. Bernas, P. Laukkanen, N. Kumar, P. Mäki-Arvela, J. Väyrynen, E. Laine, B. Holmbom, T. Salmi and D. Y. Murzin: J. Catal. 210, 354 - 366, **2002**.

[7] G. W. Parshall: Inorg. Syn. 15, 48-49, **1974**.

[8] D. V. Bavykin, V. N. Parmon, A. A. Lapkin and F. C. Walsh: J. Mater Chem. 14, 3370 - 3377, **2004**.

[9] J. Cao, J. Z. Sun, H.-L. Li, J. Hong and M. Wang: J. Mater. Chem. 14, 1203 - 1206, **2004**.

[10] M. Hodos, E. Horvath, H. Haspel, A. Kukovecz, Z. Konya and I. Kiricsi: Chem Psyc Lett. 399, 512 - 515, **2004**.

[11] M. Wang, D.-J. Guo and H.-L. Li: J. Solid State Chem. 178, 1996-2000, **2005**.

[12] C. H. Lin, C. H. Lee, J. H. Chao, C. Y. Kuo, Y. C. Cheng, W. N. Huang, H. W. Chang, Y. M. Huang and M. K. Shih: Catal Lett. 98, 61-66, **2004**.

[13] V. Idakiev, Z. Y. Yuan, T. Tabakova and B. L. Su: Appl. Catal. A: General. 281, 149 - 155, **2005**.

[14] J. Qu, X. Zhang, Y. Wang and C. Xie: Electrochim acta. 50, 3576-3580, **2005**.

[15] D. V. Bavykin, A. A. Lapkin, P. K. Plucinski, J. M. Friedrich and F. C. Walsh: J. Catal. 235, 10-17, **2005**.

[16] D. V. Bavykin, J. M. Friedrich and F. C. Walsh: Adv Mater. 18, 2807 – 2804, **2006**.

[17] H. Chang and P. J. Huang: J. Raman Spectrosc. 29, 97 - 102, **1998**.

[18] D. V. Bavykin, A. A. Lapkin, P. K. Plucinski, L. Torrente-Murciano, J. M. Friedrich and F. C. Walsh: Topics in Catal. 39, **2006**.

[19] D. Zhao, D. Feng, J. Feng, Q. Huo, N. Melosh, G. Fredrickson, B. Chmelka and G. Stucky: Science. 279, 548 - 552, **1998**.

[20] International Zeolite Association: www.iza-online.org. **2007**.

[21] V. Ananikov, M. Kabeshov and I. Beletskaya: Synlett. 6, 1015 - 1017, **2005**.

[22] R. Jackstell, S. Harkal, H. Jiao, A. Spannenberg, C. Borgmann, D. Rottgere, F. Nierlich, M. Elliot, S. Niven, K. Cavell, O. Navarro, M. Viciu, S. P. Nolan and M. Beller: Chem-Eur. J. 10, 3891 - 3900, **2004**.

[23] F. Benvenuti, C. Carlini, A. M. Raspolli Galletti, G. Sbrana, M. Marchionna and R. Patrini: J. Mol. Catal. A-Chem. 137, 49 - 63, **1999**.

[24] F. Benvenuti, C. Carlini, M. Marchionna, R. Patrini, A. M. Raspolli Galletti and G. Sbrana: J. Mol. Catal. A-Chem. 139, 177 - 187, **1999**.

[25] B. Blanco, M. Brissart, M. Moreno-Manas, R. Pleixats, A. Mehdi, C. Reyé, S. Bouquillon, F. Hénin and J. Muzart: Appl. Catal. A-Gen. 297, 117 - 124, **2006**.

[26] B. Altava, M. Burguete, E. García-Verdugo, S. V. Luis and M. Vicent: Tetrahedron. 57, 8675 - 8683, **2001**.

[27] G. Bond and I. Hellier: J. Catal. 4, 1 - 5, **1965**.

[28] F. J. Harrod and J. Chalk: J. Am. Chem. Soc. 86, 1776-1779, **1963**.

[29] B. Corain and G. Puosi: J. Catal. 30, 403 - 408, **1973**.

[30] H. Wakamatsu, M. Nishida, N. Adachi and M. Mori: J. Org. Chem. 65, 3966-3970, **2000**.

[31] J. K. Hambling, Catalyst preparation and use, Patent: 1,007,325, **1962.**

[32] E. D'Incan and P. Viout: Tetrahedron. 40, 3421-3424, **1984**.

[33] C. S. John, A. Tada and L. V. F. Kennedy: J. Chem. Soc. Farday Trans. I. 74, 498-505, **1978**.

[34] M. A. Aramendía, V. Borau, C. Jiménez, A. Marinas, J. R. Ruiz and F. J. Urbano: J. Mol. Cat. A: Chem. 218, 81 - 90, **2004**.

[35] J. N. Kondo, K. Domen and F. Wakabayashi: J. Phys. Chem. 101, 5477 - 5479, **1997**.

[36] J. N. Kondo, K. Domen and F. Wakabayashi: Micropor Mesopor Mat. 21, 429 - 437, **1998**.

[37] D. M. Hamilton, Terminal to interior double bond isomerization process for an olefinic molecule with reduced dimerization, Patent. **1988.**

[38] M. A. Parent and J. B. Moffat: J. Catal. 177, 335 - 342, **1998**.

[39] D. Kishore and S. Kannan: J. Mol. Cat. A: Chem. 223, 225-230, **2004**.

[40] A. Lambert, E. G. Derouane and I. V. Kozhevnikov: J. Catal. 211, 445 - 450, **2002**.

[41] K. Borzeky, T. Mallat and A. Baiker: Catal. Lett. 59, 95-97, **1999**.

[42] R. J. Grau, P. D. Zgolicz, G. Gutierrez and H. A. Taher: J. Mol. Cat. A: Chem. 148, 203 - 214, **1999**.

[43] G. V. Smith, J. A. Roth, D. S. Desai and J. L. Kosco: J. Catal. 30, 79 - 85, **1973**.

[44] M. M. P. Zieverink, M. T. Kreutzer, F. Kapteijn and J. A. Moulijn: Ind. Eng. Chem. Res. 44, 9668-9675, **2005**.

[45] P. v. d. Plank: J. Catal. 26, 42-50, **1972**.

[46] D. E. Portlock, D. Naskar, L. West, W. L. Seibel, T. Gu, H. J. Krauss, X. S. Peng, P. M. Dybas, E. G. Soyke, S. B. Ashton and J. Burton: Tetrahedron Lett. 44, 5365-5368, **2003**.

[47] A. Bernas, P. Laukkanen, N. Kumar, P. Mäki-Arvela, J. Väyrynen, E. Laine, B. Holmbom, T. Salmi and D. Y. Murzin: J. Catal. 210, 354 - 366, **2002**.

[48] A. Bernas, P. Maki-Arvela, N. Kumar, B. Holmbom, T. Salmi and D. Y. Murzin: Ind Eng Chem. 42, 718 - 727, **2003**.

[49] A. Bernas, N. Kumar, P. Mäki-Arvela, N. V. Kul'kova, B. Holmbom, T. Salmi and D. Y. Murzin: Appl. Catal. A: General. 245, 257 - 275, **2003**.

[50] A. Bernas, N. Kumar, P. Mäki-Arvela, B. Holmbom, T. Salmi and D. Y. Murzin: Org. Proc. Res. Dev. 8, 341 - 352, **2004**.

[51] A. A. Petrov, Catalytic isomerization of hydrocarbons, **1960**, Olbourne Press.

[52] F. E. Condor, Catalysis VI: Hydrocarbon catalysis, **1958**, Reinhold Publishing Corporation.

[53] Cornils and Herrmann, Applied homogeneous catalysis with organometallic compounds, vol. 3, **2002**.

[54] T. C. Morril and C. A. D'Souza: Organometallics. 22, 1626 - 1629, **2003**.

[55] R. Cramer and R. V. Lindsey: J. Am. Chem. Soc. 88, 3534 - 3544, **1966**.

[56] Conti, Raimondi, Pregaglia and Ugo: Journal of organometallic Chemistry. 70, 107-120, **1974**.

[57] M. B. Sparke, L. Turner and A. J. M. Wenham: J. Catal. 4, 332 - 340, **1965**.

[58] A. Salvini, F. Pacenti, P. Frediani, A. Devescov and M. Caporali: J. Org. Chem. 625, 255 - 267, **2001**.

[59] R. C. v. d. Drift, E. Bouwman and E. Drent: J. Organomet. Chem. 650, 1-24, **2002**.

[60] R. Uma, C. Crévisy and R. Grée: Chem. Rev. 103, 27-51, **2003**.

[61] D. Kishore and S. Kannan: Appl. Catal. A: General. 270, 227 - 235, **2004**.

[62] B. Hudson, D. E. Webster and P. B. Weels: J. Chem. Soc. Dalton. 12, 1204-1207, **1972**.

[63] M. Mirza-Aghayan, R. Boukherroub, M. Bolourtchian, M. Hoseini and K. Tabar-Hydar: J. Org. Chem. 678, 1 - 4, **2003**.

[64] D. B. Dahl, C. Davies, R. Hyden, M. L. Kirova and W. G. Lloyd: J. Mol. Cat., A: Chemical. 123, 91 - 101, **1997**.

[65] A. Sen and T.-W. Lai: Inorg Chem. 23, 3257-3258, **1984**.

[66] R. J. Topping, L. D. Quin and A. L. Crumbliss: J. Org. Chem. 385, 131 - 145, **1990**.

[67] H. Hirai, H. Sawai, E. Ochiai and S. Makishima: J. Catal. 17, 119 - 120, **1969**.

[68] D. F. Ewing, B. Hudson, D. E. Webster and P. B. Weels: J. Chem. Soc. Dalton. 12, 1287-1293, **1972**.

[69] H. A. Tayim and J. C. Bailar: J. Am. Chem. Soc. 89, 3420-3424, **1967**.

[70] N. B. Dobroserdova, G. S. Barkhmet'eva, A. I. Leonova, I. V. Gostunskaya and B. A. Kazanskii: Petrol Chem USSR. 4, 61 - 65, **1965**.

[71] D. Bingham, D. E. Webster and P. B. Wells: J Chem Soc Dalton. 18, 1928-1932, **1972**.

[72] I. Heertje, G. K. Koch and W. J. Wosten: J. Catal. 32, 337 - 342, **1974**.

[73] A. Bernas, N. Kumar, P. Laukkanen, V. Váyrynen, T. Salmi and D. Y. Murzin: Appl. Catal. A: General. 267, 121 - 133, **2004**.

[74] P. Van der Plank and H. J. Van Oosten: J. Catal. 38, 223 - 230, **1975**.

[75] D. Mukesh, C. S. Narasimhan, D. V.M. and K. Ramnarayan: Ind Eng Chem. 27, 409 - 414, **1988**.

[76] M. Skotak, Z. Karpinski, W. Juszczyk, J. Pielaszek, L. Kepinski, D. V. Kazachkin, V. I. Kovalchuk and J. L. d'Itri: J. Catal. 227, 11 - 25, **2004**.

[77] P. B. Weels and G. R. Wilson: J. Catal. 9, 70 - 75, **1967**.

[78] N. C. Ramani, D. L. Sullivan and J. G. Ekerdt: J. Catal. 173, 105 - 114, **1998**.

[79] R. Touroude and F. G. Gault: J. Catal. 37, 193 - 203, **1975**.

[80] H. Sertchook, D. Avnir, J. Blum, F. Joo, A. Katho, H. Schumann, R. Weimann and S. Wernik: J. Mol. Cat., A: Chemical. 108, 153-160, **1996**.

[81] A. Zoran and Y. Sasson: J. Org. Chem. 46, 255 - 260, **1981**.

[82] D. Hamilton Jr, Terminal to interior double bond isomerization process for an olefinic molecule with reduced dimerization, Patent. **1988.**

[83] Aramedía, Borau, Jiménez, Marinas and Urbano: Journal of Catalysis. 211, 556 - 559, **2002**.

[84] M. P. Rosynek, J. S. Fox and J. L. Jensen: J. Catal. 71, 64 - 77, **1981**.

[85] M. P. Rosynek and J. S. Fox: J. Catal. 49, 285 - 293, **1977**.

[86] K. Na, T. Okuhara and M. Misono: J. Catal. 170, 96-107, **1997**.

[87] M. A. Parent and J. B. Moffat: Langmuir. 12, 3733 - 3739, **1996**.

[88] E. A. Cagnola, M. E. Quiroga, D. A. Liprandi and P. C. L'Argentiere: Appl. Catal. A: General. 274, 205 - 212, **2004**.

[89] L. Torrente-Murciano, A. A. Lapkin, D. V. Bavykin, F. C. Walsh and K. Wilson: J. Catal. 245, 270 - 276, **2007**.

[90] A. Bernas, N. Kumar, P. Mäki-Arvela, N. V. Kul'kova, B. Holmbom, T. Salmi and D. Y. Murzin: Appl. Catal. A: General. 245, 257-275, **2005**.

[91] M. Wang, D.-J. Guo and H.-L. Li: J. Solid State Chem. 178, 1996-2000, **2005**.

[92] A. Behr and M. Urschey: J. Mol. Catal. A-Chem. 197, 101 - 113, **2003**.

[93] J. M. Takacs, S. Venkataraman, R. N. Andrews and L. S. W. Pelter: J. Organomet. Chem. 690, 6205 - 6209, **2005**.

[94] Y. Chauvin, L. Magna, G. P. Noccolai and J. M. Basset, Process of telomerizing conjugated dienes, Patent: **2002.**

[95] A. Behr, M. Urschey and V. A. Brehme: Green Chem. 5, 198 - 204, **2003**.

[96] R. Jackstell, S. Harkal, H. Jiao, A. Spannenberg, C. Borgmann, D. Rottgere, F. Nierlich, M. Elliot, S. Niven, K. Cavell, O. Navarro, M. Viciu, S. P. Nolan and M. Beller: Chem-Eur. J. 10, 3891 - 3900, **2004**.

[97] R. Jackstell, A. Frisch, M. Beller, D. Rottgere, M. Malaun and B. Bildstein: J. Mol. Catal. A-Chem. 185, 105 - 112, **2002**.

[98] B. In Lee, K. Hee Lee and J. Sung Lee: J. Mol. Catal. A-Chem. 166, 233 - 242, **2001**.

[99] G. Santos-Fonseca, R. F. de Souza and J. Dupont: Catal. Commun. 3, 377 - 380, **2002**.

[100] A. Behr and R. Ugo, Aspects of homogeneous Catalysis, Volume 5, **1984**, D. Reidel Publishing Company.

[101] F. Benvenuti, C. Carlini, M. Lami, M. Marchionna, R. Patrini, A. M. Raspolli Galleti and G. Sbrana: J. Mol. Catal. A-Chem. 144, 27 - 40, **1999**.

[102] A. Krotz, F. Vollmuller, G. Stark and M. Beller: Chem. Commun. 195 -196, **2001**.

[103] F. Vollmuller, J. Krause, S. Klein, W. Magerlein and M. Beller: Eur. J. Inorg. Chem. 1825 - 1832, **2000**.

[104] D. Nielsen and K. Cavell, N-Heterocyclic Carbenes in synthesis, Chapter 4, **2006,** Wiley-VCH.

[105] B. In Lee, K. Hee Lee and J. Sung Lee: J. Mol. Catal. A-Chem. 156, 283 - 287, **2000**.

[106] M. Basato, L. Crociani, F. Benvenuti, A. M. Raspolli Galletti and G. Sbrana: J. Mol. Catal. A-Chem. 145, 313 - 316, **1999**.

[107] S. M. Maddock and M. G. Finn: Organometallics. 19, 2684 - 2689, **2000**.

[108] E. Dinjus and W. Leitner: Appl. Organomet. Chem. 9, 43 - 50, **1995**.

[109] P. Braunstein, D. Matt and D. Nobel: J. Am. Chem. Soc. 110, 3207 - 3212, **1988**.

[110] P. Braunstein, D. Matt and D. Nobel: Chem. Rew. 88, 747 - 764, **1988**.

[111] F. Bouachir, P. Grenouillet, D. Neibecker, J. Poirier and I. Tkatchenko: J. Organomet. Chem. 569, 203 - 215, **1998**.

[112] F. Benvenuti, C. Carlini, A. M. Raspolli Galletti, G. Sbrana, M. Marchionna and R. Patrini: J. Mol. Catal. A-Chem. 137, 49 - 63, **1999**.

[113] L. Magna, Y. Chauvin, G. P. Niccolai and J. M. Basset: Organometallics. 22, 4418 - 4425, **2003**.

[114] F. Benvenuti, C. Carlini, M. Marchionna, R. Patrini, A. M. Raspolli Galletti and G. Sbrana: J. Mol. Catal. A-Chem. 140, 139 - 155, **1999**.

[115] M. Camargo, P. Dani, J. Dupont, R. F. de Souza, M. Pfeffer and I. Tkatchenko: J. Mol. Catal. A-Chem. 109, 127 - 131, **1996**.

[116] B. Estrine, B. Blanco, S. Bouquillon, F. Hénin, M. Moreno-Manas, J. Muzart, P. Pena and R. Pleixats: Tetrahedron Lett. 42, 7055 - 7057, **2001**.

[117] Y. Ding, R. Goddard and K.-R. Porschke: Organometallics. 24, 439 - 445, **2005**.

[118] G. W. Nyce, T. Glauser, E. F. Connor, A. Mock, R. M. Waymouth and J. L. Hedrick: J. Am. Chem. Soc. 125, 3046 - 3056, **2003**.

[119] F. Benvenuti, C. Carlini, M. Marchionna, R. Patrini, A. M. Raspolli Galletti and G. Sbrana: J. Mol. Catal. A-Chem. 139, 177 - 187, **1999**.

[120] B. Blanco, M. Brissart, M. Moreno-Manas, R. Pleixats, A. Mehdi, C. Reyé, S. Bouquillon, F. Hénin and J. Muzart: Appl. Catal. A-Gen. 297, 117 - 124, **2006**.

[121] B. Estrine, R. Soler, C. Damez, S. Bouquillon, F. Henin and J. Muzart: Green Chem. 5, 686 - 689, **2003**.

[122] K. Kaneda, H. Kurosaki, M. Terasawa, T. Imanaka and S. Teranishi: J. Org Chem. 46, 2356 - 2362, **1981**.

[123] K. Kaneda, H. Kurosaki, M. Terasawa, T. Imanaka and S. Teranishi: J. Org Chem. 46, 2356 - 2362, **1981**.

[124] J. C. Mol: J. Mol. Cat. A: Chem. 213, 39 - 45, **2004**.

[125] A. Seayad, M. Ahmed, H. Klein, R. Jackstell, T. Gross and M. Beller: Science. 297, 1676 - 1678, **2002**.

[126] Cornils and Herrmann, Applied homogeneous catalysis with organometallic compounds, 3, **2002**,

[127] R. Cramer and R. V. Lindsey: J. Am. Chem. Soc. 88, 3534 - 3544, **1966**.

[128] F. Benvenuti, C. Carlini, M. Lami, M. Marchionna, R. Patrini, A. M. Raspolli Galleti and G. Sbrana: J. Mol. Catal. A-Chem. 144, 27 - 40, **1999**.

[129] F. Vollmuller, J. Krause, S. Klein, W. Magerlein and M. Beller: Eur. J. Inorg. Chem. 1825 - 1832, **2000**.

[130] A. Krotz, F. Vollmuller, G. Stark and M. Beller: Chem. Commun. 195 -196, **2001**.

[131] R. Jackstell, A. Frisch, M. Beller, D. Rottgere, M. Malaun and B. Bildstein: J. Mol. Catal. A-Chem. 185, 105 - 112, **2002**.

Appendix I

IDENTIDICATION OF TELOMERIZATION PRODUCTS BY MASS SPECTRA

I.1 INTRODUCTION

Telomerization products of isoprene, 1,3-pentadiene and 1,3-hexadiene with different alcohols such as methanol, ethanol, propanol and butanol were identified by their mass spectra. The analyses were carried out at Cardiff University using a GC-MASS instrument which was equipped with the same column that the one described in Chapter 2. Same method was also used. In this appendix, the mass spectra of all products are shown.

I.2 IDENTIFICATION OF TELOMERIZATION PRODUCTS OF ISOPRENE WITH ALCOHOLS

Telomerization of isoprene with methanol

Only the telomerization products of isoprene with methanol were isolated by distillation and identified by NMR spectroscopy (analyses done between Cardiff and Rostock Universities). Figure I.1 shows the mass spectrum of the identified head-to-tail product.

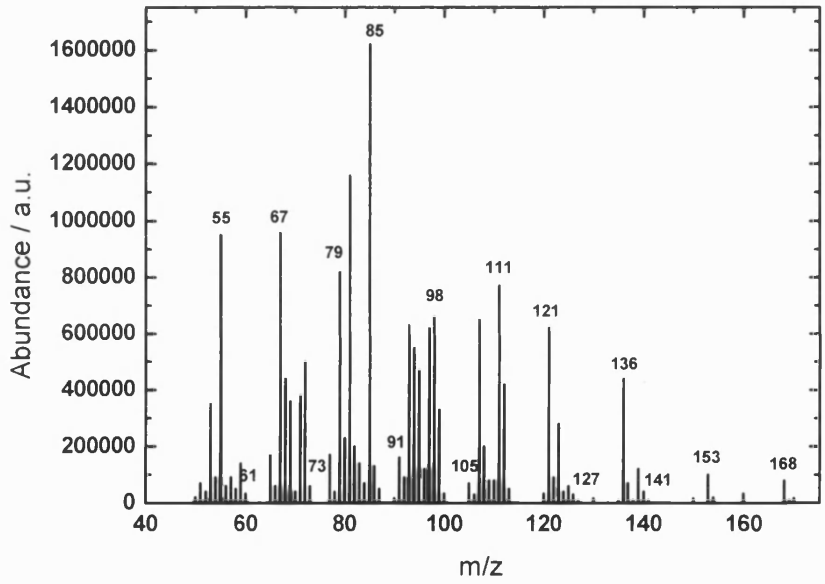

Figure I.1: Mass-spectrum of head-to-tail telomerization product of isoprene with methanol.

The total mass of this molecule is 168 g/mol which corresponds with the last peak of the spectrum. ChemSketch program was used in order to simulate the fragmentations of the molecules in the MASS detector, obtaining Figure I.2 in this case. It is believed that the first groups to be broken are the carbons attached to the ether group correspondening to the nucleophile molecule. The total mass of two isoprene molecules is 122 g/mol, peak which is observed in all mass-spectra of the telomerization of isoprene products independent of the alcohol used as nucleophile.

Slightly different spectra are obtained for different isomers, depending on where the double bonds and the branched are situated.

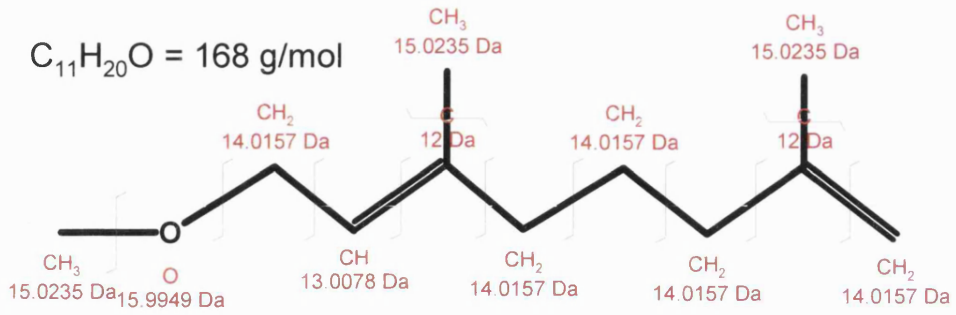

Figure I.2: Head-to-tail telomerization of isoprene with methanol product and its mass-spec fragmentations.

Mass spectra and potential fragmentations of all non-identified telomerization products are shown.

Telomerization of isoprene with ethanol

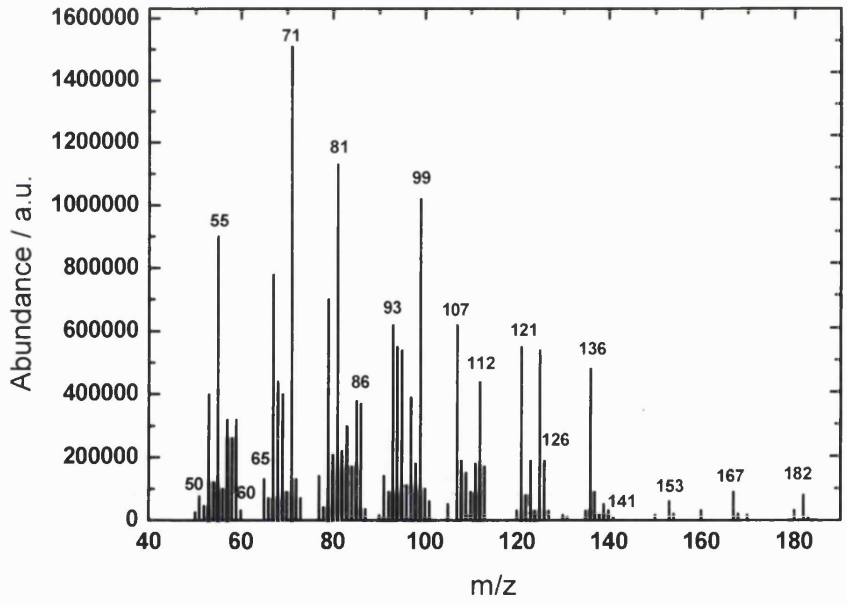

Figure I.3: Mass-spectrum of a product of the telomerization of isoprene with ethanol.

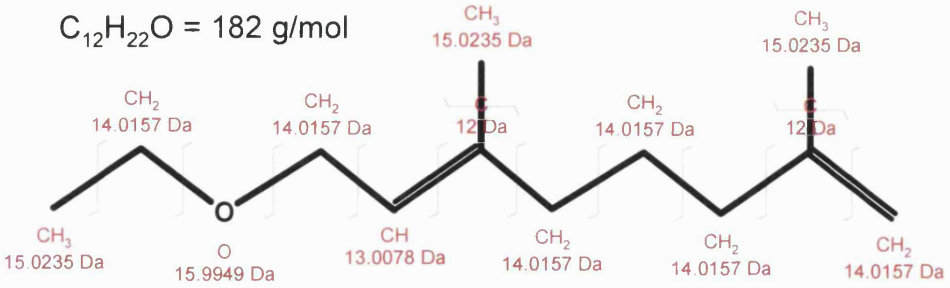

Figure I.4: Telomerization of isoprene with ethanol product and its mas-spec fragmentations.

Telomerization of isoprene with propanol

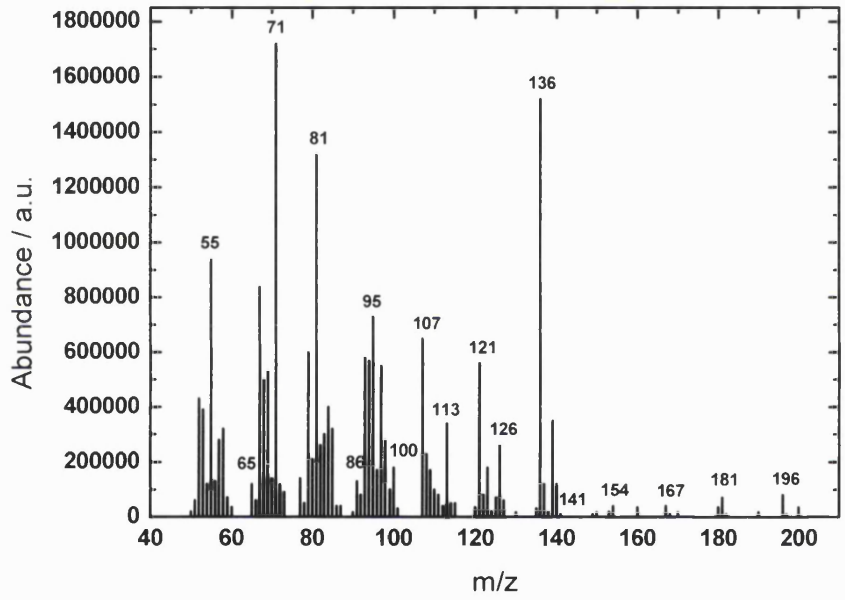

Figure I.5: Mass-spectrum of a product of the telomerization of isoprene with propanol.

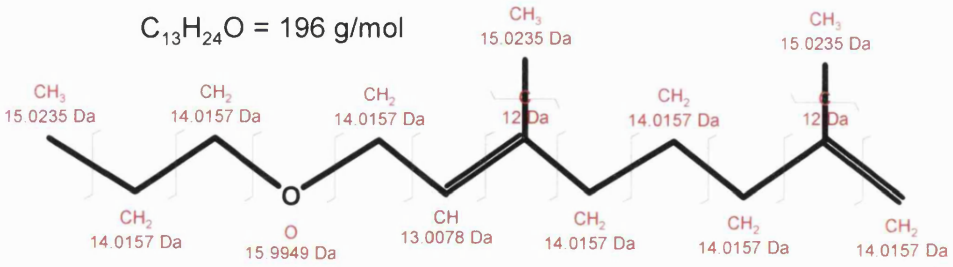

Figure I.6: Telomerization of isoprene with propanol product and its mas-spec fragmentations.

Telomerization of isoprene with butanol

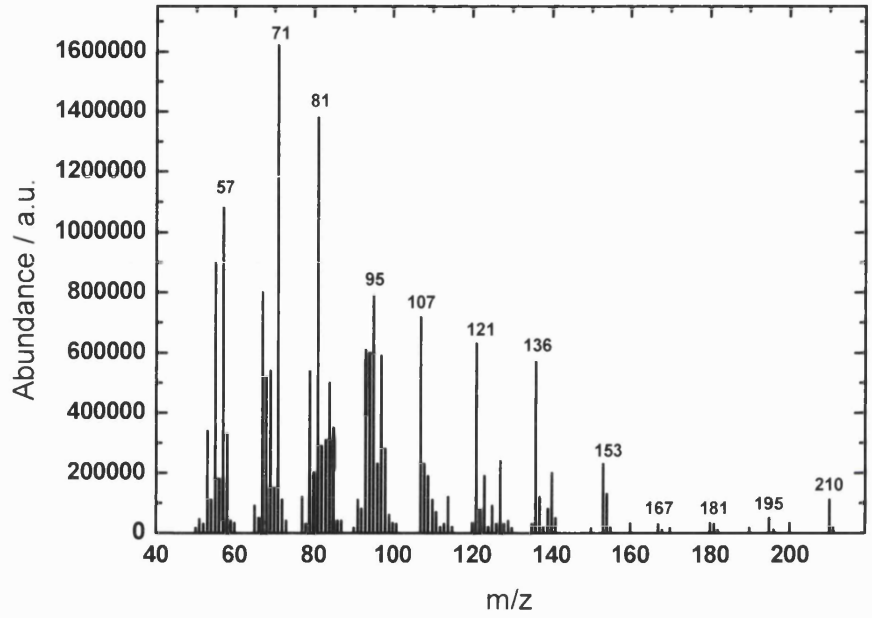

Figure I.7: Mass-spectrum of a product of the telomerization of isoprene with butanol.

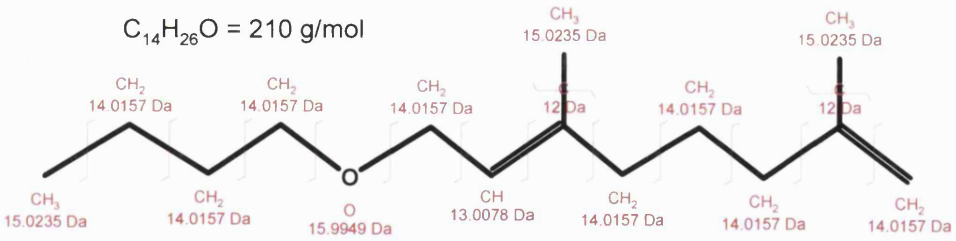

Figure I.8: Telomerization of isoprene with butanol product and its mas-spec fragmentations.

I.2 IDENTIFICATION OF TELOMERIZATION PRODUCTS OF 1,3-PENTADIENE WITH ALCOHOLS

Telomerization of 1,3-pentadiene with methanol

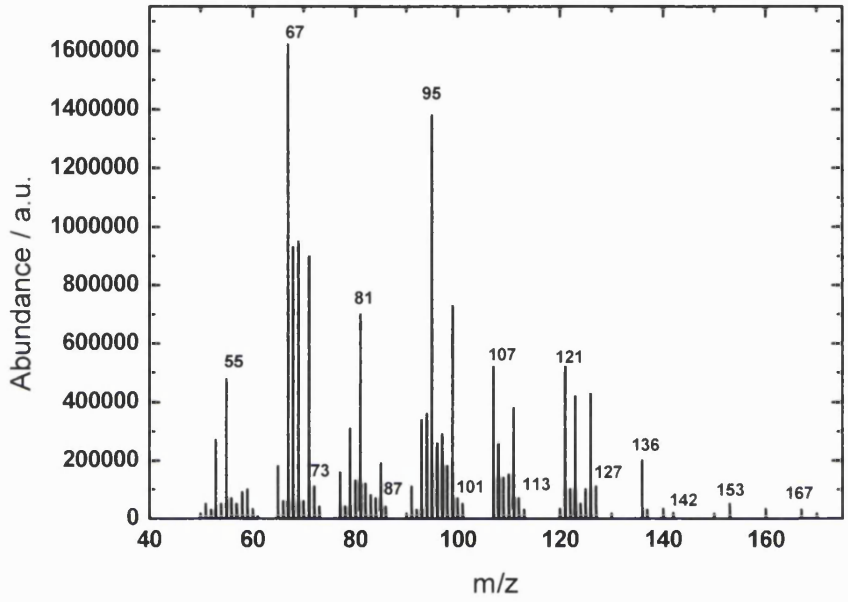

Figure I.9: Mass-spectrum of a product of the telomerization of 1,3-pentadiene with methanol.

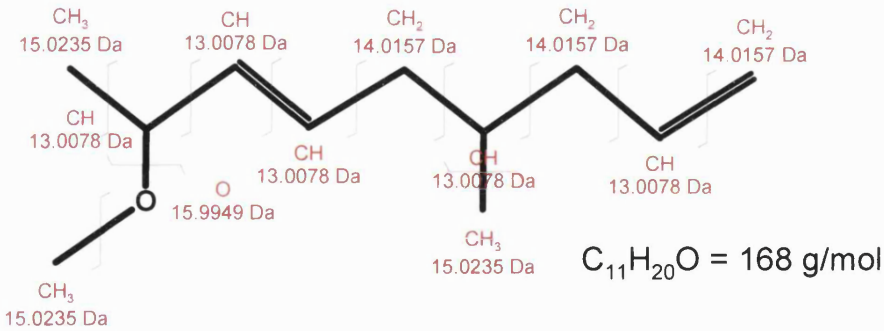

Figure I.10: Telomerization of 1,3-pentadiene with methanol product and its mas-spec fragmentations.

Telomerization of 1,3-pentadiene with ethanol

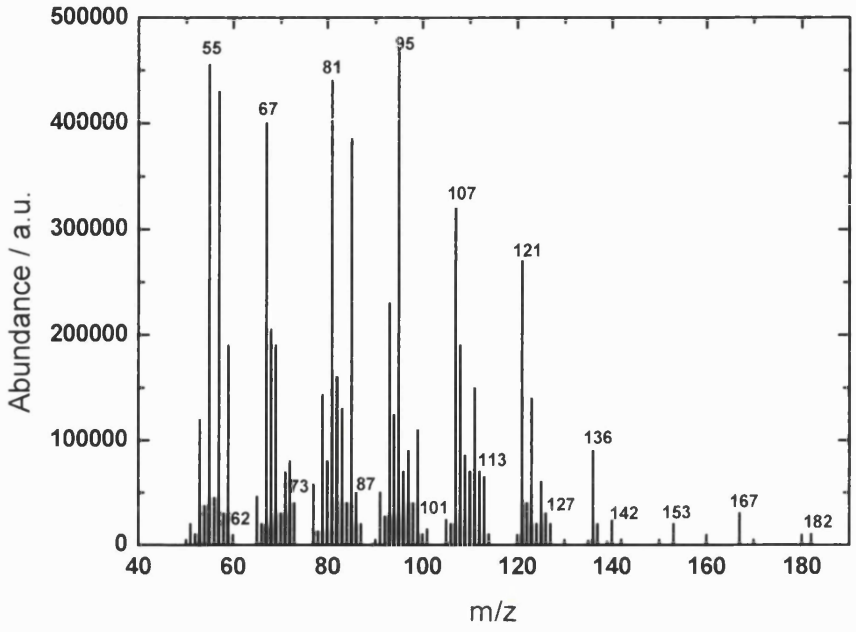

Figure I.11: Mass-spectrum of a product of the telomerization of 1,3-pentadiene with ethanol.

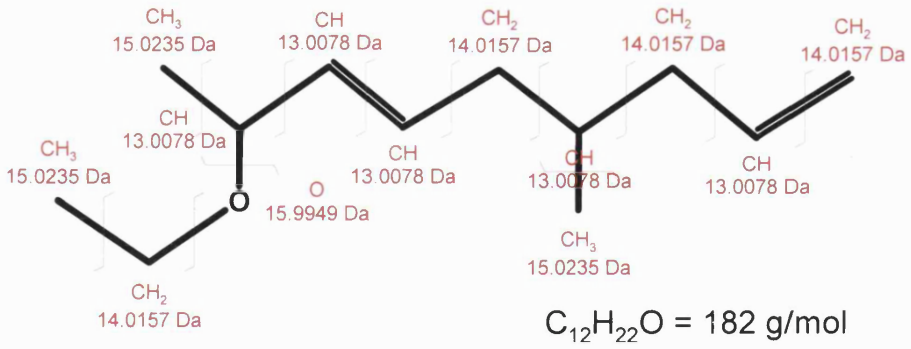

Figure I.12: Telomerization of 1,3-pentadiene with ethanol product and its mas-spec fragmentations.

Telomerization of 1,3-pentadiene with propanol

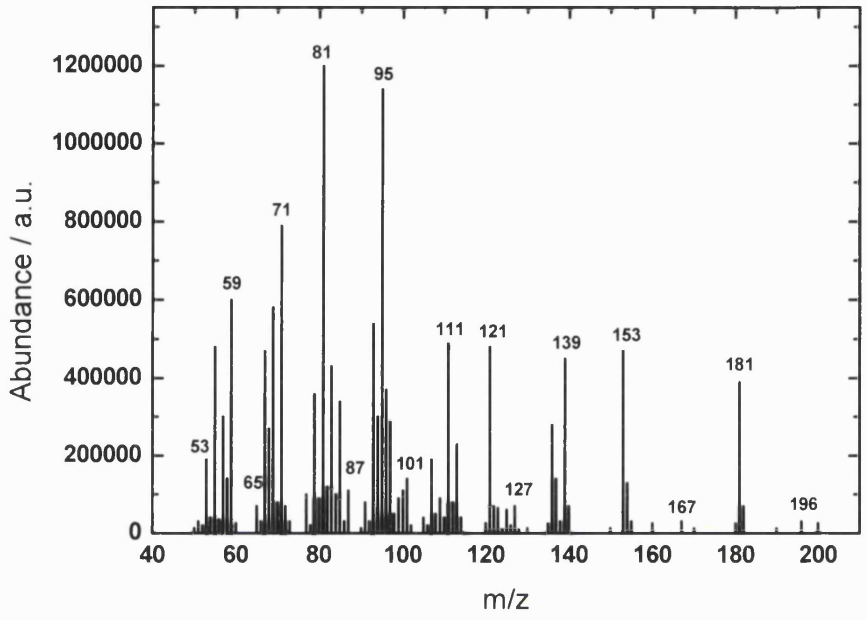

Figure I.13: Mass-spectrum of a product of the telomerization of 1,3-pentadiene with propanol.

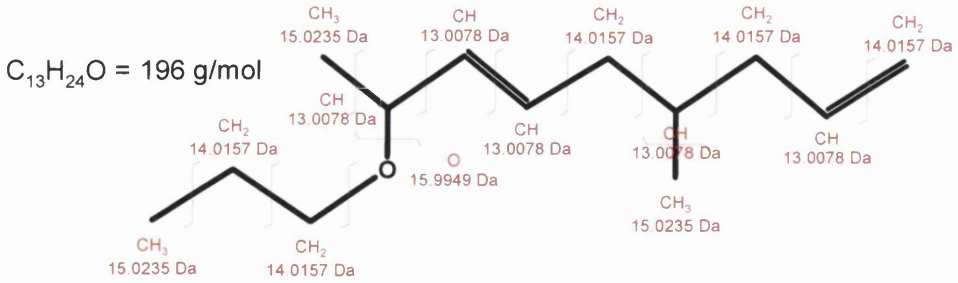

Figure I.14: Telomerization of 1,3-pentadiene with propanol product and its mas-spec fragmentations.

Telomerization of 1,3-pentadiene with butanol

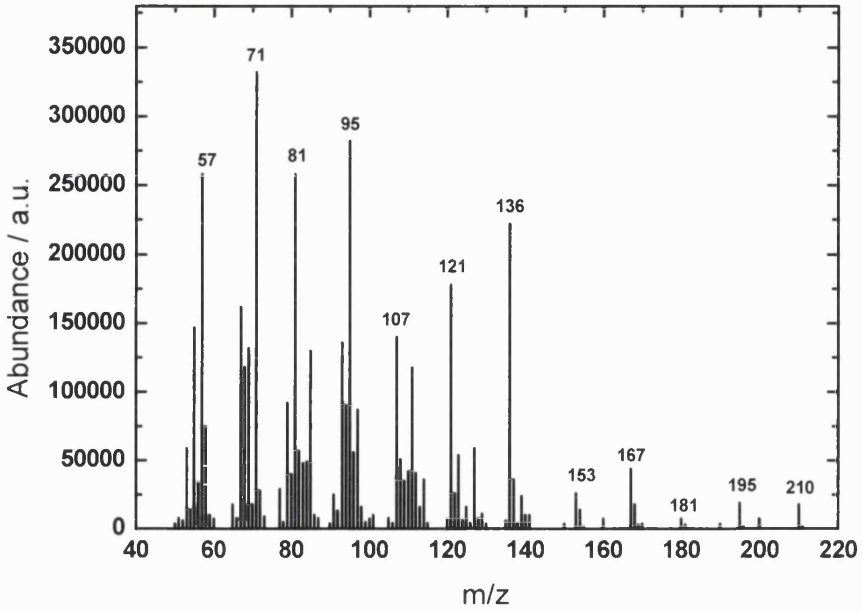

Figure I.15: Mass-spectrum of a product of the telomerization of 1,3-pentadiene with butanol.

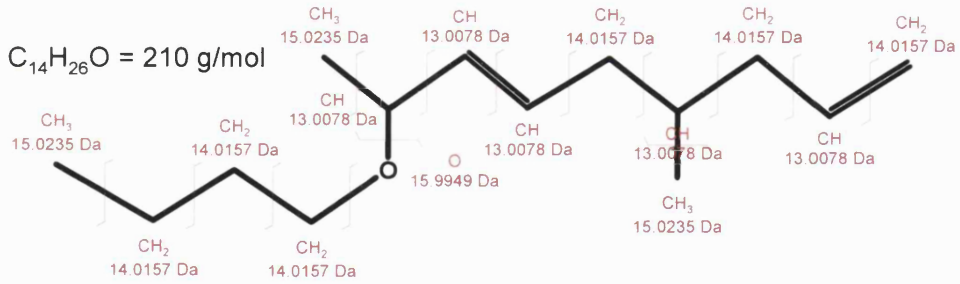

Figure I.16: Telomerization of 1,3-pentadiene with butanol product and its mas-spec fragmentations.

I.3 IDENTIFICATION OF TELOMERIZATION PRODUCTS OF 1,3-HEXADIENE WITH ALCOHOLS

Telomerization of 1,3-hexadiene with ethanol

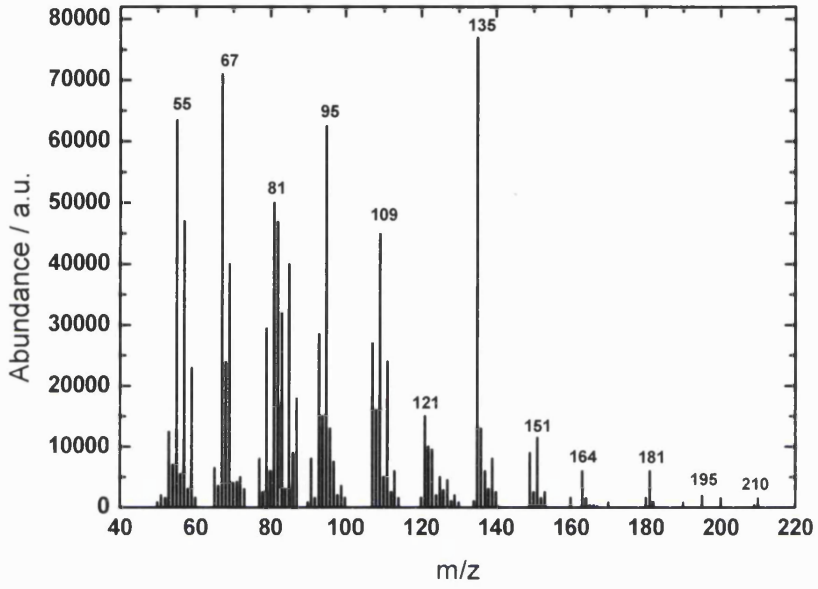

Figure I.17: Mass-spectrum of a product of the telomerization of 1,3-hexadiene with ethanol.

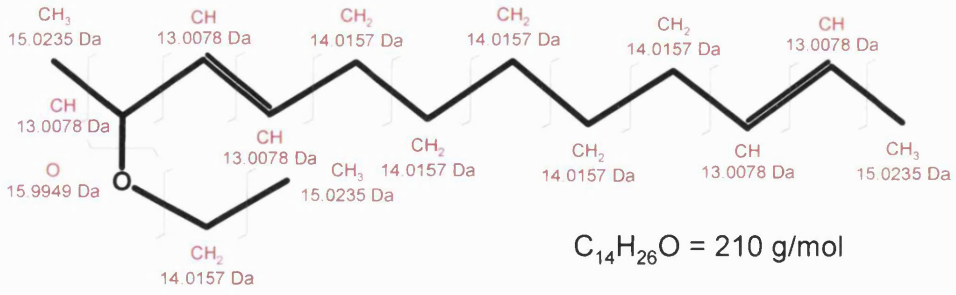

Figure I.18: Telomerization of 1,3-hexadiene with ethanol product and its mas-spec fragmentations.

Telomerization of 1,3-hexadiene with propanol

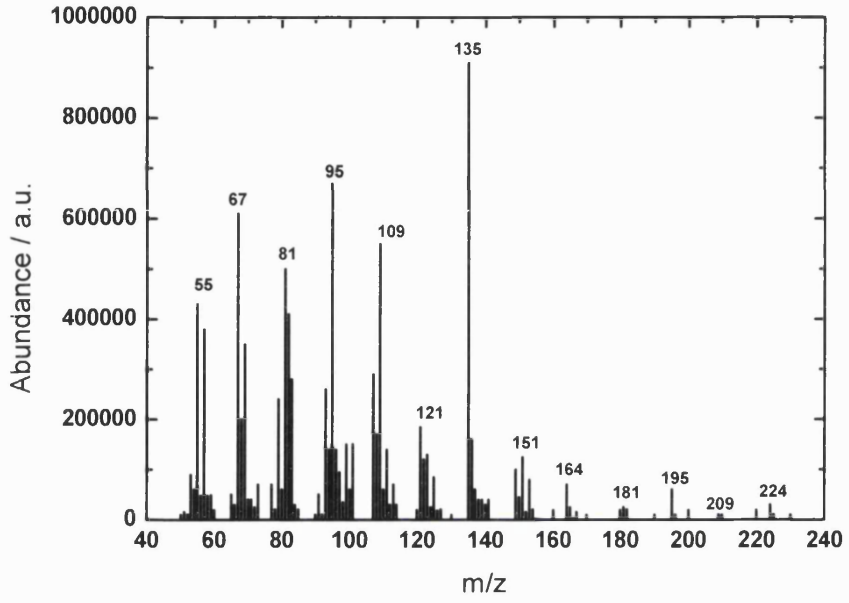

Figure I.19: Mass-spectrum of a product of the telomerization of 1,3-hexadiene with propanol.

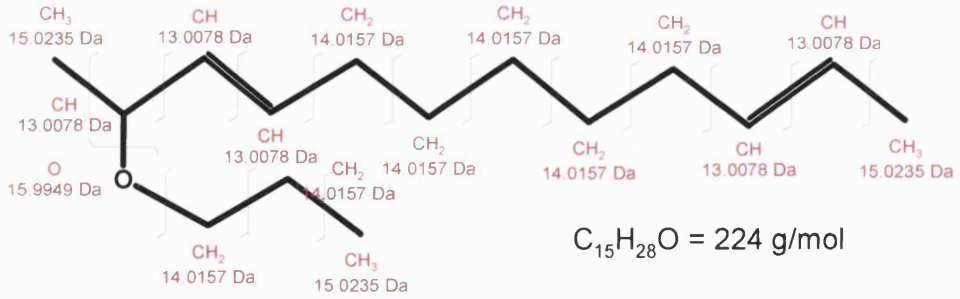

Figure I.20: Telomerization of 1,3-hexadiene with propanol product and its mas-spec fragmentations.

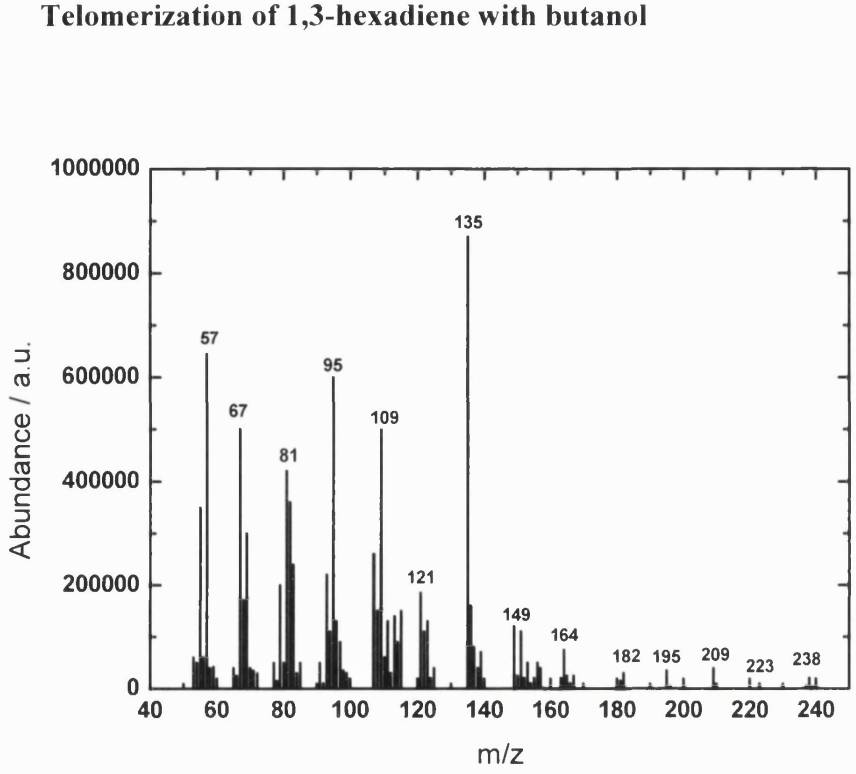

Figure I.21: Mass-spectrum of a product of the telomerization of 1,3-hexadiene with butanol.

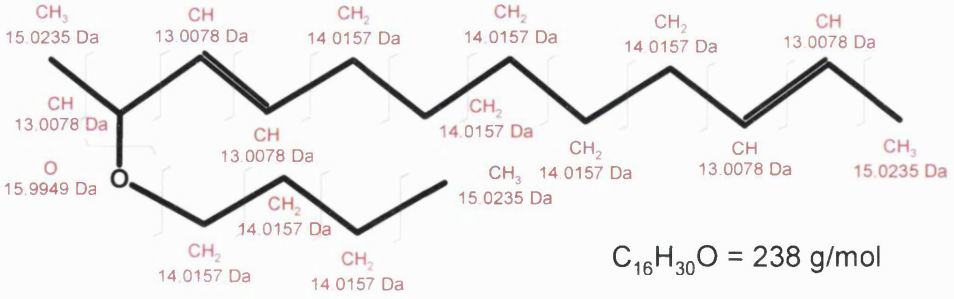

Figure I.22: Telomerization of 1,3-hexadiene with butanol product and its mas-spec fragmentations.

Appendix II

ERROR ANALYSIS

II.1 INTRODUCTION

For evaluation of the accuracy of the experimental data obtained, the experimental errors were estimated using the standard error propagation shown in Equation (II.1).

$$for F = f(A,B,C) \quad F = F_0 + \Delta A\left(\frac{\partial A}{\partial f}\right)_{B,C} + \Delta B\left(\frac{\partial B}{\partial f}\right)_{A,C} + \Delta C\left(\frac{\partial C}{\partial f}\right)_{A,B} \qquad \textbf{(II.1)}$$

where A,B and C are variables. Deltas represent the deviation from an exact value which are either the instrumental error or need to be determined from the accuracy of experimental measurements such as in the case of the gas chromatography analyses.

II.2 CALCULATION OF THE ERROR IN GC ANALYSES

Gas chromatographic analyses were carried out using an autoinjector CP-8400 from Varian with a 0.4% RSD. However, higher deviations were observed and the error was calculated doing several continuous analyses of the same sample and calculating the deviation standard according to Equation (II.2).

$$\sigma = \sqrt{\frac{\sum_{i=1}^{N}(X_i - \overline{X_i})^2}{N}} \qquad \textbf{(II.2)}$$

where N is the number of samples, and $\overline{X_i}$ is the average value. The standard deviation of seven consecutive analyses of initial concentrations of 4.3 M and 1 mM is **± 5%**.

II.3 CALCULATION OF ERROR IN METAL LOADING IN SUPPORTS

As it was described in Chapter 3, loading of metals over different supports was carried out by ion-exchange or reaction with a metal salt solution. The remaining solutions were collected and measured by atomic absorption spectroscopy. Metal loading was calculated by the Equation (II.3).

$$\%wt\ metal = \frac{g\ of\ supported\ metal}{g\ of\ support} \cdot 100 \qquad \textbf{(II.3)}$$

The deviation of the weight of support is given by the accuracy of the scale, in this case (± 0.001g). Total weight of supported metal is calculated as the difference between the weight of metal in the initial solution (whose deviation is given by the accuracy of the scale (± 0.00001)) and the weight of metal in the remaining

solution after the synthesis, determined by AAS (whose accuracy is ± 0.1 ppm = ±0.001g.

$$\Delta g\ of\ supported\ metal = \Delta\ Initial\ weight - \Delta\ Final\ weight = 0.00001 + 0.001 \approx 0.001 \quad \textbf{(II.4)}$$

Therefore, the deviation of the metal loading (Equation (II.3) is calculated in Equation (II.5) as ± **0.1%**.

$$\Delta wt\ metal = \Delta g\ of\ supported\ metal \cdot |100| + \Delta g\ of\ support = 0.001 \cdot 100 + 0.001 \approx 0.1\% \quad \textbf{(II.5)}$$

II.4 CALCULATION OF ERROR IN CONVERSION, SELECTIVITY AND TON VALUES

Conversion values in Chapters 4 and 5 are calculated by the Equation (II.6).

$$Conversion\ (\%) = \frac{Final\ moles \cdot 100}{Initial\ moles} \quad \textbf{(II.6)}$$

Initial number of moles was converted in volume using density and molecular weight of the different reactants before being added into the solution using a micropipette whose accuracy is ± 10^{-5} mL. Equation (II.7) calculates the deviation in the case of isoprene (ρ = 0.68 g/mL and M_w = 68.12 g/mol).

$$Initial\ moles = V(mL) \cdot \frac{\rho}{M_w}\left(\frac{mol}{mL}\right) \qquad \Delta\ Initial\ moles = \Delta V \cdot |cte| = 9 \cdot 10^{-8} \quad \textbf{(II.7)}$$

Considering an initial number of moles of 0.03244 (used for isoprene 4.3M), this error supposes only the 0.0003 %. This value is negligible compared to the error

committed by GC analysis in the final number of moles calculations, therefore, according to Equation (II.8), the deviation of conversion values is ± 5%.

$$\begin{aligned} \Delta\, Conversion\ (\%) &= \Delta\, Final\ moles + \Delta\, Inital\ moles \\ &= 5\% + 0.003\% \approx 5\% \end{aligned} \qquad \textbf{(II.8)}$$

Selectivity to a determined product is calculated by the Equation (II.9), deviation of the initial numbers of moles was previously estimated in ± 0.003%. Final moles of any compound are determined by gas chromatography analyses which error has been calculated in ± 5%. Therefore, deviation of selectivity values is **± 5%**.

$$Selectivity\ to\ X\ (\%) = \frac{Final\ moles\ of\ X \cdot 100}{Initial\ moles}$$

$$\begin{aligned} \Delta\, Selectivity\ to\ X\ (\%) &= \Delta\, Final\ moles\ of\ X + \Delta\, Inital\ moles \\ &= 5\% + 0.003\% \approx 5\% \end{aligned} \qquad \textbf{(II.9)}$$

Turn over number (TON) was calculated according to Equation (II.10).

$$TON = \frac{moles\ converted}{moles\ of\ catalyst} \qquad \textbf{(II.10)}$$

Moles converted are calculated as the difference between initial and final number of moles. According to previous calculations, there is an error of ± 5%. In reactions with the highest initial concentration (4.3 M), it supposes ± 0.002 moles.

In homogeneous and commercial catalysts, the deviation of moles of catalyst consists of the accuracy of the scale (± 0.00001 g) multiply by the inverse of the molecular weight. For palladium, rhodium and ruthenium catalysts, the error consists of $\pm\ 9 \cdot 10^{-8}$.

In prepared supported metal catalysts, the deviation is calculated by the Equation (II.11).

$$moles\ of\ catalyst = \%\ metal \cdot weight\ catalyst \cdot \frac{1}{M_w}$$

$$\Delta\ moles\ of\ catalyst = 0.1 \cdot \frac{1}{M_w} + 0.00001 \cdot \frac{1}{M_w} \qquad \textbf{(II.11)}$$

In the case of Pd, Rh and Ru $\Delta\ moles\ of\ catalyst = \pm 9 \cdot 10^{-8}\ moles$

The error committed in the calculation of number of moles of the catalysts is in both cases, homogeneous and heterogeneous, negligible compared to the error in the calculation of the number of moles converted (± 0.002 moles). Therefore, the deviation in the TON values is estimated as ± **0.002**.

$$\Delta\ TON = \Delta\ moles\ converted + \Delta\ moles\ of\ catalyst$$

$$\Delta\ TON_{\text{hom}\,ogeneous} = 0.002 + 9 \cdot 10^{-8} \approx \pm 0.002 \qquad \textbf{(II.12)}$$

$$\Delta\ TON_{heterogeneous} = 0.002 + 9 \cdot 10^{-8} \approx \pm 0.002$$

Appendix III

PUBLISHED PAPERS

Some of the results shown in this thesis have been already published in international journals. Copies of the papers are included in this Appendix. Other papers were in preparation at the time that this thesis was submitted.

Available online at www.sciencedirect.com
ScienceDirect
Journal of Catalysis 245 (2007) 272–278
JOURNAL OF CATALYSIS
www.elsevier.com/locate/jcat

Highly selective Pd/titanate nanotube catalysts for the double-bond migration reaction

Laura Torrente-Murciano [a], Alexei A. Lapkin [a,*], Dmitry V. Bavykin [b], Frank C. Walsh [b], Karen Wilson [c]

[a] *Catalysis and Reaction Engineering Group, Department of Chemical Engineering, University of Bath, Bath BA2 7AY, UK*
[b] *Electrochemical Engineering Group, School of Engineering Sciences, University of Southampton, Highfield, Southampton SO17 1BJ, UK*
[c] *Department of Chemistry, University of York, York YO10 5DD, UK*

Received 9 August 2006; revised 13 October 2006; accepted 17 October 2006

Available online 17 November 2006

Abstract

Pd(II) and Pd(0) catalysts supported onto titanate nanotubes ($H_2Ti_3O_7$) were prepared by an ion-exchange technique. The catalysts are characterised by narrow size distribution of metal nanoparticles on the external surface of the nanotubes. Pd(II) catalysts show high selectivity toward double-bond migration reaction versus hydrogenation in linear olefins. The catalytic activity exhibits a volcano-type dependence on the metal loading, with the maximum activity observed at ca. 8 wt%. The Pd(II) was shown to be rapidly reduced to Pd(0) by appropriate choice of solvent. Prereduced Pd(0) catalysts were found to be less active toward double-bond migration and more selective toward hydrogenation. The DBM reaction was faster in protic solvents, such as methanol or ethanol.

Keywords: Titanate nanotubes; Double-bond migration; Olefin isomerisation

1. Introduction

The double-bond migration (DBM) reaction is known to be catalysed by both liquid and solid state acids and bases, transition metal salts, organometallic complexes of transition metals, as well as supported transition metals, especially Pd, Ru, and Rh. DBM often occurs as an unwanted side reaction of olefins, as in the case of Wacker-type oxidation by the Pd(II)-polyoxometalate catalytic pair [1], or in the hydrogenation of olefins [2–5]. The DBM reaction is also important in synthesis. Examples of synthetically useful DBM reactions include deconjugation of enons [6], transformation of allylic alcohols into carbonyls [7,8], production of higher olefins as part of the SHOP process [9], isomerisation of eugenol [10] and flavonoids [11], and conjugation of linoleic acid [12]. More significantly, a number of tandem or one-pot sequences of reactions involving DBM have been successfully demonstrated and, in the case of hydroformylation of internal olefins, commercialised [13–17].

Among the many examples of DBM catalysis, the most active, selective, and well-researched catalysts are almost exclusively homogeneous transition metal salts and organometallic compounds; examples include $PdCl_2$, $PdCl_2{\cdot}2C_6H_5CN$ [18], $RhCl_3{\cdot}3H_2O$ [19], $Ni[P(OEt)_3]_4$ [20], and $RuClH(CO)(PPh_3)_3$ [21]. Homogeneous catalysis in conventional solvent systems necessarily raises the problem of catalyst recovery. Loss of transition metals into the product stream at the ppm level is becoming prohibitive to commercialisation. This drawback can be overcome in some cases by working in a multiphase system with immiscible solvents, such as the $scCO_2$-ionic liquid couple, or "smart" solvents with controllable solvatation power [22]. However, there is significant interest in developing truly heterogeneous catalytic processes that facilitate catalyst recovery and involve simpler process engineering, leading to cleaner chemical syntheses.

A number of heterogeneous catalysts with double-bond migration activity have been reported. The nontransition metal

* Corresponding author. Fax: +44 1225 385713.
E-mail address: a.lapkin@bath.ac.uk (A.A. Lapkin).

0021-9517/$ – see front matter
doi:10.1016/j.jcat.2006.10.015

catalysts are either solid bases or acids. The earlier literature describes supported alkali metals [23] and a dispersed alkali hydroxide [6] as isomerisation catalysts. The DBM reaction was used to estimate the number of acid sites in the alumina catalyst [24] and to evaluate the activity of magnesium mixed oxide catalysts [25]; it was found that the DBM reaction was catalysed by strong Brønsted sites in some zeolites [26,27]. Silylated large-pore acidic zeolites were reported to be more selective toward double-bond migration versus dimerisation [9], and Keggin-type polyoxometalate salts were found to be active in the gas-phase DBM reaction [28]. More recently, hydrotalcites were found to be efficient in synthetic applications of the DBM reaction to produce high-value speciality molecules [10,29].

In the case of transition metal catalysts, including important reactions of hydrogenation of vegetable oils [5] and enantioselective reactions promoted by cinchona modifiers [2], DBM is often cited as an undesirable side reaction in hydrogenation [3,30,31]. There are also few reports of synthetically important DBM reactions. Rhodium supported on alumina or carbon catalysts were shown to selectively steer DBM toward a more stable higher substituted unsaturated carbon position in quinine and quinidine, whereas a commercial Pd(0)/C catalyst was inactive [32]. In a series of papers. Murzin et al. reported conjugation of linoleic acid catalysed by supported transition metals in work aimed at producing two specific isomers known for their health effects [12,33,34]. Supported ruthenium catalysts were found to be most active, stable, and selective [35].

Recently, we have reported preparation of Au, Pt, Ru, Ni, and Pd supported on a novel structured mesoporous material: multilayered titanate nanotubes [36]. For Ru, Pt, and Pd, the ion-exchange mechanism of deposition resulted in the formation of small (1.4–5 nm) metal nanoparticles with a narrow size distribution over a broad range of metal loadings (up to 10 wt%). In the case of Ru(III)/titanate catalyst, this resulted in the independence of catalyst activity (expressed as turnover frequency) on the metal loading, observed in the reaction of liquid-phase selective oxidation of alcohols [37]. It is interesting to investigate the activity of Pd/titanate nanotube catalysts in the DBM reaction, because of this reaction's sensitivity to the nature of the active sites. In most previous studies of heterogeneous Pd catalysts of DBM reaction, the metal deposited from a salt solution was reduced by hydrogen or formic acid before catalytic tests, generating Pd(0) catalytic species. It was also shown that unreduced, supported Pd catalysts exhibit higher selectivity toward double-bond migration than reduced catalysts, which tend to be more selective toward hydrogenation [38].

It is known that interaction with reducible supports, such as TiO_2, may promote generation of ionic metal species, which can be either beneficial or detrimental to catalytic activity, the so-called SMSI effect [39]. The nature of the titanate support and the ion-exchange preparation mechanism may allow the stabilisation of the ionic metal species and could give rise to high selectivity toward the DBM reaction. There is only one report in the open literature of a Pd/titanate nanotubes catalyst, prepared by reduction of $PdCl_2$ by glycol [40], that was found to be very active for the electrooxidation of methanol. This paper reports recent data on the selective double-bond migration reaction promoted by in situ generated active species of the mixed Pd(II)/Pd(0) catalyst supported on the external surface of ion-exchangeable, titanate nanotubes.

2. Experimental

2.1. Catalyst preparation and characterisation

The titanate nanotubes were prepared by a hydrothermal method described elsewhere [41]. In a typical synthesis, 20 g of TiO_2 (Fisher Chemicals) was added to 300 mL of 10 M NaOH solution and heated in an autoclave for 20 h at 413 K. After synthesis, the titanate nanotubes were washed several times with demineralised water. The powder was repeatedly washed with demineralised water and 0.1 M H_2SO_4 until the pH of the wash was approximately 7. The samples were dried overnight at 393 K.

Palladium(II) was deposited by ion exchange from aqueous palladium chloride solutions of different concentrations. HCl was added to palladium chloride solutions to avoid precipitation of palladium black. The initial pH of the solution depended on the salt and HCl concentration. For example, in the case of the 8.86 wt% catalyst, the initial pH of salt-HCl solution was 1.9; the final pH was about 4. Titanate powder was added to the solution under vigorous stirring and left at ambient temperature for 2 h. After ion exchange, the catalyst colour changed from white to orange-brown, depending on the palladium concentration. Samples were filtered and washed with the minimum quantity of demineralised water. The remaining solutions were analyzed by atomic absorption spectroscopy (Perkin Elmer) to determine the quantity of deposited palladium. Some catalysts were left in the "as prepared" condition, and others were reduced at room temperature by reaction with aqueous $NaBH_4$. After preparation, all catalysts were dried at 393 K.

XPS measurements were performed using a Kratos Axis HSi instrument equipped with a Mg$K\alpha$ X-ray source and charge neutraliser. Spectra were acquired using a pass energy of 20 eV with an X-ray power of 169 W. Spectra were energy-referenced using valence band and adventitious carbon, whereas quantification and deconvolution was performed using CASA-XPS version 2.3.9 software. TEM images were obtained using JEOL 3010 electron microscope. The solid power samples were deposited on a perforated copper grid coated with gold. XRD spectra were recorded using a Bruker AXS D8 Discoverer X-ray diffractometer, with CuK_α radiation $\lambda = 0.154$ nm and a graphite monochromator, in the 2θ range of 5°–75°.

2.2. Catalytic tests and materials

The performance of Pd(II) and Pd(0) supported onto titanate nanotubes catalysts was tested in the reaction of isomerisation of allylbenzene (**I**). This is a simple reaction with a narrow product distribution. The double-bond migration produces *trans*-phenyl propene (**II**) as the desired product (the *cis*-isomer is <5% in equilibrium, and its formation is unfavourable), the

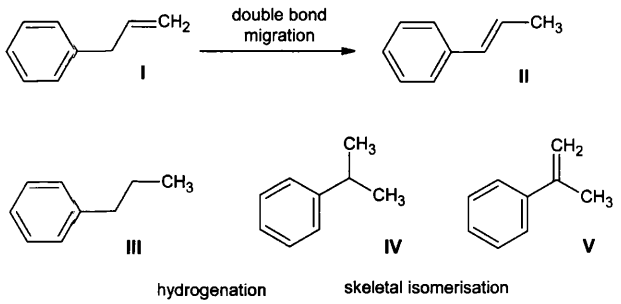

Fig. 1. Potential products (II–V) of reaction of allylbenzene (I) in the presence of an isomerisation catalyst.

skeletal isomerisation produces α-methyl styrene (V), and hydrogenation produces propylbenzene (III) and cumene (IV) (see Fig. 1).

Allylbenzene, *trans*-phenyl propene, and propylbenzene (99% purity), along with methanol, ethanol, *N*-methylpyrrolidone (NMP), and *n*-hexane, were obtained from Sigma-Aldrich. Reactions were performed in a 100-mL, three-necked glass flask under reflux. The initial concentration of allylbenzene was 0.002 M in most experiments. In a typical experiment, solvent and reactants were preheated to reaction temperature (348 K in the case of ethanol, and 333 K with methanol, *n*-hexane, and NMP). Once temperature was stabilised, the reaction was initiated by adding 200 mg of a catalyst. Samples (1 mL) were periodically withdrawn from the reactor. These samples were filtered with 0.2 μm nylon filters and analyzed by gas chromatography (Varian 3800) using a capillary column (Alltech, EC-WAX) and a flame ionization detector (FID). The catalysts were recovered after reaction by filtration for XPS analysis. The material balance was closed in all reactions to within ±10%, and the accuracy of determination of concentrations was better than ±6%. Turnover frequency (TOF) was calculated per unit amount (mol) of Pd, disregarding the oxidation state and the mean metal particle surface area.

3. Results and discussion

3.1. Preparation and characterisation of catalysts and titanate nanotubes

Their high ion-exchange capacity and open pore mesoporous structure makes titanate nanotubes good supports for metal nanoparticles [36]. The powder XRD pattern of the nanotubes, shown in Fig. 2, corresponds well with the reflections of a trititanate $H_2Ti_3O_7$, which is believed to be the most likely structure of the nanotubes [36]. This confirms that the starting material is the same as that used in the study of a supported Ru(III) catalyst [42] and that the nanotubes had not been significantly affected by rapid washing with sulfuric acid.

The isotherm of adsorption of palladium onto titanate nanotubes was determined at room temperature by measuring the initial and equilibrium palladium concentrations in the stock solutions (Fig. 3). The ion-exchange deposition method results in high loadings (up to 10.1 wt%) of palladium metal nanoparticles supported on the surface of the nanotubes. This also

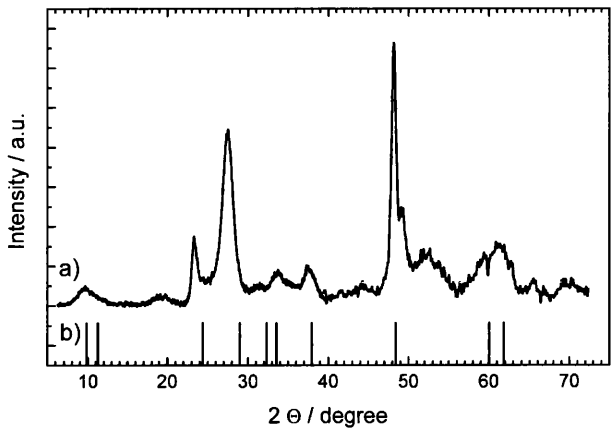

Fig. 2. XRD pattern of titanate nanotubes: (a) 'as prepared' powder, (b) reflections of the trititanate [42].

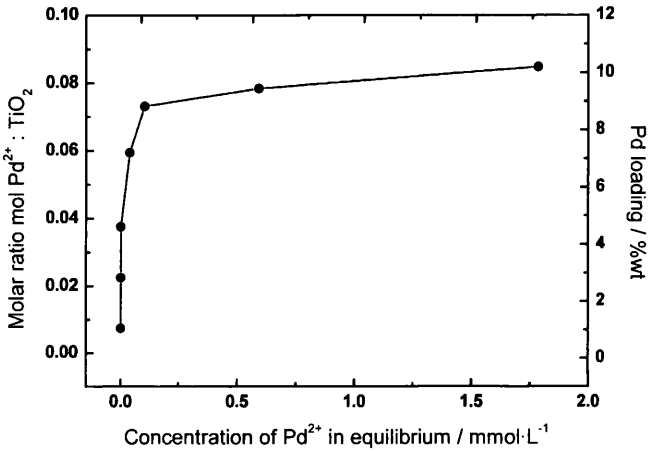

Fig. 3. Isotherm for adsorption of palladium from an aqueous $PdCl_2$ solution onto titanate nanotubes at 298 K.

indicates the high degree of palladium proton exchange; for example, the reaction of Pd(II) with protons in the titanate nanotubes from a 2 mM solution of $PdCl_2$ results in a Pd^{2+}/Ti ratio of 0.08, whereas a maximum value 0.33 would correspond to $PdTi_3O_7$. In other words, almost 25% of all protons in the titanate nanotubes can be replaced by Pd(II) from relatively dilute solution of a salt. The isotherm of adsorption is characterised by a very sharp increase in metal loading with a small increase in the concentration of the stock solution; nearly quantitative sorption of Pd(II) results in negligible residual equilibrium concentration in solution, as shown in Fig. 3. Such a small equilibrium concentration of Pd(II) in water suspension of palladium-exchanged titanate nanotubes should result in a negligible rate of palladium leaching from the catalysts.

The TEM images of titanate nanotubes decorated with palladium nanoparticles for various metal loadings are shown in Fig. 4. The distribution of Pd particles for the 4.75 wt% sample is not uniform; areas of nanotubes with a low density of Pd particles are accompanied by areas with a much higher density. The deposition of metal particles is more uniform for the samples with 6.97 and 8.86 wt% Pd loading. However, the size and shape of metal particles are very similar in all metal loadings

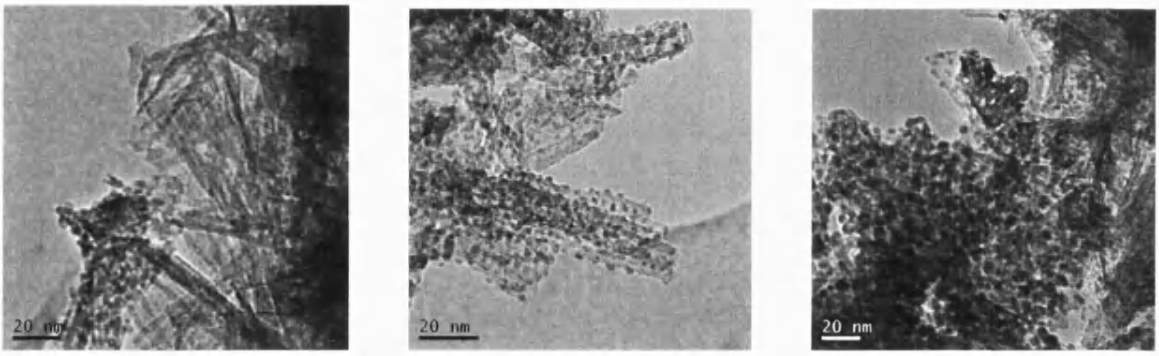

Fig. 4. TEM images of as 'prepared' Pd(II)/titanate nanotubes catalysts: (a) 4.75 wt% Pd, (b) 6.97 wt% Pd, (c) 8.86 wt% Pd.

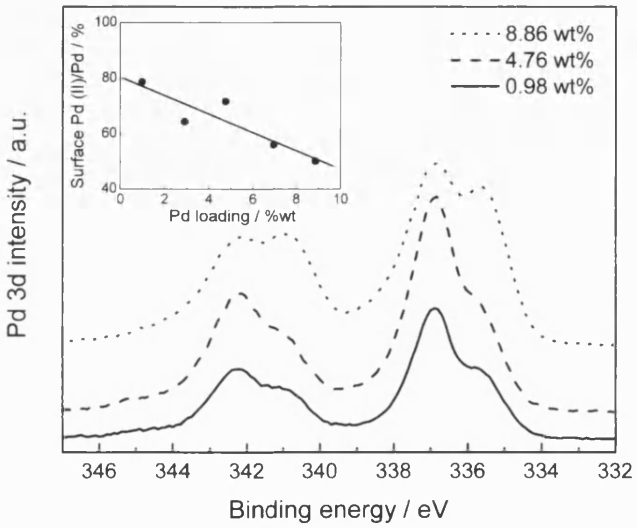

Fig. 5. XPS spectra of 'as prepared' Pd(II)/titanate nanotubes catalyst having different Pd loadings.

tested, with particle sizes of 1.9–4.8 nm and a slightly flattened, spheroidal metal particle shape. A similar, nonuniform deposition has also been found in the case of Pt/titanate nanotubes catalysts [36]. The nonuniform deposition of Pd at low metal loadings may be due to nonuniformity of the nanotube sample; the parts of a sample with higher surface energy react first, leaving the remaining nanotubes bare. However, it is also feasible that nonuniformity in metal deposition may be due to the ion-exchange method used; that is, in very fast ion exchange, the addition of dry titanate powder to the salt solution results in significant metal deposition onto the first portion of the sample that reaches the liquid phase. This is quite feasible; monitoring of pH during ion exchange has shown that 95% of pH change occurs in the first 8 min of reaction. Under different preparation conditions, such as vigorous stirring and slow addition of diluted metal salt solution (or simultaneous addition of metal salt and the nanotube powder/dispersion), the uniformity could be improved through reduction in the external mass transfer limitation. This is currently under investigation.

Fig. 5 shows the Pd 3d XP spectra for the series of Pd/titanate nanotubes samples with 0.98–8.86 wt% loading. The spectra can be deconvoluted into 2 components with Pd $3d_{5/2}$ binding energies of 337.1 and 335.5 eV, which are consistent with Pd(II) and Pd(0), respectively. Fig. 5, inset, shows that the percentage of the Pd(II) component decreases with the bulk Pd content, which is consistent with the Pd clusters becoming more metallic at higher loadings. Quantitative analysis of the XP spectra revealed that the surface Pd loadings for the series of catalysts were in the range of 18–42 wt%, somewhat higher than the bulk Pd content. Such observations are consistent with attenuation of the underlying Ti 2p signal occurring through exclusive coating of the external surface of the nanotubes with Pd, which is in accordance with the observations from TEM.

3.2. Catalytic results

Catalytic tests were performed with both prereduced catalysts and as-prepared catalysts assumed to contain a significant proportion of Pd(II) species, as confirmed by XPS. Reactions performed at 323 K showed no conversion; the following reactions were carried out at 348 K. Typical reaction profiles obtained with Pd(II)/titanate nanotubes and Pd(0)/titanate nanotubes catalysts are shown in Fig. 6. In all reactions with the Pd(II)/titanate catalysts, the main reaction was the double-bond migration to trans-phenyl propene. Dimerisation (based on the retention time, the unidentified product shown in Fig. 6 was assumed to be a dimer) and hydrogenation products were also formed in much smaller concentrations. Reaction proceeded without induction time until a ca. maximum 80% yield of the main desired product (Fig. 6a) was achieved and no skeletal isomers were found. Both the rate of reaction and selectivity were considerably lower for the prereduced Pd(0)/titanate catalysts (Fig. 6b). This suggests that the active species responsible for the double-bond migration reaction are not Pd(0), or else the catalyst could be poisoned by impurities of sodium and boron from a $NaBH_4$ reagent.

Varying the initial concentration of reactant (allylbenzene) between 0.001 and 0.01 M resulted in different conversions and selectivities (see Table 1). In all cases, a high selectivity of around 90% of the double-bond migration product was obtained at high conversions. Lower selectivity was observed in reaction with the lowest initial reactant concentration and the highest catalyst/reactant ratio (Fig. 7). In this case, almost 100% con-

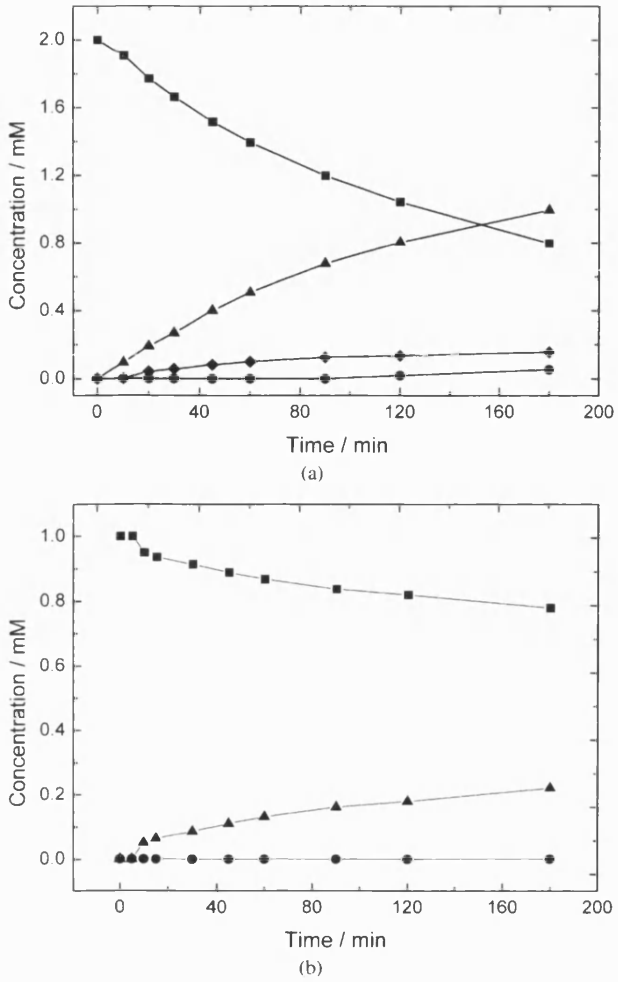

Fig. 6. Isomerisation reaction profiles in MeOH at 333 K. (a) Using a 6.97 wt% Pd(II)/titanate nanotubes. (b) Using a 7.33 wt% Pd(0)/titanate nanotubes prereduced in an aqueous solution of $NaBH_4$. (■) Allylbenzene, (▲) *trans*-phenyl propene, (●) propylbenzene and (◆) unidentified.

Table 1
Conversions and selectivities obtained with different reactant concentrations using 6.97 wt% Pd(II)/titanate nanotubes catalyst. Reaction conditions: allylbenzene reactant in ethanol solvent at 348 K

Initial conc. (mol L^{-1})	Conversion (%)		Selectivity (%)	TOF @ 30 min (h^{-1})	Initial rate (10^{-6} mol s^{-1} g^{-1})
	At 30 min	At 3 h			
0.001	68	100	69	1.0	2.7
0.002	74	96	93	2.3	5.9
0.005	13	33	86	1.1	2.8
0.01	5	12	86	0.8	2.0

version of allylbenzene was achieved in 2 h of reaction time. The considerable extent of hydrogenation reaction decreased the selectivity. The concentration versus time profile of *trans*-phenyl propene suggests a consecutive reaction mechanism; the decreased main product concentration appeared to coincide with an increase rate of hydrogenation byproduct formation. Data showing the dependence of selectivity on conversion (see below) suggest that double-bond migration and hydrogenation are parallel mechanisms and that the apparent acceleration of

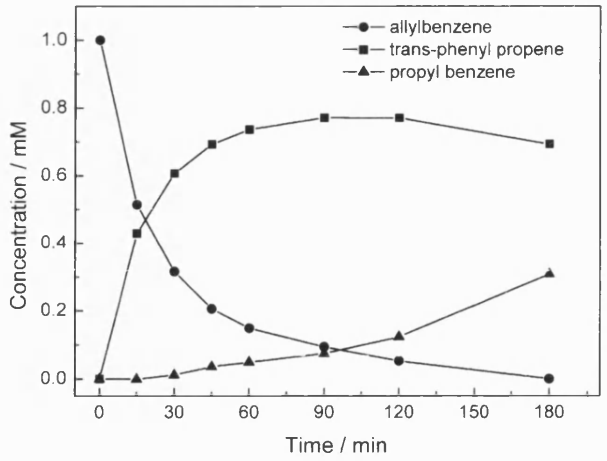

Fig. 7. Reaction profile for an initial allylbenzene reactant concentration of 0.001 M using a 6.97 wt% Pd(II)/titanate nanotubes catalyst, in ethanol at 348 K.

Table 2
Activity and selectivity data on Pd(II)/titanate nanotubes for isomerisation reaction. Reaction conditions: initial concentration of allylbenzene 0.002 M, in ethanol at 348 K

Pd (wt%)	Conversion (%)		Selectivity (%)	TOF @ 30 min (h^{-1})	Initial rate (10^{-6} mol s^{-1} g^{-1})
	At 30 min	At 3 h			
2.90	28	68	77	2.2	5.7
6.97	74	96	93	2.3	5.9
8.86	77	98	86	1.8	4.8
10.13	61	86	88	1.3	3.3

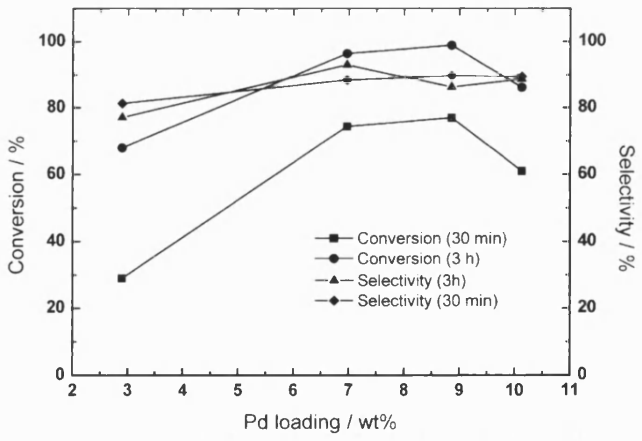

Fig. 8. Conversion and selectivity at different loadings of palladium on titanate nanotubes. Reaction conditions: initial concentration of allylbenzene reactant 0.001 M, in ethanol at 348 K.

the hydrogenation reaction relates to the generation of active catalytic sites for hydrogenation during the course of reaction.

The influence of metal loading on activity and selectivity is shown in Table 2. The conversion as a function of Pd(II) loading follows a typical volcano plot, as shown in Fig. 8, with the maximum at ca. 8–9 wt% Pd. Selectivity was found to be a weak function of metal loading and varied between 80 and 90%. This can be explained by the similar particle sizes of the metal ob-

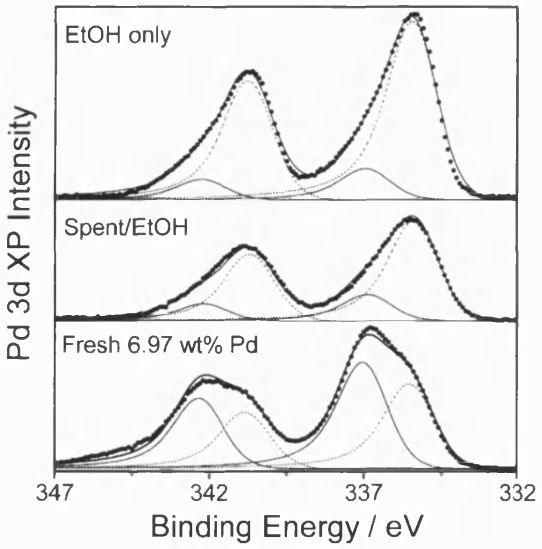

Fig. 9. XPS analysis of Pd(II)/titanate nanotubes catalysts with a 6.97 wt% Pd loading: equilibrated in ethanol: under reaction conditions (top), after reaction (middle) and fresh 'as prepared' catalyst (bottom).

served on TEM for catalysts with 5–9 wt% metal loading (see Fig. 4) and also corresponds well with the hypothesis of parallel hydrogenation and isomerisation reactions.

In all reactions, the orange-brown catalysts became completely black within the first 5 min. This colour change was due to the reduction of Pd(II) into Pd(0) as confirmed by XPS. XPS analysis of the fresh catalyst after a blank reaction (using ethanol as solvent) and after the double-bond migration reactions were performed to determine the oxidation state of palladium in all cases. Fig. 9 shows the Pd 3d region, revealing a mixture of Pd(II) and Pd(0) in the fresh catalysts, as indicated by the Pd $3d_{5/2}$ components at 337.1 and 335.5 eV, respectively. The initial catalyst started off with ~56% of the Pd present as Pd(II); however, the Pd(II) component decreased to 12.5% after exposure to EtOH and to 18.3% after the isomerisation reaction. The corresponding increase in the relative intensity of 335.5 was attributed to Pd(0), indicating that catalyst reduction occurred.

Comparing our results on catalyst activity and selectivity with the literature data is difficult. The reported initial overall rate and TOF of Pd(0)/C in the isomerisation of linoleic acid are approximately 1.7×10^{-5} mol s^{-1} g^{-1} and 2.6 h^{-1}, respectively [35], slightly higher than the values found in this study. But the isomerisation of linoleic acid and allylbenzene are very different reactions, and these results do not permit direct comparison of the catalysts. Gas-phase isomerisation of allylbenzene over mixed-oxide base catalysts [43] was reported in units that do not allow comparison.

3.3. Influence of solvent

Different solvents were evaluated for the double-bond migration reaction (Table 3). For the same palladium loading on titanate nanotubes (6.97 wt%), a high conversion was obtained when an alcohol was used as solvent (ethanol or methanol),

Table 3
Influence of the solvent on the activity and selectivity of 6.97 wt% Pd(II)/titanate nanotubes catalyst for isomerisation of allylbenzene with an initial reactant concentration of 0.002 M

Solvent	Temperature (K)	Conversion (%)		Selectivity (%)
		At 30 min	At 3 h	
Ethanol	350	74	96	93
MeOH	333	16	60	82
MeOH:EtOH	333	20	49	85
NMP	350	0	0	0
Hexane	333	3	16	100

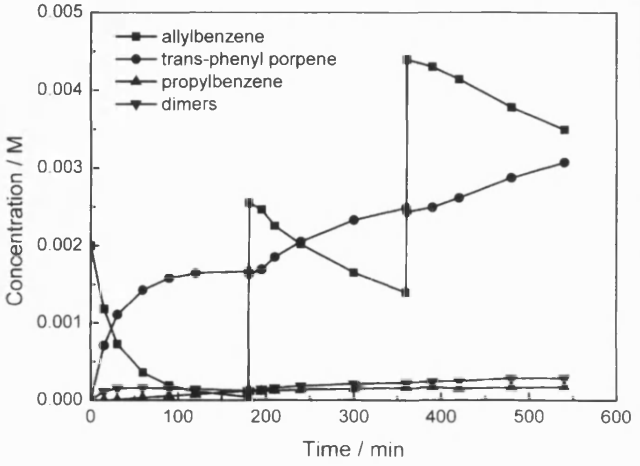

Fig. 10. Concentration profiles in three consecutive runs. Reaction conditions: 0.2 g of 10.1 wt% Pd(II)/titanate nanotubes catalyst; initial concentration of allylbenzene 0.002 M, in ethanol at 350 K.

with a higher value in the case of ethanol. When nonpolar solvents, *n*-hexane and NPM, were used, much lower conversions were obtained than in the case of the protic solvents or even null.

The solvent is clearly important, with ethanol and methanol promoting rapid reduction of Pd(II), as evidenced by the colour changes in the catalyst samples and detected by XPS (see Fig. 9). The change in catalyst colour occurred much more slowly when *n*-hexane or NPM was used than when alcohols were used. In the case of reduced metal catalysts, the effects of solvent have been attributed to the competitive sorption of solvent molecules on the active metal [2,44], with ethanol considered a special case. In Pd(II)/titanate nanotube catalysts, the role of the solvent is different, however. Clearly, alcohols as solvents promote the main reaction and at the same time result in the fastest reduction of Pd(II) species on the support.

3.4. Catalyst stability

No leaching of Pd was detected through atomic absorption measurements of the filtered reaction solutions. Catalyst stability and reusability were tested by adding fresh reactant to the reaction mixture after completion of reaction; the reaction profiles are shown in Fig. 10. Taking into account the dilution factor, the initial rates in the three consecutive reactions were 4.8×10^{-6}, 1.3×10^{-6}, and 7.2×10^{-7} mol s^{-1} g^{-1}. The apparent decrease

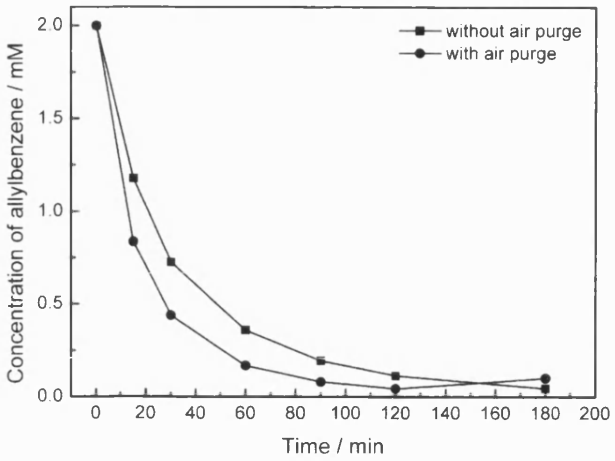

Fig. 11. Reactant concentration profiles with and without bubbling air into the reaction medium. Reaction conditions: catalyst: 0.2 g of 10.1 wt% Pd(II)/titanate nanotubes catalyst; initial concentration of allylbenzene 0.002 M, in ethanol at 350 K.

in the rate of reaction is probably due to the irreversible reduction of Pd(II) into the less active Pd(0) species. Direct oxidation of Pd(0) by oxygen has been suggested as a method of in-situ catalyst regeneration. The results obtained with and without air purge during the reaction are shown in Fig. 11. A higher initial reaction rate was found when the reaction was performed in the presence of air likely due to a temporary stabilisation of the active species by oxygen. Consecutive addition of fresh reagent after completion of the reaction resulted in the same reaction rate as seen in the absence of oxygen.

4. Conclusion

Catalysts containing Pd(II) supported on multilayered titanate nanotubes with a high loading of metal particles of small size and a narrow particle distribution were synthesised. After reduction in situ by methanol or ethanol solvents, the Pd(II)/titanate nanotube catalysts had high activity and very high selectivity toward double-bond migration during the isomerisation of allylbenzene. Reaction in the presence of oxygen promoted stability of the active catalyst. Other solvents, such as *n*-hexane and NMP, showed very low or zero activity. Ex situ reduction of the catalysts resulted in a loss of selectivity and activity toward isomerisation.

Acknowledgment

EPSRC funding of experimental studies at the University of Bath (grant GR/S86112/01) is gratefully acknowledged.

References

[1] A. Lambert, E.G. Derouane, I.V. Kozhevnikov, J. Catal. 211 (2002) 445–450.
[2] K. Borzeky, T. Mallat, A. Baiker, Catal. Lett. 59 (1999) 95–97.
[3] R.J. Grau, P.D. Zgolicz, C. Gutierrez, H.A. Taher, J. Mol. Catal. A Chem. 148 (1999) 203–214.
[4] G.V. Smith, J.A. Roth, D.S. Desai, J.L. Kosco, J. Catal. 30 (1973) 79–85.
[5] M.M.P. Zieverink, M.T. Kreutzer, F. Kapteijn, J.A. Moulijn, Ind. Eng. Chem. Res. 44 (2005) 9668–9675.
[6] E. D'Incan, P. Viout, Tetrahedron 40 (1984) 3421–3424.
[7] R. Uma, C. Crévisy, R. Grée, Chem. Rev. 103 (2003) 27–51.
[8] R.C. van der Drift, E. Bouwman, E. Drent, J. Organometallic Chem. 650 (2002) 1–24.
[9] D.M. Hamilton, US4727203 (1988), S.O. Company, USA.
[10] D. Kishore, S. Kannan, Appl. Catal. A Gen. 270 (2004) 227–235.
[11] Y. Hoshino, N. Takeno, Bull. Chem. Soc. Jpn. 67 (1994) 2873–2875.
[12] A. Bernas, P. Laukkanen, N. Kumar, P. Mäki-Arvela, J. Väyrynen, E. Laine, B. Holmbom, T. Salmi, D.Y. Murzin, J. Catal. 210 (2002) 354–366.
[13] H. Klein, R. Jackstell, M. Beller, Chem. Commun. (2005) 2283–2285.
[14] A. Seayad, M. Ahmed, H. Klein, R. Jackstell, T. Gross, M. Beller, Science 297 (2002) 1676–1678.
[15] B. Schmidt, Eur. J. Org. Chem. (2003) 816–819.
[16] A.E. Sutton, B.A. Siegal, D.F. Finnegan, M.L. Snapper, J. Am. Chem. Soc. 124 (2002) 13390–13391.
[17] G. Dyker, H. Markwitz, Synthesis (1998) 1750–1754.
[18] G. Bond, I. Hellier, J. Catal. 4 (1965) 1–5.
[19] F.J. Harrod, J. Chalk, J. Am. Chem. Soc. 86 (1963) 1776–1779.
[20] B. Corain, G. Puosi, J. Catal. 30 (1973) 403–408.
[21] H. Wakamatsu, M. Nishida, N. Adachi, M. Mori, J. Org. Chem. 65 (2000) 3966–3970.
[22] B. Cornils, W.A. Herrmann, I.T. Horváth, W. Leitner, S. Mecking, H. Olivier-Boubigou, D. Vogt, Multiphase Homogeneous Catalysis, Wiley–VCH, New York, 2005.
[23] J.K. Hambling, UK Patent 1,007,325 (1962).
[24] C.S. John, A. Tada, L.V.F. Kennedy, J. Chem. Soc. Faraday Trans. I 74 (1978) 498–505.
[25] M.A. Aramendía, V. Borau, C. Jiménez, A. Marinas, J.R. Ruiz, F.J. Urbano, J. Mol. Catal. A Chem. 218 (2004) 81–90.
[26] J.N. Kondo, K. Domen, F. Wakabayashi, J. Phys. Chem. 101 (1997) 5477–5479.
[27] J.N. Kondo, K. Domen, F. Wakabayashi, Microporous Mesoporous Matter. 21 (1998) 429–437.
[28] M.A. Parent, J.B. Moffat, J. Catal. 177 (1998) 335–342.
[29] D. Kishore, S. Kannan, J. Mol. Catal. A Chem. 223 (2004) 225–230.
[30] G.V. Smith, J.A. Roth, D.S. Desai, J.L. Kosco, J. Catal. 30 (1973) 79–85.
[31] P.V.D. Plank, J. Catal. 26 (1972) 42–50.
[32] D.E. Portlock, D. Naskar, L. West, W.L. Seibel, T. Gu, H.J. Krauss, X.S. Peng, P.M. Dybas, E.G. Soyke, S.B. Ashton, J. Burton, Tetrahedron Lett. 44 (2003) 5365–5368.
[33] A. Bernas, N. Kumar, P. Mäki-Arvela, N.V. Kul'kova, B. Holmbom, T. Salmi, D.Y. Murzin, Appl. Catal. A Gen. 245 (2003) 257–275.
[34] A. Bernas, N. Kumar, P. Laukkanen, V. Väyrynen, T. Salmi, D.Y. Murzin, Appl. Catal. A Gen. 267 (2004) 121–133.
[35] A. Bernas, N. Kumar, P. Mäki-Arvela, B. Holmbom, T. Salmi, D.Y. Murzin, Org. Proc. Res. Dev. 8 (2004) 341–352.
[36] D.V. Bavykin, A.A. Lapkin, P.K. Plucinski, L. Torrente-Murciano, J.M. Friedrich, F.C. Walsh, Top. Catal. 39 (2006); doi:10.1007/s11244-006-0051-4.
[37] D.V. Bavykin, A.A. Lapkin, P.K. Plucinski, J.M. Friedrich, F.C. Walsh, J. Catal. 235 (2005) 10–17.
[38] A. Bernas, N. Kumar, P. Mäki-Arvela, N.V. Kul'kova, B. Holmbom, T. Salmi, D.Y. Murzin, Appl. Catal. A Gen. 245 (2005) 257–275.
[39] M. Bowker, P. Stone, P. Morrall, R. Smith, R. Bennett, N. Perkins, R. Kvon, C. Pang, E. Fourre, M. Hall, J. Catal. 234 (2005) 172–181.
[40] M. Wang, D.-J. Guo, H.-L. Li, J. Solid State Chem. 178 (2005) 1996–2000.
[41] D.V. Bavykin, V.N. Parmon, A.A. Lapkin, F.C. Walsh, J. Mater. Chem. 14 (2004) 3370–3377.
[42] D.V. Bavykin, A.A. Lapkin, P.K. Plucinski, J.M. Friedrich, F.C. Walsh, J. Catal. 235 (2005) 10–17.
[43] M.A. Aramendía, V. Borau, C. Jiménez, A. Marinas, J.M. Marinas, F.J. Urbano, J. Catal. 211 (2002) 556–559.
[44] A. Bernas, P. Mäki-Arvela, N. Kumar, B. Holmbom, T. Salmi, D.Y. Murzin, Ind. Eng. Chem. Res. 42 (2005) 718–727.

Topics in Catalysis Vol. 39, Nos. 3–4, October 2006 (© 2006)
DOI: 10.1007/s11244-006-0051-4

Deposition of Pt, Pd, Ru and Au on the surfaces of titanate nanotubes

Dmitry V. Bavykin[a,*], Alexei A. Lapkin[b], Pawel K. Plucinski[b], Laura Torrente-Murciano[b], Jens M. Friedrich[a], and Frank C. Walsh[a]

[a] *Electrochemical Engineering Group, School of Engineering Sciences, University of Southampton, Highfield, Southampton, SO17 1BJ, UK*
[b] *Catalysis and Reaction Engineering Group, Department of Chemical Engineering, University of Bath, Bath, BA2 7AY, UK*

Nanoparticles of different metals (Pt, Pd, Au) or a metal hydroxide (Ru) have been immobilized on the surface of mesoporous titanate nanotubes produced by alkali hydrothermal treatment of TiO_2, and have been characterized by HRTEM. Two different approaches have been utilised for the deposition of metal particles into the internal pores of titanate nanotubes: (*i*) deposition from solution confined inside the nanotubes and (*ii*) blocking the external surface of the nanotubes. A third method, ion-exchange of protons onto metal cations in titanate nanotubes followed by reduction or alkali treatment (in the case of Ru hydroxide), has been used for deposition of metal nano-particles on both the internal and external surfaces of the nanotubes. Nanoparticles of metal or metal hydroxide deposited by the ion-exchange method are characterised by an average size in the range of 1.2–5 nm, and deposits are uniformly distributed on the surface, resulting in a very high loading density. An increase in the amount of deposited metal resulted predominantly in a higher nanoparticle loading density, without growth in the particle size. This was correlated with the retention of high specific catalytic activity of ruthenium hydrated oxide deposited on titanate nanotubes in the reaction of selective oxidation of benzyl alcohol over a wide range (0.6–8.7 wt%) of ruthenium loading. The methods for metallization of titanate nanotubes are critically discussed.

KEY WORDS: multilayered wall titanate nanotubes; incipient wetness; impregnation; titanate nanotubes; mesoporous catalyst supports.

1. Introduction

Nanotubular titanium (IV) oxide materials, produced by alkali hydrothermal treatment [1], are novel and intensively studied materials which possess a unique combination of physico-chemical properties. The characteristics of these materials include: a high ion-exchange capacity for cations of different metals [2,3], open mesoporous morphology, a high specific surface area [4], a wide bandgap semiconductor properties [5], pronounced proton conductivity [6], relatively good stability at elevated temperatures [7] of the alkali metal saturated form of the nanotubes [2]. These multilayered nanomaterials have a well developed lamellar structure corresponding to one of the following crystal structures: $H_2Ti_3O_7$ [8], $H_2Ti_2O_4(OH)_2$ [9], $H_2Ti_4O_9{\cdot}H_2O$ [10] or TiO_2-B [3]. The material shows promise in a variety of applications including hydrogen sensors [11], a substrate for hydrogen sorption [12,13], photocatalysis [14,15], acid catalysis [16] solar cell photosensitising [17], ion-exchange [18] and as a new generation of electrodes for lithium batteries [19,20] as well as for electrocatalysis [21,22].

Titanate nanotubes are of great interest for catalysis since their high cation exchange capacity provides the possibility of achieving a high loading of active catalyst with an even distribution and high dispersion. Besides, the open mesoporous morphology of nanotubes, the high specific surface area and the absence of micropores facilitate transport of reagents to the active sites during the catalytic reaction. The semiconducting properties of titanate nanotubes result in strong electronic interaction between the support and a catalyst, improving catalytic performance in redox reactions. A high proton conductivity provides the possibility of acid based catalysis. The relatively low cost of the titanate nanotubes compared to the TiO_2 nanotubes produced by sol-gel template assisted methods, renders the present materials attractive for technological applications. Although titanate nanotubes demonstrate moderate catalytic activity as acid base catalysts [16,23] there are few demonstrated examples of the successful utilisation of titanate nanotubes as mesoporous catalyst supports for different nanoparticles: CdS decorated titanate nanotubes [24,25] in reaction of photocatalytic oxidation of dyes, Pd/TiO_2 nanotubes catalyst [26] for electro-oxidation of methanol, Pt/TiO_2 nanotubes photocatalyst for generation of H_2 [14], Au/TiO_2 nanotubes catalyst for water-gas shift reaction [27], RuO_2/TiO_2 nanotubes electro-catalyst for reduction of CO_2 [22] and ruthenium (III) hydrated oxide deposited on titanate nanotubes for selective oxidation of alcohols [28].

The nanotubular morphology of titanate could also be exploited in shape-selective catalysis. Deposition of catalysts onto the internal cavities of nanotubes only might provide the possibility of adjusting catalyst selectivity to favour the formation of non-bulky molecules, by adjusting the diameter of the nanotubes.

* To whom correspondence should be addressed.
E-mail: D.Bavykin@soton.ac.uk

1022-5528/06/1000-0151/0

To study this hypothesis it is necessary to develop a method of deposition of catalyst nanoparticles inside the internal cavities of nanotubes. In this paper two different approaches for immobilisation of metal nanoparticles inside the titanate nanotubes, by means of confinement of the solution of metal salts inside the nanotube and by protection of the external surface of nanotubes using bulky surfactant molecules, are presented. The localisation of metal particles was studied by TEM microscopy. Both methods are critically discussed.

2. Experimental details

2.1. Reagents

Titanium dioxide (anatase, TiO_2), sodium hydroxide (NaOH), sulfuric acid (H_2SO_4), hydrochloric acid (HCl), palladium chloride ($PdCl_2$), ruthenium (III) chloride hydrate ($RuCl_3 \cdot nH_2O$), dihydrogen hexachloroplatinate (H_2PtCl_6), hydrogen tetrachloroaurate (III) hydrate ($HAuCl_4 \cdot H_2O$), ethylendiamine (en), diethylentriamine (dien), didodecyl-dimethylammonium chloride (SR142, $(C_{12}H_{25})_2(CH_3)_2NCl$), sodium tetraborohydrate ($NaBH_4$), pure grade were obtained from Aldrich and were used without further purification.

2.2. Preparation of titanate nanotubes

The method of preparation of titanate nanotubes was based on alkali hydrothermal transformation [29]. Twenty grams of titanium dioxide was added to 300 mL of 10 mol dm^{-3} NaOH solution and heated for 22 h at 140 °C. The white, powdery TiO_2 product was thoroughly washed with water, 0.05 mol dm^{-3} H_2SO_4, and distilled water, followed by drying in vacuum at 80 °C.

2.3. Deposition of platinum from solution inside nanotubes

In order to produce 0.5 wt% Pt/TiO_2 nanotubes, 1 g of nanotube titanium dioxide was mixed with 25 mL of water and 0.5 mL of 0.05 mol dm^{-3} (2 wt%) H_2PtCl_6. The mixture was ultrasonically treated for 30 min then slowly evaporated in a rotary vacuum evaporator at 50 °C until almost dry. The yellowish powder was placed into a controlled humidity chamber for 7 days. To adjust the humidity, $MgCl_2$ (P/P_0 = 0.3) salt was used [30]. Reduction of H_2PtCl_6 in titanate nanotubes was carried out in a quartz U-tube with hydrogen at a flow rate of approximately 20 mL min^{-1} at room temperature. On contact with hydrogen, the powder changed from white to grey in colour. Once all of the powder had turned grey, the temperature was increased to remove the residue of HCl and water. The reaction sample was dried in vacuum at 80 °C. In order to prepare samples of different Pt loading, the volume of H_2PtCl_6 used in the initial solution was modified.

2.4. Deposition of gold by blocking the external surface with surfactants

One gram of titanate nanotubes was mixed with 0.5 g of SR142 surfactant and 100 mL water was added. The suspension was ultrasonically treated at 60 °C for 30 min then the powder was filtered and washed with 5 mL of water. To achieve ca. 2 wt% gold loading, the powder was mixed with 50 mL of 2×10^{-3} mol dm^{-3} solution of $[Au(en)_2]Cl_3$, which was prepared by mixing 2 mL of 0.05 mol dm^{-3} $HAuCl_4$ with 100 μL of ethylendiamine in 48 mL of water. When the white titanate nanotube powder was contacted with the yellow solution of gold complex, the powder turned yellow and the solution became white. To achieve equilibrium of ion-exchange the mixture was stirred over 12 h. It was then filtered and washed with 10 mL of water added under vigorous stirring to 20 mL of 0.1 mol dm^{-3} $NaBH_4$ solution. The yellow powder immediately changed to dark violet. The Au/TiO_2 nanotube powder was filtered and washed with copious amounts of water, followed by drying in vacuum at 80 °C. For deposition of different gold loading, the volumes of 0.05 mol dm^{-3} $HAuCl_4$ and ethylendiamine solutions were adjusted.

2.5. Deposition of ruthenium (III) hydrated oxide by ion exchange

The weight of $RuCl_3 \cdot nH_2O$ was varied in the range 25–200 mg; the material was dissolved in 25 mL of water with addition of 100 μL of 37 wt% HCl. 2 g of nanotubular powder was added and the mixture was vigorously stirred for 30 min at 25 °C. During this process the dark brown colour of the solution turned white while the (previously white) TiO_2 turned grey. The obtained powder was filtered and washed with large amounts of demineralised water. The dark powder was placed in a 100 mL beaker and 50 mL water was added. Under vigorous stirring, 1 mol dm^{-3} NaOH was slowly added until the solution reached pH 10. The colour of the powdery products changed in the sequence: light green, dark green, black when the catalyst loading was increased. The solids were filtered, washed with water and dried in vacuum at 80 °C for 2 h.

2.6. Deposition of palladium by ion exchange

One gram of titanate nanotubes was added under stirring to the 250 mL of $PdCl_2$ solution in water. The concentration of $PdCl_2$ solution varied in the range from 5×10^{-5} mol dm^{-3} to 3×10^{-3} mol dm^{-3}. After 2 h of ion-exchange at room temperature, the solids (having a colour which varied from orange to brown, depending on the initial concentration of $PdCl_2$) were filtered, washed with water and dried in vacuum at 120 °C for 12 h. 50 mL of 0.1 mol dm^{-3} $NaBH_4$ solution was added to the powder under vigorous stirring. The colour of the (yellow or brown) powder changed immediately

to grey. After 30 min, the Pd/TiO_2 nanotubular powder was filtered and washed with a large amount of water and dried in vacuum at 80 °C.

2.7. Measurement of the adsorption isotherm of metal

The adsorption isotherms of various metals or metal complexes onto the titanate nanotubes were determined at room temperature (ca. 22 °C) by measuring the concentration of the remaining metals in solution after ion-exchange with powdered titanate nanotubes. The relative amount of adsorbed metal a [mol(M)×mol $(TiO_2)^{-1}$] was determined using the formula:

$$a = \frac{80 \times (C_0 - C) \times V}{m}, \quad (1)$$

where C_0 is the initial concentration of metal salt, C is the concentration of metal salt after adsorption, m is the mass of nanotubes and V is the volume of solution.

The concentration of Ru^{3+} and Pd^{2+} in remaining solutions was analysed using atomic absorption spectrophotometry (Perkin Elmer). Concentrations of $[Au(en)_2]Cl_3$, $[Au(dien)Cl]Cl_2$ and $HAuCl_4$ were determined using a Shimadzu UV-1601 spectrophotometer.

2.8. Characterisation of samples

BET surface area and BJH pore distribution of the TiO_2 samples were calculated from measurements of nitrogen adsorption at −195 °C using a Micromeritics ASAP 2010 instrument. Adsorption of water vapour was measured using an Intelligent Gravimetric Analyzer IGA-001 (Hiden Isochema, UK) having 0.0001 mg sensitivity. 100 mg of titanate nanotube sample was sealed in the reactor equipped with a temperature control unit. The adsorption isotherm was measured at 25 °C using a standard sequence, with a 30 min timeout for each point.

TEM images were obtained using a JEOL 3010-TEM transmission electron microscope. SEM images were obtained with a JEOL 6500 FEG-SEM scanning electron microscope.

The catalytic activity of ruthenium hydrated oxide deposited on titanate nanotubes in the selective oxidation of benzyl alcohol with oxygen was studied in a continuous flow multichannel reactor [31]. The specific catalytic activity (turnover frequency, TOF) of catalyst was normalised to the amount of ruthenium. The reactor has been used in differential mode with conversion less then 10%. This was achieved by dilution of catalyst with pure titanate nanotubes. Details of the experimental arrangement are published elsewhere [28].

3. Results and discussion

There are several well established techniques for the metallization of non-conductive surfaces, including electroless deposition, incipient wetness impregnation, electron beam lithography, vacuum vapour deposition and template assisted deposition [32]. In the case of the present titanate nanotubes, we have selected wet chemical impregnation methods of deposition accompanied by chemical reduction of precious metal salts by gaseous hydrogen or solution of $NaBH_4$. This approach provides a simple and fast method which is capable of producing dispersed, high surface metal deposits suitable for catalytic and electrochemical applications. Our approach has been motivated by the need to decorate nanotube surfaces by active, finely divided metals using an inexpensive technique.

3.1. Method of metal salts solution inside the nanotubes, Pt catalyst

By using the phenomenon of capillary condensation, i.e. stabilization of a liquid phase coexisting with its vapour at relative vapour pressures less than unity by means of spatial confinement, it is possible to selectively fill pores of a certain size with liquid by adjusting its vapour pressure. The maximum diameter of filled pores depends on the relative pressure of water according to the Kelvin equation. In the case of nanotubes, the pore structure of the powdered samples consists of the internal cavities (ca. 4–6 nm diameter) of individual tubes, as well as the pores (ca. 6–12 nm diameter) between the tubes within the secondary aggregates [4]. This was clearly demonstrated by combining ultrasonic treatment with pore-size distribution measurements using nitrogen adsorption technique. In this method of metal deposition it is assumed that during the slow drying of aqueous metal salt solution, impregnated by means of incipient wetness technique, the majority of metal would diffuse into the narrow internal tube cavities where the liquid phase is stabilised by controlling humidity (see figure 1). It is, therefore, necessary to know the vapour pressure of water corresponding to capillary condensation in the internal cavities of the nanotubes and not in the larger pores between the nanotubes. Metal nanoparticles could then be obtained by reduction with gaseous hydrogen without disturbing the liquid phase.

Isotherms of adsorption and desorption of water on titanate nanotubes at 25 °C are shown in figure 2(a). From the desorption curve, using the Halsey formula for water film thickness calculation and taking the water surface tension parameter as 72.9 mN m^{-1}, the pore size distribution for titanate nanotubes was calculated and results are shown in figure 2(b). Numbers above the data points are the corresponding values of relative pressure at which the pores with less of equal size are filled with water. From these data it follows that if pores with radii of less than 3 nm need to be filled, then it is necessary to dry the sample at a relative water pressure of $P/P_0 = 0.59$ (see figure 2(b)). In order to avoid

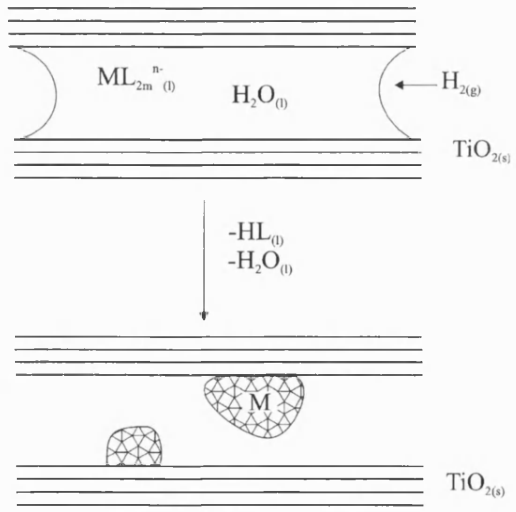

Figure 1. Cartoon illustrating the process of deposition of metals inside the pores of titanate nanotubes by confinement of liquid in a capillary followed by gas phase reduction with hydrogen.

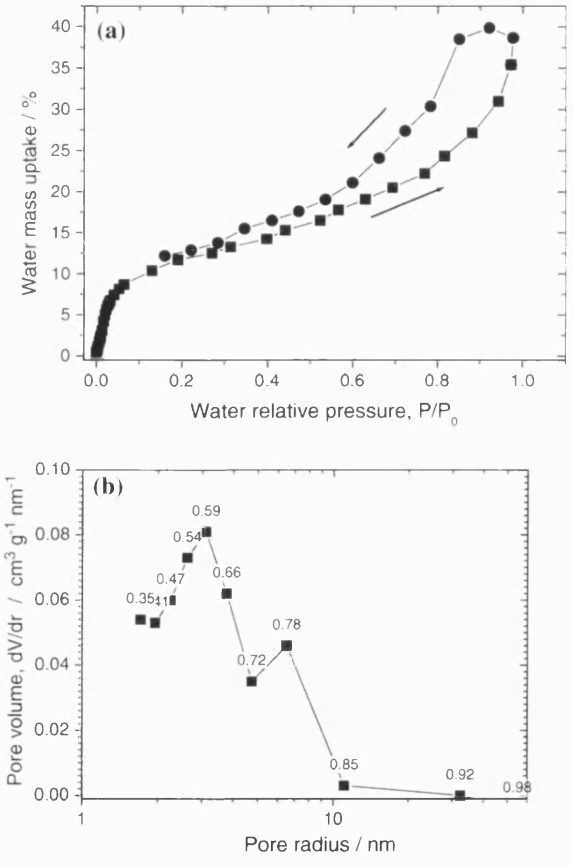

Figure 2. Isotherm of water adsorption (■) and desorption (●) at 25 °C on the surface of titanate nanotubes (a), and pore size distribution calculated from desorption curve (b); numbers in graph (b) correspond to the relative pressure of water, see text.

overlap with external pores, which are usually slightly larger than internal pores [4] a relative pressure of $P/P_0 = 0.3$ was chosen.

Titanate nanotubes in aqueous suspension have a relatively high negative zeta-potential over a wide range of pH, e.g. for pH = 8 the zeta potential is equal to −43 mV [21]. An aqueous solution of hydrogen hexachloroplatinate is dissociated into protons and negatively charged $[PtCl_6]^{2-}$ anions, which are characterised by low adsorption on the surface of negatively charged titanates nanotubes due to the electrostatic repulsion. Platinum (IV) in an aqueous solution of H_2PtCl_6 can easily be reduced to metal platinum by gaseous hydrogen at relatively low temperatures. Thus, this system is appropriate for testing the concept of metal deposition from confined liquids.

For low platinum loadings, incipient wetness impregnation of the powdered titanate nanotubes with H_2PtCl_6 followed by very slow drying at relative pressure $P/P_0 = 0.3$ and consecutive reduction with gaseous hydrogen resulted in a very uneven distribution of platinum. A TEM image of titanate nanotubes with 0.5 wt% deposited Pt nanoparticles is shown in figure 3. One bundle of nanotubes is covered with ca. 2 nm Pt nanoparticles with a very high particle density, whereas part of the surface is bald. Metal nanoparticles are deposited onto the external as well as the internal surfaces of nanotubes. This irregular deposition of Pt nanoparticles may be due to the characteristics of the incipient wetness impregnation method; during drying the front of solution/gas interface is moving through the solid powder and the composition of the liquid phase is continuously varying. This problem is intrinsic to the method of incipient wetness impregnation and might be solved by agitation of the solid powder during drying. This would allow a better distribution of metal within the solid support. On the scale of hundreds of nanometers, however, the distribution of metal remains uneven.

An increase in platinum loading results in the increase in the metal particles size (see figure 3(b)). Metal particles formed inside the cavities of titanate nanotubes have a rod like shape, with the diameter of rods corresponding to the internal diameter of nanotubes. Similar Pt-entrapped titanate nanotubes were recently produced by impregnation of nanotubes with the melt of H_2PtCl_6 at elevated temperatures in the atmosphere of hydrogen [33]. In this case, however, the metal was also deposited unevenly.

3.2. *Method of blocking the external surface of nanotubes, Au catalyst*

In order to avoid the problem of uneven deposition of metal nanoparticles onto the surface of titanate nanotubes, it is important to realise that, in aqueous suspension, the nanotubes have a negative charge and should readily adsorb metals in the cationic form from diluted solutions. This would eliminate the stage of sample drying, which results in the movement of

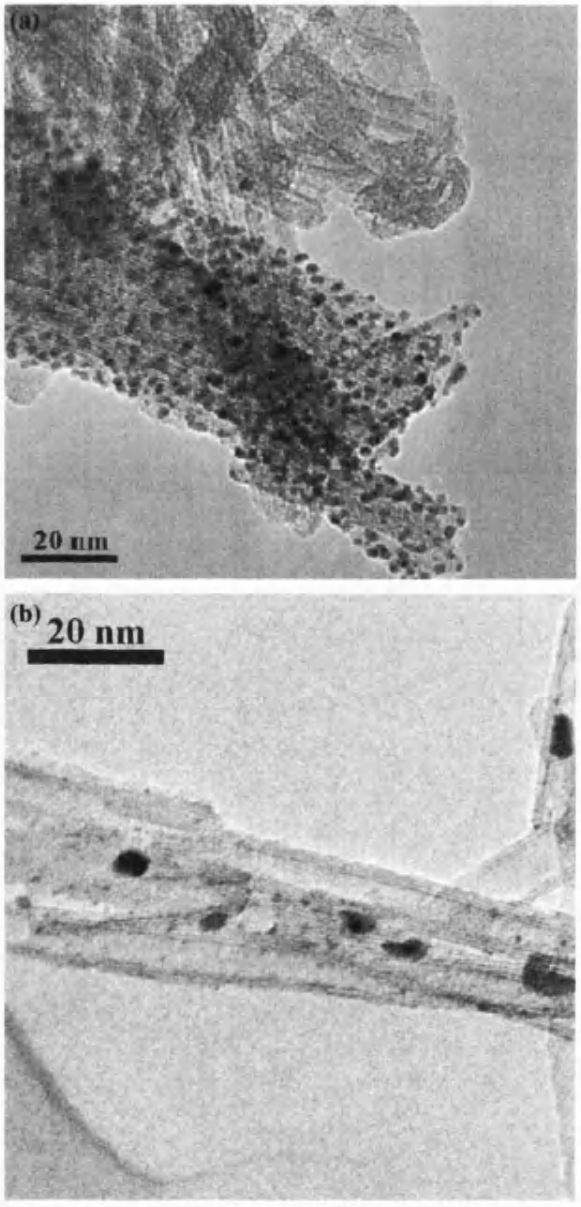

Figure 3. TEM image of platinum nanoparticles deposited into the pores of titanate nanotubes by the method of liquid confinement followed by hydrogen reduction for different platinum loadings: (a) 0.5 wt%, (b) 5 wt%.

gas–liquid interface and high variability of metal concentration along the sample. In this case, slow diffusion of cations from solution to the surface on nanotubes promotes a more uniform distribution of a metal.

In protonated form of layered nanotubular titanic acid protons occupy either side of the wall surface (convex and concave) as well as the interstitial cavities between the layers of the nanotube walls. The approximately 0.72 nm gap between the layers is not accessible to nitrogen gas molecules [4]. Small hydrogen molecules [12] from the gas phase, however, can intercalate between these layers. Protons and cations from aqueous solutions (H^+, Me^{n+}) can easily be exchanged between protons in the nanotube wall according to:

$$x\mathrm{Me}^{n+} + \mathrm{H_2Ti_3O_7} \rightarrow \mathrm{Me}_x\mathrm{H}_{2-x}\mathrm{Ti_3O_7}^{x(n-1)+} + x\mathrm{H}^+ \quad (2)$$

where x is the number of metal ions exchanged with protons.

Here, we have assumed that the crystal structure of titanate nanotubes corresponds to trititanic acid [8] since it was recently demonstrated [28] that sodium cations are able to exchange the protons of titanates nanotubes with a molar ratio close to 0.67. This value is the ratio of the number of moles of ion-exchanged Na^+ to the number of moles of titanium in the nanotube. When the molar ratio is equal to 0.67, corresponding to an x value of 2 in reaction (2). Other alkali metal cations, e.g. lithium ions [3,19,20], are also capable of participating in rapid ion exchange.

The adsorption isotherms of different metals from aqueous solution of their salts onto the titanate nanotubes at room temperature (22 °C) are shown in figure 4. Below a certain, relatively high, ion-exchange molar ratio (0.02 for Ru^{3+} and 0.04 for Pd^{2+}) the

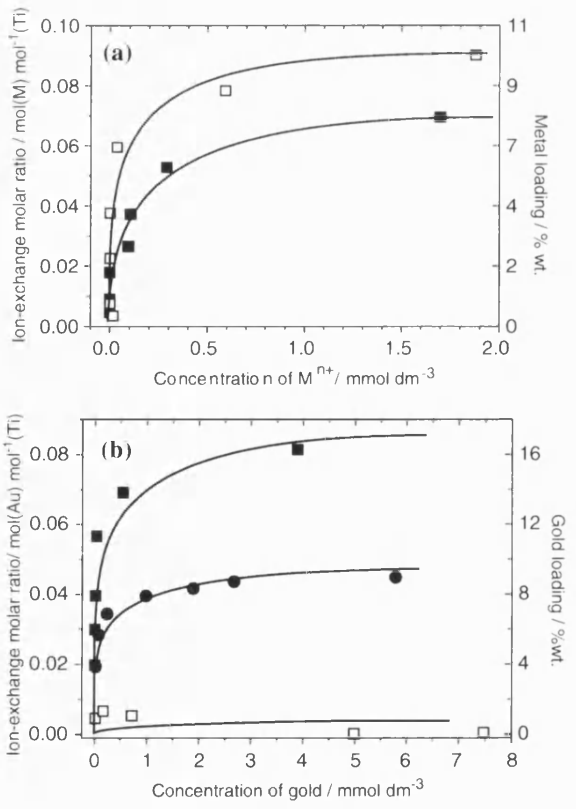

Figure 4. Isotherm of different metals adsorption on titanate nanotubes in water suspension at 22 °C. (a) Adsorption of Ru^{3+} from $RuCl_3$ solution (■), adsorption of Pd^{2+} from $PdCl_2$ solution (□); (b) adsorption of Au (III) from different complexes: $[Au(en)_2]Cl_3$ (■), $[Au(dien)Cl]Cl_2$ (●), $H[AuCl_4]$ (□).

process of ion exchange is almost complete, resulting in a very small residual concentration of metal in solution. Such behaviour is potentially very useful, for example, in recovering precious metals from aqueous solutions. A further increase in the concentration of metal in solution results in saturation of ion-exchange sites in titanate nanotubes, establishing an equilibrium distribution of metal between aqueous solution and the solid nanotubes.

The effect of speciation of the metal complex on its ability to participate in ion-exchange process with titanate nanotubes was studied on the example of polyamine complexes of gold. Three complexes, namely $[Au(en)_2]Cl_3$, $[Au(dien)Cl]Cl_2$ and $H[AuCl_4]$, were selected and the resulting isotherms of adsorption are shown in figure 4(b). The highest molar exchange ratio (0.081) was observed for $[Au(en)_2]Cl_3$ complex of gold, cation of which has a charge of +3. The $[Au(dien)Cl]Cl_2$ complex of gold, which has cation of +2 charge adsorbs onto the titanate nanotubes with a lower value of the maximum ion exchange ratio (ca. 0.045). This result is similar to the recently observed adsorption behaviour of polyamine complexes of nickel on the surface of SiO_2 [34], where the $[Ni(en)_2(H_2O)_2]^{2+}$ complex also has better adsorption properties than the $[Ni(dien)(H_2O)_3]^{2+}$ complex, probably due to differences in molecular recognition of specific adsorption sites between different complexes. The negatively charged tetrachloride complex of gold demonstrates very poor ion-exchange properties with the negatively charged titanate nanotubes, showing the significance of electrostatic interactions for the adsorption of metal salts from aqueous solution onto the titanate nanotubes.

Knowing that adsorption of positively charged molecules from aqueous solution onto the surface of nanotubular titanates readily occurs, it is possible to selectively block the external surface of nanotubes using, for example, $(C_{12}H_{25})_2(CH_3)_2NCl$ surfactant as a surface blocking agent. Indeed, the cationic part of the molecule will easily be attached to the negatively charged surface of the titanate nanotubes, whereas two bulky dodecyl groups will prevent adsorption of surfactant molecules inside the nanotube (see figure 5). The consecutive ion-exchange of metal cation will distribute the metal throughout the crystal structure of the titanate nanotube. Note, that metal cations may occupy proton positions located on either side of the nanotubes (concave and convex), as well as in the interstitial spacing between the layers of the nanotubes walls. Addition of a reducing agent would result in reduction of metal cations and formation of metal nanoparticles on the surface of titanate nanotubes. The choice of reducing agent may affect selectivity of preferentially forming metal nanoparticles on the outer or inner surface of the nanotubes. A hydrophilic reducing agent, such as $NaBH_4$, could possibly attack the internal surface of nanotubes, which is not blocked with hydrophobic

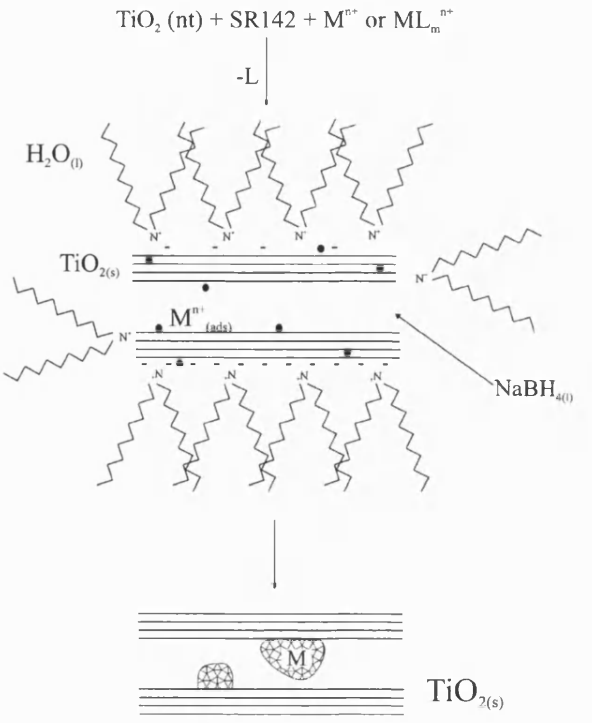

Figure 5. Cartoon illustrating the method of metal deposition inside the pores of titanate nanotubes by blocking the external surface with the $(C_{12}H_{25})_2(CH_3)_2NCl$ – SR142 surfactant followed by reduction with a hydrophilic reducing agent ($NaBH_4$).

molecules, thus resulting in the formation of metal nanoparticles only inside the titanate nanotubes (see figure 5). On the other hand, addition of a hydrophobic reducing agent could result in the formation of metal nanoparticles exclusively on the external surface.

The method of deposition of gold nanoparticles into the internal cavities of nanotubes by blocking the external surface of nanotubes was tested using SR142 as a blocking surfactant, $[Au(en)_2]Cl_3$ complex as a precursor of gold and $NaBH_4$ as a hydrophilic reducing agent. The TEM images of resulting samples of gold deposited onto the surface of titanate nanotubes with 2 wt% and 10 wt% gold loadings are shown in figure 6. The Au nanoparticles produced have a spheroidal shape, a wide distribution in particle size and a relatively large average particle diameter. In the sample with 2 wt% gold loading the average gold particle size is ca. 4 nm, with particles of much larger size than the internal diameter of nanotubes also present in the sample. This clearly indicates that deposition of gold nanoparticles occurs on the external surface of nanotubes. An increase in gold loading results in the appearance of rod like gold nanoparticles (see the arrows in figure 6(b)), with the diameter equal to the internal diameter of the nanotubes, proving that deposition of gold also occurs inside the titanate nanotubes. Despite blocking of the external surface of nanotubes during reduction with $NaBH_4$, nanoparticles of gold coat both the internal and external

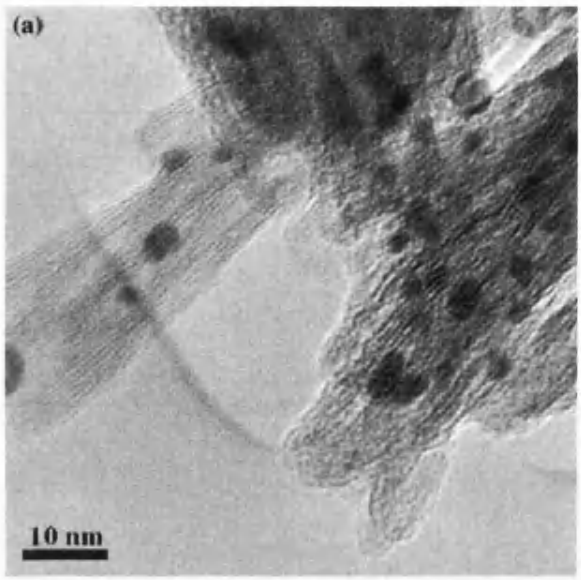

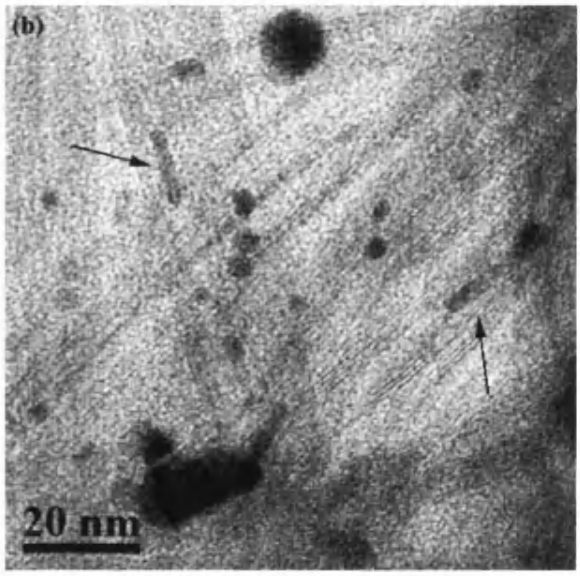

Figure 6. TEM images of gold deposited to the titanate nanotubes by the method of external surface blocking (a) Au loading of 2 wt%, (b) Au loading of 10 wt%.

surfaces of nanotubes. This is probably due to inefficient "protection" of the external surface from $NaBH_4$ molecules by the surfactant layer, allowing the $NaBH_4$ to diffuse both inside the internal nanotube cavities (to the internal surface) and through the surfactant molecules to the external surface with a similar rate. Modification of the reducing agent or surfactant molecules could be a viable strategy to control the location of deposited metal nanoparticles.

3.3. *Conventional ion-exchange method, Pd and Ru catalysts*

Figure 7 shows a TEM image of nanoparticles of metal palladium deposited on both the internal and external surfaces of titanate nanotubes. The metal was deposited by ion-exchange from $PdCl_2$ solution followed by reduction with $NaBH_4$. The average diameter of metal particles is ca. 2–4 nm and the particles have a spheroidal shape. The particles are well dispersed on either surface of the nanotubes. This material is potentially very promising for catalysis and it is important to know how dispersion and uniformity of metal nanoparticles deposition depends on metal loading.

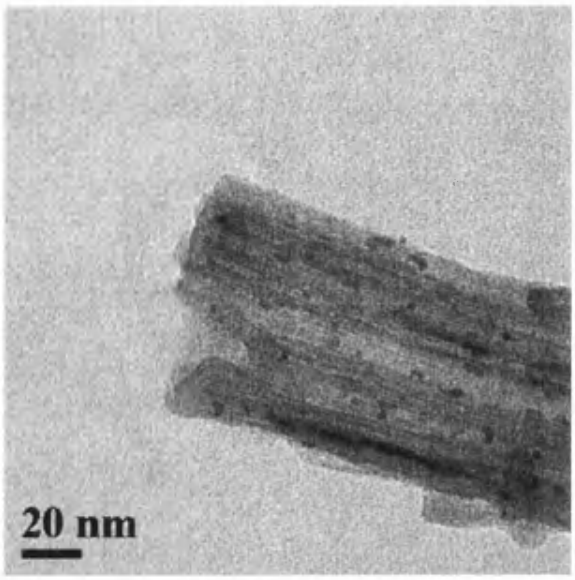

Figure 7. TEM image of palladium nanoparticles deposited on titanate nanotubes, with a Pd loading of 2.3 wt%.

The effect of catalyst loading on the morphology and dispersion of catalyst nanoparticles deposited on the surface of titanate nanotubes was studied for the case of ruthenium (III) hydrated oxide catalyst deposited by ion-exchange followed by alkali fixation. The catalytic activity of $Ru(III)/TiO_2$ nanotube catalyst was tested in the reaction of selective oxidation of alcohols with oxygen in a continuous flow multichannel compact reactor [28,31]. The TEM images and histograms of ruthenium (III) hydrated oxide nanoparticles deposited on the surface of titanate nanotubes for three different loading are shown in figure 8. Spheroidal ruthenium nanoparticles were evenly distributed on internal and external surfaces of titanate nanotubes and the density of particles reached ca. 0.1 nm^{-2} for 8.7 wt% ruthenium loading. An increase in ruthenium loading from 0.6 to 8.7 wt% results in an increase in the density of deposited particles, whereas the average size of the particles remains constant (see figure 8, histograms). The catalytic activity of $Ru(III)/TiO_2$ nanotube catalyst during the selective oxidation of benzyl alcohol to benzaldehyde is maintained at a very high value over the wide range of ruthenium loadings (see table 1). The independence of specific catalyst activity from loading correlates well with the independence of ruthenium average

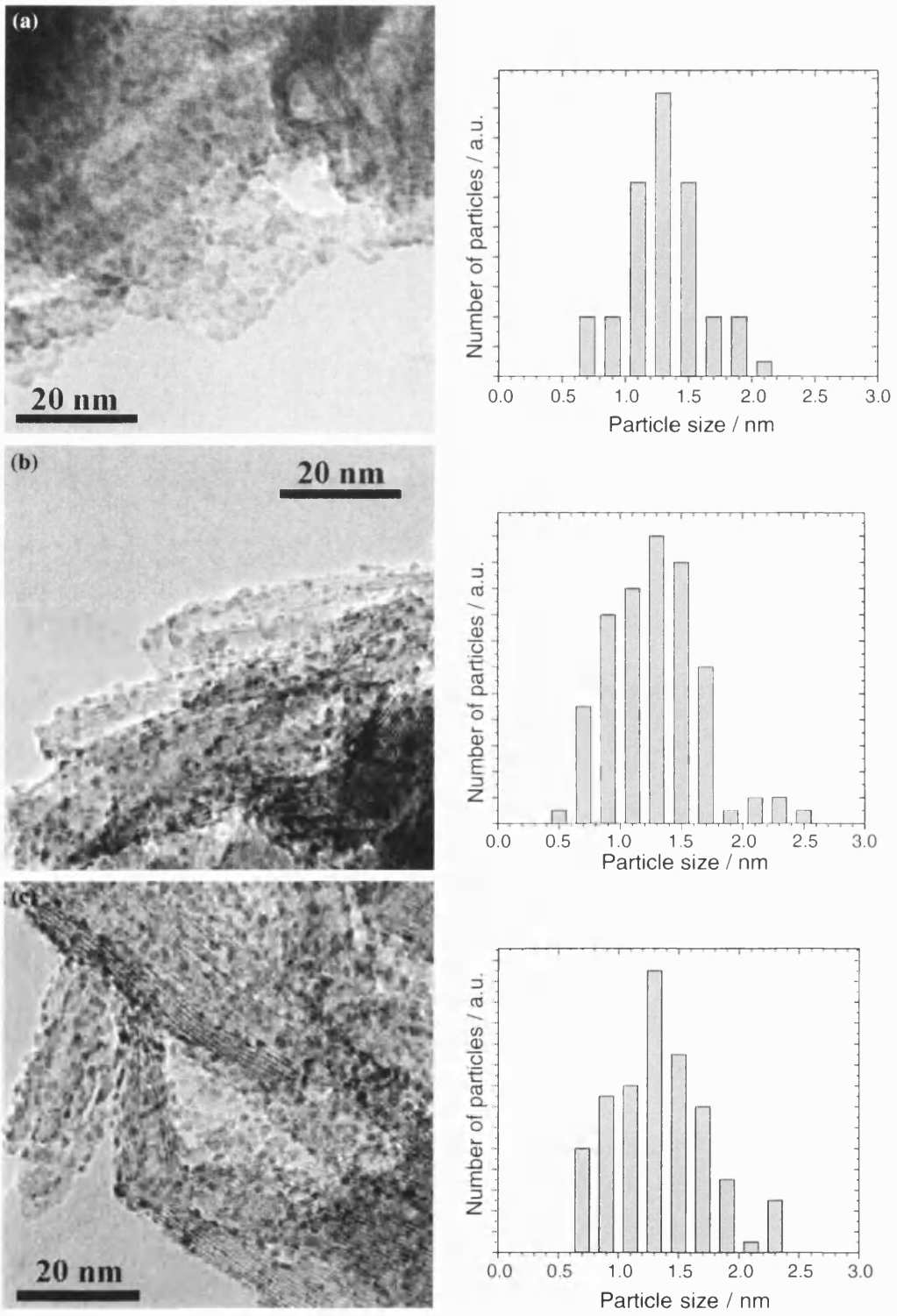

Figure 8. TEM images of ruthenium (III) hydrated oxide nanoparticles deposited onto titanate nanotubes and histograms of particle size distribution for different Ru loadings: (a) 1.1 wt%, (b) 3.4 wt%, (c) 8.7 wt%.

Table 1
Correlation between the average size of ruthenium hydrated oxide nanoparticles deposited on the surface of titanate nanotube and the rate of benzyl alcohol oxidation (TOF) catalysed by Ru(III)/TiO_2 with different catalyst loading

Catalyst loading/wt%	TOF[a]/h^{-1}	Average size[b]/nm
0.6	254	1.3
1.1	404	1.3
2.2	440	1.2
3.3	444	1.2
4.7	361	1.2
6.6	347	1.2
8.7	334	1.2

[a]Experimental conditions: initial concentration of alcohol is 1 mol dm^{-3}, solvent is toluene, liquid flowrate 2 mL min^{-1}, P = 8 bar, T = 117 °C.
[b]Determined from TEM images.

particle size from loading. The high value of specific catalytic activity (TOF $\leq$450 h^{-1}) is attributed to a high dispersion of deposited ruthenium hydrated oxide in the catalysts with a high loading, which was confirmed by the microscopy studies.

4. Conclusions

1. Two different approaches towards deposition of metal nanoparticles inside titanate nanotubes have been demonstrated.
2. The first method involves liquid constriction in the internal cavities of the nanotubes by controlled drying at certain vapour pressure after incipient wetness impregnation, followed by reduction with gaseous hydrogen. The method allows the deposition of nanowires of metal inside the nanotubes but suffers from an unsatisfactory distribution of catalyst.
3. The second method involves the blocking of the external surface of nanotubes by cationic surfactants with bulky hydrophobic groups after ion-exchange of titanate nanotubular protons onto metal cations, followed by reduction with $NaBH_4$. The method produces samples of metal nanoparticles which coat both the external and internal sides of titanate nanotubes. Further modification of the reducing agent and/or surfactant is required in order to ensure deposition of nanoparticles selectively inside the nanotubes.
4. The third method of metal nanoparticles deposition on the both sides of nanotubes utilises the high ion-exchange capacity of titanate nanotubes. This method allows to achieve a high loading of metal nanoparticles which are distributed evenly on the surface of nanotubes, making it a promising support for a variety of catalysts.
5. Further, comprehensive studies of the physico-chemical properties of metal nanoparticles on the surface of titanate nanotubes are required as are methods which provide highly localised metal deposition.

Acknowledgments

This work was funded through the EC project "CREATION" G5RD-CT-2002-00724. The authors are grateful to the electron microscopy unit at Johnson Matthey Research Centre, Sonning Common, Reading, UK, for assistance with TEM studies.

References

[1] T. Kasuga, M. Hiramatsu, A. Hoson, T. Sekino and K. Niihara, Langmuir 14 (1998) 3160.
[2] X. Sun and Y. Li, Chem. Eur. J. 9 (2003) 2229.
[3] G. Armstrong, A.R. Armstrong, J. Canales and P.G. Bruce, Chem. Commun. 19 (2005) 2454.
[4] D.V. Bavykin, V.N. Parmon, A.A. Lapkin and F.C. Walsh, J. Mater. Chem. 14 (2004) 3370.
[5] D.V. Bavykin, S.N. Gordeev, A.V. Moskalenko, A.A. Lapkin and F.C. Walsh, J. Phys. Chem. B 109 (2005) 8565.
[6] A. Thorne, A. Kruth, D. Tunstall, J.T.S. Irvine and W. Zhou, J. Phys. Chem. B 109 (2005) 5439.
[7] M. Zhang, Z. Jin, J. Zhang, X. Guo, J. Yang, W. Li, X. Wang and Z. Zhang, J. Mol. Catal. A: Chem. 217 (2004) 203.
[8] Q. Chen, G.H. Du, S. Zhang and L.M. Peng, Acta Cryst. B 58 (2002) 587.
[9] J.J. Yang, Z.S. Jin, X.D. Wang, W. Li, J.W. Zhang, S.L. Zhang, X.Y. Guo and Z.J. Zhang, Dalton Trans. 20 (2003) 3898.
[10] A. Nakahira, W. Kato, M. Tamai, T. Isshiki, K. Nishio and H. Aritani, J. Mater. Sci. 39 (2004) 4239.
[11] O.K. Varghese, D. Gong, M. Paulose, K.G. Ong and C.A. Grimes, Sens Actuators B 93 (2003) 338.
[12] D.V. Bavykin, A.A. Lapkin, P.K. Plucinski, J.M. Friedrich and F.C. Walsh, J. Phys. Chem. B 109 (2005) 19422.
[13] S.H. Lim, J. Luo, Z. Zhong, W. Ji and J. Lin, Inorg. Chem. 44 (2005) 4124.
[14] C.H. Lin, C.H. Lee, J.H. Chao, C.Y. Kuo, Y.C. Cheng, W.N. Huang, H.W. Chang, Y.M. Huang and M.K. Shih, Catal. Lett. 98 (2004) 61.
[15] J.C. Xu, M. Lu, X.Y. Guo and H.L. Li, J. Mol. Catal. A 226 (2005) 123.
[16] C.H. Lin, S.H. Chien, J.H. Chao, C.Y. Sheu, Y.C. Cheng, Y.J. Huang and C.H. Tsai, Catal. Lett. 80 (2002) 153.
[17] M. Adachi, Y. Murata, I. Okada and S. Yoshikawa, J. Electrochem. Soc. 150 (2003) G488.
[18] R. Ma, T. Sasaki and Y. Bando, Chem. Commun. 7 (2005) 948.
[19] J. Li, Z. Tang and Z. Zhang, Electrochem. Commun. 7 (2005) 62.
[20] L. Kavan, M. Kalbac, M. Zukalova, I. Exnar, V. Lorenzen, R. Nesper and M. Graetzel, Chem. Mater. 16 (2004) 477.
[21] D.V. Bavykin, E.V. Milsom, F. Marken, D.H. Kim, D.H. Marsha, D.J. Riley, F.C. Walsh, K.H. El-Abiary and A.A. Lapkin, Electrochem. Commun. 7 (2005) 1050.
[22] J. Qu, X. Zhang, Y. Wang and C. Xie, Electrochim. Acta 50 (2005) 3576.
[23] A. Kleinhammes, G.W. Wagner, H. Kulkarni, Y. Jia, Q. Zhang, L.-C. Qin and Y. Wu, Chem. Phys. Lett. 411 (2005) 81.
[24] J. Cao, J.-Z. Sun, H.-Y. Li, J. Hong and M. Wang, J. Mater. Chem. 14 (2004) 1203.
[25] M. Hodos, E. Horvath, H. Haspel, A. Kukovecz, Z. Konya and I. Kiricsi, Chem. Phys. Lett. 399 (2004) 512.
[26] M. Wang, D.J. Guo and H.L. Li, J. Solid State Chem. 178 (2005) 1996.

[27] V. Idakiev, Z.Y. Yuan, T. Tabakova and B.L. Su, Appl. Catal. A 281 (2005) 149.
[28] D.V. Bavykin, A.A. Lapkin, P.K. Plucinski, J.M. Friedrich and F.C. Walsh, J. Catal. 235 (2005) 10.
[29] T. Kasuga, M. Hiramatsu, A. Hoson, T. Sekino and K. Niihara, Adv. Mater. 11 (1999) 1307.
[30] L.B. Rockland, Anal. Chem. 32(10) (1960) 1375.
[31] D.V. Bavykin, A.A. Lapkin, S.T. Kolaczkowski and P.K. Plucinski, Appl. Catal. A 288 (2005) 175.
[32] B. Kasemo, S. Johansson, H. Persson, P. Thormahlen and V.P. Zhdanov, Top. Catal. 13 (2000) 43.
[33] A. Nakahira, T. Kubo, Y. Yamasaki, T. Suzuki and Y. Ikuhara, Jpn. J. Appl. Phys. 44(22) (2005) L690.
[34] S. Boujday, J.F. Lambert and M. Che, J. Phys. Chem. B 107 (2003) 651.

Synthesis of novel composite materials via the deposition of precious metals onto protonated titanate (TiO_2) nanotubes

F. C. Walsh*[1], D. V. Bavykin[1], L. Torrente-Murciano[2], A. A. Lapkin[2] and B. A. Cressey[3]

Methods for the deposition of precious metals (Au, Pt, Pd and ruthenium hydrated oxide) onto the surface of nanotubular titanates are considered. Viable techniques include preliminary ion exchange of precious metal cations onto the nanotubes followed by chemical, electrochemical or photochemical reduction to the metal. The morphology and size of the metal nanoparticles ranged from spheroidal particles of a few nanometres to larger, rod like particles. The deposits, which were densely loaded onto the surface and were uniformly distributed, had a high surface area and good chemical stability. The size of metal nanoparticles ranged from 1 to 50 nm.

Keywords: Adsorption, Nanostructure, Ion exchange, Metal particles

Introduction

Nanostructured composites have become an important new class of engineering materials. In the case of metal/ceramic composites, one method of manufacture is to coat the ceramic substrate with a metallic deposit.[1] The nanoporous ceramic substrates are produced by a variety of techniques including an anodic route,[2] sol–gel methods or hydrothermal routes.

The recently developed nanotubular titanates,[3] produced by alkaline hydrothermal treatment of raw TiO_2, have a reasonable capacity for cation exchange[4] combined with an open mesoporous morphology,[5] providing an accessible surface having controlled chemical properties. Such nanotubes are usually agglomerated into secondary particles. The size of these particles is affected by the conditions of synthesis as shown in Fig. 1*a*. In Fig. 1*b* and *c* the TEM images show the structure of titanate nanotubes, which have a multiwall structure and an internal diameter in the range of several nanometres. These nanotubular titanates are attracting much attention owing to their potential use in industrial applications such as hydrogen storage,[6,7] lithium batteries,[8,9] photovoltaic devices[10] and catalysis.[11] Nanotubes with a high aspect ratio (i.e. they are long compared with their diameter) can be used as a reinforcement particle in composite coatings, providing a high shock resistance to mechanical loads.[12]

Precious metals are intensively used in applications ranging from heterogeneous catalysis to electronic materials. Owing to their high cost, it is important to prepare such metals either as dispersed ultra small metal particles on the surface of porous materials or as continuous, thin coatings of metal on the surface of a support. A uniform distribution of precious metal on the substrate is important since it allows the cost to be minimised while maintaining the performance of the coatings. Ideally, a uniform atomic scale distribution of precious metal on the surface of a support would provide such a uniform, monolayer distribution of metal. This can be achieved if the precursor of the deposited metal (usually a metal ion) reacts with the surface of the support in a chemical reaction. Ion exchange is a suitable process to facilitate an atomic scale distribution of the metal precursor.

Common techniques include adsorption of metal ions followed by chemical reduction. In the case of titanate nanotubes, their enhanced ion exchange properties suggest the combination of ion exchange and chemical reaction. Using this approach, CdS (Refs. 13 and 14) and TiO_2 (Ref. 15) decorated titanate nanostructures have been synthesised.

In this work, the metallisation of titanate nanotubes with several precious metals, using the method of ion exchange of metal cations into the nanotube structure followed by reduction in the metal ion, is considered. The effect of the metal precursor ionic charge on the efficiency of metal adsorption is studied and methods for the reduction in the ion exchanged metal ions are discussed.

Experimental Details

Reagents

Titanium dioxide (anatase, TiO_2), sodium hydroxide (NaOH), sulphuric acid (H_2SO_4), hydrochloric acid (HCl), palladium chloride ($PdCl_2$), ruthenium(III) chloride hydrate ($RuCl_3.nH_2O$), dihydrogen hexachloroplatinate (H_2PtCl_6), hydrogen tetrachloroaurate(III) hydrate ($HAuCl_4.H_2O$), ethylendiamine (en), diethylentriamine (dien), didodecyl-dimethylammonium chloride [SR142, $(C_{12}H_{25})_2(CH_3)_2NCl$], thioglycerol (thy), sodium

[1]Electrochemical Engineering Group, School of Engineering Sciences, University of Southampton, Highfield, Southampton SO17 1BJ, UK
[2]Catalysis and Reaction Engineering Group, Department of Chemical Engineering, University of Bath, Bath, BA2 7AY, UK
[3]Science and Engineering Electron Microscopy Centre, School of Chemistry, University of Southampton, Highfield, Southampton SO17 1BJ, UK

*Corresponding author, email F.C.Walsh@soton.ac.uk

Published by Maney on behalf of the Institute
Received 13 July 2006; accepted 9 October 2006
DOI 10.1179/174591906X149077

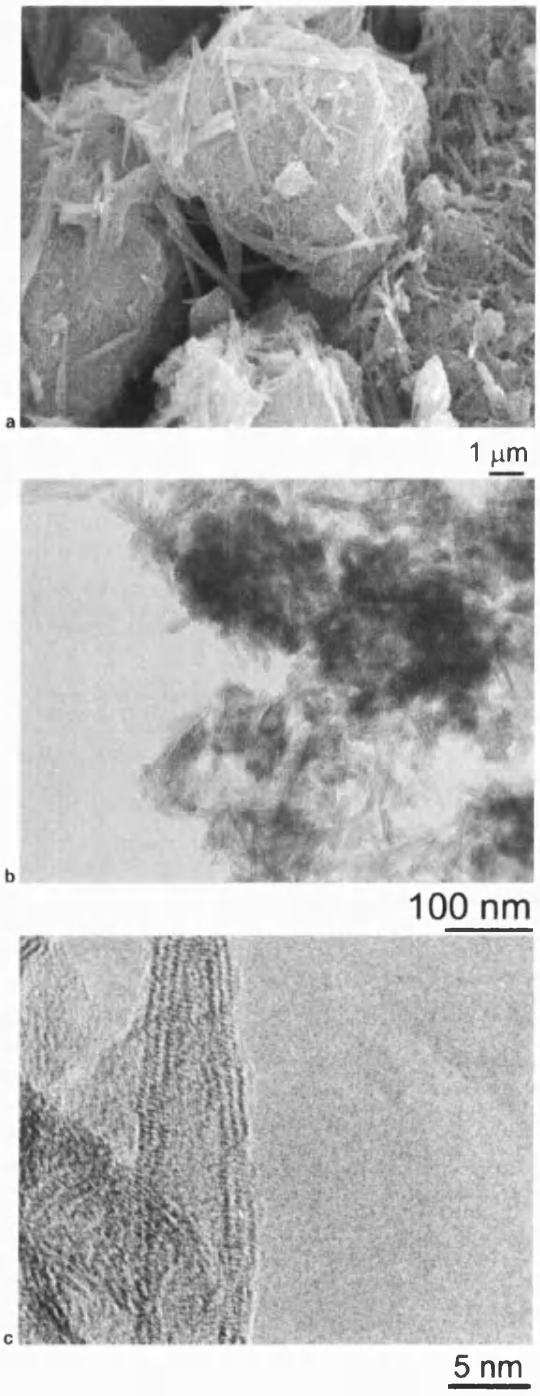

1 Titanate nanotube support produced by alkaline hydrothermal treatment (a) image (SEM); (b) image (TEM); (c) image (high resolution TEM)

tetraborohydrate ($NaBH_4$), 'pure grade' were obtained from Aldrich and were used without further purification.

Preparation of titanate nanotubes

The method of preparation of titanate nanotubes was based on alkaline hydrothermal transformation.[16] Titanium dioxide of 20 g was added to 300 cm^3 of 10 mol dm^{-3} NaOH solution and heated for 22 h at 140°C. The white, powdery TiO_2 product was thoroughly washed at 25°C with water, 0·05 mol dm^{-3} H_2SO_4 and distilled water, followed by drying in vacuum at 80°C.

Ion exchange of metal cations with protons of titanate nanotubes

Dry titanate nanotubes powder (1 g) was suspended in 10 cm^3 of water and 40 cm^3 of the precious metal precursor solution was slowly added under vigorous stirring. The concentration of the metal precursor was adjusted to meet the required metal loading, taking into account the isotherm of adsorption of ions in the surface of titanate nanotubes.[17] The mixture was kept for 2 h at 25°C, under stirring, to complete the ion exchange process. The mixture was filtered, thoroughly washed with water at 25°C and air dried.

Chemical reduction of metal ions

When $NaBH_4$ was used as the reducing agent, the powdered titanate nanotubes (saturated with metal cations) were suspended in water with (or without) addition of 0·1 mol dm^{-3} thioglycerol. The excess of 0·1 mol dm^{-3} $NaBH_4$ solution was added under vigorous stirring accompanied by a colour change of the powder as reduction to finely divided metal occurred.

When gaseous hydrogen was used as the reducing agent, the titanate nanotubes powder, saturated with diethylenediamine gold(III) $[Au(en)_2]^{3+}$ ions, was placed in a quartz U tube and hydrogen was pumped through the tube at a flowrate of ≈20 mL min^{-1}. The temperature was set to 50°C. On contact with hydrogen, the powder changed from yellow to purple in colour. Once the powder had completely turned purple, the temperature was increased, to 150°C, to remove residual HCl and water as vapour.

Photochemical reduction of metal

Titanate nanotubes (1 g) were ion exchanged with gold ions from a 2×10^{-3} mol dm^{-3} $[Au(en)_2]Cl_3$ solution. The powder was suspended in 50 cm^3 of water and illuminated for 1 h with UV light using a Muller TYPLAX × 1000 mercury arc lamp. The colour of the light yellow powder turned to purple blue. The sample was filtered, washed with water at 25°C and dried in vacuum at 80°C.

Electrochemical reduction of metal

For electrochemical reduction, the titanate nanotubes were immobilised on the surface of a carbon electrode using a doctor blade technique.[8] Titanate nanotubes of 2 g were dispersed in 8 cm^3 of dimethylformamide (DMF) using a shear blade mixer (Silverstone L4RT) for 60 min until a thick slurry was formed (0·25 g cm^{-3}). The 0·5 g carbon (acetylene black, Chevron Philips, BET area 75 m^2 g^{-1}) was dispersed in 8 cm^3 of DMF 2 cm^3 of titanate nanotubes slurry was mixed with 1 cm^3 of acetylene black slurry and 1·25 cm^3 of a 5 wt-% solution of polyvinyliden fluoride (PVDF, Solef 6020/1001) was added. The mixture was deposited at 25°C on the surface of a carbon plate electrode by a doctor blade technique and dried at 80°C. The prepared electrode was immersed in 50 cm^3 of 2×10^{-3} mol dm^{-3} diethylendiamine gold trichloride, $[Au(en)_2]Cl_3$, solution in water for 20 min, rinsed with cold water at 4°C several times and dried at 25°C. The direct electrochemical reduction to gold was undertaken in 6 mol dm^{-3} KOH electrolyte at 25°C at a potential of −1·4 V versus SCE for 30 min.

Transmission electron microscopy images of all samples were obtained using a JEOL 3010 TEM instrument. The powder sample was 'dry' deposited on a copper grid covered with a perforated carbon film. Scanning electron microscopy images were obtained with a JEOL 6310 SEM.

Results and discussion

Generally, the method of wet chemical deposition of metal on a surface includes the stage of dispersion of the metal precursor on the surface of substrate followed by reduction to the metal. In most of the conventional methods (e.g. incipient wet impregnation) the phenomenon of adsorption of metal precursor on the surface of support is used, which limits the amount of depositing metal. If the metal precursor is able to react not only with surface of substrate but also with its volume (absorption of the precursor) then the amount of deposited metal can be increased and the quality of the metal distribution maintained. The ion exchange of precious metal ions with titanate nanotubes can facilitate a good metal distribution and high metal loading throughout the nanoporous support.

Ion exchange

Titanate nanotubes produced by alkaline hydrothermal treatment of TiO_2 have characteristic multilayered wall, tubular morphology. Each layer consists of edge sharing TiO_6 octahedra forming zigzag structure. The distance between layers is ~0·72 nm. The proton exchangeable OH groups of titanic acid are located between these layers inside the wall of nanotubes as well as on the internal and external surfaces (Fig. 2).[3] The exact crystal structure is disputed between $H_2Ti_3O_7$ (Ref. 18), $H_2Ti_2O_4(OH)_2$ (Ref. 19) and $H_2Ti_4O_9.H_2O$ (Ref. 20), but the result of titration of protons with NaOH favours the trititanic acid as a stochiometric formula of titanate nanotubes[11]. The ion exchange reaction of trititanate nanotubes with a singly charged metal cation, M^+ can be expressed as

$$xM^+ + H_2Ti_3O_7 \rightarrow M_xH_{2-x}Ti_3O_7 + xH^+ \quad (1)$$

where the parameter x reflects how well the cations M^+ can exchange with protons in the nanotubular trititanic acid. For alkaline metals, the value of x is very close to 2 whereas for other cations the change is smaller, suggesting that not all OH groups in the titanate nanotubes have the same accessibility. For example, the ion exchange of Pd^{2+} and Ru^{3+} with protons in the titanate nanotubes from a 2 mmol dm^{-3} solution of the corresponding chloride salt results in the following M/Ti ratios 0·09 (maximum 0·33) and 0·07 (maximum 0·22) respectively. The maximum M/Ti ratio occurs when all protons in the titanate support are substituted by metal cations.[17]

During ion exchange of the precious metal precursor with titanate nanotubes, it is important to use suitable ionic form of the metal. Since titanate nanotubes in aqueous suspension have a negative zeta potential[21] owing to the dissociation of titanic acid, only cations of the metal interact well with the substrate. In the sequence $[Au(en)_2]Cl_3$, $[Au(dien)Cl]Cl_2$, $H[AuCl_4]$ the following corresponding values of M/Ti ratios have been obtained from a 2 mmol dm^{-3} solution: 0·08, 0·04, 0·005. The metals in a cationic form can be easily attached to the titanate nanotubes, substituting titanate protons, whereas anions of the metal tend to remain in solution.

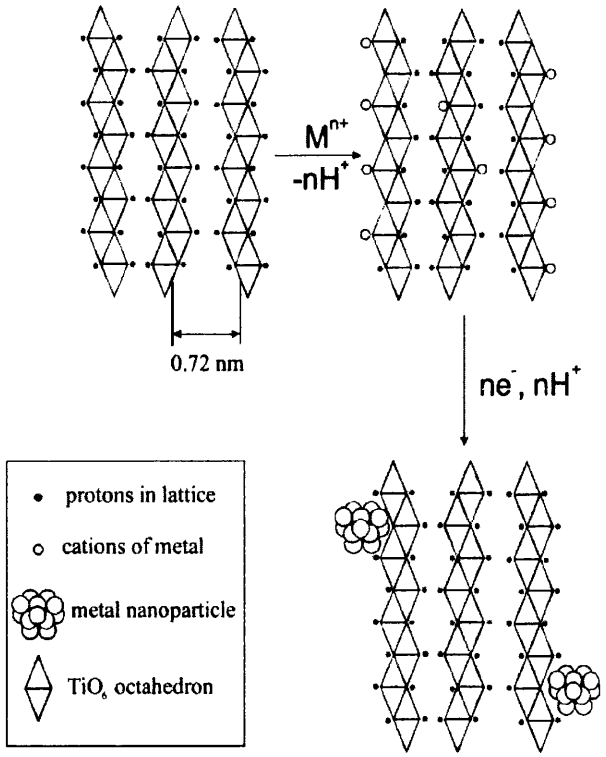

2 Process of metal cation exchange with protons in titanate nanotube lattice followed by reduction to metal on surface of nanotube

Such an ionic distribution of metal into the substrate leads to the dispersed deposits of metal nanoparticles after reduction. Using this method, the increase in metal loading does not change the size of metal nanoparticles.[17] In Fig. 3 TEM images of Pd nanoparticles deposited on the surface of titanate nanotubes, which were deposited by the method of ion exchange from aqueous solution of $PdCl_2$ followed by reduction with $NaBH_4$, are shown. The metal nanoparticles are uniformly distributed on the surface on nanotubes and their size varies in range from 2 to 5 nm. The increase in metal loading from 4·8 to 8·9 wt-% resulted in an increase in amount of nanoparticles rather than their size (Table 1).

Reduction of metal

The stage of reduction of the metal precursor incorporated into the titanate nanotubes controls the morphological properties, particularly the size and shape of the metal nanoparticles. The rate of the reduction as well as the presence of surfactant or ligand additives are major factors which affect the reduction stage. The following examples illustrate various methods for the reduction in $[Au(eu)_2]^{3+}$ moieties incorporated into the titanate nanotubes.

Chemical reduction

Chemical reduction is the widely used method of preparation metal nanoparticles. The strength of reducing agent can affect the rate of metal cations reduction, which regulates the morphology of metal particles. Aqueous $NaBH_4$, which has been used as a reducing agent for electroless deposition of metals, is characterised by a

Table 1 Comparison of methods for metal deposition on titanate nanotubes

Method	Precious metal	Metal loading, wt%	Time of reduction/min	Size of metal particles/nm
Ion exchange with Pd^{2+}, reduction with $NaBH_{4(aq)}$	Pd	4·8	<1	2·1–4·8
	Pd	7·0	<1	2·4–4·4
	Pd	8·9	<1	1·9–4·5
Ion exchange with Ru^{3+}, treatment with $NaOH_{(aq)}$*	Ru	1·1	10–15	0·6–2·1
	Ru	3·4	10–15	0·5–2·5
	Ru	8·7	10–15	0·6–2·3
Ion exchange with $[Au(en)_2]^{3+}$ followed by reduction with $NaBH_{4(aq)}$	Au	2	<1	2–6
Reduction with $NaBH_{4(aq)}$ and thioglycerol	Au	2	<1	25–50
Reduction with $H_{2(g)}$	Au	2	10–20	8–25
Photoreduction	Au	10	60	4–35
Electrochemical reduction	Au	15	30	10–50
Impregnation by $H_2PtCl_{6(aq)}$ then reduction with $H_{2(g)}$†	Pt	0·5	<1	1–3

*See Ref. 11 for details.
†See Ref. 17 for details.

very high rate of reduction. The reduction in Au(III) by sodium borohydride can be expressed as

$$3NaBH_4 + 8[Au(en)_2]Cl_3 + 9H_2O = 3H_3BO_3 + 8Au + 16en + 3NaCl + 21HCl \quad (2)$$

Figure 4*a* shows a TEM image of titanate nanotubes with 2 wt-% of gold deposited by method of ions exchange followed by reduction with $NaBH_4$. The gold nanoparticles are distributed uniformly on the both sides of nanotubes (inside and outside) and have an average size of ≈4 nm (Table 1). No large agglomerates of gold particles were observed.

Sulfur containing organic molecules are well known stabilisers of gold clusters in solution interacting with the surface of metal via the -SH group.[22] In contrast to the general tendency to stabilise small gold particles by addition of -SH containing molecules, addition of thioglycerol during reduction in gold on titanate nanotubes results in formation of massive gold particles, as shown in Fig. 4*b*. The size of the spheroidal particles varied in the range from 25 to 50 nm (Table 1).

The reaction of gas phase reduction in ion exchanged gold with hydrogen

$$3H_2 + 2[Au(en)_2]Cl_3 = 2Au + 4en + 6HCl \quad (3)$$

Table 2 Types of metallised nanotubes (corresponding to various metal loadings) and their possible application areas

Loading	Type of metallisation	Electron micrograph	Application
	Metal particle inner nanotube diameter outer nanotube diameter Multiwalled tube	10 nm	Functionalisation for hydrogen storage
		10 nm	Catalysis; electrocatalysis; photocatalysis; fuel cell; solar cell
		*	Nanowires; thermoconductive nanofluids; magnets
		*	Reinforced composite coatings

*Work in progress.

is slower than that with $NaBH_4$. As a result, the average size of gold particles is higher (Table 1). Some of the particles have an ellipsoidal shape with a small diameter, corresponding to the internal diameter of titanate nanotubes (Fig. 4*c*). The similar shape of nanoparticles of Pt has been observed previously[17,23] during gas phase reduction in solution of metal precursor constricted inside the nanotubes. Indeed, if the gold exchanged titanate nanotubes sample contained water or was exposed to the humid air, the water could undergo capillary condensation and fill the internal pores of the nanotubes. This might result in desorption of gold salts from nanotubes into the solution inside the tube. The following reduction in the solution will result in formation of metal particles having a cylindrical shape.

Photochemical reduction

Photochemical reduction of metal on the surface of TiO_2 is a popular method of deposition of precious metals on the surface of TiO_2 photocatalysts since it allows contamination of photocatalyst with sodium ions to be avoided. The TiO_2 absorbs a quantum of light and generates an electron hole pair. The hole can react with any reducing materials or molecules of water. The electron reaches the interface and reacts with salts forming metal nanoparticles. The overall reaction can be written as

$$2[Au(en)_2]Cl_3 + 3H_2O + 6h\nu = 2Au + 1{\cdot}5O_2 + 4en + 6HCl \quad (4)$$

Since the absorption of light occurs mainly on the TiO_2 photocatalyst, the reduction in metal in the bulk solution is minimised.[24] The titanate nanotubes have wide bandgap semiconductor properties[25] and demonstrate photocatalytic activity.[26] Thus, the photochemical reduction in metal on the surface of titanate nanotubes can be achieved. In Fig. 4*d* the TEM image of gold nanoparticles produced by ion exchange followed by photochemical reduction is shown. The particle size distribution is very wide (Table 1): the very small nanoparticles of 4 nm coexist with massive 35 nm nanoparticles of gold. All particles show good adhesion to the substrate.

Electrochemical reduction

Electrochemical reduction has the advantage of using an additional adjustable parameter: electrode potential, which allows control over the rate of the reduction and morphological properties of metal nanoparticles. Electrochemically reduced metal tends to show good electrical contact with the support. The electrode reaction can be written as

$$[Au(en)_2]Cl_3 + 3e^- = Au + 2en + 3Cl^- \quad (5)$$

Electrochemical reduction in ion exchanged cations of Au(III) incorporated into the titanate nanotubes at a potential of −1·4 V versus SCE resulted in the formation of relatively large spheroid particles of typical size in range from 10 to 50 nm (Table 1, Figs. 4*e* and 5).

In Fig. 6, four TEM images of precious metal nanoparticles deposited on the surface of titanate nanotubes are shown. Although the methods of metal deposition are not absolutely identical, one can see the general tendency of larger particles in the sequence Ru<Pt<Pd<Au.

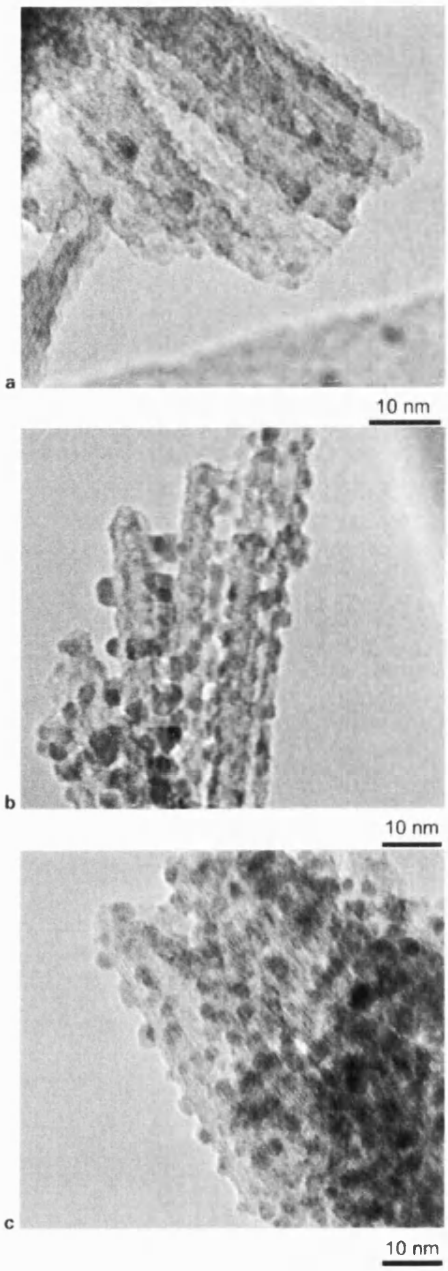

3 Images (TEM) of various loadings of Pd nanoparticles deposited on surface of titanate nanotubes by the method of ion exchange from aqueous solution of $PdCl_2$ followed by reduction with $NaBH_4$ at 25°C (a) 4·8 wt-%Pd; (b) 7·0 wt-%Pd; (c) 8·9 wt-%Pd

Applications of metallised nanotubes

In Table 2 the prospective applications of titanate nanotubes metallised with precious metals with different loading are summarised. The titanate nanotubes with low metal loading (<0·1 wt-%) having typically one metal nanoparticle per nanotubes will probably find application as novel functionalised materials for hydrogen storage.[6,7] When densely decorated with precious metal nanoparticles, the titanate

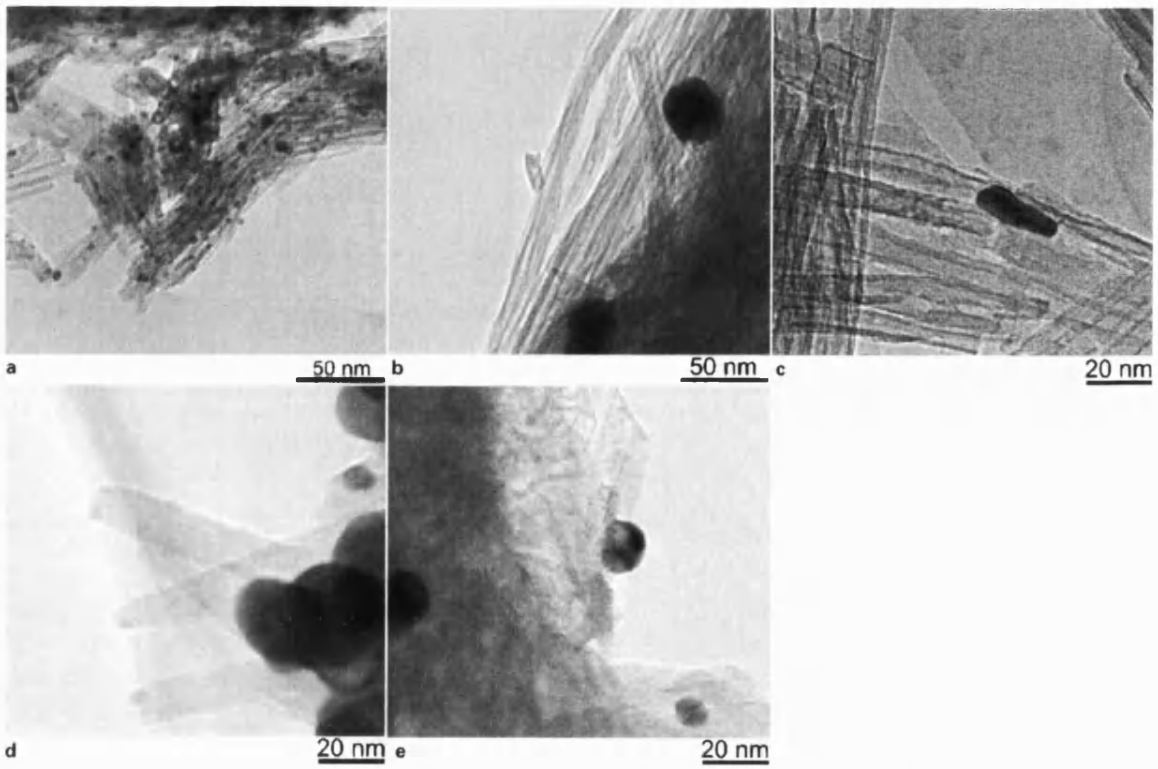

4 TEM images of gold nanoparticles deposited into the pores of titanate nanotubes by ion-exchange with diethylendiamine gold (III) ions ($[Au(eu)_2]^{3+}$) followed by reduction with (a) $NaBH_4$, (b) $NaBH_4$ in the presence of 0·1 mol dm^{-3} thioglycerol, (c) gaseous hydrogen, (d) photoreduction and (e) electrochemical reduction

nanotubes are prospective materials for heterogeneous catalysis,[11,27,28] photocatalysis[26] and electrocatalysis.[29] It is particularly important to have a uniform deposition of highly dispersed metal particles in many of the applications, since this will lead to a high specific surface area of precious metal and a lower materials cost. The practical range of loading was typically from 5 to 15 wt-%.

Further increases in the metal loading (up to 50 wt-%) and maintaining the uniformity of metal distribution should result in continuous coating of the nanotubes surface with metal (Table 2). Such composite nanostructures have not yet been reported but may find application in areas where nanostructured metals with a high aspect ratio are needed (e.g. thermoconductive nanofluids, electroconductive wires for nanodevices or supermagnet nanoparticles).

The complete filling of nanotubes pores with metal will result in the formation of a continuous metal phase with incorporated titanate nanotubes. In the case of titanate nanotubes, such structures await synthesis as a novel class of composite materials.

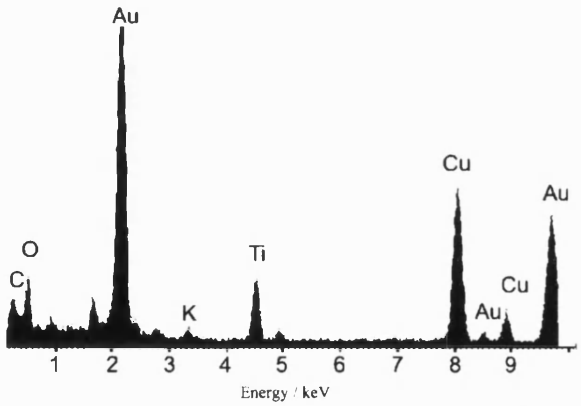

5 EDX spectrum of gold electrodeposited on titanate nanotubular electrode from Figure 4*e*. The Cu peaks result from the specimen support grid and holders

Conclusions

1. Nanotubular titanates have been decorated with nanoparticles of precious metal including Au, Pt, Pd and Ru. The method of metal nanoparticle deposition includes the stage of ion exchange of protons of titanate nanotubes with cations of precious metal followed by reduction to the metal. The nanoparticles were uniformly distributed on the internal and external surfaces of the nanotubes.
2. Ion exchanged Au(III) ions in titanate nanotubes were reduced chemically, photochemically or electrochemically. The highest dispersions of metal were achieved using the aqueous BH_4^- ion as the reducing agent.
3. It was demonstrated that an increase in Pd loading up to 8·9 wt-% results in Pd particles having an average size of ≈3·5 nm.

Acknowledgement

The authors gratefully acknowledge financial support from a NATO/Royal Society Fellowship and the University of Southampton's Research Institute for Industry.

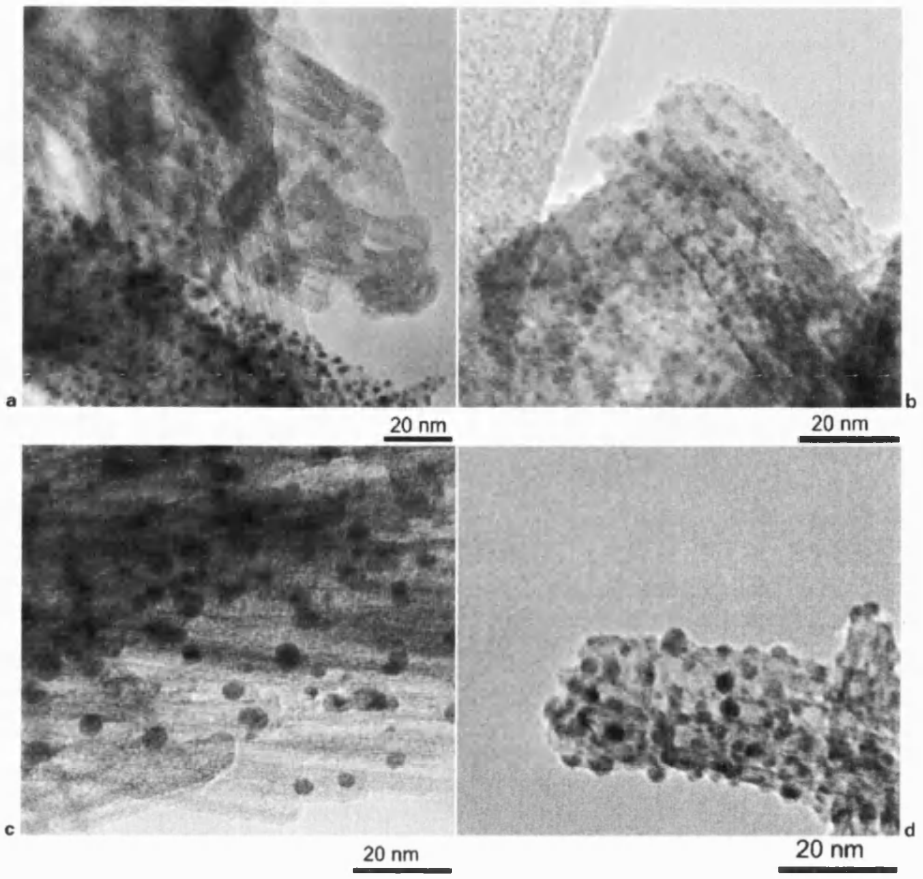

6 TEM images of titanate nanotubes decorated with (a) Pt,[17] (b) $Ru(OH)_3$,[11] (c) Au and (d) Pd nanoparticles

References

1. C. T. J. Low, R. G. A. Wills and F. C. Walsh: *Surf. Coat. Technol.*, 2006, **201**, 371.
2. E. Schofield: *Trans. IMF*, 2005, **83**, 35–42.
3. D. V. Bavykin, J. M. Friedrich and F. C. Walsh: *Adv. Mater.*, 2006, **18**, 2807–2824.
4. X. M. Sun and Y. D. Li: *Chem. Eur. J.*, 2003, **9**, 2229–2238.
5. D. V. Bavykin, V. N. Parmon, A. A. Lapkin and F. C. Walsh: *J. Mater. Chem.*, 2004, **14**, 3370–3377.
6. D. V. Bavykin, A. A. Lapkin, P. K. Plucinski, J. M. Friedrich and F. C. Walsh: *J. Phys. Chem. B*, 2005, **109B**, 19422–19427.
7. S. H. Lim, J. Luo, Z. Zhong, W. Ji and J. Lin: *Inorg. Chem.*, 2005, **44**, 4124–4126.
8. A. R. Armstrong, G. Armstrong, J. Canales and P. G. Bruce: *J. Power Sources*, 2005, **146**, 501–506.
9. J. Li, Z. Tang and Z. Zhang: *Chem. Phys. Lett.*, 2006, **418**, 506–510.
10. Y. Ohsaki, N. Masaki, T. Kitamura, Y. Wada, T. Okamoto, T. Sekino, K. Niiharab and S. Yanagida: *Phys. Chem. Chem. Phys.*, 2005, **7**, 4157–4163.
11. D. V. Bavykin, A. A. Lapkin, P. K. Plucinski, J. M. Friedrich and F.C. Walsh: *J. Catal.*, 2005, **235**, 10–17.
12. Y. Q. Zhu, T. Sekine, K. S. Brigatti, S. Firth, R. Tenne, R. Rosentsveig, H. W. Kroto and D. R. M. Walton: *J. Am. Chem. Soc.*, 2003, **125**, 1329–1333.
13. J. Cao, J. Z. Sun, H. Y. Li, J. Hong and M. Wang: *J. Mater. Chem.*, 2004, **14**, 1203–1206.
14. M. Hodos, E. Horvath, H. Haspel, A. Kukovecz, Z. Konya and I. Kiricsi: *Chem. Phys.*, 2004, **399**, 512–515.
15. H. G. Yang and H. C. Zeng: *J. Am. Chem. Soc.*, 2005, **127**, 270–278.
16. T. Kasuga, M. Hiramatsu, A. Hoson, T. Sekino and K. Niihara: *Adv. Mater.*, 1999, **11**, 1307–1311.
17. D. V. Bavykin, A. A. Lapkin, P. K. Plucinski, L. Torrente-Murciano, J. M. Friedrich, and F. C. Walsh: *Top. Catal.*, 2006, **39**, DOI: 10.1007/S11244-006-0051-4.
18. Q. Chen, G. H. Du, S. Zhang and L. M. Peng: *Acta Cryst. B*, 2002, **58**, 587–593.
19. J. J. Yang, Z. S. Jin, X. D. Wang, W. Li, J. W. Zhang, S. L. Zhang, X. Y. Guo and Z. J. Zhang: *Dalton Trans.*, 2003, **20**, 3898–3901.
20. A. Nakahira, W. Kato, M. Tamai, T. Isshiki, K. Nishio and H. Aritani: *J. Mater. Sci.*, 2004, **39**, 4239–4245.
21. D. V. Bavykin, E. V. Milsom, F. Marken, D. H. Kim, D. H. Marsha, D. J. Riley, F. C. Walsh, K. H. El-Abiary and A. A. Lapkin: *Electrochem. Commun.*, 2005, **7**, 1050–1058.
22. K. V. Sarathy, G. Raina, R. T. Yadav, G. U. Kulkarni and C. N. R. Rao: *J. Phys. Chem. B*, 1997, **101B**, 9876–9880.
23. A. Nakahira, T. Kubo, Y. Yamasaki, T. Suzuki and Y. Ikuhara: *Jpn J. Appl. Phys.*, 2005, **44**, L690–L692.
24. T. Soejima, H. Tada, T. Kawahara and S. Ito: *Langmuir*, 2002, **18**, 4191–4194.
25. D. V. Bavykin, S. N. Gordeev, A. V. Moskalenko, A. A. Lapkin and F. C. Walsh: *J. Phys. Chem. B*, 2005, **109B**, 8565–8569.
26. C. H. Lin, C. H. Lee, J. H. Chao, C. Y. Kuo, Y. C. Cheng, W. N. Huang, H. W. Chang, Y. M. Huang and M. K. Shih: *Catal. Lett.*, 2004, **98**, 61–66.
27. V. Idakiev, Z. Y. Yuan, T. Tabakova and B. L. Su: *Appl. Catal. A*, 2005, **281A**, 149–155.
28. T. Akita, M. Okumura, K. Tanaka, K. Ohkuma, M. Kohyama, T. Koyanagi, M. Date, S. Tsubota and M. Haruta: *Surf. Interf. Anal.*, 2005, **37**, 265–269.
29. Y. G. Wang and X. G. Zhang: *Electrochim. Acta*, 2004, **49**, 1957–1962.